APPLICATION OF MOLECULAR GENOMIC ANALYSIS TOOLS TO ASSESS BACTERIAL GENOMES AND BOVINE REGULATORY ELEMENTS FOR FOOD SAFETY AND MEAT QUALITY

A Dissertation

by

DUSTIN AARON THERRIEN

Submitted to the Graduate and Professional School of
Texas A&M University
in partial fulfillment of the requirements for the degree of

DOCTOR OF PHILOSOPHY

Chair of Committee,	Penny K. Riggs
Committee Members,	H. Russell Cross
	Thomas Matthew Taylor
	Jason J. Gill
Head of Department,	Graham Cliff Lamb

May 2022

Major Subject: Animal Science

ABSTRACT

In recent years due to drastic reductions in cost, sequencing-based technologies have become more accessible to the scientific community. As a result, these tools have become commonplace within the contemporary literature and have displaced several older genome-based methodologies/techniques. Despite the apparent benefits that these tools possess over the older counterparts, several technical hurdles remain that must be addressed. As such, the current research was conducted to explore and demonstrate the utility and limitations of sequencing-based technologies within two aspects of the agricultural sciences: food safety and meat quality.

In the first study, whole genome sequencing (**WGS**) of a group of U.S. Department of Agriculture (**USDA**)-approved non-pathogenic *Escherichia coli* (***E. coli***) surrogates and their rifampicin-resistant counterparts was conducted via two popular next generation sequencing (**NGS**) technologies. The strengths and weaknesses of both long- and short-read sequencing were demonstrated. Neither approach was sufficient for generating a closed bacterial genome, but by combining the short- and long-read assemblies in a hybrid fashion, complete genomes were produced. The hybrid genome and short-read assemblies were most effective for identifying virulence factors and single nucleotide polymorphism (**SNP**s) that conferred rifampicin resistance. These completed genomes will be valuable for future food safety research activities and our results support recommendations for how WGS can be effectively utilized within industry food safety programs.

The second study sought to further elucidate the physiological mechanisms that contribute to the development of the dark cutting phenotype in beef cattle. Through RNA-

sequencing of microRNAs from total RNA extracts of *Longissimus lumborum* biopsies, expression profiles were generated for each steer carcass. Differential expression analyses compared microRNA expression between normal carcasses and those displaying the dark, firm, and dry (**DFD**) phenotype via two statistical approaches. These analyses resulted in the identification of 10 candidate microRNAs (**miRNA**s) that were found to possess potential biological relevance to the DFD phenotype. These findings represent a starting point in uncovering the relationship between of miRNAs and the DFD phenotype and can contribute to the development of screening/intervention-based strategies that can be utilized in better understanding physiological/genomic mechanisms in order to reduce the occurrence of this economically important trait.

DEDICATION

I would like to dedicate this dissertation to the memory of Dr. Sarah Canterberry.

Thank you for believing in me.

I hope that I would have made you proud.

ACKNOWLEDGEMENTS

To begin I would like to thank God, all things are possible through your grace and all that I have is due to your generosity. Next, I would like to thank my parents for all the sacrifices that you all have made in order to make this possible. I hope that I have made you all proud, and sorry for not being present in your lives more over the years due to my work. Furthermore, I would like to thank my best friends Alex Buckner, John Lopez, and Walker Lazo for their friendship, loyalty, and support over the years. A special thanks as well to my friend Marissa Rotenberry, who spent countless hours on the phone with me discussing various aspects of statistical analysis. I would like to acknowledge my girlfriend, Hannah Valigura. I know that I am not the easiest person to get along with, but thank you for all of your patience, encouragement, and support through this whole process. I would like to also thank her dad, Mike Valigura, for giving me a place to stay while I travelled back and forth between Mississippi and Texas in the final stages of my work.

Additionally, I would like to thank the faculty members of the Biology Department at Stephen F. Austin State University for the support and encouragement throughout the years. The faculty within that department offered countless opportunities that allowed me to get where I currently am, and I can honestly say gave me the best educational experience out of my entire college career. However, of these individuals I would like to single out and personally thank Mr. Ronald Havner. You provided me with a job in the microbiology lab during a very difficult time (financially) in my life, and throughout my time as an undergraduate and a master's student you always provided me exceptional counsel. No matter what problem or obstacle I was facing, you always gave the impression

that you genuinely cared, and I can't express how thankful I am for that, you are a real Dude. Higher education as a whole would benefit tremendously if there were more educators like you. Furthermore, as much as I hate chemistry, I would like to acknowledge and thank Dr. Franks at the Stephen F. Austin State University Chemistry Department as well. You were always hard but fair and I respect you for that. Additionally, no matter how difficult the challenge was that I was facing, I would think back on the time that I had to take one of those God awful 3-hr tests of yours with a piece of 0.5 mm pencil lead because my pencil broke, and I didn't have a spare. That memory has served as a source of strength during my entire academic career because I don't think anything I have currently done has ever been that difficult or stressful.

Furthermore, I would like to thank the numerous other individuals who made this work possible and assisted me in this journey. My committee members, for guiding me through this process, for assisting with my work, and overall, for making all of this possible. Kelli Kochan, for maintaining an immaculate working environment within the laboratory, training me in numerous protocols, and for assisting me in experimental design and troubleshooting. Dr. Andrew Hillhouse, for not only handling the sequencing portions of my experiments but also for letting me tag along and for answering questions I had pertaining to those procedures. Kranti Konganti and Dr. Wes Brashear, for offering bioinformatic assistance, quick turnover times on analyses, for thoroughly answering questions regarding the data analysis portions of these experiments, and for most importantly replying to emails within a timely manner. Lastly, I would like to offer a special thanks to Dr. Riggs for not only taking me on as a graduate student but for all of the support and guidance along the way. Life threw in a few curve balls along the way, and

I am sorry it took longer than expected. However, despite this I deeply appreciate all of the patience that you showed me during this process and for not giving up on me over these last couple of rough years.

CONTRIBUTORS AND FUNDING SOURCES

Contributors

The dissertation committee that endorsed this research consisted of Dr. Penny Riggs (chair), Dr. Russell Cross, Dr. Jason Gill of the Department of Animal Science, and Dr. Matthew Taylor of the Graduate Faculty of the Department of Food Science and Technology.

Funding Sources

This work is partially supported by the Texas Beef Council and Texas A&M AgriLife Research. Additional support for this work (samples and pedigree info) was provided by Agriculture and Food Research Initiative [Grant No. 2012-68003-30155] from the USDA National Institute of Food and Agriculture.

NOMENCLATURE

β-AA	Beta-adrenergic agents
%BCTRC	Boneless, closely trimmed, retail cuts
%KPH	Kidney, pelvic, and heart
A/E	Attaching and effacing
AGO	Argonaute
AN	Angus-sired
ARE	AU-rich elements
ATCC	American Type Culture Collection
ATP	Adenosine triphosphate
a_w	Minimum water activity
BCP	1-bromo-3-chloropropane
BFP	Bundle forming pili
BLAST	Basic Local Alignment Search Tool
bps	Base pairs
BUSCO	Benchmarking Universal Single-Copy Orthologs
CASR	Calcium-sensing receptor
CCP	Critical control point
CCR4-NOT	Carbon catabolite repressor 4-negative on TATA
CDC	Centers for Disease Control and Prevention
CDT	Cytolethal distending toxin
CF	Colonization factor

CFA/I	Colonization factor antigen I
CNF1	Cytotoxic necrotizing factor 1
Contig	Contiguous segment/sequence
CPM	Counts per million
CPT	Center of Phage Technology
CSDC2	Cold-shock domain-containing protein 2
DAEC	Diffusely adherent *Escherichia coli*
DCP	de-capping protein
DDX6	DEAD-BOX helicase 6
DFD	Dark, firm, and dry
DGCR8	Di George Syndrome Critical Region 8
DKK1	Dickkopf-1
DOE	U.S. Department of Energy
EAEC	Enteroaggregative *Escherichia coli*
EAF	EPEC adherence factor plasmid
E. coli	*Escherichia coli*
EHEC	Enterohemorrhagic *Escherichia coli*
EIEC	Enteroinvasive *Escherichia coli*
EPEC	Enteropathogenic *Escherichia coli*
ETEC	Enterotoxigenic *Escherichia coli*
FBDO	Foodborne disease outbreak
FD	Fold difference
FDA	Food and Drug Administration

FDR	False discovery rate
FXR1	Fragile X mental retardation-relation protein 1
GI	Gastrointestinal
GTP	Guanosine triphosphate
HACCP	Hazard Analysis and Critical Control Point
HIF-α	Hypoxia-inducible factor α
HPCC	High Performance Computing Cluster
HSP	Heat-shock protein
HUS	Hemolytic uremic syndrome
IPA	Ingenuity Pathway Analysis
isomiR	miRNA isoforms
LEE	Locus of enterocyte effacement
LT	Heat-labile toxin
MAC	MacConkey Agar
MAPK	Mitogen-activated protein kinase
MRE	miRNA recognition elements
mRNA	Messenger RNA
miRNA	MicroRNA
MLST	Multi-locus Sequencing Typing
MRC	Molecular Research Center Inc.
MYC	Myelocytomatosis oncogene
MYOD1	Myoblast determination protein 1
NA	Nellore-sired

NACMCF	National Advisory Committee on Microbiological Criteria for Food
NBQA	National Beef Quality Audit
NCBI	National Center for Biotechnology Information
NGS	Next-Generation Sequencing
NIH	National Institute of Health
NMEC	Neonatal meningitis-associate *Escherichia coli*
NON	Non-dark cutter
ONPG	O-nitrophenyl-beta-D-galactopyranoside
P53	Tumor protein P53
PABPC	Polyadenylate-binding protein
PAN2/PAN3	Poly(A)-nuclease deadenylation complex subunits 2 and 3
pap	P fimbriae
P bodies	Processing bodies
Per	Plasmid-encoded regulator
PFGE	Pulse-field Gel Electrophoresis
Pol II	RNA polymerase II
pre-miRNA	Precursor miRNA
pri-miRNA	Primary miRNA
RaGOO	Reference-guided contig ordering and orienting tool
RAN	ras-related nuclear protein
rif^R	Rifampicin-Resistance
RISC	RNA-induced silencing complex
RNase III	Ribonuclease III

rpoB	RNA polymerase (β-subunit)
RRDR	Rifampicin resistant determining region
SBS	Sequence by Synthesis
SMRT	Single molecule real time
SNP	Single-nucleotide polymorphism
ST	Heat-stable toxin
STEC	Shiga-toxigenic *Escherichia coli*
Stx	Shiga-toxin
TBE	Tris/Borate/EDTA
TIGSS	Texas A&M Institute for Genome Sciences and Society
TNF-α	Tumor necrosis factor-α
TRBP	TAR RNA binding protein
TSA	Tryptic soy agar
TSA-R	Tryptic soy agar-Rifampicin
TSB	Tryptic soy broth
TTSS	Type III secretion system
UPEC	Uropathogenic *Escherichia coli*
USDA	U.S. Department of Agriculture
USDA-AMS	USDA Agricultural Marketing Service
USDA-FSIS	USDA Food Safety and Inspection Service
UTR	Untranslated region
VTEC	Verocytotoxin-producing *Escherichia coli*
VFDB	Virulence Factor Database

VP	Voges-Proskauer
WGS	Whole Genome Sequencing
XPO5	Exportin 5
XRN1	Exoribonuclease 1
ZEB1/2	Zinc finger E-box-binding homeobox 1/2

TABLE OF CONTENTS

Page

LIST OF FIGURES

Page

LIST OF TABLES

Page

CHAPTER I FOOD SAFETY:

INTRODUCTION & LITERATURE REVIEW

Overview

Despite the existence of stringent food safety standards, illnesses attributable to foodborne microbial pathogens persist. In order to alleviate and respond to this ongoing issue, the U.S. Department of Agriculture Food Safety and Inspection Service (**USDA-FSIS**) transitioned from using genomic analysis techniques such as pulsed-field gel electrophoresis (**PFGE**), to WGS for foodborne disease outbreak- and recall-associated isolates identification. While sequencing-based methodologies have been shown to be more effective than PFGE for pathogen identification and trace back investigations, many hurdles remain before this technology's full potential can be realized within the food industries. One hurdle is the lack of a standardized assessment process due to the broad diversity of capability across existing sequencing platforms, and lack of a standardized bioinformatics workflow for data analysis. To address this, long-read and short-read sequencing methods are compared directly for analysis of bacterial genomes from a group of USDA-FSIS approved *E. coli* bacterial surrogates currently used for in-plant validation of antimicrobial interventions. These non-pathogenic *E. coli* isolates (American Type Culture Collection (**ATCC**) BAA-1427, BAA-1428, BAA-1429, BAA-1430, and BAA-1431) possess useful similarities (*e.g.* temperature and pH tolerance) to Shiga-toxigenic *E. coli* and *Salmonella enterica*.

As the food industries incorporate high-throughput sequencing within food safety programs, these data will be beneficial for better understanding of this technology and for

developing a standardized workflow that can be applicable for processors and regulators. It is expected that data generated here will be beneficial in not only providing insight to the virulence and genetic make-up of these strains, but also in aiding decision-making for the incorporation and application of WGS within industry food safety programs.

Foodborne pathogens

Foodborne pathogens are broadly defined as any biological agents (*e.g.* bacteria, viruses, and parasites) that when ingested via the consumption of contaminated food or water result in an infection or intoxication that leads the consumer host to experience discomfort, illness, and/or potentially death (Scannell, 2012). When consumed, foodborne pathogens possess the potential to lead to foodborne disease outbreaks (**FBDOs**) which are defined as incidents in which two or more persons experience a similar illness resulting from the ingestion of a common food (CDC, 2015). This notion that certain illnesses coincide with the consumption of food has been well documented throughout history, with reports existing as early as Hippocrates (460 B.C.) who was one of the earliest to document a strong correlation between humans' health and the food they consumed (Hutt & Hutt II, 1984). However, it was not until 1888 during a FBDO where 57 individuals became ill from consuming blood sausages contaminated with *Salmonella enteritidis* that undoubtable evidence for this suspicion arose, marking it as the first incident in which an illness was linked to a specific pathogenic organism (Frenzel et al., 2017, Karlinski, 1889; Tauxe & Pavia, 1998). Since then, numerous measures have been implemented by the food industry and providers in order to improve and protect food safety. This task remains difficult, and it is currently estimated that globally, foodborne illnesses are responsible for ~600 million (1 in 10 people) illnesses and ~420,000 deaths per year (World Health Organization,

2019). Among these cases the Center of Disease Control and Prevention (**CDC**) estimates that FBDOs lead to ~48 million isolated illnesses and ~3,000 deaths within the United States each year alone (CDC, 2018a).

While numerous organisms have been documented as associated with the manifestation of foodborne illnesses and resultant FBDOs the most prevalent causes of illness are Norovirus, *Salmonella*, *Clostridium*, *Campylobacter*, *Staphylococcus*, *Clostridium*, *Listeria*, *Escherichia coli*, *Yersinia*, *Shigella*, and *Vibrio* (Bintsis, 2017). Of these, *E. coli* remains one of the most well-known and studied of these pathogens to date and has been responsible for multiple FBDOs within the United States. *E. coli* was first identified to be a foodborne pathogen in 1971; however, it was not until 1982 where it was associated with outbreaks of bloody diarrhea that resulted from the consumption of contaminated ground beef meat in Oregon and Michigan (Lim et al., 2010; Riley et al., 1983). However, one of the most widely known incidents regarding this pathogen occurred between 1992 - 1993 when 4 children died, and more than 700 illnesses occurred due to the consumption of contaminated hamburger meat from ~73 different Jack in the Box fast food chain locations within California, Idaho, Washington, and Nevada (CDC, 1993). Since then, it was estimated that in 2013 *E. coli* O157:H7 was responsible for ~$271 million in healthcare expenses, and in 2016 was reported by the CDC to be responsible for 839 foodborne disease outbreaks that resulted in 14,259 illnesses, 875 hospitalizations, and 17 deaths alone (Batz et al., 2014; CDC, 2018b; Hoffman et al., 2012; USDA, 2013). Despite the vast improvements in the realm of food safety over the years, this pathogen remains problematic, its detection/elimination currently remains a hurdle for the food safety programs of the beef and poultry industries.

Escherichia coli

Escherichia coli, formerly known as *Bacterium coli commune* (the common colon bacterium) was first observed in 1885 by the German pediatrician, Theodor Escherich (1857 – 1911) via his studies of the intestinal and fecal microflora of neonates and infants. Since then, this bacterium has become one of the most thoroughly studied and researched organisms on the planet (Cooper, 2000; Escherich, 1885). Due to its ability to be easily and quickly grown and cloned within a laboratory setting and its amenable/flexible genomic characteristics, *E. coli* has served as a key model organism in multiple disciplines of study, and has contributed to much of our understanding regarding fundamental principles (*e.g.* metabolism, gene expression, DNA replication, various biochemical pathways, *etc*.) in fields of research such as biochemistry and molecular biology (Cooper, 2000). To date more than 23,000 *E. coli* genomic assemblies and annotations have been submitted to the National Center for Biotechnology Information (**NCBI**), with median total genome length ~5.13 Mbs, and median protein count of >4,000 on average across all species (National Center for Biotechnology Information, 2017). *E. coli* are unicellular microorganisms that have been reported to be gram-negative, straight rod-shaped (2.0-6.0μm x 1.1-1.5μm), facultative anaerobic mesophiles that do not produce spores, may produce capsules/microcapsules depending on strain type, and may present mobility if pertitrichous flagella are present (Hardy Diagnostics, 2016; Lim, et al. 2010; Percival and Williams, 2014). Additionally, this bacterial species has been reported to be catalase-positive, oxidase-negative, fermentative, methyl-red-positive, reduce nitrates, citrate-negative, H_2S-negative, urease-negative, O-nitrophenyl-beta-D-galactopyranoside (**ONPG**)-positive, Voges-Proskauer (**VP**)-negative, and can produce acids from carbohydrates (Adams and

Moss, 2008; Hardy Diagnostics, 2016; Percival and Williams, 2014). It has been reported that *E. coli* can generally grow in temperatures that range from 7 ºC to 50 ºC (optimally at 37ºC), show no marked heat resistance (D-value at 60 ºC on the order of 0.1min), can withstand being stored in extremely cold conditions (*i.e.* refrigerators & freezers) for extended periods of time, can survive in an environment with a slightly acidic pH (lowest: 4.4) but thrives at a more neutral pH (optimal: 7), and in foods with a minimum water activity ($\mathbf{a_w}$) of 0.95 (Adams and Moss, 2008; World Health Organization, 2018).

E. coli is one of six members (*i.e. E. albertii, E. blattae, E. coli, E. fergusonii, E. hermannii, and E. vulneris*) of the genus *Escherichia*, and resides within the family *Enterobacteriaceae* along with other notable enteric pathogens (*e.g. Salmonella* spp., *Shigella* spp., and *Yersinia* spp.) (Adams and Moss, 2008; Castellani and Chalmers, 1919; Gordon, 2013). Of these prokaryotic species, *E. coli* and many species of the genus *Shigella* share many distinct genetic similarities (*e.g.* potentially sharing up to ~ 80 - 90% similarity at the nucleotide level) when observed and are often difficult to distinguish (Adams and Moss, 2008; Ud-Din and Wahid, 2014). However, unlike *Shigella* spp., a large majority of *E. coli* species are mobile, prototrophic, typically more biochemically active, possess the ability to actively ferment lactose among many other sugars, are indole positive, can decarboxylate lysine, and produce gas from D-glucose (Adams and Moss, 2008; Percival and Williams, 2014; Ud-Din and Wahid, 2014). *E. coli* commonly exists as a non-pathogenic member of the indigenous intestinal microbiota located within the gastrointestinal (**GI**) tract of most warm-blooded animals (*e.g.* humans, ruminants, chickens, pigs, *etc*.). However, there are select serotypes that have acquired pathogenesis and are responsible for wide spectrum of human illnesses (Gordon, 2013; Lim et al., 2010;

World Health Organization, 2018). These pathogenic groupings are typically categorized via a serotyping system established in 1947 by Kauffman that incorporates their somatic (O), capsular (K), and flagellar (H) surface antigens as a means of identification (Kauffmann, 1947). In combination to this the CDC currently further categorizes these pathogenic *E. coli* into subsets based on the nature of their associated illnesses (*e.g.* pathogenic mechanisms, clinical symptoms, virulence factors, *etc*.) into six diverse pathogroups/pathotypes: Enterotoxigenic *E. coli* (**ETEC**), Enteropathogenic *E. coli* (**EPEC**), Enteroaggregative *E. coli* (**EAEC**), Enteroinvasive *E. coli* (**EIEC**), Diffusely adherent *E. coli* (**DAEC**), and Enterohemorrhagic *E. coli* (**EHEC**), which may also be referred to as Shiga-toxin producing *E. coli* (**STEC**) or Verocytotoxin-producing *E. coli* (**VTEC**) (CDC, 2014; Croxen et al, 2013; Garcia et al., 2010).

Of these, the subset of opportunistic EHEC species (*i.e.* O26:H11, O91:H21, O111:H8, O157:NM, O157:H7), specifically *E. coli* O157:H7 has been reported to be among the most common *E. coli* species associated with illnesses in humans worldwide (Law, 2000; Melton-Celse et al., 1996; Michino et al., 1998; Paton and Paton, 1999). Common reservoirs for *E. coli* O157:H7 are predominately the intestinal tracts of ruminants, particularly those of cattle and sheep, who are typically unaffected by the pathogen. (Sharma, et al., 2011; The Center for Food Security & Public Health, 2016). The primary mode of transmission of O157:H7 is via the fecal-oral route that can occur from direct contact with the host-animal, direct contact with an infected person, and with the consumption of water that has been contaminated with fecal matter that contains O157:H7 cells (Adams and Moss, 2008; Percival and Williams, 2014; The Center for Food Security & Public Health, 2016). Foodborne illness/outbreaks caused by O157:H7 have historically

been attributed to the consumption of undercooked beef, notably ground beef, and raw milk or contaminated beef products exposed to fecal contaminants via the hide during extraction and harvest processes (Adams and Moss, 2008; The Center for Food Security & Public Health, 2016; World Health Organization, 2018). However, it is of note that recently a significant increase in O157:H7 outbreaks has been attributed to the consumption of leafy vegetables (*e.g.* lettuce, spinach, *etc.*) that were contaminated via exposure to feces from animals or contaminated water sources (World Health Organization, 2018). It has been reported that following the ingestion of <100 cells in humans, a ~3 – 8 days incubation period occurs, followed by illness for ~1 – 12 days. (Percival and Williams, 2014; Sharma, et al., 2011; The Center for Food Security & Public Health, 2016; World Health Organization, 2018).

While the onset of symptoms varies depending on factors such as the concentration of EHEC cells consumed and the age/overall health of the afflicted individual, they typically consist of abdominal cramps, watery diarrhea, hemorrhagic colitis (bloody diarrhea), fever, vomiting, nausea, and dehydration (Adams and Moss, 2008; Percival and Williams, 2014; The Center for Food Security & Public Health, 2016; World Health Organization, 2018). However, in about 10% of the incidents, predominately in the elderly, young children (>5 years old), and immunocompromised, the infection can result in the life-threatening complication known as hemolytic uremic syndrome (**HUS**), which is characterized by thrombocytopenia, anemia, and acute renal failure (Adams and Moss, 2008; Percival and Williams, 2014; The Center for Food Security & Public Health, 2016; World Health Organization, 2018).

Generally, *E. coli* pathogenesis is often a multi-step process that relies on the naïve species acquiring a set of genetic virulence factors via the acquisition of plasmids, transposons, bacteriophages, and/or pathogenicity islands (Lim et al., 2010). One of the primary key virulence factors for O157:H7 subspecies is shiga-toxin (**Stx**), which is a highly potent bacteriophage-encoded verocytotoxin that can present itself in two forms: Stx_1 and Stx_2 (Lim et al., 2010). Stx_1 shares a highly similar homolog to that of the Stx in *Shigella dysenteriae I* and is reported to differ by <100 nucleotides in genetic differences, while Stx_2 is reported to be slightly more distant. It is reported to possess higher levels of toxicity and is more frequently associated with more severe symptoms (*i.e.* hemorrhagic colitis and HUS) (Boerlin et al., 1999; Lim et al., 2010; Ostroff et al., 1989). The structure of Stx is highly conserved and consists of five separate but identical receptor binding subunits (B5) that bind with the host's globotriaosylceramide (Gb3) receptors, in addition to a single enzymatic subunit (A1) that is responsible for the inhibition of protein synthesis via alterations of the 28S rRNA (Gordon, 2013; Lim et al., 2010; Naseer et al., 2017).

Another hallmark feature of O157:H7 is its ability to infect/colonize the host's intestinal mucosa lining and then manifest highly distinctive attaching and effacing (**A/E**) lesions (Adams and Moss, 2008; Gordon, 2013; Lim et al., 2010; Naseer et al., 2017). To achieve this feat, it utilizes a series of genes that are located within the chromosomal pathogenicity island that is referred to as the locus of enterocyte effacement (**LEE**) (Adams and Moss, 2008; Gordon, 2013; Lim et al., 2010; Naseer et al., 2017). This locus contains the genetic information that encodes for three vital components: the type III secretion system (**TTSS**; responsible for the secretion/export of effector molecules), the *eae* gene encodes for the adherence protein intimin and its receptor Tir, and a variety of

Esp proteins that alter cellular signal transduction of the host's cells during A/E lesion formation (Adams and Moss, 2008; Lim et al., 2010; Naseer et al., 2017). Lastly, in addition to Stx and the LEE pathogenicity island it has been reported that in a vast majority of the O157:H7 clinical isolates that were associated with illness also contained the highly conserved virulence pO157 plasmid that contains *ehx* (hemolysin) (Lim et al., 2010; Naseer et al., 2017). Hemolysin has been reported to be highly conserved with various EHEC serotypes that are commonly associated with HUS and is often used as a diagnostic probe for STEC (Adams and Moss, 2008; Fu et al., 2018; Lim et al., 2010). However, despite this accumulation of knowledge, O157:H7 continues to persist as a threat to public health, and in turn has forced regulatory agencies and food safety programs to continue to evolve their offensive strategies in order to combat it.

Food safety

In 1982 following its association with outbreaks of bloody diarrhea that resulted from the consumption of contaminated ground beef in Oregon and Michigan, U.S.A., the USDA-FSIS officially recognized *E. coli* O157:H7 as a causative agent in human illnesses and began to implement food safety and regulatory measures to protect the health of the general public (Lim et al., 2010; Riley et al., 1983). Between 1992 – 1993 occurred possibly one of the most high-profile O157:H7 outbreaks in the United States, which resulted in several hundred illnesses and the deaths of four children along the Pacific Northwest due to the consumption of undercooked hamburgers purchased from the Jack in the Box food chain (CDC, 1993; Murano et al., 2018). This prompted immediate action from the U.S. government, and in 1993 the USDA-FSIS mandated the Cattle Clean Meat Program, which served as a zero-tolerance standard requiring that beef carcasses should be

purged of all fecal matter, ingesta, and udder fluids (Marshall et al., 2005; USDA, 1993). Following this action, in 1994 the USDA-FSIS notified the public that *E. coli* O157:H7 was now considered to be an adulterant of raw ground beef and began a microbiological testing program dedicated to the detection of O157:H7 in raw ground beef products (USDA, 2020). In 1996, the USDA-FSIS released the Pathogen Reduction; Hazard Analysis and Critical Control Point (**HACCP**) Systems; Final Rule, which mandated a set of principles adopted from the National Advisory Committee on Microbiological Criteria for Food (**NACMCF**) that aimed at reducing and preventing the prevalence of foodborne adulterants commonly associated with meat and poultry products (Doyle et al., 2015; National Advisory Committee on Microbiological Criteria for Foods, 1992; USDA, 1996). The implementation of this legislation focused primarily on the prevention and reduction of pathogenic bacteria related to foodborne illnesses, and mandated that meat and poultry related processing establishments/facilities adopt the HACCP system in concordance with the established requirements laid out in 9 CFR Part 417 and submit to routine federal inspections (Code of Federal Regulations, 1996; USDA, 1996).

In order to achieve the requirements of 9 CFR Part 417, the HACCP management system utilizes seven principles: (*i*) Conduct a hazard analysis, (*ii*) Identify the critical control points (**CCP**), (*iii*) The establishment of critical limits for each CCP, (*iv*) Establishing CCP monitoring requirements, (*v*) Establishing corrective action in the case of potential deviations, (*vi*) Developing and maintaining an effective recordkeeping procedure that documents the HACCP system in its entirety, and (*vii*) HACCP systems must be systematically verified (Hogue et al., 1998; USDA, 1996). While numerous antimicrobial intervention strategies (*e.g.* hot water washes, acid washes, chlorine and trisodium

phosphate treatments, knife trimming, *etc*.) have been utilized within various food processing facilities, under this system verification holds extreme importance within a HACCP program and must be performed frequently to ensure the effective application of the control measure (Marshall et al., 2005). Within the HACCP system, the verification principle consists of four distinct processes: (*i*) The initial validation where the establishment determines if the HACCP plan is operating as intended; (*ii*) Ongoing and systematic verification activities (*i.e.* calibration of machines, the review of records, *etc.*); (*iii*) Annual reassessment and modification of the establishments HACCP plan to maintain scientific relevance; and (*iv*) Verification of the establishment's HACCP plan (USDA, 1996, 2015a). To date, the HACCP system still serves as an internationally accepted, science-based food safety management system that focuses on limiting and identifying potential food safety risks via the analysis and control of biological, chemical, and physical hazards from raw material production, procurement, and handling, to manufacturing, distribution, and consumption of the finished product (FDA, 2018a). Following this legislation, the USDA-FSIS, in 1999 announced that the public health risk of O157:H7 should be expanded beyond just ground beef and should also encompass all products containing non-intact beef as well (USDA, 1999). In 2012 the USDA-FSIS declared that raw beef manufacturing trimmings must also be tested for STEC serogroups: O26, O45, O103, O111, O121, and O145 in addition to O157:H7 (USDA 2012).

Additionally, in 2012 the U.S. Food and Drug Administration (**FDA**) began developing GenomeTrakr, an open-access genomic reference database (FDA, 2017, 2021a,b). Though the FDA has been incorporating the use of WGS since 2008, GenomeTrakr was designed to serve as the first distributed network of laboratories to

utilize WGS as a means to identify and track foodborne pathogens on a global scale (FDA, 2018b) swiftly and accurately. For example, once these individual laboratories/researchers have collected the genomic and geographical data relating to these foodborne pathogens, the data are stored within the NCBI public databases where they can be actively shared among public health officers and researchers (FDA, 2021a,b). This approach is highly advantageous because not only does it afford a means for real time comparison and analysis of data but having such a comprehensive database allows health officials to precisely locate the sources of the outbreaks, differentiate potential sources/routes of contamination, decipher which ingredients became adulterated, and trace the illnesses back to the original facility and geographical location (FDA, 2018b). To date, GenomeTrakr has become a global initiative that is currently comprised of 54 U.S. laboratories (*i.e.* federal, hospital, health, and university) as well as 21 labs outside the U.S., and reports to have sequenced 630,000 isolates resulting in more than 300 closed bacterial genomes since its founding (FDA, 2021a,b). Among these labs are the USDA-FSIS labs which announced in 2013 that it too would begin to retire older technologies such as PFGE and transition to WGS and NGS based approaches for its investigations of foodborne disease outbreaks- and recall-associated pathogen identifications.

However, while the technological benefits of the GenomeTrakr network warrant the recent adoption of WGS and NGS technologies by these government and regulatory agencies, it remains to be seen how the private food industry will incorporate and utilize this technology within its facilities and what standards they will be held to by their regulators if they indeed do so.

Surrogate *Escherichia coli* strains

A successful HACCP plan relies heavily upon its seventh principle, verification, as this allows for the ascertainment of whether the individual control points of the plan are indeed operating as intended. In order to challenge these control points and verify their effectiveness against the pathogens that they were designed to control for it becomes necessary to perform investigative studies that utilize pathogen specific testing. However, for the purposes of in-plant validation this can be problematic, as the pathogens in question will only be present in relatively low concentrations, and their introduction is strictly prohibited by the USDA and FDA due to the grave risk it would pose to the potential consumers (Marshal et al., 2005). In such an instance it is appropriate for a plant to utilize non-pathogenic surrogates or indicator organisms that are native microflora of the carcass as a means to evaluate the efficiencies of antimicrobial interventions (Marshal et al., 2005).

A surrogate is a non-pathogenic bacterial species or strain that shares an identical fate or response to a specific treatment or environment in an equivalent manner to a pathogenic species or strain of interest (Beuchat et al., 2001; Hu and Gurtler, 2017; Sinclair et al., 2012). This is not to be confused with the term indicator organism, which has been previously defined as a specific and/or group of microorganisms that are indicative that a food product has been exposed to environmental conditions that pose an inherent risk that the food may have been contaminated with a pathogen or held under conditions conducive for pathogen growth (Busta et al. 2006). In comparison, while both surrogate and indicator organisms are highly similar in their biology and research-based applications, surrogate organisms are highly controlled, often created/highly tested within a laboratory setting, and are not naturally occurring on the food item of interest but are

instead introduced artificially to imitate the survival of their pathogenic counterparts (Busta et al., 2006).

To date the USDA-FSIS has approved the use of a variety of non-pathogenic surrogates for the validation of in-plant intervention strategies and process challenge studies as a means of determining the efficiency of these antimicrobial interventions and their ability to reduce foodborne pathogens. This model of intervention validation is highly beneficial as it not only allows one to determine the efficiencies of their current interventions but allows them to do so without any inherent risk of contaminating their testing equipment or facilities. In order to be classified as a surrogate the microorganism possess the following characteristics: non-pathogenic, possess similar inactivation characteristics, behave in a manner like the pathogen of interest within a similar environment, genetically stable, easily prepared and enumerated, easily distinguishable from native microflora, and be susceptible to similar injuries as the species of interest (Busta et al., 2006; Hu and Gurtler, 2017). Currently, the USDA-FSIS-approved bacterial surrogates include a group of non-pathogenic *E. coli* (ATCC BAA-1427, BAA-1428, BAA-1429, BAA-1430, and BAA-1431) that have been shown to possess similar properties to pathogenic *E. coli and Salmonella enterica* (USDA, 2015b). Prior to their release for commercial use these strains of non-pathogenic *E. coli* originated from the facilities in the Department of Animal Science at Iowa State University where they were isolated from cattle hides (Dickson, Personal Communication). Following their isolation, the isolates were sent to the *E. coli* Reference Center of Pennsylvania State University (State College, PA) for further verification.

These surrogate organisms were verified to not express forms of antibiotic resistance or genes associated with pathogenesis. Thereafter, they underwent further toxin testing via the application of commercial kits as well as tissue culture testing (African green monkey kidney (Vero) cells) by the depositor (ATCC, 2012a, 2012b; Dickson, Personal Communication). Further analysis by Marshall et al. (2005) demonstrated that when these surrogate isolates underwent antimicrobial wash treatments (*i.e.* utilized different temperatures of water wash treatments as well as similar water wash treatments followed by various washes of lactic acid, chlorine, and trisodium phosphate.) on beef carcasses and compared with compared with isolates of *E. coli* O157:H7 undergoing similar treatments, these surrogates when combined possessed the utility to validate antimicrobial treatments (Marshall et al., 2005). Subsequently, Niebuhr et al. (2008) successfully demonstrated that when subjected to antimicrobial treatments and compared with cultures of *Salmonella* undergoing identical treatments, that on average the strains of non-pathogenic *E. coli* possessed a higher tolerance to the designated treatments than their *Salmonella* counterparts. These findings were the first to demonstrate that these select strains of *E. coli* could also potentially be utilized as surrogates for various species of *Salmonella* as well under these types of intervention (Niebuhr et al., 2008). Additionally, Cabrera-Diaz et al. (2009) further expanded upon these findings by conducting comparative analysis between the various growth, tolerance (*i.e*. acid & thermal), and attachment properties of these select surrogates and strains of pathogenic *E. coli* O157:H7 and *Salmonella* counterparts. Their findings demonstrated that when hot water and lactic acid treatments were applied to a beef carcass, the surrogates possessed equal and, in some

cases, higher heat and acid tolerances to pathogenic counterparts, thus broadening the scope of their utility as surrogates (Cabrera-Diaz et al., 2009).

Furthermore, Keeling et al. (2009) compared these five *E. coli* biotype I isolates against *E. coli* O157:H7 under four commonly used meat processing conditions (*i.e.* freezing, refrigerating, fermentation, and thermal inactivation). The findings of this study revealed that no significant differences were observed between isolates BAA-1427, BAA-1429, and BAA-1430 and *E. coli* O157:H7 in the presence of the treatments and that these select surrogates would make them suitable surrogates for all four processes (Keeling et al., 2009). However, despite their widespread use as surrogates for the validation of intervention strategies as well as experimental control in research pertaining to antimicrobial intervention strategies, substantial genomic information for these strains was lacking, providing the rationale for the work described herein.

Whole-genome sequencing

Over the last few decades, WGS has not only become a household name within the research community, but has also completely revolutionized the biosciences, and has illuminated much of what researchers currently know and understand regarding gene function as well as its role in the development of disease. However, despite its increasing popularity, the phrase WGS is often used as misnomer, or as an all-encompassing phrase to describe NGS and its associated applications. Such misuses of this phrase have led to a degree of uncertainty and confusion in the semantics of phrases such as WGS and NGS within the current academic literature as well as regulatory settings, as both are often used to describe genomic assemblies that are in fact drafts that have not and may never be fully

resolved. Next-generation sequencing, also known as high-throughput sequencing, is a broad term that is used to describe second-generation/post-Sanger sequencing technologies that simultaneously sequences thousands – millions of DNA molecules in parallel. There currently exists numerous applications of NGS, all of which typically focus on individual aspects of the genome of interest and typically result in draft/incomplete genomes comprised of numerous contiguous sequences (**contigs**). While varying definitions exist for the term WGS, also known as complete -, entire-, full-genome sequencing, it can be loosely defined as an application of next-generation that produces a comprehensive resolution of the genome of interest and reduces it into a complete singular contig.

While varying landmarks of significance pertaining to development and success of genomic sequencing, it was in 1977 with the major-breakthrough by Frederick Sanger in his development of the Sanger's chain-termination or dideoxy technique (first-generation sequencing) that modern era of DNA sequencing began (Heather and Chain, 2016; Sanger et al., 1977). In the following years, vast improvements to many aspects of this sequencing method led to robust increases in the utilization of this technology, and the eventual founding of GenBank, in 1983 which serves as the sequence database for the U.S. National Institute of Health (**NIH**; Giani et al., 2020; Heather and Chain, 2016; NIH, 2021a). In 1986, the field was further revolutionized with the release of the first semi-automated DNA sequencing method, known as dye primer sequencing, was developed by Lloyd Smith and LeRoy Hood, which utilized synthesized fluorescent DNA primers (Hood and Galas, 2003; Smith et al., 1986). Soon after in 1990, the U.S. Department of Energy (**DOE**) and NIH announce the beginning of the Human Genome Project, which proceeded into 2003, and due to its incredibly high throughput demands further accelerated the speed in which

automated sequencing technologies were developed (Barba et al., 2014; Giani et al., 2020; Hood and Galas, 2003; NIH, 2021b). Following this in 2005, another major paradigm shift in sequencing technology occurred when the company 454 Life Sciences (purchased by Roche in 2007) released the first commercially available NGS technology, the 454 FLX pyrosequencing platform. This breakthrough was followed by numerous other parallel sequencing-based techniques and marks the beginning of the second-generation sequencing (short-read sequencing) (Barba et al., 2014; Barzon et al., 2011; Heather and Chain, 2016; Rajesh and Jaya, 2017).

Lastly, it was in early 2010 when the company Pacific Biosciences introduced its patent single molecule real time (**SMRT**) sequencing technology that could yield long-reads that spanned between 5-15 kbps in length that the field of genomics saw the emergence of the third-generation sequencing technologies (Giani et al., 2020; Heather and Chain, 2016; Kchouk et al., 2017; Lee et al., 2016). Despite all of the various technologies that have come and gone over the recent decades, WGS is primarily conducted using second- and third-generation sequencing methodologies, which can be differentiated by the length of sequence fragments or "read-lengths" (*i.e.* short- and long-read) they yield (Jagadeesan et al., 2019; Taboada et al., 2017). Of these, two of the most prevalent brands that are seen within the contemporary literature are the Illumina MiSeq short-read sequencing platforms (Illumina, San Diego, CA), and its long-read counterpart the MinION manufactured by Oxford Nanopore (Oxford Nanopore, RI 02903, UK). The Illumina MiSeq incorporates the use of sequencing by synthesis (**SBS**), a widely adopted NGS technology, and utilizes massively parallel sequencing that generate read lengths of ~100 to 300 base pairs (**bps**) in size, a high degree of accuracy (*i.e.* error rate in base

calling typically >1%) , and result in ~95% coverage of most bacterial genomes (Goodwin et al., 2016; Illumina, 2017, 2010, 2021; Jagadeesan et al., 2019; Maio et al., 2019; Ronholm et al., 2016; Taboada et al., 2017). The Illumina SBS workflow consists of four primary steps: (*i*) Library preparation, (*ii*) Cluster generation, (*iii*) Sequencing, (*iv*) Data analysis (Illumina, 2017, 2010, 2021). The first step, library preparation, consists of the fragmentation (*i.e.* physically or enzymatically) of double-stranded DNA and the addition of unique adapters to each end of the DNA fragments. The second step, cluster generation, is a process in which each molecule within the generated library is hybridized to the oligos on the flow cell and then isothermally amplified in order to generate numerous copies of the DNA fragments.

Once the individual fragment strands bind to the complementary oligos located on the flow-cell, a polymerase binds to it and generates a complementary strand with the hybridized fragment, which are then denatured, removing the original template leaving the copy behind. The reverse strand that was generated from the original template is then clonally amplified via bridge amplification, which is repeated continuously as well as simultaneously for millions of other clusters. Once bridge amplification has occurred the reverse strands are denatured, linearized, and are washed off leaving behind the forward strands which remain bound to the flow-cell oligos. The 3’ ends of these forward strands are then blocked to prevent any further priming. The third step, sequencing, consists of the extension of the first sequencing primer to produce the first read, and with each cycle fluorescently tagged nucleotides will then compete for addition to the extending chain. Only one nucleotide will bind to that location which is dependent on the template’s

sequence; once successfully bound to the clusters it is excited by a light source which will emit a fluorescent signal.

Once this first read has been completed the generated read product is denatured and removed, and then the index-1 read primer will then bind to the template in its place generating a read of its own. Afterwards, this index-read it is denatured along with the 3' barrier freeing the template strand to bridge over to a neighboring oligo located on the surface of the flow-cell. Following this, index-2 will bind and be processed similarly as index-1, polymerases will hybridize with the template strand and synthesize a double-stranded bridge. This yields a complement strand to that of the template strand. These two strands are then linearized and the 3' ends of each are blocked. The original template strand will be released from its flow-cell oligo, and this process continues until millions of reads are generated.

The fourth step, data analysis, consists of the pooling of the generated sequences based on their designated indices that were added during the sample preparation phase. Lastly, each of these sample reads that contain similar regions of base calls are then clustered together, and the forward- and reverse-reads are paired together creating contigs which are further aligned with a reference genome of interest for further analysis (Illumina, 2017, 2010, 2021). Short-read approaches such as the Illumina MiSeq process are beneficial as they allow for researchers to develop somewhat comprehensive estimations regarding the total gene number for an organism, their classification and approximate degree of relatedness to other similar species, and the overall relatedness of their distinct gene sets to other organisms. However, despite the effectiveness these methods offer regarding comparative gene-based studies, short-read sequencing in unable to produce

sequences that span long repetitive genomic regions and large areas that are prone to rearrangement (*e.g.* deletions, insertions, repeats, and inversions), and frequently results in incomplete genomic assemblies (draft genomes) of contigs that are oriented incorrectly or contain other structural errors (Jagadeesan et al., 2019; Maio et al., 2019; Pollard et al., 2018; Ronholm et al., 2016; Taboada et al., 2017). Drawbacks and deficiencies such as these that have strongly driven the development of third-generation sequencing technologies such as the Oxford Nanopore MinION. In contrast, for DNA sequencing the Oxford Nanopore MinION incorporates the use of single-strand sequencing method that sequences in real-time and generates read lengths wildly ranging from ~1 kbps to hundreds of kilobases on average, with some being reported as being in the millions of base pairs in a single read (Giani et al., 2020; Payne et al., 2019).

Despite this vast improvement in sequence read-lengths, the MinION sequence results often result in significantly lower levels of base-calling quality and sequence accuracy, with base calling error rates ranging from ~5-40% (Goodwin et al., 2015; Goodwin et al., 2016; Jagadeesan et al., 2019; Jain et al., 2018; Loman et al., 2015; Pollard et al., 2018; Ronholm et al., 2016). The Oxford Nanopore workflow consists of three primary steps: (*i*) Library preparation, (*ii*) Sequencing, (*iii*) Data analysis (Oxford Nanopore Technologies, 2016, 2018, 2020). The first step, library preparation, can be highly variable depending on the nature of the experiment depending on which Oxford Nanopore library prep kit is utilized. However, in the commonly used Rapid Barcoding Sequencing kit library preparation consists of mixing high molecular weight genomic DNA with a barcoded transposome complex that consists of a transposase enzyme and sequence adapters. This transposase enzyme contains multiple functions and serves as a

means to cleave the DNA and attach the sequence adapters to each end. It can act as a molecular anchor that binds the DNA complex to the nanopore, and also functions as a motor protein (*i.e.* a processive enzyme) that serves as a breaking system that allows the user to control the speed in which the DNA will be sequenced.

The second step, sequencing, incorporates the use of a protein nanopore (1 nm in scale) that is located within the electrically resistant flow-cell membrane composed of synthetic polymers. From there an electrical current is then applied on the surface of the polymer membrane that is passed through the opening at the surface of the pore, which allows for individual or single molecules to pass through. These molecules depending on their molecular sizes will lead to signature disruptions within the electrical current flowing through the pore. This process begins with the double-stranded DNA molecule binding with the transposase enzyme forming a DNA-enzyme complex. The transposase enzyme functions as a motor that guides the DNA molecule to the nanopore, where upon reaching this destination anchors itself onto the nanopore. Upon anchoring to the nanopore, the double-stranded DNA is unzipped by the processive enzyme and only a single-stranded will be fed through the nanopore. These k-mers (4 nucleotides) begin travelling through the narrowest part of the nanopore located within the polymer membrane where it will lead to the previously described electrical disruptions within the potential. Each nucleotide possesses its own characteristic disruption pattern that allows for each base pair to be distinguished in real-time based on the size of disruption it causes to the electrical current. Once the initial strand has been completed the nanopore binds with another DNA-enzyme complex and this process begins to repeat.

The third step, data analysis, takes place in real-time and begins to upload data as soon as the sequencing begins. While sequencing occurs the output data is simultaneously uploaded on the Oxford Nanopore Metrichor cloud-based data analysis system where the user can actively monitor it until sufficient data has been collected (Oxford Nanopore Technologies, 2016, 2018, 2020). Long-read approaches such as the Oxford Nanopore MinION approach have been highly beneficial in the bioscience fields of research as they have not only allowed for researchers to for the first time more accurately resolve regions of the genome that contain large quantities of repeated sequences. This in turn has allowed for the closing of significantly more draft genomes and has also provided the ability to read RNA transcripts in their entirety (Giani et al, 2020; Giordano et al., 2017).

However, despite the effectiveness of third-generation sequencers such as the MinION, this technology suffers in its ability to successfully sequence homopolymeric regions that exceed its designated k-mer length (Goodwin et al., 2016). Furthermore, there still remains much within the literature regarding the accuracy of the MinION, and it has been shown to display significant inconsistencies in the ranges of its reported errors in base-calling (numerous indels) (Goodwin et al., 2015; Goodwin et al., 2016; Jagadeesan et al., 2019; Jain et al., 2018; Loman et al., 2015; Pollard et al., 2018; Ronholm et al., 2016).

CHAPTER II:

COMPLETE WHOLE GENOME SEQUENCES OF *ESCHERICHIA COLI* SURROGATE STRAINS AND COMPARISON OF METHODOLOGIES FOR APPLICATION TO THE FOOD INDUSTRY[*]

INTRODUCTION

Over recent decades, the landscape of food safety has undergone paradigm shifts as technological advancements in genomics enabled implementation of numerous measures for ensuring a safe and secure food supply (Murano et al., 2018). However, despite these stringent food safety standards/practices in the United States, illnesses attributable to foodborne microbial pathogens continue to persist. The CDC estimates that illnesses attributed to foodborne pathogens are responsible for approximately 48 million illnesses (1 in 6 people), 128,000 hospitalizations, and 3,000 deaths each year within the United States alone (Allard et al., 2016; CDC, 2018; Doyle et al., 2015; Lüth et al., 2018; Sekse et al., 2017). Furthermore, among these it has been estimated that *E. coli* O157:H7 alone was responsible for ~$271 million in healthcare expenses and economic losses (Batz et al., 2014; Hoffman et al., 2012; USDA, 2013). Traditionally in order to combat this persistent dilemma various methodologies and technologies (*e.g.* PFGE), serotyping, phage typing, multi-locus sequence typing (**MLST**), *etc.*) have been utilized for identification and characterization of foodborne pathogens at the clinical level. Regrettably, while these

---

[*] Reprinted with permission from Therrien, D. A.; Konganti, K.; Gill, J. J.; Davis, B. W.; Hillhouse, A. E.; Michalik, J.; Cross, H. R.; Smith, G. C.; Taylor, T. M.; Riggs, P. K., Complete Whole Genome Sequences of *Escherichia coli* Surrogate Strains and Comparison of Sequence Methods with Application to the Food Industry; Published by Multidisciplinary Digital Publishing Institute, **2021**.

molecular profiling techniques have undoubtedly saved lives as well as served invaluable roles in food safety, they remain highly time consuming, technically laborious, difficult to replicate, and lack the resolution necessary for differential identification of closely related bacterial strains.

However, rapid technological advancements and drastic reductions in cost have made applications such as WGS via high throughput sequencing NGS and 3rd generation sequencing) appealing alternatives to these previous characterization methods (Allard et al., 2017; Jagadeesan et al., 2019; The National Human Research Institute, 2019). Currently, WGS is achieved via two types of sequencing methods that can be distinguished by the length of sequence fragments or "read lengths" (*i.e.* short- and long-read) produced (Jagadeesan et al., 2019; Taboada et al., 2017). Short-read sequencing platforms, such as those manufactured by Illumina, utilize massively parallel sequencing that yields read lengths of about 100 to 300 bps with a high level of accuracy. Typically, error rates in nucleotide identification (base calling) are less than 1% and result in 95% coverage of most bacterial genomes (Goodwin et al., 2016; Jagadeesan et al., 2019; Maio et al., 2019; Ronholm et al., 2016; Taboada et al., 2017). The short-read approach allows a researcher to make comprehensive estimations regarding the total number of genes present within the organism of interest, their classification in relation to other species, and the overall relatedness of their distinct gene sets to other organisms. While highly informative and effective for comparative gene-based studies, this technique is inadequate for producing sequences that span long repetitive genomic regions and large areas that are prone to rearrangement (*e.g.* deletions, insertions, repeats, and inversions).

This limitation frequently results in incomplete genomic assemblies (draft genomes) of contigs that are oriented incorrectly or contain other structural errors (Jagadeesan et al., 2019; Maio et al., 2019; Pollard et al., 2018; Ronholm et al., 2016; Taboada et al., 2017). In contrast, long-read sequencing platforms can generate read lengths ranging from ~1,000 bps to hundreds of kilobases in a single read. Unfortunately, the increased sequence length is offset by a significant reduction in sequence accuracy, with base calling error rates ranging from ~5-40% (Goodwin et al., 2015; Goodwin et al., 2016; Jagadeesan et al., 2019; Jain et al., 2018; Loman et al., 2015; Pollard et al., 2018; Ronholm et al., 2016). Despite the differences among WGS technologies, sequencing-based approaches consistently provide greater resolution and discriminatory power for distinguishing closely related bacterial species compared to previous methods, thus improving foodborne pathogen surveillance systems and trace back investigations (Deng et al., 2016; Jackson et al., 2016; Lakicevic et al., 2017; Lüth et al., 2018; Lysty et al., 2017; Rantsiou et al., 2018; Sekse et al., 2017). WGS datasets can be simultaneously used in multiple investigative analyses (*e.g.* subtyping, antibiotic resistance profiling, virulence genetic markers, screening of mobile genetic markers, *etc*.) or stored for future analyses. For these reasons, WGS is being adopted by federal regulatory and public health related entities (*e.g.* CDC, FDA, USDA-FSIS) as one of the primary methods for surveillance, tracing of transmission routes, and for foodborne disease outbreak- and recall associated isolates identification for select bacterial species and outbreak investigation (Deng et al., 2016; Jagadeesan et al., 2019; Rantsiou et al., 2018; Wang et al., 2016).

The technological benefits of WGS support the recent adoption by government and regulatory agencies, but certain aspects must be addressed before WGS can be widely

incorporated as routine screening within the food industry, if at all. Arguably, one area of greatest difficulty pertaining to this technology is the abundant diversity in workflows that exist for processing and sequencing of the samples, as well as bioinformatic analyses and interpretation of large volumes of data. Genomic technologies have undergone rapid advancements that enabled innovations and accessibility but have also resulted in a large variety of preparatory workflow procedures, sequencing platforms with diverse utility, and innumerous bioinformatic analytical tools (Deng et al., 2016; Jagadeesan et al., 2019; Portmann et al., 2018; Rantsiou et al., 2018; Ronholm et al., 2016; Riggs, 2019; Taboada et al., 2017).

To address a number of these questions while contributing relevant and novel data, the overall objective of this project was to produce long-read, short-read, and hybrid genomic assemblies for a group of USDA-FSIS-approved non-pathogenic *E. coli* surrogates (ATCC BAA-1427, BAA-1428, BAA-1429, BAA-1430, and BAA-1431). The USDA-FSIS has previously supported the use of non-pathogenic surrogate organisms (*i.e.* must be non-pathogenic, genetically stable, easily prepared and enumerated, easily distinguishable from native microflora, possess similar inactivation characteristics and behave in a manner like the pathogen of interest within a similar environment) for the validation of in-plant intervention strategies to reduce the presence of foodborne pathogens (Busta, et al., 2006). This model of intervention is highly beneficial because it allows one to determine the efficacy of a current intervention strategy without inherent risk of contaminating testing equipment or facilities. This group of surrogates is of particular interest because they been shown to possess similar properties to pathogenic *E. coli* and *Salmonella enterica* and are widely used in contemporary research and intervention

validation (Cabrera-Diaz et al., 2009; Ingham et al., 2010; Keeling et al., 2009; Marshall et al., 2005; Niebuhr et al., 2008; USDA, 2015b). Despite their widespread use, genetic information for these strains is not readily available within the literature. The data presented here contribute to the existing body of knowledge regarding sequencing approaches for detection of genes associated with pathogenesis and antibiotic resistance. In addition, with the recent transition by the USDA-FSIS to WGS to improve monitoring of foodborne disease outbreak- and recall-associated microbial isolates these data will provide completed genomes for these widely used surrogates that will be an invaluable resource for processors and regulatory officers in differentiating these strains from pathogenic strains of *E. coli* and supporting decision-making for the incorporation and application of WGS for food safety applications.

METHODS & MATERIALS

Bacterial surrogates

Five non-pathogenic *E. coli* biotype I strains (isolates BAA-1427, BAA-1428, BAA-1429, BAA-1430, and BAA-1431) were obtained from the American Type Culture Collection (ATCC; Manassas, VA, USA) and revived according to ATCC guidance (Table 1.1) (ATCC, 2012a). The surrogates originated as isolates from cattle hides at facilities in the Department of Animal Science at Iowa State University (Marshall et al., 2005; Dickson, Personal Communication). The strains were confirmed to lack antibiotic resistance or a subset of known virulence factors by the *E. coli* Reference Center of Pennsylvania State University and underwent further toxin testing via the application of commercial kits as well as tissue culture testing (African green monkey kidney (Vero) cells) by the depositor (Table 1.2) (ATCC, 2012a,b; Dickson, Personal Communication).

These *E. coli* isolates were propagated twice in 5.0 mL of tryptic soy broth (**TSB**; Becton, Dickinson and Co., Sparks, MD, USA) (24 h, 35°C), and then grown on tryptic soy agar (**TSA**; Becton, Dickinson and Co.) slants, TSA petri plates, TSA + rifampicin (100.0 mg/L; **TSA-R**) plates, and MacConkey agar (**MAC**; Becton, Dickinson and Co.) Petri plates (24 h, 35°C). Following overnight incubation, colonies of parent *E. coli* isolates grown on the TSA slants and streaked on plates were verified as rifampicin-sensitive or rifampicin-resistant (**rif^{R}**). API® 20E (bioMérieux, Inc. N.A., Durham, NC, USA) tests were used to identify organisms as *E. coli* according to manufacturer guidance. Following verification of parent strain identities, three isolates (isolates BAA-1427, BAA-1428, and BAA-1430) were used for generation of rif^{R} mutants, coded BAA-1427 rif^{R}, BAA-1428 rif^{R}, and BAA-1430 rif^{R} (Frenzel et al., 2017; Kaspar and Tamplin, 1993). The rif^{R} strains were verified as described above with respect to *E. coli* identification, and via overnight growth on TSA-R media (24 h, 35°C).

DNA extraction & quantification

For DNA extraction, *E. coli* (parents, rif^{R} mutants) were propagated from working stocks incubated in 5.0 mL TSB (24 h, 35°C) as previously described. TSA streak plates were created from each bacterial isolate and incubated likewise (24 h, 35°C). A single bacterial colony was selected and grown in 5.0 mL TSB (24 hr, 35°C) for DNA extraction. The samples were centrifuged at 10,000 x g for 2 min and cell pellets were frozen at -80°C until used. A phenol/chloroform DNA extraction protocol was used to isolate genomic DNA from cell pellets (Ausubel et al., 1989). The extraction procedure was modified with the substitution of 1-bromo-3-chloropropane (**BCP**; Molecular Research Center Inc., Cincinnati, OH, USA) for 24:1 chloroform:isoamyl alcohol prior to ethanol precipitation

(Chomczynski and Mackey, 1995). DNA samples were quantified via spectrophotometry (NanoDrop ND-1000), visualized by electrophoresis through a 1.0% agarose SFR gel (AMRESCO, Solon, OH) in a 1x Tris/Borate/EDTA (TBE) buffer solution, and stained with SYBR green.

Genomic sequencing

Bacterial genomic DNA was sequenced at the Texas A&M Institute for Genome Sciences and Society (**TIGSS**) core facility (College Station, TX) by Illumina MiSeq and Oxford Nanopore MinION gene sequencing platforms. The derivative group of rif^R mutants were sequenced only via MiSeq. Prior to sequencing, the bacterial DNA was re-quantified via the Qubit 2.0 Fluorometer as recommended by the Illumina MiSeq and Oxford Nanopore MinION library preparation kit protocols. Libraries were prepared with the Nextra XT v2 library preparation kit for the Illumina MiSeq platform, and the Rapid Barcoding Kit (SQK-RBK004) for the MinION. Quality of all sample libraries was evaluated via the Agilent 2200 TapeStation prior to sequencing.

Genome assembly

Upon completion of sequencing reactions, the raw sequence data were downloaded from the Illumina BaseSpace and Oxford Nanopore Metrichor cloud-based storage systems and uploaded onto the TAMU TIGSS High Performance Computing Cluster (**HPCC**) for further processing. The sequence data produced by the MinION were converted from the FAST5 to FASTQ format via the Oxford Nanopore Albacore v2.0.1 base caller (Lannoy et al., 2019). Sequence quality was assessed via FastQC, and low-quality sequence data and the adapter sequences were removed with Trimmomatic v0.32 (Andrews, 2010; Bolger et al., 2014). The SPAdes software tool (v3.13.0) was used to generate a short-read assembly

from the MiSeq data, and the Canu v2.0 single-molecule sequence assembler was used to generate long-read assembly from the MinION data (Bankevich et al., 2012; Koren et al., 2017). Once assembled the contigs for each bacterial sample were screened and those contigs that were < 1000 bps (MinION), <500 bps (MiSeq), possessed low coverage scores, and/or were poorly associated with *E. coli* species were removed from the assemblies. After low-quality contigs had been removed, sequence statistics were calculated for each sample, with overall rates of coverage being calculated via the BEDTools software (Quinlan and Hall, 2010).

Polishing and error correction

Raw unfiltered MiSeq reads and the Canu FASTA long-read assemblies were combined into hybrid assemblies using the Unicycler genomic assembler (Wick et al., 2017a). During this process, the generated hybrid assemblies underwent various cycles of polishing and error correction using the integrated Pilon software tool v1.23 (Walker et al., 2014). Following this the degree of completeness of each hybrid genome was assessed using the Benchmarking Universal Single-Copy Orthologs (**BUSCO**) software v4 and was compared with the lineage enterobacteriales (composed of 216 species and 781 orthologs) (Seppey et al., 2019). To further close these genomes, each was processed using the reference-guided contig ordering and orienting tool (**RaGOO**) with the *E. coli* K12 substr. MG1655 (NC_000913.3) reference genome (Alonge et al., 2019). Lastly, for the samples that were not reduced to a single contig, analysis was conducted via BLASTn to align the nucleotide sequences of the surplus contigs to known sequence to identify their origins (Altschul et al., 1990).

Virulence factor screening and verification

Serotyping and MLST for the three assemblies of each bacterial surrogate was determined with the open access SeroTypeFinder 2.0 and MLST 2.0 software (Joensen et al., 2015; Larsen et al., 2012). The generated assemblies for each of the *E. coli* surrogates were analyzed by translated BLAST analysis (BLASTx) against a dataset of *E. coli* virulence factors extracted from the Virulence Factor Database (**VFDB**) using an e-value cutoff of 10^{-5} (Table 1.3) (Chen et al., 2005; Chen et al., 2012; Chen et al., 2016; Yang et al., 2008). The genome of the known non-pathogenic *E. coli* str. Nissle 1917 (NZ CP022686) was used as a control to filter spurious hits by subtraction of BLASTx hits shared between the surrogates and Nissle with the remaining factors undergoing further investigation. Analyses were conducted on the Texas A&M University Center of Phage Technology (**CPT**) Galaxy instance (Afgan et al., 2018).

The remaining detected virulence factors were examined to confirm the presence of complete genes and/or gene modules as appropriate. Individual bacterial contigs were opened with Sanger Artemis (v.18.0.0) and the regions containing suspected virulence determinants based on BLASTx coordinates were manually annotated and their protein sequences compared to those of known functional virulence factors by BLASTp to determine if they were complete and free of alterations that may render them non-functional (Carver et al., 2012). The percent identities for each of the potential pathogenic elements found within the hybrid assemblies were calculated using the Sørensen-Dice coefficient (Dice, 1945; Sørensen, 1948).

$$SDC = {2|x \cap y|}\Big/{|x| + |y|}$$

The rif^{R}-mutants were excluded from this analysis, as it was expected that their matches would correspond with their surrogate parent strains.

Detection of known RNA polymerase β-subunit (rpoB) rifampicin resistance mutations

The *rpoB* DNA sequences of the parental surrogates BAA-1427, BAA-1428, and BAA-1430 assemblies (*i.e.* long-read, short-read, and hybrid), and their corresponding short-read rif^{R}-mutants BAA-1427 rif^{R}, BAA-1428 rif^{R}, and BAA-1430 rif^{R} counterparts were compared to that of *E. coli* str. K-12 substr. MG1655 (NC_000913.3) via BLASTn to detect mutations commonly associated with rifampicin resistance (Blattner et al., 1997).

RESULTS

Comparison of sequence assembly statistics

Assembly summaries for the MinION and MiSEQ assemblies were calculated and compared along with their Serotypes and MLSTs (Tables 1.4 & 1.5). Sequence generated from the Oxford Nanopore MinION platform resulted in read lengths that were approximately 10-fold longer than read outputs from the Illumina MiSeq sequencer (Tables 1.4 & 1.5). The longer read lengths enabled assembly of sequence reads into fewer and longer contigs and resulted in greater overall genome coverage for each bacterial sample (Table 1.4). The draft assemblies produced from MinION data resulted in a large singular contig for each assembly (4 - 5 Mbs) with a subset of smaller contigs averaging 1kb in size. In contrast, the MiSeq platform resulted exhibited greater uniformity in the size distribution of contigs, with the largest ranging from ~300 - 500 kbs with a steady decline in size to the smallest contig which was ~70 bps (Figures 1.1 & 1.2). These results are consistent with expected ranges for each platform, as a consequence of the unique chemistry and mechanisms for each technology. However, the total assembled lengths for

each bacterial genome differed by only 100 - 300 kb between the MinION and MiSeq sequencing platforms, reflecting a 2 - 6% difference among surrogate counterparts (Tables 1.4 & 1.5).

Hybrid assembly statistics and analysis

The MinION and MiSeq assemblies were combined to improve the overall genome assembly of each surrogate. For each hybrid assembly, summary statistics were calculated and serotypes and MLSTs were identified for comparison with the long- and short-read counterparts. Total lengths of the hybrid assemblies for all five *E. coli* surrogates increased when compared with the MiSeq assemblies and slightly decreased when compared to that of the MinION assemblies (Tables 1.4, 1.5, and 1.6). In considering the total number of contigs and the overall completeness of the genomes, significant improvements were observed in the hybrid assemblies in (Tables 1.4, 1.5, and 1.6). In most cases the genomes were reduced to a single contig. The remaining additional contigs observed for two of the surrogates (BAA-1428 & BAA-1430) were identified via BLASTn to be residual fragments of existing plasmids. Additionally, when the hybrid genomes were compared with the lineage enterobacteriales (216 species and 781 orthologs) within BUSCO, each sample's genome was reported to be between ~99.8 – 99.9% complete (Table 1.6). Lastly, the hybrid assembly's quality was further improved compared with the other assemblies as it underwent multiple rounds of polishing via Pilon which resulted in numerous corrections within each genome (Table 1.6). GenBank Genomes database accession numbers for each genomic assembly are included in Table 1.6, and each sample was annotated via the automated NCBI prokaryotic genome annotation pipeline (Benson et al., 2013; Tatusova et al., 2016).

For three of the bacterial genomes (BAA-1427, BAA-1429, and BAA-1431), each assembly was closed and reduced to a single observable contig that was within the range of a standard *E. coli* genome. The BAA-1428 genome contained one contig that was comparable in size with the three completed genomes, and a smaller 6,762 bps. From BLASTn analysis, the smaller, non-chromosomal contig was found to be identical (100% coverage) to several plasmid sequences existing in public databases: *Salmonella enterica* serovar Newport plasmid pSNE1-1926 (CP025235.1) (6,761 bps), *Salmonella enterica* serovar 1,4[5],12:i- plasmid p11-0813.1 (CP039594.1) (6,760 bps), and *Salmonella enterica* serovar Enteritidis plasmid p4.4 (MG948564.1) (6,760 bps). Of these, the proposed plasmid differed the most from *Salmonella enterica* serovar 1,4[5],12:i- plasmid p11-0813.1 (CP039594.1) by only 50 nucleotide alterations that existed primarily between nucleotides 1201 - 1315. Both *Salmonella enterica* serovar Newport plasmid pSNE1-1926 (CP025235.1) and *Salmonella enterica* serovar Enteritidis plasmid p4.4 (MG948564.1) possessed a nucleotide shift (A → G) at nucleotide 1371 when compared with the proposed BAA-1428 plasmid. Additionally, the proposed plasmid was compared with the other plasmids, they all possessed deletions within a region of low-complexity sequence (*i.e.* homopolymeric guanines) that spans between nucleotides 426 - 436. With the only notable differences existing within this region of low-complexity sequence and at nucleotide 1371 (A → G) it could not be determined if the proposed BAA - 1428 plasmid was more similar to the *Salmonella enterica* serovar Newport plasmid pSNE1-1926 (CP025235.1) or *Salmonella enterica* serovar Enteritidis plasmid p4.4 (MG948564.1).

The result for BAA-1430 however was enigmatic when compared with the others as not only was it on average ~300 kbps larger than the other assembled genomes in total

length but despite all further processing, remained at five observable contigs. Of these the largest was 4,988,672 bps in overall size which is more comparable to the other genomes. Four smaller contigs that were present ranged from 96,846, 9,368, 6,077, and 5,649 bps in length. When BLASTn analysis was performed on these remaining non-chromosomal contigs it was found that the second contig (96,846 bps) displayed the highest genetic identity to the *E. coli fergusonii* plasmid pRHB23-C01_2 (CP057566.1; 99.74% identity, 83% coverage). The third contig (9,368 bps) most resembled the *Serratia liquefaciens* plasmid pS12 (CP048786.1; 99.97% identity, 94% coverage. The fourth contig (6,077 bps) shared a 100% identity and 100% coverage with the *E. coli* plasmid pRHB08-C23_3 (CP057955.1). Lastly, the fifth and smallest contig (5,649 bps) revealed a 99.83% identity and 96% coverage when compared with an unnamed plasmid previously associated with *E. coli* strain RHB13-C21 (CP055721.1).

Virulence factor presence/absence determination and characterization

The MinION, MiSeq, and hybrid genome assemblies from each of the five *E. coli* surrogates encoded genes associated with a subset of predicted regulatory protein adherence factors (Table 1.7). However, the genomes lacked many of the necessary genes that encode vital structure elements/subunits necessary for assembly of the full protein complexes, thus rendering these adherence factors non-functional (Table 1.7). The genomes assembled from MinION sequence were of lower resolution, containing multiple indels and higher errors rates that significantly reduced statistical confidence for detection of many of the adherence factor sequences that were examined, in comparison with those generated by the MiSeq and hybrid assemblies (Table 1.7). However, the MinION, MiSeq, and hybrid genome assemblies indicate that strains BAA-1427, and BAA-1431 encode

complete cytolethal distending toxin (**CDT**) A, B, and C, and cytotoxic necrotizing factor 1 (**CNF1**) (Table 1.7). The percent identities of each of the identified pathogenesis factors for each hybrid assemblies were calculated with the Sørensen-Dice coefficient (Dice, 1945; Sørensen, 1948). Predicted amino acid sequences identified as CDT A, -B, and -C within both surrogate sequences were 56.03%, 69.87%, and 40.56% similar to their functional CDT A, -B, and -C counterparts (GenBank: CAD48849.1, CAD48850.1, and CAD48851.1), respectively (Janka et al., 2003). Additionally, the CNF1-like amino acid sequence in BAA-1427 and BAA-1430 possessed 53.48% percent identity to functional CNF1 (GenBank: CAA50007.1) (Falbo et al., 1993).

Detection of known rpoB rifampicin resistance mutation

The *rpoB* DNA sequences of the parental surrogates BAA-1427, BAA-1428, and BAA-1430 assemblies (*i.e.* long-read, short-read, and hybrid), and their corresponding short-read rif^R-mutants BAA-1427 rif^R, BAA-1428 rif^R, and BAA-1430 rif^R were compared to that of *E. coli* str. K-12 substr. MG1655 (NC_000913.3) to gauge each method's utility for enabling detection of known mutations that confer rifampicin resistance (Table 1.8). When screened, it was found that the three BAA-1427 assemblies (parent strains) and the BAA-1427 rif^R assembly (mutant child strain) shared a silent mutation (A206 to A), while the rif-resistant strain contained an additional L533 to P mutation. The BAA-1428 genomes and BAA-1428 rif^R shared a silent mutation (T486 to T), and BAA-1428 rif^R also possessed a mutation in S512 to P. Additionally, the parent BAA-1430 genomes and the BAA-1430 rif^R genome shared a series of silent mutations (P489 to P, L623 to L, and G846 to G) when compared to *E. coli* K-12. Lastly, in addition to those silent mutations the BAA-1430 rif^R mutant possessed an additional mutation of

H526 to Y. However, it is of note that while the MinION assemblies did contain the same mutations as the Miseq, hybrid, and rif-resistant assemblies, they also contained a large number of additional indels and were ultimately deemed unsuitable for the reliable identification of rif^R-associated single-nucleotide polymorphisms (**SNPs**) (Table 1.8). While elements known to confer rif^R could be detected in the MinION assemblies, this would not be a reliable approach for detecting novel mutations

DISCUSSION

We conducted WGS of a group of USDA-approved non-pathogenic *E. coli* surrogates via two popular NGS technologies and also performed short-read sequencing on rif^R derivatives that exist for three of them. Our objective was to generate and characterize complete genome sequences for these important resources. At the same time, we used the opportunity to directly compare two common sequencing platforms and evaluate their usefulness for identification of potential pathogenic elements or known SNPs that confer rifampicin resistance. Both sequencing methods enabled production of draft genome assemblies for each bacterial strain, although key differences were apparent - notably in the distribution of contig size between the two platforms.

Despite producing draft genomes that typically contained less than 100 contigs of quality sufficient for comparative genomic analysis, with some exception to the MinION genomes due to high error rates, a complete, closed genome was not produced by either method alone (Tables 1.4 & 1.5). However, sequence from the MinION enabled assemblies for each sample in which a single contig comprised ~94 - 99% of the total assembly length (Table 1.4). Consistent with previous findings, when the MinION and Miseq assemblies were utilized in producing hybrid de novo assemblies, the unique

strengths of each method combined to overcome their individual limitations (Boža et al., 2017; Maio et al., 2019; Tyler et al., 2018; Wick et al., 2017a,b). The combined hybrid MinION and MiSEQ assembly resulted in drastic quality improvements in each of the bacterial genomes assemblies (Table 1.6). The hybrid assembly was similar in overall length but had greatly reduced contigs and improved quality for bacterial assembly. Analysis of each hybrid for completeness (via BUSCO using lineage enterobacteriales), indicated that each genome assembly was ~99.8 - 99.9% complete (Table 1.6). Overall, the hybrid assemblies proved to be superior for closing the bacterial genomes and provide an invaluable tool for precisely distinguishing between multiple closely related species of interest.

For assessing pathogenesis, all three assembly strategies enabled identification of genetic sequence associated with various adherence factors and regulatory elements within all the isolates. Differences were observed between methods due to statistical cut-offs for identity established prior to the analysis (Table 1.7). On average the MinION genome assemblies lacked the same degree of resolution and confidence in predicting the presence of several of the adherence factors resulting in several false negatives. The MinION assemblies also appeared to possess multiple frameshifts and duplications, further complicating virulence factor analysis. The hybrid assemblies resulted in more accurate representation of the genomes of these bacteria.

The genome assemblies for the surrogate strains were scanned for the presence of gene sequences that encode virulence factor subunits (Table 1.7; details of virulence factors provided in Table 1.3). Although these lines were previously shown to lack functional virulence factors by other methods, the availability of these new complete

genome assemblies enabled a more detailed investigation of the strains (ATCC, 2012b). Four strains (BAA-1427, BAA-1429, BAA-1430, and BAA-1431) possessed genetic sequences similar to those found within the enteropathogenic *E. coli* adherence factor plasmid (**EAF**) pB171. Sequences for bundle-forming pili (**BFP**) subunits BfpB (secretin), BfpE (inner membrane protein), and BfpH (transglycolase) were identified in three MiSeq assemblies (BAA-1427, BAA-1430, and BAA-1431) (Tobe et al., 1999). Three of the hybrid and MinION counterparts (BAA 1427, BAA-1430, BAA 1431) lacked BfpH, and the MinION BAA-1430 lacked all three Bfp subunits. However, the noted absences following BLAST**x** analysis resulted from failure to meet the statistical threshold, likely reflecting nucleotide sequence variations. Additionally, all the assemblies for two strains (BAA-1429 and BAA-1430) encoded the BfpW/PerC transcriptional activators, which are part of the plasmid-encoded regulator (**Per**) responsible for BFP formation and activation of select genes within the LEE (Gómez-Duarte and Kaper, 1995; Mellies et al., 1999; Shin et al., 2001; Tobe et al., 1996). Despite the presence of some subunits, these sequence elements are insufficient for formation of fully functional pili due to the absence of key accompanying subunit genes.

Apparent homologs of various P fimbriae (**pap**) subunits such as PapE (tip fimbriae), PapG (digalactoside-binding adhesion), and PapJ (assemble/integrity), were observed for all three assemblies of the BAA-1429 strain genome. These elements help comprise the pyelonephritis-associated pili/P fimbriae commonly seen in uropathogenic *E. coli* (Kuehn et al., 1992; Lane and Mobley, 2007; Lillington et al., 2014; Tennent et al., 1990). The pap operon is responsible for the formation of this pilus and has been previously described as encoding eleven distinct proteins (*i.e.* PapA, -B, -C, -D, -E, -F, -G,

-H, -I, -J, -K). However, the presence of a fully functional P fimbriae pilus is unlikely due to the absence of fundamental structural and assembly elements (Goetz et al., 1999; Tennent et al., 1990; Waksman and Hultgren, 2009; Wult et al. 2002).

Some form of a colonization factor (**CF**) that is typically observed in ETEC species was observed in genome assemblies from all the strains. The most prevalent CF was the protein CsnA, which is a component of the major pilin monomer of the CS20 fimbriae (Mortezaei et al., 2015; Nada et al., 2011; Valvatne et al., 2004). However, in almost every instance, sequence similarity of these remained close to the statistical cut-off for identity, indicating lack of similarity to functional virulence factors. In addition to CFs, the BAA-1428 and BAA-1430 genomes contained genes similar to the CswA factor, commonly associated with the formation of the structural CS12 fimbriae subunits (Nada et al., 2011). Lastly, *E. coli* BAA-1430 exclusively possessed sequence similarity to the CfaB, CooA, and CsbA CFs, associated with the colonization factor antigen I (**CFA/I**), CSI pilin major subunit, and the CS17 fimbrial subunit (Galkin et al., 2013; Nada et al., 2011; Nataro and Kaper, 1998). The CFs found within these genomes are associated with virulent ETEC; for pathogenesis to arise within these species there are two primary factors that must be present, which are the enterotoxins: heat-labile (**LT**) and/or heat-stable (**ST**) toxins, of which are frequently transported within the same plasmid as the CFs (Nada et al., 2011; Nataro et al., 1998; Wiley et al., 2010). Their absence indicates these CFs may represent fimbriae/adherence factors that are not associated with pathogenesis but confer similar structural properties to those that are. It is not uncommon that *E. coli* isolates, whether pathogenic or non-pathogenic, possess some mix of colonization and/or adherence factors (Frömmel et al., 2013; Grozdanov et al., 2004; Rendón et al., 2007). However, in this

experiment none of the identified sequences with resemblance to any putative virulence factor is expected to be functional or pose a hazard. The findings here indicate that the isolates of interest harbored no other detectable factors typically associated with virulent ETEC.

In two strain genomes (BAA-1427 and BAA-1430) potential homologous sequences encoding toxins associated with pathogenic *E. coli* were detected, but with only weak similarity -thus not likely functional. For example, the CNF1 holotoxin, an AB toxin, is documented to operate via RhoGTPases activity within eukaryotic cells but shared only 53.48% percent translated amino acid identity with the known functional toxin (Caprioli et al., 1987; Khan et al., 2002; Knust et al., 2009). Documented regions within CNF1 that are responsible for host cell binding, as well the C-terminal portion that expresses the catalytic activity of this protein, were each ~50% identical in the surrogates when compared to the respective regions within their functional counterpart (Fabbri et al., 1999; Fabbri et al., 2010; Lemichez et al., 1997). Additionally, the BAA-1427 and BAA-1430 genomes all appeared to harbor sequences sharing similarities with that of CDT (Friedrich et al., 2006; Guerra et al., 2011). CDT is a tripartite holotoxin responsible for cell cycle arrest and apoptosis within mammalian cells and is composed of a deoxyribonuclease-like toxin B-subunit and A and C subunits responsible for transporting the B subunit to the surface of the host cell (Ceelen et al., 2006; Elwell et al., 2001; Nesic et al., 2004; Pickett and Whitehouse, 1999; Tejero and Galán, 2001). Upon examination of these identified subunits, it was found that our samples only shared a 56.03% identity to subunit A (CAD48849.1), 69.87% to subunit B (CAD48859.1), and 40.56% to subunit C (CAD48851.1) when compared with functional toxins.

The availability of rifampicin-resistant strains derived from the surrogates also enabled screening for antibiotic resistant strains. All three sequencing and assembly methods enabled successful identification of SNPs within the *rpoB* gene known to confer rifampicin resistance (Goldstein, 2014, Jin and Gross, 1988). As discussed, the genome assemblies generated from MinION data reflected the lowest quality assembly. While potentially useful for analysis of highly specific, known SNPS, these data would be difficult to utilize for discovery of new mutations (Table 1.8). Two isolates (BAA-1427 and BAA-1427 rif^R) appeared to share a silent mutation encoding amino acid A206, while the rif-mutant contained an additional L533 to P mutation, a change previously documented to confer rifampicin resistance (Jin and Gross, 1988). Two strains (BAA-1428 and BAA-1428 rif^R) shared a silent mutation (T486 to T) compared to *E. coli* K-12. BAA-1428 rif^R also possessed an additional S512 to P mutation, which has not been previously reported to confer rifampicin resistance but resides within the first cluster of the rifampicin resistant determining region (**RRDR**) (Goldstein, 2014). Lastly, the BAA-1430 genomes and BAA-1430 rif^R both shared silent mutations (P489 to P, L623 to L, and G846 to G), and the BAA-1430 rif^R possessed a H526 to Y mutation, also documented to confer drug resistance (Jin and Gross, 1988). Ultimately, each technique was useful for identification of key differences between the parent surrogate strains and the K-12 reference *rpoB* gene, but the long-read genomes lacked the precision to accurately distinguish consistent key differences that conferred rifampicin resistance due to a high concentration of nucleotide deletions and false amino acid shifts.

In closing, this study provided a direct comparison of two common sequencing platforms and discussion of genome assembly characteristics applied to surrogate bacterial

strains for which genome sequences were not available. From both research and regulatory standpoints, the application of WGS and subsequent bioinformatic analyses are indeed the tools of the future - unifying many traditionally used microbiological analyses into a singular workflow and enabling greater precision in surveillance of foodborne pathogens for quicker and more efficient regulatory response to foodborne outbreaks. Institutes such as the Center for Genomic Pathogen Surveillance have already adopted and standardized WGS-based pathogen detection. Similar research and application in both academe and industry will continue to accelerate. Both long- and short-read sequencing methods serve valuable, yet distinct roles for construction of complete microbial genomes. Long-read capacity facilitates better genome assembly and reveals structural properties of the genome that are not readily sequenced by other means. Short-read methods improve precision and resolution required for investigative studies and certain targeted analyses. As demonstrated in this study, when combined in hybrid fashion, the two sequencing approaches together are invaluable in enabling completed high-quality genomes to be constructed and accessible within databases for utilization in traceback and recalls in the instance of foodborne outbreaks in which a high degree of resolution is required for distinguishing between closely related bacterial strains. Libraries of high quality, complete genomes also serve a valuable research function, and provide a resource for further understanding of genomic sequences or alterations that can confer pathogenesis.

The application of true WGS (*i.e.* production of a complete genome comprised of a single contiguous sequence) as a means for daily routine screening within a food processing facility's food safety program is impractical and other forms of high-throughput sequencing may be more optimal. As demonstrated here, short-read platforms such as

MiSeq provide a time- and cost-efficient means of simple of known pathogenic elements or antibiotic resistance genes. For the purposes of a food processing facility, confirmation of elements that confer pathogenesis is required, and while the methods described within this paper offered a means to achieve this, a fully closed bacterial genome is not required for most routine screening. While the cost of sequencing has greatly diminished and the quality of generated output continues to increase, WGS remains a data intensive process, relies on evaluation of DNA extracted from a pure bacterial culture, and is largely inefficient for routine screening. Ultimately, while routine WGS of samples taken within the food processing facility would serve a valuable means for differentiating what is being transported into the facility from the native microflora that pre-existed within the facility, it is impractical as a means for routine screening for outgoing lots. Although WGS enables sequence discrimination of genetic elements associated pathogenic and non-pathogenic strains, the current findings demonstrate that this outcome can be achieved more optimally via high-throughput targeted sequencing. Regardless, high-throughput sequencing methods will become increasingly important in food safety applications. These analyses enable insight into the genetic make-up of the surrogate strains studied that is useful for a variety of research applications and can also help inform decision-making for the incorporation and application of WGS within industry food safety programs.

CHAPTER III MEAT QUALITY:

INTRODUCTION & LITERATURE REVIEW

Overview

Despite being the subject of extensive research and investigation, the phenomenon known as dark-cutting beef, also commonly referred to as DFD beef, remains a significant beef quality deficit, resulting in substantial price discounts at the packer. In order to alleviate this ongoing issue, numerous on- and off-farm management practices have been proposed and implemented over the years in order to improve handling practices and welfare of the animals to reduce occurrence of DFD carcasses. However, while reports in the 2016 U.S. National Beef Quality Audit (**NBQA**) indicate significant reductions in DFD incidences (1.9%) from the previous audit conducted in 2011 (3.2%), DFD beef still represents a significant financial burden within the beef-industry (Moore et al., 2012; Boykin et al., 2017). While it has been thoroughly documented within the literature that DFD is a multifactor phenomenon that occurs when an animal's muscle glycogen levels are significantly depleted following prolonged ante-mortem stress, many of the physiological mechanisms responsible for this undesirable phenotype remain elusive. While it has been repeatedly demonstrated that miRNAs serve as potent regulators in the cellular processes of myogenesis and adipogenesis, recently they have also been shown to serve similar roles in the regulation of stress reaction pathways (physiological and psychological) within fully developed tissues (Leung and Sharp, 2010; Mendell and Olson, 2012; Fatima and Morris, 2013; Wang and Taniguchi, 2013; Olejniczak et al., 2018; Oliveira et al., 2019). Due to their functional roles within these physiological processes, it

is hypothesized that a subset of miRNAs may also serve as regulators within the genetic signaling networks that contribute to the DFD phenotype.

To examine this problem, RNA-Seq was performed on total RNA that was extracted from dark-cutting and normal muscle biopsies taken from a contemporary group of F_2 and F_3 *Bos taurus* - *Bos indicus* steers for evaluation of miRNA expression. It is believed that data gathered here will not only provide beneficial insight into the etiology of DFD and the potential roles that miRNAs serve in its manifestation as well as stress responses in general but will also lead to a further reduction in both its prevalence and the economic losses it causes for the beef industry at a global level.

Meat grading & quality

The USDA beef grading standard is a nationally unvarying grading standard that promotes uniformity and an assurance of product quality that is desired by the consumers, retailers, institutions, and export markets on a continuous basis, regardless of the supplier (USDA-AMS, 2021). In addition to satisfying the consumer and retail portions of the market, the grading of beef carcasses also hold extreme importance to the producers as this grade reflects quality, and directly affects compensation (*i.e.* purchase prices) for the cattle that they produce (Tatum, 2007, 2020). This grading system was first proposed during the early 1900's and is currently maintained and applied by the USDA Agricultural Marketing Service (**USDA-AMS**) (Harris et al., 1996; USDA-AMS, 2021). Following harvest, the beef grading process begins after a post-harvest chilling process (24 - 48hrs), which may be preceded by an electrical stimulation phase depending on the processing facility, in order to enhance the favorable eating characteristics of color and tenderness of the beef (Savell, 2012).

Once chilled, the beef carcasses undergo the ribbing process. The ribbing of a beef carcass consists of the severing of the vertebral column of the carcass at the location that bisects the twelfth thoracic vertebra, which is then followed by an incision through the *longissimus dorsi* muscle (ribeye area) forming a cross section between the 12^{th} and 13^{th} rib. Following this incision, the *longissimus dorsi* of the 12^{th} rib is allowed to rest and be exposed to oxygen, which leads to the oxygenation of the muscle myoglobin which results in the blooming effect (*i.e.* changing in color; primary from a dark state to one that is bright/cherry red in color) of the muscle. Once the muscle has had ample time to bloom, the beef carcass of interest is then ready to be presented to the USDA-AMS meat graders for grade designation. The grading of beef is a highly regulated process that must be conducted by certified USDA-AMS meat graders. Grading is a voluntary, fee-for-service that is offered by the USDA-AMS to meatpacking companies; and the graders themselves are not employed or compensated by the producers or companies for whom they are performing these grading services (Harris et al., 1996, USDA-AMS, 2017a, b). These USDA-AMS graders implement the current USDA-AMS beef carcass grading system, which is comprised of two separate grading standards, the Yield Grade & Quality Grade (Hale et al., 1988; Hale et al., 2013; Tatum, 2007, 2020; USDA-AMS, 2017a). The goal of the first beef grading standard, yield grade, is to assess and estimate the cutability of the carcass, which is described as the amount of boneless, closely trimmed (1/2'' fat or less), retail cuts (**%BCTRC**) from the high-value parts (*i.e.* square-cut chuck, rib, short loin, round, and sirloin) that will be yielded from the carcass at the point of harvest (Hale, 1988; Hale, 2013; Tatum, 2007, 2020; USDA-AMS, 2017a).

The current USDA-AMS yield grade scores are quantified and ranked numerically (*i.e.* 1, 2, 3, 4, and 5) and are inversely proportional to the amount lean meat that the carcass will produce (Hale, 1988; Hale, 2013; Tatum, 2007, 2020; USDA-AMS, 2017a). Categorically speaking this means that when a beef carcass receives a yield grade score of "1" this indicates the carcass of interest will net the highest yield of lean red meat, and as the yield grade score increases the yield value begins to depreciate with those that are graded at a "5" representing the lowest yields of meat, respectively (Hale, 1988; Hale, 2013; Tatum, 2007, 2021; USDA-AMS, 2017a). Four primary carcass characteristics are evaluated by meat graders when assigning the yield grade of a beef carcass*:* (*i*) the amount of external fat/thickness of the fat surrounding the ribeye, (*ii*) the total hot carcass weight (*i.e.* hot or un-chilled carcass weight immediately post-slaughter), (*iii*) the percentage of fat within the kidney, pelvic, and heart **(%KPH**), and (*iv*) the total area of the ribeye muscle (Hale, 1988; Hale, 2013; Tatum, 2007, 2020; USDA-AMS, 2017a). Once these characteristics have been observed and estimations for each have been recorded this information can be applied to the following equation:

$$\begin{aligned} Yield\ Grade = {} & 2.5 + 2.5\ (adjusted\ fat\ thickness, inches) \\ & - 0.2\ (kidney, pelvic\ and\ heart\ fat\ \%) \\ & - 0.0038\ (hot\ carcass\ weight\ \%) \\ & + 0.74\ (ribeye\ area, square\ inches) \end{aligned}$$

in order to derive an estimate yield grade and cutability value for the carcass (Hale, 1988; Hale, 2013; Tatum, 2007, 2020; USDA-AMS, 2017a). While the yield grade is used to determine the amount of lean meat that is produced by the carcass, the second beef grading standard, quality grading, serves as an estimate of the overall eating satisfaction or

palatability (*i.e.* tenderness, juiciness, and flavor) (Hale, 1988; Hale, 2013; USDA-AMS, 2017a). Eight quality grades are assigned by the USDA during the grading process and are listed in descending quality value: Prime, Choice, Select, Standard, Commercial, Utility, Cutter, and Canner (Hale, 1988; Hale, 2013; USDA-AMS, 2017a).

The grading score of USDA-Prime represents the most desirable cuts that are typically sold in restaurants/hotels, USDA-Choice & Select often appears as "block beef" sold in retail markets/grocery stores, and the remaining are often sold at discounted prices and make up most of the manufactured beef products (*e.g.* ground beef, pre-cooked meats, canned meats, frankfurters, *etc*.) (Hale, 1988; Hale, 2013; USDA-AMS, 2017a). In order to calculate these quality grades, the USDA-AMS will evaluate the carcass and measure two primary factors: the physiological maturity of the animal & the degree of intramuscular marbling (Hale, 1988; Hale, 2013; Tatum, 2007, 2020; USDA-AMS, 2017a). The maturity of the animal is divided into five groups that are ranked from youngest to oldest (*i.e.* A: 9 to 30 months, B: 30 – 42 months, C: 42 – 72 months, D: 72 – 96 months, and E: > 96 months), and are determined via two primary physiological indicators, the degree of ossification that has occurred within the cartilage and the color/texture of the ribeye portion within the carcass (Hale, 1988; Hale, 2013; Tatum, 2007, 2020; USDA-AMS, 2017a). As an animal begins to age, significant changes occur within its skeletal system. Around the time in which an animal's physiological age reaches 42 – 72 months, its ribs begin to lose their redness and roundness, becoming paler in color and wide/flat in shape (Hale, 1988; Hale, 2013). Additionally, the cartilage surrounding the chine bone, also called the "button", which is located in the vertebral column (*i.e.* progresses from the sacral to the thoracic vertebrae) begins to harden and ossify around the time the animal

reaches ~30 months of age (Hale, 1988; Hale, 2013). Following this, the color and texture of the ribeye muscle are evaluated and categorized from youngest, which are cuts that are visually light cherry-red in coloration with a very fine textural quality, to older which are typically coarser/tough in texture and dark- to very dark red in their coloration (Hale, 1988; Hale, 2013).

These two values are then combined in the following equation:

$$Skeletal\ Maturity + Lean\ Maturity = Overall\ Maturity$$

to produce the overall estimated maturity of the carcass (Hale, 1988; Hale, 2013). Next, the second major, and primary criterion that is used to determine beef quality is marbling, which is described as the flecks of intramuscular fat that are dispersed within the ribeye muscle that resides between the 12^{th} - 13^{th} rib cross-section (Hale, 1988; Hale, 2013; USDA-AMS, 2017a). Marbling quantity is described according to nine degrees (*i.e.* Abundant, Moderately Abundant, Slightly Abundant, Moderate, Modest, Small, Slight, Traces, and Practically Devoid), and each of these degrees are further divided into 100 subunits and are discussed in terms of tenths of quantity (*e.g.* Abundant $^{00\text{-}100}$, Moderately Abundant $^{00\text{-}100}$, *etc.*) (Hale, 2013). Following the calculation of the carcass marbling score it can then be applied to the following equation:

$$Overall\ Maturity + Marbling\ Score = USDA\ Quality\ Grade$$

to derive the final USDA quality grade (Hale, 1988; Hale, 2013; USDA-AMS, 2017a). However, in certain instances the carcass may display some imperfection, defect, abnormality, or undesirable trait (*e.g.* bruises, bloodshot/clots, dark cutters, contain abscesses/cysts, *etc.*), commonly referred to as “no-rolls” in which the packers may forgo the grading of these outliers and sell them at discounted prices (Hale, 1988). Those outliers

classified as dark cutters are especially problematic, because while a carcass might meet all the characteristics to be labelled at USDA-Prime, -Choice, or -Select, it is often downgraded one full grade and sold at heavily discounted prices due to off-putting dark coloration (Hale, 1988; USDA-AMS, 2017a).

While it has been established that as an animal ages, the coloration of their meat begins to darken, dark cutters are not a product of age, but rather are byproducts of physiological stress that occurred to animals prior to slaughter that results in the failure of adequate muscle blooming (Hale, 1988; USDA-AMS, 2017a). While numerous meat quality attributes have been shown to influence consumers' decision-making process when purchasing beef product, the coloration of the cut is often considered an indication of freshness and quality (Mahmood et al., 2017; McKeith et al., 2016; Willis et al., 2017; English et al., 2016). This darker appearance remains highly aesthetically unattractive and suffers heavy discrimination/rejection from consumers and retailers alike, and results in substantial economic losses for the beef industry globally each year.

Dark, Firm, and Dry beef

Dark, firm, and dry beef, alternatively known as dark-cutting beef, is an undesirable phenotypic condition in which a beef carcass fails to adequately bloom due to its pH remaining abnormally elevated (*i.e.* ≥ 5.8). These beef carcasses will fail to achieve the desirable bright, cherry red pigmentation, and will instead possess an abnormally dark pigmentation (Miller, 2007; Ponnampalam et al., 2017). In addition to its failure to achieve the bright, cherry red pigmentation that is desired by customers, the manifestation of this condition also results in several other undesirable characteristics within the beef carcass. Despite being just as safe and nutritional for consumption as normal cuts of beef, these

unaesthetic qualities result in DFD beef to be frequently rejected on the retail level and suffers strict consumer bias. At the point of sale, consumers tend to reference color as an indication of quality and freshness, with a strict bias favoring cuts of beef that are bright, cherry red in appearance, and reject those that are darker in appearance as they are perceived as being lower in quality (English et al., 2016; McKeith et al., 2016; Mahmood et al., 2017; Willis et al., 2017). Due to this increased rejection at the retail level, DFD carcasses are subjected to harsh meat grading standards by the USDA-AMS, leading them to be sold at a discounted prices to the foodservice industry where the meat is utilized in producing pre-cooked food products (Moiseev and Cornforth, 1999; Savell, 2013; USDA-AMS, 2017a, b).

Currently, it was estimated in the 2016 NBQA report that within the United States, the overall presence of dark cutting beef had fallen to 1.9%, the lowest percentage surveyed in NBQA history (Moore et al., 2012; Boykin et al., 2017). However, despite the manifestation of the DFD phenotype being relatively infrequent within the United States, incidence of DFD beef continues to fluctuate seasonally, and remains a significant contributor to the depreciation of meat quality world-wide (Ponnampalam et al., 2017). It was estimated that in 2020 when U.S. cattle numbers reached ~32.8 million, the cost of DFD carcasses when discounted at $281/head was responsible for ~$95 - 100M in lost revenue for the U.S. beef industry alone (USDA, 2021). As a result of these persistent economic losses, DFD beef and its contributing factors have been the subject of numerous investigative studies. However, to date the DFD phenotype remains a highly complex phenomenon, and there currently still exists no method(s) that allow for its consistent prediction, prevention, nor replication within a given population. While the attributes and

associated causal factors of DFD beef have been thoroughly described since the 1940s, little advancement has been made in our understanding regarding the underlying physiological mechanisms that contribute to its manifestation.

Biochemistry and physiology of DFD beef

The DFD phenotype has been shown to sporadically manifest in beef carcasses (> 30 months of age) that have been subjected to elevated degrees of prolonged stress prior to slaughter (Lawrie, 1958; Cross et al., 1983; Mahmood et al., 2017). These prolonged levels of ante-mortem stress result in the depletion of the intramuscular glycogen reserves within the meat from these carcasses, resulting in ultimate pH values of the carcasses to remain abnormally high (*i.e.* ≥ 5.8) which significantly inhibit their ability to effectively bloom (Hedrick et al., 1959). Blooming refers to a 30-to-60-minute process in which the surface of a cut of meat will be exposed to oxygen leading it to undergo a change in color (*i.e.* dark purple/brown to bright cherry red) (Jacob, 2020). This change in color is heavily driven by the rate in which the surface level myoglobin or deoxymyoglobin is oxygenated (Ponnampalam et al., 2017). Fresh cuts of meat will initially appear to possess a dark purple pigmentation due to high concentrations of deoxymyoglobin, but as oxygen penetrates the surface of the carcass the deoxymyoglobin molecules will become oxygenated forming oxymyoglobin, giving the carcass a bright red pigmentation (Jacob, 2020). This inability of DFD beef carcasses to bloom results in an abnormal deviation in their coloration that is significantly darker than the bright, cherry red color that is desired by consumers. As a result, dark-cutting carcasses are less desirable and valued at a discounted price.

In a normal/healthy beef carcass not exposed to prolonged ante-mortem stress, a large reservoir of intramuscular glycogen remains immediately post-mortem, and is key for the biochemical process of blooming to occur (Abril et al., 2001; Jacob, 2020). At the point of death, the muscle tissue continues to function normally, utilizing its glycogen reserves to generate adenosine triphosphate (**ATP**) as a source of energy via the metabolic pathway of glycolysis (Savell & Gehring, 2018). As a result, lactic acid is produced, and in the absence of a functioning circulatory system, lactic acid accumulates within the muscle. After ~24-hours post-harvest, the pH of the carcass will decline from a neutral state (*i.e.* pH 7.0: neutral value found in living animals) to a pH that ranges from ~5.3 - 5.7 (*i.e.* that of desirable cuts of beef) (Tarrant, 1989; Miller, 2007; Savell & Gehring, 2018). This reduction in pH results in the breakdown/shrinkage of structural fibers located within the muscle, and significantly lower the respiratory activity of the muscle tissue and its mitochondria (Lawrie, 1958; Seideman, et al., 1984; McKeith et al., 2016; Ponnampalam et al., 2017; Jacob, 2020). This process not only allows for oxygen to easily penetrate the surface of the beef carcass, but also promotes the formation of a thick oxymyoblogin layer, thus allowing the cut of meat to bloom to a more desirable bright red pigmentation (Ponnampalam et al., 2017). On the contrary, when an animal is exposed to chronic levels of pre-harvest stress, its muscle glycogen content becomes depleted, leading to an increased occurrence in the DFD phenotype.

Without sufficient concentrations of muscle glycogen to serve as a substrate in the post-mortem glycolysis pathway, less lactic acid is produced within the muscle. These low volumes of intramuscular lactic acid prevent the beef carcass from reaching a normal level of acidification (*i.e.* pH 5.5 - 5.7) resulting in elevated carcass pH with values greater than

or equal to pH 5.8 (Miller, 2007; Ponnampalam et al., 2017). When the pH of meat remains too high, the isoelectric points of muscle proteins are altered, resulting in an increased capacity to associate with and hold water (Miller, 2007; Ponnampalam et al., 2017; Savell & Gehring, 2018). As these proteins begin to associate with water, the muscle fibers in the DFD carcass begin to swell in size and become tightly compressed (Seideman, et al., 1984; Abril et al., 2001). Tightly packed myofibrils form a barrier that obstructs oxygen from deeply diffusing along the surface of the meat (Lawrie, 1958; Seideman, et al., 1984; Abril et al., 2001). This process results in decreased quantities of deoxymyoglobin that can be oxygenated, and results in only a very thin superficial layer of oxymyoglobin (Lawrie, 1958; Seideman, et al., 1984; Abril et al., 2001; Ponnampalam et al., 2017; Jacob, 2020).

Furthermore, it has been reported that in DFD beef, tightly packed myofibrils also result in decreased ability to scatter light across the meat's surface, giving it a darker, more translucent appearance (Seideman, et al., 1984; Abril et al., 2001; Ponnampalam et al., 2017; Jacob, 2020). Additionally, when pH remains high in meat tissue the muscle's respiratory activity is accelerated, enhancing its mitochondrial activity and oxygen consumption rate (*i.e.* rate at which mitochondria utilize substrates to produce ATP via the Krebs cycle.) (Lawrie, 1958; Ledward, 1985; Seideman et al., 1984; English et al., 2016; McKeith et al., 2016; Jacob, 2020). Increased mitochondrial respiration rate accelerates the deoxygenation of the oxymyoglobin molecules, making the purple deoxymyoglobin the dominant form of myoglobin in the meat (Ashmore et al., 1972; English et al., 2016; McKeith et al., 2016; Ponnampalam et al., 2017; Jacob, 2020). An overabundance of deoxymyoglobin prevents the meat tissue from successfully blooming and result in an

abnormally dark pigmentation that can range from a dark purplish/maroon to an almost completely black color, depending on severity of dark-cutting (Miller, 2007; Ponnampalam et al., 2017).

Carcass quality and characteristics

Aside from the undesirable color of these DFD beef carcasses, this condition also consequentially leads to other prominent and unfavorable characteristics. It has been reported that cuts from more severe DFD beef phenotypes (*i.e.* pH > 6.0) are more difficult to handle and prepare. This meat often retains a persistent red/pink color that makes it appear to be undercooked despite reaching an adequate internal temperature (Mendenhall, 1989; Trout, 1989; Cornforth et al., 1991; Moiseev and Cornforth, 1999). This characteristic is attributed to the abnormally high pH value of the meat, which acts as a buffer that prevents the denaturation of the muscular myoglobin (Mendenhall, 1989; Trout, 1989; Cornforth et al., 1991; Moiseev and Cornforth, 1999). Furthermore, beef characterized as DFD is often associated with increased incidence of diminished quality and poor sensory properties. Dark-cutting beef has been reported to possess a greater variability in its tenderness, dependent on its severity and the method in which the cooked meat was prepared, as well as an unsavory texture that has been described as firm, sticky, and dry (Bouton et al., 1973; Wulf et al., 2002; Calkins and Hodgen, 2007; Miller, 2007; English, 2016; Ponnampalam et al., 2017).

Additionally, DFD beef cuts on average were found to be less palatable than their normal counterparts and tended to exhibit a variety of undesirable off-putting flavors (*i.e.* bland, musty, slightly soapy, sour, and metallic) (Yancey et al., 2005; Calkins & Hodgen, 2007; Miller, 2007; Grayson et al., 2016; Ponnampalam et al., 2017). However, when

considering the juiciness of DFD steaks, many studies tended to indicate that no significant differences found in consumer's preference between normal vs DFD cuts of meat (Dransfield, 1981; MacDougall et al., 1979; Wulf et al., 2002). Lastly, in addition to its unaesthetic appearance and unsavory organoleptic properties, DFD beef has decreased shelf life and is more prone to microbial spoilage (Gill and Newton, 1977, 1979, 1981-1982; Vanderzant, 1983; Ferguson et al., 2001; Miller, 2007; Ponnampalam et al., 2017). This increased rate of degradation has been largely attributed to DFD beef's increased ability to hold water and its high pH, which creates a more favorable environment for the proliferation of meat spoilage bacteria (Gill and Newton, 1977, 1979, 1981-1982; Vanderzant, 1983; Ferguson et al., 2001; Miller, 2007; Ponnampalam et al., 2017). Under normal circumstances, many of these spoilage microorganisms will preferentially utilize the glucose reserves of the muscle as their primary energy source before seeking other sources of nutrition (Gill and Newton, 1977, 1979, 1981-1982; Vanderzant, 1983; Ferguson et al., 2001; Miller, 2007; Ponnampalam et al., 2017). Unfortunately, since most of those reserves had been previously exhausted, hydrogen-sulfide producing microorganisms begin utilizing the meat's amino acids immediately, leading to the rapid generation of spoilage odors and green discoloration in vacuum sealed meat (Gill and Newton, 1977, 1979, 1981-1982; Vanderzant, 1983; Ferguson et al., 2001; Miller, 2007; Ponnampalam et al., 2017).

Causes and associated contributing factors

It has been established that the occurrence of dark cutting in beef cattle has been shown to follow a seasonal trend, occurring more frequently in the fall months (*i.e.* in North America: highest in September and October), and is heavily influenced by drastic

fluctuations in the weather (Grandin, 1992; Smith et al., 1993; Scanga et al., 1998; Miller, 2007; Boykin et al., 2017; Savell and Gehring, 2018; Loredo-Osti et al., 2019). While incidence of DFD beef can be caused by extreme heat, it typically occurs at greatest levels when animals are exposed to extremely cold weather 24 to 48-hrs prior to slaughter (Grandin, 1992; Smith et al., 1993; Scanga et al., 1998; Miller, 2007; Boykin et al., 2017; Savell and Gehring, 2018; Loredo-Osti et al., 2019). The risk of dark cutting is further increased when prolonged exposure to freezing weather is combined with strong winds and precipitation (Grandin, 1992; Smith et al., 1993). When exposed to extremely cold weather, the animal's body temperature can be drastically decreased, causing the animal to shiver uncontrollably and consume muscle glycogen (Scanga et al., 1998). Furthermore, it is believed that several intrinsic characteristics (*e.g.* sex, temperament, age, weight, and breed) of the animal may influence its predisposition to become stressed, and thus increase the likelihood for the animal to express the DFD phenotype. There exists contrasting evidence within the literature regarding the correlation between sex and its impact on dark cutting.

Some studies have previously demonstrated that sex did not have a significant impact on the expression of the dark cutting phenotype (Araujo et al., 2016; Page et al., 2001). However, heifers have been shown to possess an inherently higher risk of dark cutting due to their more excitable temperament, as well as the tendency for them to be aggressively mounting when mixed with unfamiliar animals (Kenny and Tarrant, 1987; Scanga et al., 1998; Voisinet et al., 1997a, b). It has also been reported that there is an increased prevalence of dark cutting in intact bulls due to their aggressive behavior and tendency to fight when mixed with unfamiliar animals prior to slaughter (Warriss et al.,

1984; Miller, 2007). Older animals may also be more prone to display dark meat due to increased levels myoglobin since possess naturally lower levels of muscle glycogen and their overall pH increases as they age (Ponnampalam et al., 2017). McGilchrist et al. (2012) observed reduced incidence of dark cutting in carcasses that possessed larger ribeye areas, heavier weights, and higher concentrations of rib fat. Mixed findings regarding the association between breed and dark cutting have been reported, but it has been suspected that tropically adapted breeds with nervous temperaments such as *Bos indicus* are more prone to exhibit dark cutting (Shackelford et al., 1994; Voisinet et al., 1997a).

Proper handling and management of animals by experienced handlers and personnel has been shown to drastically decrease incidents of DFD beef (Hedrick et al., 1959; Shackelford et al., 1994; Grandin, 2020). It has been extensively reported that the mixing of unfamiliar animals at a processing plant prior to harvest will significantly increase the prevalence of DFD carcasses. When unfamiliar animals are mixed, they begin to establish a new hierarchy of dominance that results in an increase of fighting, aggression, and mounting behaviors (Miller, 2007; Ponnampalam et al., 2017; Grandin, 2020). Numerous studies have comprehensively established that pre-harvest transportation, especially over long distances with inexperienced drivers, is one of the largest sources of pre-harvest stress for beef cattle (Swanson and Morrow-Tesch, 2001; Ponnampalam et al., 2017). Extended transportation times have been associated with higher levels of stress and agitation making the cattle difficult to unload which leads to higher incidents of dark cutting (Mounier et al., 2006; Miller 2007; Warren et al., 2010). Immonen et al. (2000) demonstrated that by feeding beef cattle a high energy diet a couple of weeks prior to transport can assist in reducing dark cutting.

Warren et al. (2010) also reported that cattle shipped and sourced from saleyards tended to possess darker beef than those obtained directly cosigned from farms to abattoirs. Loredo-Osti et al. (2019) observed that lairage time and improper desensitization were directly correlated with manifestation of DFD beef. The use of electrical prods has been associated with higher degrees of lactate, cortisol, and overall stress in beef cattle (Hemsworth et al., 2011; Grandin, 2020). Lastly, the utilization of certain implant strategies and the use of beta-adrenergic agents (**β-AA**) is suspected to increase the prevalence of DFD beef carcasses. Others have observed that steers implanted and re-implanted with implants containing a combination of androgens and estrogens resulted in a higher percentage (> 6%) of dark cutting overall (Scanga et al., 1998). Additionally, similar findings were observed in heifers that were initially treated with only estrogen implants, with incidence further worsened when the animals were re-implanted with estrogen (Scanga et al., 1998).

Furthermore, this effect could be alleviated across all sexes and implantation type if > 100 days had passed between the final implant and harvest, except for steers that had been re-implanted with androgens and heifers that had been re-implanted with estrogens (Scanga et al., 1998). Tarrant (1989) reported that the use aggressive β-AA's, such as clenbuterol and cimaterol can lead to the breakdown of muscle glycogen, and when combined with even a moderate amount of stress can potentially lead to DFD carcasses (Tarrant, 1989). However, ractopamine is the only growth promotant β-AA currently used in livestock in the United States, and when used according to manufacturer's guidelines is not shown to significantly increase the likelihood of dark cutting (Baszczak et al., 2006; Dikeman, 2007; Lean et al., 2014; Ponnampalam et al., 2017).

Experimental interventions and manifestations of the DFD phenotype

In addition to investigating its attributes and sources, a variety of approaches have been used to manifest, as well as improve the undesirable qualities of dark cutting once it has already manifested. Howard and Lawrie (1956) were able to induce DFD occurrence within select beef carcasses via ante-mortem injection of large concentrations of insulin. Hedrick et al. (1959) attempted to administer injections of hydrocortisone, insulin, Thorazine, Diquel, and Reserpine. These researchers found that Thorazin, Diquel, and Reserpine had limited success in preventing dark-cutting; however, the insulin and hydrocortisone had no significant impact on manifestation of the defect (Hedrick et al., 1959). Ashmore et al. (1973) managed to simulate dark cutting in select sheep via injections of epinephrine, which could be reversed in some cases with the application of the epinephrine inhibitor propranolol. Cornforth and Egbert (1985) revealed that when dark pre-rigor muscle was treated with rotenone (a mitochondrial respiratory inhibitor) or oversaturated with oxygen, the muscles would lighten in color.

Multiple investigations have shown that treatment of dark cutting steaks with lactic acid could enhance their color as well as reduce the persistent pink appearance they exhibit when cooked (Sawyer et al., 2009; Apple et al., 2011; Ponnampalam et al., 2017). English et al. (2016) found that when DFD strip loins at pH 6.4 were aged for extended periods of time (0-, 21-, 42-, and 62-days) their blooming effect was improved (English et al., 2016). Wills et al. (2017) also revealed that when DFD beef was enhanced with 0.1% and 0.2% rosemary and packaged in high-oxygen or carbon-monoxide modified atmospheric packaging their coloration could be improved (Wills et al., 2017). However, while some of these approaches have been successful, success often remains inconsistent, costly, and can

result in other negative qualities as a result (*e.g.* bland flavor, significant increase in bitter and soapy flavors, *etc*.), making overall prevention of its manifestation the most feasible option (Yancey et al., 2005; Ponnampalam et al., 2017).

microRNA

MicroRNAs are a major class of small (*i.e.* ~17-27 nucleotides), single-stranded, non-coding RNA molecules that function as fine-tuned regulators of gene expression at a post-transcriptional level. The first miRNA, *lin-4*, was discovered in 1993, within the nematode species *Caenorhabditis elegans* via the combined efforts of the Ambros and Ruvkun laboratories (Lee et al., 1993; Wightman et al., 1993; Almeida et al., 2011). It was found that *lin-4* did not encode for a protein, but rather a small RNA transcript that regulated the developmental timing of *C. elegans* larvae via repressing the translation of the lin-14 protein (Horvitz and Sulston, 1980; Chalfie et al., 1981; Lee et al., 1993; Wightman et al., 1993; Saliminejad et al., 2018). Seven years following this discovery, a second small regulatory RNA, *let-7*, was also identified and reported play a similar role as lin-4 in controlling the regulation of development during the later larval stages in *C. elegans* (Reinhart et al., 2000). However, it was soon realized that *let-7* was not confined merely to *C. elegans* and was soon identified to be highly conserved among many different organisms, including *Homo sapiens* (Pasquinelli et al., 2000; Lee and Ambros, 2001; Lagos-Quintana et al., 2002; Lim et al., 2003; Roush and Slack; 2008). Soon after their discovery this new class of regulatory RNAs were coined “microRNAs” and added layers of complexity to our perception of the mechanisms involved in gene expression (Lau et al., 2001; Lee and Ambros, 2001; Lagos-Quintana et al., 2002; Jeffries et al., 2009).

Since their discovery, miRNAs have become recognized as one of the most abundant gene families and have been found to be highly conserved among a wide range of organism (*e.g.* animals, plants, protists, and viruses) (Li et al., 2010; Friedlander et al., 2014; Ha and Kim, 2014; O'Brien et al., 2018). According to the miRNA repository (miRBase (v22.1)) it has been reported that miRNA sequences from 271 organisms: 38,589 hairpin precursors, and 48,860 mature miRNA sequences have been catalogued (Kozomara et al., 2019). Of these it has been reported that currently 1,917 annotated hairpin precursors and 2,654 mature miRNA sequences have been identified within the human genome alone, and that >60% of human protein-coding genes possess a predicted miRNA-binding sites (Friedman et al., 2009; Kozomara et al., 2019). The genes that encode for miRNAs have been found to be widely distributed throughout the genome, and many of these genes have been found to be noncoding with the miRNA being their sole transcript (Hammond, 2015). It has been found that miRNAs can be transcribed monocistronically or they can appear in clusters and be expressed in a polycistronic fashion (Rodriguez et al., 2004; Zeng, 2006; Ha and Kim, 2014; Hammond, 2015). These miRNAs genes have been found to reside within noncoding intergenic regions, within the introns of coding transcripts, and in rarer instances been found to exist within exonic regions (Roush and Slack, 2008; Ha and Kim, 2014; Hammond, 2015; Kalla et al., 2015; O'Brien et al., 2018; Saliminejad et al., 2018).

While the exact locations of these intergenic miRNA promoters have not all been mapped, it is believed that they either possess their own unique promoters and undergo transcription individually or share a common promoter with a neighboring gene (Zeng, 2006; Ha and Kim, 2014; Saliminejad et al., 2018). Alternatively, those miRNA genes that

are encoded within an exon or the intron of coding transcript will often utilize the promoters of their respective host genes (Zeng, 2006; Ha and Kim, 2014; Saliminejad et al., 2018). The biogenesis of miRNAs is a multistep process that begins within the cell's nucleus and can be occur via two distinct pathways: canonical and non-canonical (Ha and Kim, 2014; Hammond, 2015; O'Brien et al., 2018; Olenjniczak et al., 2018; Saliminejad et al., 2018; Gerbert and MacRae, 2019). In the canonical model of biogenesis miRNA genes are typically transcribed by RNA polymerase II (**Pol II**) and regulated by its associated transcription factors. However, there are exceptions regarding some viral miRNA in which RNA polymerase III is used instead (Lee et al., 2004; Ha and Kim, 2014; Hollins and Cairns, 2016). These transcribed miRNAs will initially begin as large (*i.e.* >1 kilobase), single-stranded primary miRNAs (**pri-miRNA**s), and can house either a single miRNA or multiple and potentially related miRNAs (Lee et al., 2002; Zeng, 2006; Ha and Kim, 2014). These pri-miRNA transcripts will possess a typical 5' 7-methyl guanosine cap and a 3' poly(A) tail, as well as at least one stem-loop (hairpin) structure that ranges from ~33 - 35 nucleotides in length (Cai et al., 2004; Zeng, 2006; Ha and Kim, 2014).

Once a pri-miRNA has been transcribed its hairpin structure will be recognized by and bound to two Di George Syndrome Critical Region Gene 8 (**DGCR8**) double-stranded RNA binding proteins (Zeng, 2006; Ha and Kim, 2014; O'Brien et al., 2018; Gerbert and MacRae, 2019). Following this a ribonuclease III (**RNase III**) enzyme named Drosha will associate with the two DGCR8 molecules forming a heterotrimeric microprocessor complex (Zeng, 2006; Ha and Kim, 2014; O'Brien et al., 2018; Gerbert and MacRae, 2019). The catalytic drosha subunit will then interact with the double-strand RNA-single-strand RNA duplex at the base of pri-miRNA's stem-loop structure, and then cleaves it

~11 bps from its basal junction and ~22 bps from its apical junction (Han et al., 2006; Zeng et al., 2005; Zeng, 2006; Ha and Kim, 2014; O'Brien et al., 2018; Gerbert and MacRae, 2019). The cleavage of the pri-miRNA stems will result in the release of a smaller (*i.e.* ~65-100 bps) hairpin shaped precursor miRNA (**pre-miRNA**) that will possess a 5' phosphate group, a 3'-hydroxyl group, and a two nucleotide overhang at its 3' end (Han et al., 2006; Zeng et al., 2005; Hollins and Cairns, 2016). Following this the pre-miRNA will be escorted through a nuclear pore into the cellular cytoplasm by the transporter molecule, exportin 5 (**XPO5**) (Lund et al., 2004; Ha and Kim, 2014). The XPO5 molecule recognizes and strongly interacts with 3' overhang of the pre-miRNA, and it uses its ras-related nuclear protein (**RAN**)-guanosine triphosphate (**GTP**) cofactor as the driving force (Lund et al., 2004; Okada et al., 2009; Gerbert and MacRae, 2019).

Upon reaching the cytoplasm the GTP of the RAN cofactor will be completely hydrolyzed and the transport complex will begin to disassociate freeing the pre-miRNA molecule within the cytosol (Ha and Kim, 2014). The pre-miRNA's 5'phosphate, 3' overhang, hairpin structure will be recognized by a second RNase III enzyme, Dicer, and it will bind to the pre-miRNA by utilizing its double-stranded RNA binding cofactor, which for vertebrates is the TAR RNA binding protein (**TRBP**) (MacRae et al., 2007; Park et al., 2011; Tsutsumi et al., 2011; Ha and Kim, 2014; Olenjniczak et al., 2018; Gerbert and MacRae, 2019). Once the pre-miRNA has been bound to dicer it will undergo further processing and be cleaved near its terminal loop creating an intermediate double-stranded mature miRNA that is ~22 bps in length with a 2 nucleotide 3' overhang (Zhang et al., 2004; Zeng, 2006; Nicholson, 2014). Following this an argonaute (**AGO**) protein will interact with the dicer enzyme in order to bind with the mature miRNA duplex and unwind

it (Zeng, 2006; Kawamata and Tomari, 2010; Olenjniczak et al., 2018; Saliminejad et al., 2018). Once unwound the passenger strand will be discarded and degraded while the antisense/guide strand will be preserved (Kawamata and Tomari, 2010; Saliminejad et al., 2018; Gerbert and MacRae, 2019). It has been reported that in this strand selection process the strand with the less stable hydrogen bonding at its 5' end is favored, and that AGO has been revealed to show a strong preference for the strand that contains an adenine or uracil as a 5'-terminal nucleotide (Khvorova et al., 2003; Schwartz et al., 2003; Zeng, 2006).

The selected guide strand will then become integrated with the AGO protein and its associated cofactors to form the RNA-Induced Silencing Complex (**RISC**), thus completing the canonical pathway of biogenesis (Kawamata and Tomari, 2010; Saliminejad et al., 2018; Gerbert and MacRae, 2019). This miRNA induced RISC complex, often referred to as miRISC, is now capable of recognizing and repressing its target messenger RNA (**mRNA**), thus completing the canonical pathway (Pasquinelli, 2012). It is worth briefly mentioning that while the canonical pathway is the dominant form of miRNA biogenesis, various alternative non-canonical pathways have been identified as well (Ha and Kim, 2014; Hammond, 2015; O'Brien et al., 2018; Olenjniczak et al., 2018; Saliminejad et al., 2018; Gerbert and MacRae, 2019). These alternative pathways can typically be categorized as either DGCR8/drosha-independent or dicer-independent and are similar to the canonical pathway, but typically take place within a host cell that lacks certain key canonical processing factors (Ha and Kim, 2014; Hammond, 2015; O'Brien et al., 2018; Saliminejad et al., 2018). However, it has been reported that a vast majority of these non-canonical miRNAs are poorly conserved in vertebrates and only exist in minute concentrations (Ha and Kim, 2014). Once biogenesis has occurred the

mature miRNA will guide the RISC to the target mRNA, where it will negatively modulate the expression of the mRNA transcript (Hammond, 2015).

While the interactions of miRNAs on their target mRNAs have been found to be highly dynamic and dependent on a variety of variables, typically the mature miRNA will utilize a 6-8 nucleotide motif that is located at its 5' end, the "seed region", to and guide the RISC to the correct target mRNA (Sjögren et al., 2018). The seed region will recognize and enable base pairing with a complementary seed match sequence that is typically located within the 3'-untranslated region (**UTR**) of the target mRNA, known as miRNA recognition elements (**MRE**s) (Inui et al., 2010; Pasquinelli, 2012; Hollins and Cairns, 2016; O'Brien et al., 2018). The degree of complementarity that is shared between the miRNA's seed region and the MRE of the mRNA will determine the mechanism of repression that will be utilized (Pasquinelli, 2012; O'Brien et al., 2018). If the miRNA seed region is perfectly paired with its target this will result in the target mRNA to be cleaved via AGO endonuclease activity which will then be further degraded within the cytoplasm of the host cell (Pasquinelli, 2012; Hollins and Cairns, 2016; O'Brien et al., 2018). However, this is more commonly observed in species of plants, and rarely occurs in animal species which are more prone to have miRNA:mRNA interactions that only possess partial pairing (Pasquinelli, 2012; Hollins and Cairns, 2016; O'Brien et al., 2018). In the instance of partial base pairing between the miRNA and its target, the RISC will repress the expression of the target mRNA via degradation and/or the translational inhibition of its transcripts (Pasquinelli, 2012; Hollins and Cairns, 2016; O'Brien et al., 2018).

When partial pairing occurs in humans the AGO protein of the RISC will recruit a member of the glycine-tryptophan protein family, GW182, which will in turn interact with

the polyadenylate-binding protein (**PABPC**) (Behm-Ansmant et al., 2006; Braun et al., 2011; Gerbert and MacRae, 2019). The PABPC protein will provide the necessary scaffolding that will be required to further recruit other deadenylation factors such as, the poly(A)-nuclease deadenylation complex subunits 2 and 3 (**PAN2**/**PAN3**) as well as the carbon catabolite repressor 4-negative on TATA (**CCR4-NOT**) complex (Christie et al., 2013; Jonas and Izaurralde, 2015; Saliminejad et al., 2018; Gerbert and MacRae, 2019). The recruitment of CCR4-NOT by GW182 will lead to the recruitment of DEAD-BOX helicase 6 (**DDX6**) which will help repress translation during this process (Mathys et al., 2014; Bartel, 2018; Saliminejad et al., 2018). These deadenylases will begin to shorten and ultimately remove the poly(A) tail of the target mRNA causing it to become destabilized (Wu and Belasco, 2006; Inui et al., 2010; Pasquinelli, 2012; Jonas and Izaurralde, 2015). The removal of the mRNA's poly(A) tail will promote the recruitment of the mRNA de-capping protein (**DCP**), which will also lead to the removal its 5' 7-methyl guanosine cap (Behm-Ansmant et al., 2006; O'Brien et al., 2018; Gerbert and MacRae, 2019). This will result in the target mRNA to become rapidly degraded via 5'-3' exonucleolytic degradation which is carried out by the exoribonuclease 1 (**XRN1**) enzyme (Braun et al., 2012; Jonas and Izaurralde, 2015; Gerbert and MacRae, 2019).

Furthermore, while degradation is the most common form of miRNA gene silencing, instances have been reported in which miRNAs have successfully reduced the concentration of protein produced by their targets without affecting the overall levels of the target mRNA itself (Pasquinelli, 2012; Eichhorn et al., 2014). This persistence of the target mRNA infers that it is not being degraded in the traditional sense and insinuates that these mature miRNAs many also possess the ability to repress translation as well (Pasquinelli,

2012). It has been established that the previously described CCR4-NOT complex repressing agent that can block the initiation of translation (Braun et al., 2011; Chekulaeva et al., 2011; Pasquinelli, 2012; Mathys et al., 2014; Gerbert and MacRae, 2019). There also exists increasing evidence that these mature miRNAs may induce mechanisms that not only hinder the initiation of translation and/or elongation, but also possess the ability to direct proteolytic activity on the transcript as it is synthesized by their target mRNA (Humphreys, et al., 2005; Pillai et al., 2005; Nottrott et al., 2006; Inui et al., 2010; Pasquinelli, 2012; Gerbert and MacRae, 2019). Additionally, it has also been observed that miRNAs and their targets can localize within multiple sub-cytoplasmic compartments, which may also assist in the degradation of the target mRNA of the proteolysis of its peptides (Lui et al., 2005; Parker and Sheth, 2007; Pasquinelli, 2012; O'Brien et al., 2018). An example of this can be seen in processing bodies (**P bodies**), which are cytoplasmic foci that are devoid or ribosomes and other various transcriptional factors and enriched with numerous proteins/enzymes that promote the degradation of mRNA (Lui et al., 2005; Parker and Sheth, 2007; Pasquinelli, 2012; O'Brien et al., 2018).

It has been reported miRNA:mRNA complexes can be stored in these P bodies located within the host cell's cytoplasm where they may be degraded, have their translational processes inhibited or be reversibly stored for a period of time (Inui et al., 2010; Leung, 2015). However, while it is widely believed that both modes of gene silencing that are utilized by the miRNAs are interconnected, the precise mechanisms that are utilized by miRNAs to inhibit translation have not been fully elucidated (Pasquinelli, 2012; Jonas and Izaurralde, 2015; Gerbert and MacRae, 2019). Controversially, despite typically being associated with their repressive capabilities it has been recently observed

that miRNAs may also promote the activation of genes as well (Inui et al., 2010; O'Brien et al., 2018). For example, it was not long ago reported that miR-369-3 could serve as a translation activator under conditions in which human cells have been starved of serum (Vasudevan et al., 2007a,b; Almeida et al., 2011). Upon cell cycle arrest, miR-369-3 would associate with the adenylate-uridylate-rich elements (**ARE**s) located in the tumor necrosis factor-α (**TNF-α**) mRNA, where it would mediate the activation of translation via recruiting AGO and fragile X mental retardation-related protein 1 (**FXR1**) (Vasudevan et al., 2007a,b; Almeida et al., 2011). Furthermore, they were able to demonstrate that let-7 as well as a synthetic miRNA, miRcxcr-4, were also able to induce the upregulation of their target mRNAs during cell cycle arrest but would revert to their repressive roles during resumed cellular proliferation (Vasudevan et al., 2007a, b; Almeida et al., 2011).

Additionally, it has been found that miRNAs possess the ability to promote gene expression via targeting and interacting with a target's promotor region (Place et al., 2008; Almeida et al., 2011). Place et al. (2008) were the first to observe this and revealed that both E-cadherin and cold-shock domain-containing protein 2 gene (***CSDC2***) possessed target sites within their promoters for miR-373, and readily induced expression in response to its presence (Place et al., 2008; Almeida et al., 2011). However, while multiple studies have demonstrated miRNA's ability to actively switch between the inhibition and activation of their targets, the mechanisms that are involved within this process remain unclear and more research is required to fully elucidate how these actions are achieved. To further add complexity, it has been found that miRNAs and their genes possess a number of unique attributes that may further contribute to the mechanisms that are involved in how they regulate gene expression (Bartel, 2018; Saliminejad et al., 2018; Gerbert and MacRae,

2019). It has been observed that an individual miRNA locus has the ability to yield a multitude of miRNA isoforms (**isomiRs**), which may vary from their canonical counterparts in sequence, size, or a combination of both (Bartel, 2018; Fard et al., 2020; Tomasello et al., 2021). There are multiple classes of isomiRs that have been reported and it is believed that they arise under conditions in which an alternative biogenesis pathway is utilized and/or from various forms of RNA modifications (*e.g.* deaminases, exonucleases, *etc.*) (Bartel, 2018; Fard et al., 2020; Tomasello et al., 2021).

While their precise function is currently unclear, some evidence suggests that they may function in a supportive role with their canonical counterparts, more specifically in targeting genes that are involved within cancer related pathways (Cloonan et al., 2011; Bartel, 2018; Fard et al., 2020; Tomasello et al., 2021). Furthermore, it has been reported that not all miRNAs are ubiquitously expressed, as seen with let-7, and their expression patterns can be altered at different stages of development and/or with the onset of various pathological conditions (Lee and Ambros. 2001; Langos-Quintana et al., 2003; Landgraf et al., 2007; Baek et al., 2008; Kirby and McCarthy, 2013; Lin and Gregory, 2015; Gerbert and MacRae, 2019). A majority of miRNAs have been observed to exhibit tissue-specific expression patterns, however, despite being previously classified as residual debris from cell injury it has been observed that miRNA can also appear extracellularly (Lee and Ambros. 2001; Langos-Quintana et al., 2003; Landgraf et al., 2007; Kirby and McCarthy, 2013; O'Brien et al., 2018; Gerbert and MacRae, 2019). These circulating miRNAs have been detected in a variety of biological fluids (*e.g.* serum, plasma, saliva, urine, cerebrospinal fluid, *etc.*), and they are typically shuttled in vesicles (*e.g.* apoptotic bodies, exosomes, and various microvesicles) or attached to AGO proteins and high-density

lipoproteins (O'Brien et al., 2018; Wang et al., 2018; Gerbert and MacRae, 2019). Circulating miRNAs can be brought into the recipient cell via multiple pathways (*e.g.* endocytosis, phagocytosis, *etc.*), and have been shown to not only carry out regulatory functions within these recipient cells but function as messengers in cell-to-cell communication (O'Brien et al., 2018; Gerbert and MacRae, 2019). Furthermore, the presence of these extracellular miRNAs has been predicted to have potential to serve as biomarkers in a clinical setting that could aid in the detection of cancers, as well as a diagnostic tool for interrogating mechanisms that are involved in various biological processes (*e.g.* myogenesis, adipogenesis, *etc*.) (Hammond, 2015; Kochan et al., 2017; O'Brien et al., 2018; Wang et al., 2018; Gerbert and MacRae, 2019).

While miRNAs may only at times mildly/moderately effect the translation of their target genes, it has been shown that an individual miRNA may possess the ability to repress hundreds of genes simultaneously (Selbach et al., 2008; Sjögren et al., 2018; Gerbert and MacRae, 2019). On the contrary, multiple miRNAs may even target the same gene, where they may either cooperate or antagonize each other's regulatory actions (Lu et al., 2010; Uhlmann et al., 2012; Chuang et al., 2015; Gerbert and MacRae, 2019). Given their broad diversity and versatility in impacting gene expression it should come as no surprise that miRNAs have been found to play key regulatory roles in mediating a variety of cellular processes, biological functions, and signaling pathways (Ambros, 2004; Bartel, 2004; Inui et al., 2010; Almeida et al., 2011). The importance of miRNA functionality in several cellular processes have been conclusively demonstrated within the literature, and it has been found that the inhibition of miRNA biogenesis can result in severe abnormalities in cellular proliferation, differentiation, apoptosis, embryogenesis, organogenesis, and

survival (Ambros, 2004; Bartel, 2004; Jovanovic and Hengartner, 2006; Inui et al., 2010; Huang et al., 2011; Bhaskaran and Mohan, 2015). Within the literature it has been extensively documented that an organism that lacks the ability to successfully produce miRNAs will be greatly hindered in its ability to survive and reproduce (Ketting et al., 2001; Bernstein et al., 2003; Wienholds et al., 2003; Kloosterman and Plasterk, 2006; Bhaskaran and Mohan, 2015). Multiple knock out studies using murine and fruit fly models have demonstrated that the inhibition of the endonuclease, dicer, results in significantly higher rates of embryonic death, abnormal organs and cellular morphologies, and lower counts of stem cell (Bernstein et al., 2003; Harfe et al., 2005; Harris et al., 2006; Kloosterman and Plasterk, 2006; Wang et al., 2007; Hammond, 2015; Bhaskaran and Mohan, 2015).

Additionally, Jovanovic and Hengartner (2006) thoroughly reviewed how miRNAs can profoundly influence various the development of various forms cancer and their pathways by controlling cellular proliferation/transformation via apoptosis. Moreover, various loss of function studies have illustrated the importance of miRNAs in the growth, developmental timings, life span, metabolism, and organogenesis (Ha and Kim, 2014; Saliminejad). This concept was initially described in *C. elegans*, and it was revealed that when the function of miRNAs lin-4 and let-7 were lost, the larva would fail to transition to the next stage of development, would exhibit various abnormal characteristics and additional cellular division (Reinhart et al., 2000; Rousch and Slack, 2008). Similarly, it was observed in mammalian models that a multitude of abnormal phenotypes and developmental defects in various tissues arose when varying tissue specific miRNAs were inhibited (Park et al., 2010; Hammond, 2015). McGregor and Choi (2011)

comprehensively reviewed numerous miRNAs that are associated with adipogenesis, and their regulatory roles in various biological processes that are involved with obesity, the metabolism of fat, differentiation of adipocytes, and insulin sensitivity. Several muscle enriched miRNAs that are referred to as myomiRs have been found to be key players in the regulatory networks of myogenesis and tightly control the expression of various muscle phenotypes (Kirby and McCarthy, 2013; Kochan et al., 2017; Sjogren et al., 2017).

These myomiRs have been reported to possess a large degree of control over the differentiation and proliferation of satellite cells and skeletal muscle, as well as regenerative roles in the repair of damage skeletal muscle (Chen et al., 2006; Kim et al., 2006; Cheung et al., 2012; Sjogren et al., 2017). Moreover, it has been found that when skeletal muscle specific dicer was inhibited in mice, deformed muscle morphologies, a reduction in skeletal muscle mass, and death occurred (O'Rourke et al., 2007; Sjogren et al., 2017). MyomiRs in skeletal muscle have been observed to alter their expression patterns in response to exercise, and would differ depending on the type of exercise that was being performed (*i.e.* endurance vs resistance) (Baggish et al., 2011; Davidsen et al., 2011; Dawes et al., 2015). In addition to these findings, recent reports have emerged that indicate that miRNAs have been found to aid in mediating cellular homeostasis and cellular stress responses (Leung and Sharp, 2010; Biggar and Storey, 2018; Olejniczak et al., 2018). It has been reported that when a cell becomes damaged or is exposed to drastic shifts in environmental factors, miRNAs may be upregulated or downregulated as a response by the cell to restore balance and homeostasis (Leung and Sharp, 2010). Consequently, it has been found that extreme or prolonged levels of stress that result in

DNA damage can lead to the dysregulation of miRNA biogenesis and drastically altered patterns in their expression (Wang and Taniguchi, 2013; Olejniczak et al., 2018)

MicroRNAs have been found to play a critical role in the regulation of mammalian immune responses and when their expression becomes dysregulated this can lead to a severely susceptible immune system (Huang et al., 2011). As a result it has been firmly established that the dysregulation of miRNA expression patterns in humans has been implicated as a casual factor in a wide range of chronic human illness that include but are not limited to viral pathogenesis, diabetes, multiple macro- and microvascular complications, cardiovascular disease, kidney disease, neurodegenerative disease, autoimmune diseases, metabolic disorders, and various forms of cancer (Almeida et al., 2011; Bhaskaran, M. and M. Mohan, 2015; Hammond, 2015; Bracken et al., 2016; Paul et al., 2017; Saliminejad, et al., 2018). The regulation of miRNA biogenesis and functionality has been found to be a highly controlled process that occurs on multiple levels, extending from their transcription all the way through their post-transcriptional processing (Ha and Kim, 2014). It has been reported that miRNAs that reside within the intronic or exonic regions of coding genes will frequently fall under the same transcriptional regulation network as the mRNAs that are produced by the host gene (Hammond, 2015; Bartel, 2018; Saliminejad, et al., 2018). All other miRNAs that are located within noncoding intergenic regions and transcribed by RNA Pol II using their own promoters, and can be regulated by RNA Pol II-associated transcription factors and/or various epigenetic regulators (*e.g.* DNA methylation, histone modifications, *etc.*) (Cai and Cullen, 2004; Lee et al., 2004; Davis-Dusenbery and Hata, 2010; Ha and Kim, 2014; Bartel, 2018). For example, recent studies have demonstrated that various transcriptional factors such as myoblast determination

protein 1 (**MYOD1**), tumor protein P53 (**P53**), Zinc finger E-box-binding homeobox 1/2 (**ZEB1/2**), and the myelocytomatosis oncogene (**MYC**) possess the ability to up- and down-regulate the production of miRNAs (Kim et al., 2009; Krol et al., 2010; Ha and Kim, 2014).

Additionally, various intrinsic factors and modifications such as miRNA tailing, RNA editing, and stability have been shown to alter the biogenesis of miRNAs (Ha and Kim, 2014; Gulyaeva and Kuchlinskiy, 2016; Bartel, 2018; Gerbert and MacRae, 2019). MicroRNAs have been reported to undergo various post-transcriptional modification that are induced as a cellular stress response which can lead to alteration within their expression patterns and activities (Olejniczak et al., 2018). Moreover, not only can miRNAs be regulated while they are being processed from pri-miRNA to mature miRNA by drosha and dicer, but specific changes in the activity and expression of these proteins have also been shown to negatively regulate miRNA activity (Ha and Kim, 2014; Gulyaeva and Kuchlinskiy, 2016). Post-translational modifications, such as the phosphorylation of various sites on the AGO proteins have been linked to a reduction in miRNA's ability to bind and repress their targets (Rudel et al., 2011; Ha and Kim, 2014). Furthermore, there are studies that have demonstrated that the target mRNA can affect the stability of its binding miRNA, and in cases of high complementary can even lead to degradation (Baccarini et al., 2011; Pasquinelli, 2012; Ha and Kim, 2014). Lastly, certain viruses, such as *Herpesvirus saimiri* and cytomegalovirus have been reported to utilize their own genetic sequences to destabilize, deactivate, hijacking the host's miRNAs via base pairing interactions (Ha and Kim, 2014; Gerbert and MacRae, 2019).

The discovery of miRNAs and their broad versatility to regulate genes has permanently altered the landscape of molecular biology and has added multiple levels of complexity to our previous understanding of gene expression. These small regulators have been shown to possess a wide range of abilities that allow them to not only regulate cellular pathways, but to finely tune entire networks of genes that are responsible for many physiological processes. However, despite the great strides that have been made in understanding their functions, many of their biological roles and mechanisms have not been clearly elucidated and remain a mystery.

CHAPTER IV:

DIFFERENTIAL EXPRESSION OF MIRNAS IN BOVINE SKELETAL MUSCLE THAT DISPLAY VARYING DEGREES OF THE DARK-CUTTING PHENOTYPE

INTRODUCTION

Dark, firm, and dry beef, alternatively known as dark-cutting beef, is an undesirable phenotypic condition in which the meat of a beef carcass fails to adequately bloom due to its pH (*i.e.* ≥ 5.8) remaining abnormally elevated. This beef fails to achieve the desirable bright, cherry red pigmentation, and will instead possess an abnormally dark pigmentation (Miller, 2007; Ponnampalam et al., 2017). In addition to its abnormal appearance, DFD beef also possesses a shorter shelf life, a resistance to cooking, and a variety of unsavory organoleptic properties, such as an unsavory texture (*e.g.* firm, sticky, dry, *etc*.), an undesirable flavor profile (*e.g.* bland, musty, soapy, metallic, *etc.*), and inconsistent levels of tenderness (Bouton et al., 1973; Mendenhall, 1989; Trout, 1989; Cornforth et al., 1991; Moiseev and Cornforth, 1999; Wulf et al., 2002; Yancey et al., 2005; Calkins and Hodgen, 2007; Miller, 2007; English, 2016; Ponnampalam et al., 2017). Due to these undesirable qualities, DFD beef is frequently rejected on the retail level and suffers strict consumer bias. Consumers reference color as an indication of quality and freshness, with a strict bias favoring cuts of beef that are bright, cherry red in appearance, and reject those that are darker in appearance as they are perceived as being lower in quality (English et al., 2016; McKeith et al., 2016; Mahmood et al., 2017; Wills et al., 2017). This increased rejection at the retail level has resulted in DFD carcasses to be subjected to harsh meat grading standards by the USDA, leading them to be sold at a discounted prices to the foodservice

industry where it is utilized in producing pre-cooked food products (Moiseev and Cornforth, 1999; Savell, 2013; USDA-AMS, 2017a, b).

According to the 2016 NBQA, after a survey of 30 different facilities within the United States, 1.9% of all the graded beef carcasses were determined to be DFD, the lowest percentage surveyed in NBQA history (Boykin et al., 2017). This represents a significant improvement from the 3.2% that was previously reported within the 2011 NBQA (Moore et al., 2012). However, regardless of its reduction in frequency in the U.S., incidence of DFD beef continue to fluctuate seasonally, and represent a preventable source of substantial economic losses for the beef industry world-wide. It was estimated that in 2020 when U.S. cattle numbers reached ~32.8 million, the cost of DFD carcasses when discounted at $281/head was responsible for ~$95-100M in lost revenue for the U.S. beef industry alone (USDA, 2021). As a result of these persistent economic losses, DFD beef and its contributing factors have been the subject of numerous investigative studies. It has been established that the manifestation of this undesirable phenotype occurs predominately in the carcasses of beef cattle (> 30 months of age) that have experienced increased levels of ante-mortem stress prior to slaughter (Lawrie, 1958; Cross et al., 1983; Mahmood et al., 2017).

These prolonged, high levels of pre-harvest stress have been associated with wide range production practices and stress inducing factors. Multiple extraneous factors have been identified and include but are not limited to volatile fluctuations in the weather, aggressive implant strategies, long transport distances, prolonged holding periods, prolonged withholding of food and water, improper handling and desensitization, diet prior to transport, and the mixing of unfamiliar animals (Hedrick et al., 1959; Tarrant, 1989;

Grandin, 1992; Smith et al., 1993; Shackelford et al., 1994; Scanga et al., 1998; Immonen et al., 2000; Miller, 2007; Warren et al. 2010; Boykin et al., 2017; Ponnampalam et al., 2017; Savell and Gehring, 2018; Loredo-Osti et al., 2019; Grandin, 2020). Additionally, several intrinsic characteristics (*e.g.* sex, temperament, age, weight, and breed) have been reported to influence how susceptible an animal is to stress, and increase its predisposition to develop the DFD phenotype (Warriss et al., 1984; Kenny and Tarrant, 1987; Shackelford et al., 1994; Scanga et al., 1998; Voisinet et al., 1997a, b; McGilchrist et al., 2012; Araujo et al., 2016; Page et al., 2001; Miller, 2007; Ponnampalam et al., 2017). These high levels of ante-mortem stress will result in the depletion of the animal's intramuscular glycogen reserves, leaving an insufficient amount to adequately drive forward the post-mortem glycolysis metabolic pathway (Ponnampalam, et al., 2016; Miller, 2007). This will consequently result in diminished levels of intramuscular lactic acid and prevents the beef carcass from achieving a normal level of acidification (*i.e.* pH 5.5-5.7) 24-hours post-harvest, resulting in elevated carcass pH with values greater than or equal to pH 5.8 (Miller, 2007; Ponnampalam et al., 2017). This increased pH leads to alterations in the isoelectric points of muscle proteins, resulting in an increased affinity to associate with and retain water (Miller, 2007; Ponnampalam et al., 2017; Savell & Gehring, 2018).

As these proteins begin to associate with water, the myofibrils will begin to swell and become tightly compressed together, obstructing oxygen from deeply diffusing along the surface of the meat (Lawrie, 1958; Seideman, et al., 1984; Abril et al., 2001). These tightly compressed muscle fibers lead to a diminished ability to scatter light across the meat's surface causing it to appear darker and more translucent in pigmentation

(Seideman, et al., 1984; Abril et al., 2001; Ponnampalam et al., 2017; Jacob, 2020). This process also leads to the inhibition in the oxygenation of deoxymyoglobin (purple), resulting in only a very thin, superficial layer of oxymyoglobin (red) to be formed on the meat's surface (Lawrie, 1958; Seideman, et al., 1984; Abril et al., 2001; Ponnampalam et al., 2017; Jacob, 2020). Additionally, this elevation in carcass pH leads to an acceleration in the respiratory activity within the muscle, enhancing its mitochondrial activity and the rate in which it consumes oxygen (Lawrie, 1958; Ledward, 1985; Seideman et al., 1984; English et al., 2016; McKeith et al., 2016; Jacob, 2020). This increased rate of mitochondrial respiration will accelerate the rate in which oxymyoglobin is converted into deoxymyoglobin, making the deoxymyoglobin the dominate form of myoglobin on the meat's surface (Ashmore et al., 1972; English et al., 2016; McKeith et al., 2016; Ponnampalam et al., 2017; Jacob, 2020). This combination of factors results in the afflicted beef carcasses to display an abnormal color, which can range from a dark maroon to an almost completely black appearance, depending on severity (Miller, 2007; Ponnampalam et al., 2017).

Despite being the subject of extensive study, the DFD phenotype remains a highly complex phenomenon, and there currently still exists no method(s) that allow for its consistent prediction, prevention, nor replication within a given population. While the attributes and associated causal factors of DFD beef have been thoroughly described since the 1940s, little advancement has been made in our understanding regarding the underlying physiological mechanisms that contribute to its manifestation. However, as prices in next-generation sequencing technologies continue to drop and their applications become broader and more accessible, this has afforded new avenues of study that can be applied to resolve

this dilemma. Recently, such studies have begun to elucidate the profound impacts that miRNAs can have on various traits of economic importance in livestock, as well as their critical roles in the mediation of the cellular responses of fully developed tissues to various forms physiological and pathophysiological stress (Leung and Sharp, 2010; Mendell and Olson, 2012; Fatima and Morris, 2013; Wang and Taniguchi, 2013; Olejniczak et al., 2018; Oliveira et al., 2019). MicroRNAs are a major class of small (*i.e.* ~17 - 27 nucleotides), single-stranded, non-coding RNA molecules that function as fine-tuned regulators of gene expression at a post-transcriptional level. These small RNAs have been shown to negatively modulate gene expression by repressing the translation of their target mRNA via the full or partial base pairing to complementary sequence located in its target's 3'UTR and/or promoter regions (Inui et al., 2010; Pasquinelli, 2012; Hollins and Cairns, 2016; O'Brien et al., 2018).

These potent regulators have been found to be extremely versatile in their regulatory capabilities, with reports of individual miRNAs possessing the ability to repress hundreds of genes simultaneously (Selbach et al., 2008; Sjögren et al., 2018; Gerbert and MacRae, 2019). Moreover, miRNAs have been shown to be highly conserved between a wide range of species (*e.g.* animals, plants, protists, and viruses), and to play key regulatory roles in mediating a variety of cellular processes, biological functions, signaling pathways, and the manifestation of various diseases (Ambros, 2004; Bartel, 2004; Inui et al., 2010; Li et al., 2010; Almeida et al., 2011; Ha and Kim, 2014; Friedlander et al., 2014; O'Brien et al., 2018). The roles of miRNAs in the mediation of myogenesis and the development and metabolism of skeletal muscle has been extensively covered within the literature, and their related expression patterns have been profiled in multiple domesticated

animals (*i.e.* cattle, pigs, goats, and sheep) (Luo et al., 2013; Jing et al., 2015; Sun et al., 2015; Guo et al., 2016; Horak et al., 2016; Zhao et al., 2016; Iqbal et al., 2020; Kaur et al., 2020; Raza et al., 2020). Additionally, intramuscular miRNAs have been observed to alter their expression patterns in response to exercise, and differ depending on the type of exercise that was being performed (*i.e.* endurance vs resistance) (Baggish et al., 2011; Davidsen et al., 2011; Dawes et al., 2015). The importance of miRNAs in regulating aspects of adipogenesis in mammals has been thoroughly reviewed, and it has been demonstrated that miRNAs mediate signaling pathways that influence intramuscular adipocyte differentiation, fat metabolism, obesity, and insulin sensitivity (McGregor and Choi, 2011). Emerging data also suggests that miRNAs impact various aspects of meat quality and have been shown to regulate the tenderness and intramuscular fat content in beef and pork (Zhao et al., 2012; Wang et al., 2013; Guo et al., 2017; Li et al., 2018; Ma et al., 2018; Iqbal et al., 2020; Kaur et al., 2020).

In addition to these findings, recent reports have emerged that indicate that miRNAs have been found to aid in mediating cellular homeostasis and cellular stress responses, and their expression patterns may be drastically altered by the cell to restore balance and homeostasis (Leung and Sharp, 2010; Biggar and Storey, 2018; Olejniczak et al., 2018). Zhao et al. (2012) demonstrated the effects of acute stress on beef quality in a population of Angus beef cattle and revealed that the carcasses of cattle that were subjected to stress were significantly tougher and possessed higher Warner-Bratzler shear force measurements than the control group (Zhao et al., 2012). Guo et al. (2020) utilized high-throughput sequencing to identify miRNAs in beef cattle that were differentially expressed as a result of induced transportation stress (Guo et al., 2020). Furthermore, there have been

multiple studies have also revealed that the expression profiles of stress related miRNAs in differing organisms are altered in response to environmental stress, including heat- and cold stress (Yang et al., 2011; Rao et al., 2017; Guo et al., 2020; Yadav et al., 2021). However, despite this accumulation of knowledge many of the physiological implications of miRNAs remain poorly understood and has not been thoroughly investigated in livestock species. Moreover, to the author's knowledge no research has been performed to explore the potential roles of miRNAs in development of the DFD phenotype in beef cattle.

Due to its physiological nature and strong association with stress it is believe that miRNAs likely mediate specific physiological pathways that contribute to the manifestation of the DFD phenotype, and as so will be differentially expressed in cattle that exhibit the DFD phenotype. To address this hypothesis, RNA-Seq was performed on total RNA that was extracted from muscle biopsies taken from a group of steers that expressed varying degrees of dark cutting in order to detect and profile miRNAs that were differentially expressed. The current study constitutes a starting point in the investigation of the potential roles that miRNAs play in the development of the DFD phenotype. It is believed that the data gathered here will not only provide beneficial insight into the etiology of DFD phenotype, but also a deeper understanding of the physiological and stress related implications of miRNAs in general. Such understanding will lay the foundation for potential screening and intervention-based strategies that can be utilized to not only to further decrease the prevalence of DFD beef but reduce its economic impact on the beef industry world-wide.

METHODS & MATERIALS

Animal background and lineage

The source of tissue samples for this project originates from a beef cattle herd that was established as a designed genetic mapping population for carcass quality traits and female calf production phenotypes (Riley et al., 2019). *Bos indicus – Bos taurus* steers (Cycle 1) for carcass evaluation were produced in a reciprocal F_2 mating design from Angus (A) and Nellore (N) F_1 sires and dams. Angus-sired (**AN**; pairs of letters indicate the sire and dam breeds, respectively) and Nellore-sired (**NA**) parents utilized, resulting in four parental breed-of-origin combinations (ANAN, ANNA, NAAN, NANA, where the first two letters indicate the sire, and the last two letters indicate the dam). Additionally, contemporary Cycle 3 animals (from Cycle 1 parents) were also produced each year. Although these animals are all 50% Angus and 50% Nellore, the different breeding strategies used to produce them provide for potential genetic segregation for all traits of interest. Steers were castrated at approximately 60 to 70 days of age and weaned at an average of approximately 7 months of age.

After weaning, they were penned together each year in dry lots or pastures until evaluation. Steers were evaluated and fed at the Texas A&M AgriLife Research Beef Cattle Systems facility near College Station, a commercial feedlot in South Texas, or the Texas A&M AgriLife Research Center at McGregor, TX, depending upon the year. The steers grazed native pastures for approximately 130 days after weaning, then were penned in groups of 4 and feed for approximately 140 days. Steers from Cycle 1 group were harvested at the at the Rosenthal Meat Science and Technology Center at Texas A&M University according to the procedures described by Savell and Smith (2009) (Table 2.1).

Steers in Cycle 2 and Cycle 3 groups were harvested at a commercial processing facility (Sam Kane Beef Processor, Corpus Christi, TX). It is of note that the contemporary group of 78 steers utilized in the current study also comprised part of an experimental Bovine Viral Diarrhea vaccination trial prior to slaughter (Table 2.2). During this vaccination trial 53 steers were randomly selected from the herd and administered a vaccine that either contained a modified live virus (n = 25) or a killed (inactivated) virus (n = 28) (Table 2.2). The remaining 25 steers served as experimental controls and did not receive either treatment (Table 2.2).

Skeletal muscle biopsies and characteristics

The sample set used for the current experiment consisted of skeletal muscle biopsies obtained from a contemporary set of F_2 and F_3 *Bos taurus* - *Bos indicus* steers (n = 78) (Table 2.2). The steers were harvested in 2010 at a commercial processing facility (Sam Kane Beef Processor, Corpus Christi, TX), and all muscle biopsies were acquired by Dr. Robert Neil Vaughn. Approximately 1 g of muscle was extracted from the *Longissimus lumborum* (adjacent to the 12^{th} rib steak taken for quality evaluation) of each animal immediately postmortem following electrical stimulation. Muscle biopsies were flash frozen in liquid nitrogen and stored at -80°C. Numerous carcass traits were evaluated and recorded at harvest and after processing. For this contemporary group, 25 of the 78 beef carcasses unexpectedly exhibited the dark cutter phenotype to varying degrees (1/4 = 8, 1/3 = 9, 1/2 = 3, 2/3 = 4, and 3/4 = 1) (Table 2.2).

The incidence of dark cutting was not equally distributed across families. Half of the steers (9 of 18 steers) descending from sire 8048 (9 of 18 steers) resulted in dark

cutting carcasses. Incidence of dark cutting across the 78 steers is illustrated in Figure 2.1 and Table 2.2.

RNA extraction & quantification

A modified version of the Molecular Research Center Inc. (**MRC**; Cincinnati, OH, USA) TRI reagent RNA extraction protocol was used to extract total RNA from each of the frozen *L. lumborum* skeletal muscle biopsies (n = 78). During RNA extraction, each muscle sample was removed from the -80ºC freezer and placed within dry ice to prevent them from thawing. Approximately 100-200 mg of biopsied skeletal muscle tissue was used from each sample for RNA extraction and homogenized in liquid nitrogen using a ceramic mortar and pestle as described within the protocol. Following extraction and purification, the concentration of total RNA for each sample was quantified via spectrophotometry using the NanoDrop ND-1000 spectrophotometer. Once quantified, the integrity of each sample's total RNA was verified via the Agilent 2100 series Bioanalyzer (Agilent Technologies, Santa Clara, CA) according to the designated manufacturer's protocol. Samples were then stored in the -80ºC freezer until further use.

Small RNA sequencing

Total RNA was submitted to the TIGSS facility (College Station, TX, USA) for small RNA-sequencing via the Illumina NextSeq platform (Illumina, San Diego, CA). Prior to sequencing, each sample's total RNA was re-quantified via the Quibit 2.0 fluorometer (ThermoFisher Scientific, Waltham, MA) and sample libraries were prepared with the NEXTflex Small RNA-Seq kit v3 (BIOO SCIENTIFIC, Austin, TX) library kit. The quality of all sample libraries was evaluated via the Agilent 2200 TapeStation (Agilent Technologies, Santa Clara, CA) prior to sequencing, as recommended by the manufacturer.

The raw sequence files (Accession no. GSE193003) for each sample were uploaded on the NCBI Gene Expression Omnbius (**GEO**) database.

Bioinformatics

Following sequencing, the files containing the raw sequence data were retrieved from the Illumina BaseSpace cloud-based storage system and uploaded onto the TAMU TIGSS High Performance Computing Cluster (HPCC) for further processing. Overall sequence quality of each sample was assessed via the FastQC program. Low-quality sequence data (Phred score < 20) and the adapter sequences were removed with Trimmomatic v0.32 genomic trimming program (Andrews, 2010; Bolger et al., 2014). Following this, the hairpin.bta.fa and mature.bta.fa files were extracted from the miRNA sequence database, miRBase (v.22.1), and uploaded onto the TIGSS HPCC for use in further analyses (Kozomara et al., 2019). These FASTA files contain the sequence data for known precursor hairpins and mature (miRNA hairpins = 1064 and mature miRNAs = 1030) miRNAs currently deposited in miRbase and associated with the *Bos taurus* species. Remaining filtered sequence reads that passed the initial quality control were mapped to precursor hairpins and mature miRNA sequences, then quantified via the mirDeep2 software package (Friedlander et al., 2012). This process generated a miRNA expression profile in the form of a .csv file for each sample and contained all the identified mature miRNAs along with their respective read counts.

These individual .csv files were then concatenated into a singular numerical matrix, which was then screened for duplicated miRNAs that appeared in multiple rows with either identical or slightly differing read counts. The version that possessed the highest read count were retained. Lastly, the 78 samples along with their respective miRNA read counts

were then organized within the matrix and separated into two groups, non-dark cutters (**NON**) (n = 53) and DFD (n = 25).

Statistical Analysis

The miRNA expression levels between the two sample groups: NON and DFD were evaluated for significance via two independent approaches. A Welch's two-tailed *t*-test (Welch, 1947), also referred to as an unequal variance *t*-test, was conducted, and expression was also evaluated via DESeq2 (v.1.34.0) in the Bioconductor software package (Love et al., 2014). For the first approach, sequencing read count data were normalized to counts per million (**CPM**) prior to analysis to account for variability in sequence depth across the samples using the following formula,

$$CPM = \left(\frac{Number\ of\ reads\ mapped\ to\ miRNA}{Total\ number\ of\ mapped\ reads\ in\ the\ sample}\right) \times\ 10^6$$

(Robinson and Oshlack, 2010; Tam et al., 2015; Bushel et al., 2020). Each miRNA that was not detected at a minimum threshold of 1 CPM were removed and excluded from further analyses. Once filtered, normality was tested for via the Shapiro-Wilk Test and the Kolmogorov-Smirnov Goodness of Fit Test (Massey, 1951; Shaprio and Wilk, 1965). Following this, the remaining, normalized miRNA read counts were then used to calculate geometric means for the NON and DFD groups for each of the miRNAs.

Fold differences between the NON and DFD groups were calculated and displayed as the ratio of the geometric means for DFD/NON. Significance of expression difference was determined via the Welch's *t*-test.

The Welch's *t*-test defines the statistic *t* by the following formula,

$$t = \frac{\bar{x}_1 - \bar{x}_2}{\sqrt{\frac{s_1^2}{n_1} + \frac{s_1^2}{n_2}}}$$

where $\bar{x}$ = sample mean

s^2 = sample variance

n = sample size (Welch, 1947; Ahad and Yahaya, 2014).

To control for multiple testing, *p*-values were adjusted at a false-discovery rate (**FDR**) of 5% according to the method of Benjamini-Hochberg (1995). An adjusted $p \leq 0.05$ accompanied by a fold difference ≤ 0.8 or ≥ 1.2 was set as the cut-off for differentially expressed miRNAs. This cut-off reflects an expression difference between groups of at least 20% and a maximum of 5% probability of false discovery.

For the second approach, the DESeq2 software package was utilized. Prior to analysis the data was filtered, and all miRNAs that did not possess a sum total of ≥ 10 count reads across all samples were considered to be sequencing noise and were omitted from further analysis. Once the filtered, the count matrix was then normalized using DESeq2's median of ratios method, which appropriately scale the raw count data to account sequencing depth and library composition. Afterwards, DESeq2 then performs differential expression analysis by using a generalized linear model of the form,

$$K_{ij} \sim \text{NB}(\mu_{ij}, \alpha_i)$$

where K_{ij} = read counts for miRNA *i* and sample *j*

$\mu_{ij} = s_j q_{ij}$ = fitted mean

s_j = normalization factor for sample *j*

q_{ij} = ($\log_2(q_{ij}) = x_j.\beta_i$) = parameter proportional to the expected true concentration of fragments for sample *j*

q*ij* = normalized counts for miRNA *i* and sample *j*

β_i = $\log_2$ fold changes in miRNA *i* for each column of the model matrix *x*

α_i = gene/miRNA-specific dispersion parameter (Anders and Huber, 2010; Love et al., 2014, 2021).

Using this approach, the read counts were modelled to a negative binomial distribution and a Wald test was utilized for hypothesis testing. To control for multiple testing, *p*-values generated by the Wald test were adjusted at an FDR of 5% according to the method of Benjamini-Hochberg (1995). An adjusted $p \leq 0.05$ accompanied by a fold difference ≤ 0.8 or ≥ 1.2 was set as the cut-off for differentially expressed miRNAs. This cut-off reflects an expression difference between groups of at least 20% and a maximum of 5% probability of false discovery.

RESULTS

Summary of miRNA sequencing data

A total of 289,357,401 raw sequence reads were generated across all samples. The reads produced from each sample were approximately 101 bps in length and an average of 3,709,710 reads were generated per sample. Following the excision of the adapters and removal of low-quality reads (phred score < 20), 275,932,303 sequence reads were retained with an average of approximately 3,537,594 reads per sample. According to FastQC output, miRNA sequence reads averaged a phred quality score of ~31, GC content of ~34.5%, and 15-22 nucleotides in length.

Welch t-test analysis of relative expression levels of miRNAs

Upon completing analysis, it was found that out of the 1030 mature *Bos taurus* miRNAs that were screened, 292 miRNAs met the minimum expression threshold of at least 1 CPM (Figure 2.2). Furthermore, 187 of the 292 were expressed at or above 5 CPM (Figure 2.2). When comparing the ratios of expression (DFD/NON) it was found that 170 miRNAs possessed expression ratios that ranged from 0.90 - 1.10 between groups, and 41 miRNAs exhibited differential expression of at least 20% between groups (Figure 2.3). Additionally, it was observed that out of these 41 miRNAs, a majority were expressed in higher ratios in the DFD group (DFD > NON: 34 miRNAs) when compared to those in the NON group (NON > DFD: 7 miRNAs) (Figure 2.3). With fold difference established, a Welch's *t*-test was performed for each miRNA to determine significance of differential expression between the NON and DFD groups. While 34 differentially expressed miRNAs met statistical significance at $p \leq 0.05$, only 16 miRNAs met the arbitrarily established threshold for ± 20% difference in expression (Table 2.3). However, when the *p*-values were adjusted to control for multiple testing it was found that none of the miRNAs met the threshold of statistical significance ($p_{adj} \leq 0.05$) (Table 2.3).

Identification of differentially expressed miRNAs using DESeq2

It was found that 542 out of the initial 1030 mature *Bos taurus* miRNAs passed the initial filtering threshold. Of these, 170 miRNAs exhibited differences of at least 20% in expression between DFD and NON groups (Figure 2.4 & Table 2.4). Approximately half of the miRNAs reflected an expression ratio (DFD/NON) that ranged from 0.90 - 1.10 between groups (Figure 2.4 & Table 2.4). Furthermore, it was observed that out of these 170 miRNAs a majority were expressed in higher ratios in the normal carcasses (NON >

DFD: 96 miRNAs) when compared to those in the DFD group (DFD > NON: 74 miRNAs) (Figure 2.4 & Table 2.4). Of the differentially expressed miRNAs, 42 reached statistical significance ($p \leq 0.05$), however, only 29 miRNAs met the fold difference threshold of ≤ 0.8 or ≥ 1.2 (Table 2.4). Within the DESeq2 analysis, after Wald test *p*-values were adjusted to control for multiple testing only a single miRNA, bta-miR-2422, approached statistically significant differential expression (Table 2.4).

DISCUSSION

In the current work we performed RNA-Seq on total RNA extracted from *L. lumborum* skeletal muscle that had been biopsied from the carcasses of a contemporary set of F_2 and F_3 *Bos taurus* - *Bos indicus* steer carcasses that displayed varying degrees of dark cutting. Our objective was to utilize the RNA-Seq data that had been generated from samples from each steer to detect and identify differentially expressed miRNAs that are potentially associated with the manifestation of the dark cutting phenotype. To achieve this goal, we assessed differential miRNA expression between the normal steer carcasses and those displaying the DFD phenotype via two statistical approaches. Initially, as proof of concept, a Welch's *t*-test was conducted to screen for potentially significant differences in miRNA expression between the NON and DFD groups. A *t*-test was adopted for this initial analysis because it offered a quick, highly straightforward means to calculate a simple estimation of differential expression between the two groups without the need of extensive bioinformatical expertise.

The Welch's *t*-test was chosen over the conventional Student's *t*-test because it does not require the assumption of homogeneity of variance to be met. However, if this assumption is met, the Welch's *t*-test tends to yield highly similar results to the Student's *t*-

test, especially when the sample size is large (Welch, 1947; Delacre et al., 2017). In addition, it has been reported that when the variances and/or sample sizes are unequal the Student's *t*-test has a tendency to lose power and reliability, whereas the Welch's *t*-test tends to perform more consistently (Welch, 1947; Zimmerman, 1996; Delacre et al., 2017). Using this approach, we identified 16 miRNAs out of the original 1030 mature *Bos taurus* miRNAs that initially met the threshold for statistical significance and the established threshold for ± 20% difference in expression (Table 2.3). This established threshold for fold difference was arbitrarily set at ± 20% (≤ 0.8 or ≥ 1.2) to serve as a cutoff for minimum differences in expression for the miRNAs. Traditionally, despite being somewhat arbitrary, it is common for a 2-fold and/or 1.5- fold difference to be adopted as a cutoff for mRNA differential expression analyses. However, due to the nature and characteristics of miRNA, these values were viewed as being too conservative for the purposes of the current work, because small changes in miRNA concentration can have great downstream impact.

As previously described, miRNAs have been shown as potent regulators that can profoundly impact entire networks of genes. In addition to this, miRNAs appear in extremely low concentrations and have been reported to only constitute approximately 0.01% of the total RNA in a given tissue (Peltier and Latham, 2008). It is due to these reasons that a smaller cutoff of ± 20% (≤ 0.8 or ≥ 1.2 fold DFD/non) was adopted for the current experiment, because while remaining measurable, these values appeared to be biologically relevant to the described properties of miRNAs. However, when the *p*-values were adjusted to control for multiple testing, these miRNAs no longer met the designated threshold of significance ($p_{adj} \leq 0.05$), with bta-miR-2422 being the closest to statistical

significance ($p = 0.11$) (Table 2.3). While unfortunate, these initial findings were not surprising due to the known statistical limitations of this approach and variability across animal samples.

The first limitation resides in the normalization procedure that was utilized. In general, when conducting differential gene expression analyses using RNA-seq, the input that will be used for statistical analyses will be formatted as count matrix that contains the read counts of each transcript for each sample. Each read count is derived from the number of times that an individual read was mapped to the reference sequence (*i.e.* gene or transcript of interest), and represents a relative estimation of the total abundance of that specific transcript within the sample (Soneson and Delorenzi, 2013; Evans et al., 2018; Quinn et al., 2018). Initially these raw read counts are not directly comparable between samples. This is because they likely contain various sources of non-biological variation (*e.g.* sequencing depth, library composition, *etc*.) that typically arise from various technical issues (Wang et al., 2009; Soneson and Delorenzi, 2013; Bushel et al., 2020; Li et al., 2020). Normalization is the process in which the raw RNA-seq reads counts are adjusted to account for these sources of non-biological variation, so that more accurate comparisons of true expression levels across samples can take place (Bullard et al., 2010; Soneson and Delorenzi, 2013; Evans et al., 2018).

While there currently exists no gold standard method of normalization for RNA-Seq analyses, the importance of proper normalization has been firmly established within the literature (Wang et al., 2009; Bullard et al., 2010; Evans et al., 2018; Bushel et al., 2020). When data is improperly normalized this can have profound effects on downstream analyses, which can potentially lead to increased rates of Type I errors (Evans et al., 2018;

Bushel et al., 2020). As previously stated, the CPM normalization method that was chosen for this initial analysis. Counts per million represents one of the simplest forms of normalization that has been implemented within RNA-Seq based studies. This approach adjusts the read counts of the miRNAs in each sample to account for differences in the sequencing depth (Robinson and Oshlack, 2010; Tam et al., 2015; Bushel et al., 2020). Though commonly used within the literature, there are numerous inconsistencies that have been reported regarding the effectiveness of this normalization method.

While some studies have found that the CPM approach allows for similar levels of sensitivity and accuracy in its ability to detect differential expression as the more advanced forms of normalization, others have also been reported that it can result in higher levels of bias and variability (Tam et al., 2015; Bushel et al., 2020). Furthermore, there are also arguments that this approach to normalization is far too simplistic as it only accounts for variations in sequence depth and neglects all other sources of non-biological and technical variation (Garmire and Subramaniam, 2012; Dillies et al., 2013; Tam et al., 2015). Given this information, it is believed that it is likely that this approach could potentially contribute to increased rates of Type I errors. However, to what extent remains unclear, and given the current discrepancies within the literature pertaining to this topic it is believed that at this time further studies are required to reach a definitive conclusion. The second limitation of this approach stems from the statistical test that was utilized. Although popular due to its simplicity, the *t*-test is a parametric test and is most appropriate for analyzing continuous variables (*e.g.* height, temperature, *etc*.) that follow a normal probability distribution (Tang et al., 2016).

However, the quantitative input that is used in RNA-Seq-based differential expression analyses is formatted as count data, and as such will follow a discrete probability distribution. This is because unlike continuous variables, which can take on an infinite set of values between the limits of the variable, count values are discrete variables and can only be measured as whole, non-negative integers that can only take on a finite set of values (Kiess and Green, 2010; Soneson and Delorenzi, 2013; Ott and Longnecker, 2016; Kaps and Lamberson, 2017; Evans et al., 2018; Quinn et al., 2018; Walker, 2021). Additionally, when considering count data that is indicative of gene expression, it is quiet common for a large proportion of genes to possess only a low number of read counts. Due to this occurrence, when visualized via a histogram the data will be positively skewed with most of the residuals being truncated near zero, and there will be a long right tail that is attributed to the lack of any upper limit for expression (Fang et al., 2012; Zhang et al., 2014; Walker, 2021). However, while the Shapiro-Wilk and Kolmogorov-Smirnov tests did demonstrate non-normality in various miRNAs count values between the sample groups, this was not consistent throughout the entire dataset. Instead, it was found that in most cases the assumption of normality was only mildly to moderately violated, and the distribution curves between the two groups were typically shown to only be slightly skewed and possessed relatively the same shape in most cases.

This was likely attributed to a combination of increased sample size, as well as the approach that was taken for normalization. During normalization, the read counts were transformed from whole numbers into decimals which are inherently continuous in their nature. Furthermore, in the cases of some miRNAs, this deviation from extreme non-normality could be explained by large read counts. Within the current dataset there existed

several miRNAs that possessed large read counts, which can be roughly approximated via a normal distribution (Anders and Huber, 2010; Herbison, 2011, 2015; Walker, 2021). These explanations would be consistent with the literature, as it has been reported that such factors can potentially diminish the discreteness of count data leading it to become pseudo-continuous (Conesa et al., 2016). However, despite these inconsistent deviations in normality, it was believed that the Welch's *t*-test would still be capable of providing an accurate estimation of potential differential expression in miRNAs between the two sample groups.

While violations to the assumption of normality can increase the probability of making a Type I error, it has been established that the *t*-test in general, remains quite robust despite presence of non-normality, especially with increased sample sizes (Kiess and Green, 2010; Fagerland, 2012). Moreover, it has been reported that the effect of this violation can be further minimalized when the following criteria are satisfied: (*i*) Equal sample size, (*ii*) The two distributions are of approximately the same shape, and are not overly peaked or flattened, (*iii*) Significance level is set to 0.05 rather than 0.01, and (*iv*) A two-tailed test is used even with a directional research hypothesis (Kiess and Green, 2010). However, it is of note that while most of the listed criteria was satisfied, it is impossible to fully negate the increased probability of making a Type I error when the assumption of normality has been violated. Furthermore, while there exists instances in which count data can be adequately modelled using a linear model and approximated relatively well by a normal probability distribution, it is more appropriate to model such data with a discrete probability distribution (*e.g.* Poisson, binomial, and negative binomial distributions) using a generalized linear model (Anders and Huber, 2010; Ott and Longnecker, 2016; Kaps and

Lamberson, 2017; Walker, 2021). Despite not being perfectly modelled for data such as this experiment, this simple approach was primarily exploratory in its nature, and was believed to be accurate enough to provide a quick estimation of differential expression between the miRNAs of the two sample groups. Due to the deficiency of a standardized analytical method within the literature, we sought to approximate differential expression between the two sample groups using a simple methodology that could serve as a relatable baseline that the findings of the more mathematically complexed follow-up analyses could be compared to.

Following the conclusion of this initial analysis, the DESeq2 software package was utilized for follow-up analysis. This approach was chosen because it offered several key advantages over the approach that were utilized in the initial analysis. The first advantage resides in the manner in which DESeq2 conducts normalization. DESeq2 software package incorporates a median of ratios method of normalization that focuses on calculating individual scaling factors for each sample, which are used to adjust the total mapped read counts for each sample (Anders and Huber, 2010; Love et al., 2014, 2021). DESeq2 begins this normalization procedure by taking the $\log_e$ of all the miRNA read count values across all samples, and any miRNAs that possess zero read counts will be denotated as negative infinity (Anders and Huber, 2010; Love et al., 2014, 2021). The $\log_e$ transformed miRNA read count values are then used to calculate a geometric average for each miRNA across all of the samples, which will serve as a pseudo-reference sample for that individual miRNA (Anders and Huber, 2010; Love et al., 2014, 2021).

Using the average of these logarithmic values is beneficial because it is not easily influenced by the presence of outlier count values. Following this, all miRNAs that possess

a geometric average equal to negative infinity (*i.e.* zero read counts in one or more samples) were filtered out of the dataset (Anders and Huber, 2010; Love et al., 2014, 2021). This step is highly beneficial if a researcher is comparing the miRNA expression levels between two types of tissues (*e.g.* muscle vs liver), because it helps compress the expression levels of miRNAs that are only transcribed within the muscle (or liver). The theory behind this approach is that it allows the scaling factors to focus more on the house keeping genes, or in this case miRNAs that are typically transcribed at equal levels throughout the body regardless of tissue type. Once these values have been removed, DESeq2 will then subtract the geometric mean (pseudo-reference sample) of each miRNA from each of its individual log counts across all samples (Anders and Huber, 2010; Love et al., 2014, 2021). This calculation will yield a ratio of the read counts in each sample to the geometric average across all samples, which will allow for the identification of miRNAs within each sample that are being expressed at significantly higher or lower levels than the average (Anders and Huber, 2010; Love et al., 2014, 2021).

All of the calculated miRNA ratio values within a given sample are then used to calculate a median value, the "*median of ratios*", for that individual sample (Anders and Huber, 2010; Love et al., 2014, 2021). Using the median value of these ratios is beneficial because it reduces the impact of outliers on the final scaling factor that will be used for normalization. These median values are then reverted back into normal numbers from their logarithmic state to generate the final scaling factors that will be used normalize each sample's read counts (Anders and Huber, 2010; Love et al., 2014, 2021). Lastly, each sample's raw miRNA read counts will then be divided by that sample's unique "*normalization*" scaling factor (Anders and Huber, 2010; Love et al., 2014, 2021). This

results in the total mapped miRNA read counts for each sample to be adjusted to a common scale, which will allow for more accurate comparisons between sample groups (Anders and Huber, 2010; Love et al., 2014, 2021). Unlike CPM normalization, the DESeq2 approach accounts for not only differences in each sample's sequencing depth, but also for the effect that these differences can have on each sample's library composition (or RNA composition) (Anders and Huber, 2010; Love et al., 2014, 2021).

The second advantage to this approach is that it provides a more accurate statistical model for RNA-Seq count data. RNA-Seq count data, as previously mentioned, are discrete non-negative integers that arise from the number of instances in which an individual sequencing read is mapped to/within a genomic feature of interest (*e.g.* gene, exon, miRNA, *etc.*) (Soneson and Delorenzi, 2013). This mapping process consists of a series of discrete events in which each of the sample's sequencing reads are independently sampled at random from a very large pool of reads (*i.e.* sample's library) and compared with a reference sequence (*i.e.* in this case, 1030 mature *Bos taurus* miRNAs) (Anders and Huber, 2010; Zhou et al., 2011; Love et al., 2014, 2021). As such, the total read counts for each miRNA represents the sum of a series of random events, in which the probability of a given sequencing read being successfully mapped to any specific transcript/gene of interest is very low (Zhou et al., 2011; Fang et al., 2012). By comparison, while the total number of sequencing reads that comprise a sample's library tend to be considerably large (*i.e.* millions), the actual read counts that are found to correspond with each individual transcript are relatively small (*i.e.* tens, hundreds, or thousands) (Anders and Huber, 2010; Zhou et al., 2011; Soneson and Delorenzi, 2013). Due to this, the read counts of each miRNA are not likely to follow a normal distribution, and instead would be more inclined

to fit the model of a multinomial distribution which is a generalization of the binomial distribution (Anders and Huber, 2010; Zhou et al., 2011; Kaps and Lamberson, 2017). However, when the probability of the event is extremely low and the total number of trials is relatively large, such as what is typically seen with RNA-Seq read counts, the multinomial distribution is often approximated by the Poisson distribution (Anders and Huber, 2010; Zhou et al., 2011; Kaps and Lamberson, 2017).

The Poisson distribution is a discrete probability distribution that is commonly used for determining the probability in which a rare event will occur within a fixed interval of time, volume, or area (Kaps and Lamberson, 2017). This model is often adopted due to its simplicity, as it is only defined by a single parameter (λ) which requires that the variance of the modelled variable be equivalent to that of the mean (Anders and Huber, 2010; Soneson and Delorenzi, 2013; Kaps and Lamberson, 2017). For RNA-Seq, the utilization of Poisson modelling has been verified to be an appropriate fit for analyses that utilize technical replicates, in which all of the samples are biologically identical with the only source of variation arising from sampling and/or technical effects (Marioni et al., 2008; Bullard et al., 2010; Robinson and Oshlack, 2010; Fang et al., 2012; Soneson and Delorenzi, 2013). However, in practice due to the restrictive nature of its parameter's assumption (*i.e.* mean = variance), the Poisson distribution is often not a suitable model for differential gene expression analyses that utilize biological replicates (Robinson and Smyth, 2007; Anders and Huber, 2010; Robinson and Oshlack, 2010; Fang et al., 2012; Zhang et al., 2014). This is because the read counts of biological replicates typically exhibit a high degree of over-dispersion (*i.e.* variance > mean), and as a result will possess a variability that exceeds the limits of what the Poisson distribution allows (Robinson and

Smyth, 2007; Anders and Huber, 2010; Robinson and Oshlack, 2010; Fang et al., 2012; Zhang et al., 2014). When overdispersion occurs across numerous samples, the Poisson model will not accurately estimate the biological variability between the samples and will fail to control for Type I errors (Anders and Huber, 2010; Fang et al., 2012; Zhang et al., 2014).

In order to resolve this issue of over-dispersion, DESeq2 like many other popular software tools have begun to model RNA-Seq read counts using the negative binomial distribution, also referred to as a gamma-Poisson distribution (Whitaker, 1914; Robinson and Smyth, 2007; Anders and Huber, 2010; Robinson and Oshlack, 2010). Much like the Poisson distribution, the negative binomial distribution is also a discrete probability distribution that is commonly used to model count data. However, unlike the Poisson model, the negative binomial distribution possesses an additional dispersion parameter, which allows for a more flexible framework in its ability to model more generalized mean-variance relationships (Robinson and Smyth, 2007; Anders and Huber, 2010; Soneson and Delorenzi, 2013; Love et al., 2014, 2021). Due to this flexibility, the negative binomial distribution has been widely demonstrated to not only provides a more accurate model for over-dispersed RNA-Seq read counts, but also corrects for potential biases and errors that result from using a standard Poisson model under such conditions (Whitaker, 1914; Robinson and Smyth, 2007; Zhou et al., 2011; Zhang et al., 2014; Zhou et al., 2014). In summary, DESeq2 was chosen for the follow-up analysis because it provides a highly efficient approach to normalization where minimum data would be excluded and offers highly accurate statistical modelling of the current datasets.

Using this approach, DESeq2 modelled each miRNA to a negative binomial distribution and hypothesis testing was conducted via the Wald test. It was found that out of the 542 miRNAs that were tested for differential expression, 42 were identified as differentially expressed (initial values of $p \leq 0.05$) (Table 2.4). Of these 42 miRNAs, only 29 possessed a fold difference (**FD**) that was greater than or equal to 20% (Table 2.4). However, when the *p*-values were adjusted to control for multiple testing, it was found that only *bta-miR-2422* passed the threshold for statistical significance ($P \leq 0.05$, FD $\geq \pm 0.20$) (Table 2.4). The remaining 29 miRNAs that passed the initial thresholds were all found to no longer meet the threshold of statistical significance (Table 2.4). A potential source of error in this approach is that it extremely likely that there exists an accumulation of residual artifacts/noise within the dataset that were not adequately filtered out. Prior to analyzing RNA-Seq data, it is common practice to filter out genes/transcripts with extremely low read counts, particularly those that possess an excessive quantity of zeroes across multiple samples.

Regardless of the methodology that is chosen for differential gene expression analysis, it has been shown to be incredibly difficult to reach a meaningful conclusions regarding differential expression for transcripts that possess extremely low read counts (Bullard et al., 2010; Robles et al., 2012; Rocke et al., 2015; Tam et al., 2015; Conesa et al., 2016). By filtering such genes out prior to analysis, this not only removes gene/transcripts that demonstrate very little evidence for differential expression but can also lead to higher precision and detection sensitivity of differentially expressed genes (Bourgon et al., 2010; Sha et al., 2015; Doyle et al., 2021). This is because the presence of these genes can interfere with statistical approximations that are used for analysis, such as

the estimation of the mean-variance relationships of the datasets (Law et al., 2018; Doyle et al., 2021). Furthermore, the presence of these additional genes increases the multiple testing burden by inflating the number of statistical tests that must be performed while estimating FDRs, and as such can reduce the power to detect differentially expressed genes (Law et al., 2018; Doyle et al., 2021). However, it has been demonstrated that when the appropriate genes have been adequately filtered prior to analysis, this can increase the power of detection of differentially expressed genes by making the impact of the multiple testing adjustment of the *p*-values less severe (Bourgon et al., 2010; Risso et al., 2011; Law et al., 2018; Doyle et al., 2021). Unfortunately, despite the profound impact that pre-analysis filtering can have on downstream analysis, this process remains highly subjective.

Currently within the literature there exists no clear consensus or standard that has been established regarding what parameters and/or thresholds should be utilized during this process. However, for the current study, a highly lenient cutoff was adopted which only required a miRNA to have a sum total of at least 10 read counts across all samples in order to be not considered noise. Such a liberal threshold was adopted in order to avoid excluding any potential miRNAs that were only being differentially expressed in the more severe cases of dark cutting. However, the consequence of this is that it undoubtedly increased the level of noise within the dataset. This dilemma of analyzing RNA-Seq datasets that contain several genes with extremely low read counts combined with an excessive quantity of zeroes remains challenging. As it is often incredibly difficult to distinguish between zero count values that arise from unexpressed genes, those arising from genes that are being expressed at low levels, and those that are attributed to some form of technical variation such as RNA degradation.

Such uncertainties force the researcher to either retain the genes with the low count values which can impair the ability to detect those that are truly being differentially expressed or discard them and potentially lose biologically important genes that encode for transcripts that only appear in low concentrations (Rocke et al., 2015). In conclusion, it is believed that a stricter cutoff for pre-analysis filtering would not only improve the ability to detect true differential expression but would also potentially improve the adjusted *p*-values of the dataset. Unfortunately, due to the inconsistencies within the literature it remains unclear to what extent the threshold should be set in order to optimize detection power and minimize the loss of significant miRNAs with low levels of expression. A potential option would be to re-sequence the dataset in order to increase the sequencing depth of each sample. A deeper sequencing depth could potentially provide a higher degree of resolution for those miRNAs with low count values, which could aid in optimizing a more efficient cutoff threshold for pre-analysis filtering.

Interestingly however, despite the inherent theoretical differences that exist between these two approaches, there was considerable overlap in the top miRNAs that each approach identified. It was found that a total of 18 miRNAs passed the initial threshold of statistical significance ($p \leq 0.05$) under the set conditions of both statistical approaches prior to the FDR adjustments (Table 2.3 & Table 2.4). Moreover, 9 of these miRNAs (*i.e. bta-mir-2422*, *bta-mir-1260b*, *bta-mir-493*, *bta-mir-27a-5p*, *bta-mir-136*, *bta-mir-1307*, *bta-mir-2285q*, *bta-mir-543*, and *bta-mir-1194*) also met the established fold difference threshold of ≤ 0.8 or ≥ 1.2 under both analyses (Table 2.3 & Table 2.4). Due to the consistency of the findings between the two statistical approaches the known biological functions and targets of these 9 miRNAs were further investigated to determine if there

existed any relevance to the dark cutting phenotype. Of these miRNAs, bta-miR-2422 was the top hit for both approaches and overall demonstrated the highest degree of statistically significant differential expression (Table 2.3 & Table 2.4).

A recent study investigating the role of miRNAs in bovine trypanosomiasis utilized a series of predictive analyses and reported that *bta-miR-2422* potentially targets the transcripts of the *ICAM-1*, *ITGAM*, *LBP*, *TLR-2*, and *TNF* (Morenikeji et al., 2019). In humans, these genes have been reported to be highly associated with innate immune responses, various inflammatory processes, and the regulation of humoral defense mechanisms (Morenikeji et al., 2019). In addition to these predicted targets, Shi et al. (2020) utilized the TargetScan software package to predict the targets of several miRNAs while investigating *Wnt/β-Catenin* pathway and reported *MAP3K4* to be a potential target of *bta-miR-2422* as well (Shi et al., 2020). According to previous reports, MAP3K4 is a key player in the mitogen-activated protein kinase (**MAPK**) pathway and functions as a mediator in the environmental stress-induced activation (*e.g.* inflammatory factors, wound stress, and heat shock) of p38 and JNK, which have regulatory roles in cellular apoptosis and proliferation (Takekawa et al., 1997; Zhao et al., 2020). Aside from stress responses, it has been documented that the MAPKs play a role in the regulation of normal and pathological adipogenesis, inferring that bta-miR-2422 may play a role in the development of intramuscular fat (Bost et al., 2005; Qi et al., 2018). In addition to this, it was found that bta-miR-1260b was also involved in various aspects cellular proliferation, apoptosis, stress, innate immune responses, and cellular process involved in the progression of multiple cancers. Wang et al. (2020) reported that miR-1260b played an active role in

regulating the development of eyes, smooth muscle, and nerve differentiation in various species (Seong and Kang, 2020; Wang et al., 2020).

Kong et al. (2019) demonstrated that *bta-miR-1260b* was significantly up-regulated in a stressed induced group of Jersey cattle that were subject to varying degrees of high-altitude hypoxia. Singh et al. (2020) found that miR-1260b was significantly up-regulated in water buffalo (*Bubalus bubalis*) that were suffering from brucellosis as well as Johne's disease. Furthermore, there are numerous reports within the literature that human miR-1260b is abnormally up-regulated in tumors, and is highly associated with various forms of cancer (*e.g.* cervical cancer, lung adenocarcinoma, non-small cell lung cancer, colorectal cancer, *etc*.) (Liu et al., 2016; Xia et al., 2019; Kim et al., 2020; Ren et al., 2020). Much like miR-1260b, it was also found that *miR-27a-5p* regulates various mechanisms that are related to cellular proliferation, growth signaling pathways, innate immune responses, and cellular process involved oncogenesis (Rupaimoole et al., 2016; Zhang et al., 2019). Zhang et al. (2019) comprehensively reviewed the association between dysregulated expression levels of miR-27a and the formation of tumors. While many of the oncogenic mechanisms of this miRNA remain obscure, *miR-27a* has been shown to regulate multiple signaling pathways (*e.g.* AKT, Wnt/β-catenin, Ras/MEK/ERK, TGF-β, *etc*.) during the progression of oncogenesis in humans (Zhang et al., 2019).

In cattle, Morenikeji et al. (2019) also reported that the transcripts of the *TLR-2* and *TNF* genes were predicted to be targets of *miR-27a-5p*, insinuating that this miRNA mediates aspects of inflammatory responses and innate immunity as well. Moreover, while investigating the roles of miRNAs in castration-induced fat deposition, Yang et al. (2018) reported that miR-27a-5p mediated the expression of the calcium-sensing receptor

(**CASR**). These researchers also reported that CASR gene silencing in bovine hepatocytes significantly decreased the concentration of triacylglycerol and inhibited the secretion of very low-density lipoproteins (Yang et al., 2018). The implication of these findings indicates that miR-27a-5p may potentially mediate aspects of regulating fat deposition in cattle (Yang et al., 2018). Lastly, Sun et al. (2020) reported that *miR-27a* was associated with regulating aspects of glycolysis and the mobilization of lipids in largemouth bass during stress induced hypoxia. However, the specifics of these regulatory roles on the glycolytic pathway were not thoroughly discussed and further investigation into this matter is required.

Similarly, it was found that human miR-493 was abundantly associated with various cancers in humans as well, and targets the transcripts of *IGF1R, MKK7, RhoC*, and *FZD7* that are involved in the progression of oncogenesis (Izumiya et al., 2011; Ueno et al., 2012; Do et al., 2019). In addition to these findings, it was reported by Zheng et al. (2014) that when comparing miRNAs in serum taken from normal vs. heat-stressed Holstein cattle that bta-miR-493 was significantly up-regulated in those that were subjected to heat stress. Furthermore, Do et al. (2019) while investigating potential developmental aspects of miRNAs in cattle found that *bta-miR-493* potentially serves as a key regulator of calf rumen development during the early stages of life. However, aside from these findings the biological functions and impacts of *miR-493* in cattle remains highly ambiguous to date and further research is needed if they are to be elucidated. Following this, *miR-136* was reviewed and found to be associated with the mediation of tumor growth and plays a role in the suppression and metastasis of various cancers (Yan et al 2016; Zhu et al 2018). Zhu et al. (2018) reported that *miR-136* can inhibit the

proliferation and metastasis of prostate cancer cells via repressing the expression of *MAP2K4*.

Interestingly, in addition to this there exists evidence that miR-136 also mediates regulatory roles in the synthesis of fatty acids (*i.e.* oleic acid & conjugated linoleic acid) in beef cattle (Oliveira et al., 2019). Additionally, Guo et al. (2017) reported that *miR-136* was significantly upregulated in Wagyu cattle when compared cattle from the Holstein herd. According to reports from Smith et al. (2009), Wagyu cattle possess high levels of intramuscular marbling and monounsaturated fatty acids, such as oleic acid which is one of the primary structural components of soft fat. This information coupled with the knowledge that miR-136 regulates aspects of the MAPK pathway infers that *miR-136* potentially mediates aspects of adipogenesis and the development of intramuscular fat in cattle. Like many of the other miRNAs that have been discussed, it has been widely established that the upregulation of *miR-1307* is also highly associated with oncogenesis and various forms of cancer (Sathipati and Ho, 2018; Chen et al., 2019; Zheng et al., 2019). As such, it becomes apparent that miR-1307 is a mediator biological processes that mediate cellular mechanisms that are associated with cellular proliferation and apoptosis.

Similarly, there also exists evidence that miR-1307 is a mediator of aspects of the innate immune system. A recent review by Miretti et al. (2020) reported that *miR-1307* was found to be upregulated and responsible for coordinating innate immune responses during early stage of foot-and-mouth disease virus infection within porcine (Qi et al., 2019; Miretti et al., 2020). Similar antiviral responses have been reported in humans as well. It was found that over expression of *miR-1307* limited the expression of the NS1 influenza protein, as well as the replication of wild type H1N1 virus in human cell lines (Bavagnoli

et al., 2019). However, unfortunately aside from the known roles of miR-1307 in tumorigenesis and its impact on immunological responses there remains very little consistent information within the literature pertaining to other biological roles of this miRNA. Next, it was found that multiple members of the *miR-2285* family of miRNAs have been reported to target the transcripts of various toll-like receptor genes, and as such are potential mediators of pro-inflammatory responses of the innate immune system (Zhou et al., 2011; Das et al., 2016; Morenikeji et al., 2019). It was also reported that members of this miRNA family have been shown to interact with the CD8A T-cell surface glycoprotein, which has known roles in the cellular proliferation, the formation of T and B lymphocytes, and in regulating inflammatory responses (Lawless et al., 2014; Mahjoub, et al., 2015; Hanif et al., 2018).

Additionally, these researchers also observed that miR-2285 may potentially target and regulate the expression of heat shock protein HSPN8 (Hanif et al., 2018). Heat-shock proteins (**HSP**) are highly conserved molecular chaperones that constitute the first line of defense for damaged cells that have been exposed to endogenous and/or exogenous form of stress (Jego et al., 2013; Dubrez et al., 2020). Furthermore, these proteins possess many well documented roles in protein maturation, degradation, and re-folding (Miller and Fort, 2018). Through such actions, HSPs are able to stabilize the structures of intracellular proteins when cells are subjected to above-optimum temperatures (heat stress) and restore the integrity of the damaged cells (Miller and Fort, 2018; Li et al., 2021). As such, the implications of these findings infer that miR-2285 may be a potential mediator of biological stress responses. This claim is further substantiated by the findings of Miretti et

al. (2018) that revealed that miR-2285 was significantly down-regulated in bovine mammary glands that were subjected to heat stress.

Similar findings were observed by Li et al. (2018) while characterizing the miRNA profiles dairy cattle that were exposed to heat stress. Furthermore, the researchers predicted such differences in expression were attributed to the regulation of the *Wnt/β, TGF-β,* and *MAPK* signaling pathways (Li et al., 2018). Next, miR-543 was investigated and was found to also possess roles in oncogenesis, immunity, and stress related responses. Chen et al. (2018) observed that the upregulation of miR-543 increased cellular proliferation and metastasis of renal cell carcinoma in humans. These researchers also observed that miR-543 demonstrated a strong affinity for *Dickkopf1 (**DKK1**)* and as such mediates aspects of the *Wnt/β-catenin* signaling pathway (Chen et al., 2018). *DKK1* is a known inhibitor of the *Wnt/β-catenin* pathway, which is a highly conserved pathway known to orchestrate key mechanisms involved in maintaining cellular homeostasis, proliferation, cell fate determination, cellular maintenance, cell polarity, and various aspects of the immune system (Logan and Nusse, 2004; Clevers, 2006; Staal et al., 2008; Chen et al., 2018).

Equally important, it has been reported that the upregulation of *miR-543* has been associated with lower expression levels of HSP40s (Evert et al., 2018). The members of the HSP40 family are J-domain proteins that function as co-chaperones to HSP70 (Li et al., 2009). In addition to the previously mentioned functions of HSPs, this HSP40-HSP70 complex has been reported to possess roles in the hydrolysis of ATP molecules (Li et al., 2009). Furthermore, miR-543 was found to promote the cellular proliferation and glycolysis in osteosarcoma cells via promoting the expression of hypoxia-inducible factor α (***HIF-α***) (Zhang et al., 2017). The HIF-α is a regulator of intracellular pH and a known

mediator of metabolic pathways (Weidemann and Johnson, 2008). During states of hypoxia HIF-α will regulate the metabolic utilization of O_2 and glucose in the generation of ATP (Weidemann and Johnson, 2008).

During this process, HIF-α also reduces the activity of the TCA cycle and mitochondrial respiration in order to limit the concentration of reactive oxygen species that are produced (Weidemann and Johnson, 2008). As such, it likely that miR-543 also possess roles in the mediation of cellular metabolism as well. Unfortunately, unlike the other miRNAs that were investigated, the literature pertaining to the potential targets and functions of *bta-miR-11994* were vanishingly small. Moreover, this miRNA appeared to be novel to cattle, and there were no significant homologs within other species that were found within the miRBase database that this miRNA could be compared to. The only study that was found that appeared to relevant to this miRNA was an investigative study that attempted to identify the regulatory roles of circulating miRNA in tick-resistance in beef cattle (Abeysinghe et al., 2021).

In this study the researchers reported that *miR-11994* was one of the more abundant differentially expressed exosomal miRNAs, and in most cases was found to be slightly upregulated in cattle that possessed higher levels of tick resistance (Abeysinghe et al., 2021). However, these findings were largely inconclusive and further research would be required to determine the significance of such an occurrence. The molecular mechanisms underlying tick resistance within cattle have been well studied and have been widely attributed to host immune responses (Robbertse et al., 2017). Based on this knowledge it is presumed that this miRNA may play a role in the regulation of pro-inflammatory immunological responses, however, this is purely speculative and further investigation is

required on this matter. While the lack of clarity pertaining to this miRNA is unfortunate it is not completely unexpected, nor does it rule out the possibility that this miRNA plays a role in the manifestation of dark-cutting. To date, the study of miRNAs as a whole remains a relatively new field of study, and the targets and biological roles of many miRNAs remain largely unknown, especially those miRNAs that are novel to non-model organisms.

Overall, it was found that many of the known biological processes that these 9 miRNAs have been reported to regulate (*e.g.* metabolism, adipogenesis, stress, immune responses, *etc*.) possess considerable overlap with those that contribute to the manifestation of DFD beef. Due to their biological relevance with the DFD phenotype, it is believed that these 9 miRNAs are suitable candidates for validation and follow-up experiments that further explore the physiological mechanisms that are involved in the manifestation of DFD beef. Furthermore, in addition to these 9 miRNAs, *miR-206* is also included in the list of candidate miRNAs that will be utilized in such follow-up analyses. Despite not satisfying the established threshold for fold difference when analyzed under the conditions of the DESeq2 software package, *miR-206* has been extensively reviewed and has many established functions that are of relevance to the dark-cutting phenotype. *miR-206* is a highly conserved miRNA that belongs to a subgroup of muscle specific miRNAs known as a myomiRs and is uniquely expressed specifically within skeletal muscle, more specifically those tissues primarily composed of slow-twitch/oxidative fibers (McCarthy, 2008; Ma et al., 2015). This miRNA exists as one of the most abundant miRNAs found within the skeletal muscle of vertebrates, and its regulatory roles in myogenesis have been firmly established within the literature (McCarthy, 2008; Ma et al., 2015).

This myomiR has been reported to directly mediate the expression of genes that are responsible for specification and differentiation of satellite cells during early stages of development, as well as the fiber type transitions that occur in adult skeletal muscle (McCarthy, 2008; Liu et al., 2012; Ma et al., 2015). Additionally, miR-206 plays key roles in regeneration and repair of injured skeletal muscle, as well as mediates signaling pathways that are associated with muscle hypertrophy and atrophy (Nakasa et al., 2010; Ma et al., 2015; D'Souza et al., 2017). Furthermore, it has been found that miR-206 has been associated with altered levels of aggression and stress. Chang et al. (2020) observed that mice that had been socially isolated post-weaning possessed higher expression levels of miR-206 and were more prone to exhibit more impulsive outbursts of aggression in response to acute stress. Liao et al. (2019) also observed that the expression of miR-206 was dysregulated in goats that were weaned early, which contributed to stress-induced growth retardation and poor development of skeletal muscle. Miretti et al. (2020) reported similar downregulations of miR-206 in domestic animals post-weaning.

For beef cattle the weaning process represents one of the most stressful phases during production process. During this time the calves will be subjected to numerous forms of physiological and psychological stress such as separation from their dam, alterations in diet, exposure to unfamiliar animals in new environments, a variety of physiological changes, and seasonal climates changes for those calves that were born during spring months. The effects of these stressful stimuli can negatively impact the health of the calves and the efficiency of production, potentially leading to lower daily gains in weight and a significantly lower carcass quality and tenderness (Gardner et al., 1999; McNeill, 1999; Fulton et al., 2002). It is for these reasons, that *miR-206* is believed to be a suitable

candidate for future follow-up analyses that further investigate physiological processes that influence the dark cutting phenotype.

The identification of these candidates only represents the first step in understanding the physiological roles of these miRNAs in the development of the dark cutting phenotype. Ultimately, the identification of each miRNA's target genes will be required to further alleviate this dilemma, as it will serve as the basis for truly understanding the physiological functions of these miRNAs. Unfortunately, the study of miRNAs remains relatively new, and at this time many of the target genes and regulatory roles of these candidate miRNAs have yet to be elucidated. As such, future research will consist of the identification of candidate mRNAs that are regulated by the miRNAs from the current dataset, a genome-wide association analysis to evaluate potential quantitative trait loci for susceptibility to dark-cutting phenotype, and lastly the validation of those miRNAs that are found to be statistically significant. In order to achieve this goal, the existing total RNA that was previously extracted will be re-sequenced using the Illumina NovaSeq 6000 sequencing platform to generate mRNA sequence data for each animal. This sequencer is advantageous for the current dataset because not only could all of the samples be sequenced simultaneously on a single flow cell, but this sequencer would provide the necessary sequencing depth (~ 30 million reads/sample) required for the analysis of mRNA.

While there currently is no set standard on the number of reads that are required per sample for mRNA-Seq datasets, the general consensus of the existing literature recommends between 20 - 60 million reads per sample for an accurate views of gene expression. Once sequenced, the quality of the mRNA-seq data will be assessed and any

low-quality sequence data along with the sequence adapters will be removed, and the remaining filtered mRNA sequence reads will be mapped to the most current *Bos taurus* genome (ARS-UCD1.2). The generated aligned read files will be used as input for the featureCounts or HTSeq-count software packages which will perform gene-level quantification and establish a mRNA expression profiles in the form of read counts for each sample (Liao et al., 2014; Anders et al., 2015; Conesa et al., 2016; Yao et al., 2019). Differential expression analysis will then be performed to determine the differences in mRNA expression levels between the two sample groups (NON and DFD) using the DESeq2 (v.1.34.0) software package (Love et al., 2014). Following this, the Qiagen Ingenuity Pathway Analysis (**IPA**) web-based functional analysis tool will be utilized to determine the mRNA targets for each miRNA, predict the relationship between these miRNAs and their respective targets, and identify any relevant molecular network that these miRNAs are associated with (Kramer et al., 2014). Lastly, the 10 proposed candidate miRNAs of the current study, along with any other miRNA and/or mRNA that is found to be statistically significant based on expression level and pathway analysis will be validated via qRT-PCR in order to confirm the results of this study.

Lastly, it is of note that there were limitations within the current experiment that should be taken into consideration. The first is associated with the samples and experimental design of the current study. The steers that were used in this research originally belonged to another unrelated tenderness study that took place in 2010. However, this herd was ultimately disqualified from the study due to the unexpected manifestation of high incidence of dark cutting. Meaning that there was no control or treatment groups that were designated, nor designed for the current study to prevent or

evoke the manifestation of the dark cutting phenotype. All animals within this study were subjected to varying degrees of stress that were beyond the control of the researchers (*e.g.* improper handling, fluctuations in weather, *etc*.), which resulted in random incidence of dark cutting to manifest throughout the herd. While it has been demonstrated within the literature that various forms of stress can lead to alterations in the miRNA expression patterns of domestic animals, such studies included control groups were the miRNA levels of non-stressed animals could be measured directly against those of the stressed animals (Yang et al., 2011; Zhao et al., 2012; Rao et al., 2017; Guo et al., 2020; Yadav et al., 2021).

These equally distributed levels of stress could potentially make it more difficult to identify significant changes in the expression levels of miRNAs that are associated with stress responses. Because in theory despite the presence of the dark cutting phenotype these miRNAs should also be altered in normal steers as well since they too were exposed to similar levels of chronic stress. Furthermore, another issue was that the samples are not truly independent of one another, which is an assumption of both the statistical approaches that were used in the current study. This assumption was violated because many of the steers that were incorporated within this study were genetically related. It was observed that out of the 78 steers that were utilized in the current study 70 (89%) were sired by only 13 separate bulls (Figure 2.1 & Table 2.2). Additionally, it was also found that a single bull (Sire ID 8048) sired 36% of the study's dark cutters (Figure 2.1 & Table 2.2). While this bull did indeed sire the largest number of offspring when compared to the other bulls, this increased prevalence of the DFD phenotype within the carcasses of its offspring indicates the involvement of potential heritability and genetic influences (Figure 2.1 & Table 2.2).

Lastly, there was an unexpected treatment administered to these steers without the researchers consent or knowledge until after the fact. This treatment consisted of the administration of bovine viral diarrhea vaccinations to 53 random steers within the herd, and of those 53 steers it was found that 15 developed the dark cutting phenotype (Table 2.2). While there exists no evidence to support the notion that this vaccination resulted in the manifestation of dark cutting without those steers, it is possible that the handling process during its administration could have aided to the increased stress levels of the animal. However, despite these limitations, it is believed that the findings of the current work remain significant and relevant to the understanding of the dark cutting phenotype. Despite being extensively reviewed, many of the physiological mechanisms involved in the development of this phenotype remain unknown. Furthermore, to date this phenotype remains highly difficult to study, because there still exists no method that allow for its consistent prediction or replication within a given population. So even though the acquisition of the dark cutting phenotype in multiple steers was not controlled, this sample set remains highly unique and can provide valuable insight into the enigmatic phenomenon.

In closing, the present study sought to elucidate the physiological roles and relevance of miRNAs in the manifestation of DFD beef. Using two statistical approaches, a total of 10 candidate miRNAs that possess known biological relevance to the DFD phenotype were selected for follow-up experiments and validation. Of these 10 candidates, a single miRNA (*bta-miR-2422*) was found to be upregulated in cattle with the DFD phenotype, as well as approach statistically significant ($p = 0.0541$) differential expression. Such findings are the first of their kind and establishes a starting point in the investigation

of understanding the relationship between miRNAs and the DFD phenotype, which will serve as a baseline for the findings of future studies to be compared to. As such, it is believed that these finding will not only contribute to the understanding of the physiological mechanisms that are involved in the dark cutting phenotype but will further elucidate the regulatory roles of several miRNAs that have yet to be defined. Such findings will not only serve as a comparative baseline for future studies but will ultimately lay the foundation for the development of various strategies that can be utilized in reducing the economic burden of the dark cutting phenotype.

CHAPTER V: SUMMARY & CONCLUSION

The current research was conducted to explore and demonstrate the utility of sequencing-based technologies, as well as their limitations within various aspects of the agricultural sciences. To achieve this, two independent studies were conducted using applications of high-throughput sequencing that focuses on two separate aspects of animal science: food safety and meat quality.

The first study demonstrated that both long- and short-read sequencing methodologies possess their own unique strengths and weaknesses. Long-read sequencing has a higher capacity in generating more complete genomic assemblies than the short-read sequencer, but also contained significantly more base calling errors and overall was less accurate. On the other hand, short-read methods are highly accurate and offered the precision and resolution required for investigative studies and certain targeted analyses but was not capable of producing sequences that span long repetitive genomic regions and large areas that are prone to rearrangement. However, it was found that neither of these two methods was sufficient alone to produce a completely closed microbial genome. Ultimately, the long- and short-read genome assemblies had to be combined in a hybrid fashion in order to generate a complete genome for the bacterial surrogates. Overall, the short-read and hybrid assemblies were significantly more accurate in understanding and predicting pathogenesis and antibiotic resistance than the long-read assemblies. The results of this study indicate that while there are many advantages to this technology, a fully closed bacterial genome is not required to determine pathogenesis, and that using WGS for

daily use in routine screening within a food processing facility's food safety program is highly impractical.

The second study sought to further elucidate the physiological mechanisms that contribute to the development of the dark cutting phenotype in beef cattle. This was achieved by comparing the differences in miRNA expression levels between the normal steers and those displaying the DFD phenotype via two statistical approaches. The Welch t-test offered a relatively good approximation in screening differentially expressed miRNAs between the two sample groups. However, due to the parametric nature of this test it does not offer an adequate statistical model for count data such as this and is likely to result in multiple Type I errors. Furthermore, CPM normalization is too simplistic and does not adequately control for the library composition of the dataset. DESeq2 was found offer a superior approach to normalization and statistical modeling.

Despite the theoretical differences that exist between both approaches there was considerable overlap in the top miRNAs that each identified. Ultimately, these analyses resulted in the identification of 10 candidate miRNAs for follow-up analysis that were found to possess potential biological relevance to the DFD phenotype. Of these candidate miRNA, a single miRNA (*bta-miR-2422*) was found to approach statistically significant ($p = 0.0541$) differential expression. While currently inconclusive, the results of the current study establish a starting point in uncovering the of the relationship between of miRNAs and the DFD phenotype. These findings can contribute to the development of various screening and intervention-based strategies that can be utilized in reducing the occurrence of this trait.

REFERENCES

Abeysinghe, P., N. Turner, H. Peiris, K. Vaswani, N. Cameron, N. McGhee, M. D. Mitcherll, and J. Logan. 2021. Differentially expressed extracellular vesicle, exosome and non-exosome miRNA profile in high and low tick-resistant beef cattle. *Front. Cell. Infect. Microbiol*. 11:780424.

Abril, M., M. M. Campo, A. Onenc, C. Sanudo, P. Alberti, and A. I. Negueruela. 2001. Beef color evolution as a function of ultimate pH. *Meat Sci.* 58:69-78.

Adams, M. R. and M. O. Moss. 2008. Chapter 7: Bacterial Agents of Foodborne Illness. In: Food Microbiology, 3rd Ed. Royal Society of Chemistry. Cambridge, UK. p. 182-269.

Afgan, E., D. Baker, B. Batut, M. Beek, D. Bouvier, M. Cech, J. Chilton, D. Clements, N. Coraor, B. Gruning, A. Guerler, J. H. Jackson, V. Jalili, H. Rasche, N. Soranzo, J. Goecks, J. Taylor, A. Nekrutenko, and D. Blankenberg. 2018. The galaxy platform for accessible, reproducible and collaborative biomedical analyses: 2018 update. *Nucleic Acids Res*. 46:W537-W544. doi:10.1093/nar/gky379.

Ahad, N. A. and S. S. S. Yahaya. 2014. Sensitivity analysis of welch's t-test. In: AIP Conference proceedings. 1605:888-893.

Allard, M. W., E. Strain, D. Melka, K. Bunning, S. M. Musser, E. W. Brown, and R. Timme. 2016. Practical value of food pathogen traceability through building a whole-genome sequencing network and database. *J. Clin. Micro*. 54:1975-1983.

Allard, M. W., R. Bell, C. M. Ferreira, N. Gonzalez-Escalona, M. Hoffmann, T. Muruvanda, A. Ottensen, P. Ramachandran, E. Reed, S. Sharma, E. Stevens, R. Timme, J. Zheng, and E. W. Brown. 2017. Genomics of foodborne pathogens for microbial food safety. *Curr. Opin. Biotechnol*. 49:244-229.

Almeida, M. I., R. M. Reis, and G. A. Calin. 2011. MicroRNA history: discovery, recent applications, and next frontiers. *Mutat. Res*. 717:1-8.

Alonge, M., S. Soyk, S. Ramakrishnan, X. Wang, S. Goodwin, F. J. Sedlazeck, Z. B. Lippman, and M. C. Schatz. 2019. RaGOO: fast and accurate reference-guided scaffolding of draft genomes. *Genome Biol*. 20:1-17.

Altschul, S. F., W. Gish, W. Miller, E. W. Myers, and D. J. Lipman. 1990. Basic local alignment search tool. *J. Mol. Biol.* 215:403-410. doi:10.1016/S0022-2836(05)80360-2.

Ambros, V. 2004. The functions of animal microRNAs. *Nature*. 431:350-355.

American Type Culture Collection. 2012a. Non-pathogenic *Escherichia coli* surrogate indicators panel. Available at: https://www.atcc.org/~/media/A0D8B646B84942088663F3B5A21CCAE8.ashx (Accessed 28 March 2019.)

American Type Culture Collection. 2012b. Table 1: summary of virulence testing performed by the *E. coli* reference center of pennsylvania state university (provided by the depositor). Available at: https://www.atcc.org/~/media/3C9579F7979A4968AE1F55A41360DC45.ashx (Accessed 28 March 2019.)

Anders S. and W. Huber. 2010. Differential expression analysis for sequence count data. *Genome Biol*. 11:R106.

Anders, S. P. T. Pyl, and W. Huber. 2015. HTSeq – a python framework to work with high-throughput sequencing data. *Bioninform*. 31:166-169.

Andrews, S. 2010. FastQC: a quality control tool for high throughput sequence data. Available at: http://biostars.org/p/180392/. (Accessed 26 November 2018.)

Apple, J. K., J. T. Sawyer, J-F. Meullenet. J. W. S. Yancey, and M. D. Wharton. 2011. Lactic acid enhancement can improve the fresh and cooked color of dark-cutting beef. *J. Anim. Sci*. 89:4207-4220. doi:10.2527/jas.2011-4147.

Araujo, J. P., J. M. Lorenzo, J. Cerqueira, J. A. Vazquez, P. Pires, J. Cantalapiedra, and D. Franco. 2016. Minhota breed cattle: carcass characterization and meat quality affected by sex and slaughter age. *Anim. Prod. Sci*. 56:2086-2092.

Ashmore, C. R., L. Doerr, and W. Parker. 1972. Respiration of mitochondria isolated from dark-cutting beef. *J. Anim. Sci*. 33:574-577.

Ashmore, C. R., F. Carroll, L. Doerr, G. Tompkins, H. Stokes, and W. Parker. 1973. Experimental prevention of dark-cutting meat. *J. Anim. Sci*. 36:33-36.

Ausubel, F. M., R. Brent, R. E. Kingston, D. D. Moore, J. G. Seidman, J. A. Smith, and K. Struhl. 1989. Short protocols in molecular biology, 1st ed. John Wiley & Sons, New York, NY.

Baccarini, A., H. Chauhan, T. J. Gardner, A. D. Jayaprakash, R. Scahidananda, and B. D. Brown. 2011. Kinetic analysis reveals the fate of a microRNA following target regulation in mammalian cells. *Curr. Biol*. 21:369-376. doi:10.1016/j.cub.2011.01.067.

Baek D, J. Villen, C. Shin, F. D. Camargo, S. P. Gygi, and D. P. Bartel. 2008. The impact of microRNAs on protein output. *Nature*. 455:64-71.

Baggish, A. L., A. Hale, R. B. Weiner, G. D. Lewis, D. Systrom, F. Wang, T. J. Wang, and S. Y. Chan. 2011. Dynamic regulation of circulating microRNA during acute exhaustive exercise and sustained aerobic exercise training. *J. Physiol*. 589:3983-3994. doi:10.1113/jphysiol.2011.213363.

Bankevich, A., S. Nurk, D. Antipov, A. A. Gurevich, M. Dvorkin, A. S. Kulikov, V. M. Lesin, S. I. Nikolenko, S. Pham, A. D. Prjibelski, A. V. Pyshkin, A. V. Sirotkin, N. Vyahhi, G. Tesler, M. A. Aleksetev, and P. A. Pevzner. 2012. SPAdes: a new genome assembly algorithm and its applications to single-cell sequencing. *J. Comp. Bio.* 19:455-477. doi:10.1089/cmb.2012.0021.

Barba, M. H. Czosenk, and A. Hadidi. 2014. Historical perspective, development, and application of next-generation sequencing in plant virology. *Viruses*. 6:106-136.

Bartel, D. P. 2004. MicroRNAs: genomics, biogenesis, mechanism, and function. *Cell*. 116:281-297.

Bartel, D. P. 2018. Metazoan microRNAs. *Cell*. 173:20-51.

Barzon, L., E. Lavezzo, V. Militello, S. Toppo, and G. Palu. 2011. Applications of next-generation sequencing technologies to diagnostic virology. *Int. J. Mol. Sci*. 12:7861-7884. doi:10.3390/ijms12117861.

Baszczak, J. A., T. Grandin, S. L. Gruber, T. E. Engle, W. J. Platter, S. B. Laudert, A. L. Schroeder, and J. D. Tatum. 2006. Effects of ractopamine supplementation on behavior of British, Continental, and Brahman crossbred steers during routine handling. *J. Anim. Sci.* 84:3410-3414.

Batz, M., S. Hoffman, and J. G. Morris. 2014. Disease-outcome trees, eq-5d scores, and estimated annual losses of quality-adjusted life years (qalys) for 14 foodborne pathogens in the United States. *Foodborne Pathog. Dis.* 11:395-402. doi:10.1089/fpd.2013.1658.

Bavagnoli, L., G. Campanini, M. Forte, G. Ceccotti, E. Percivalle, S. Bione, A. Lisa, F. Baldanti, and G. Maga. 2019. Identification of a novel antiviral micro-RNA targeting the NS1 protein of the H1N1 pandemic human influenza virus and a corresponding viral escape mutation. *Antiviral Res*. 171:104593.

Behm-Ansmant, I., J. Rehwinkel, T. Doerks, A. Stark, P. Bork, and E. Izaurralde. 2006. mRNA degradation by miRNAs and GW182 requires both CCR4_NOT deadenylase and DCP1:DCP2 decapping complexes. *Genes Dev*. 20:1885-1898. doi:10.1101/gad.1424106.

Benjamini, Y. and Y. Hochberg. 1995. Controlling the false discovery rate: a practical and powerful approach to multiple testing. *J. R. Stat. Soc. Series B. Stat. Methodol.* 57:289-300.

Benson, A., M. Cavanaugh, K. Clark, I. Karsch-Mizranchi, D. J. Lipman, J. Ostell, and E. W. Sayers. 2013. GenBank. *Nucleic Acids Res*. 41:D36-D42. doi:10.1093/nar/gks1195.

Bernstein, E., S. Y. Kim, M. A. Carmell, E. P. Murchison, H. Alcorn, M. Z. Li, A. A. Mills, S. J. Elledge, K. V. Anderson, and G. J. Hannon. 2003. Dicer is essential for mouse development. *Nat. Genet*. 35:215-217.

Beuchat, L. R., F. F. Busta, J. N. Farber, E. H. Garrett, L. J. Harris, M. E. Parish, and T. V. Suslow. 2001. Analysis and evaluation of preventive control measures for the control and reduction/elimination of microbial hazards on fresh and fresh-cut produce. *Compr. Rev. Food. Sci. Food Saf*. 25:1-200.

Bhaskaran, M. and M. Mohan. 2015. MicroRNAs: history, biogenesis, and their evolving role in animal development and disease. *Vet. Pathol*. 51:759-774. doi:10.1177/0300985813502820.

Biggar, K. K. and K. B. Storey. 2018. Functional impact of microRNA regulation in models of extreme stress adaptation. *J. Mol. Cell Biol*. 10:93-101.

Bintsis, T. 2017. Foodborne pathogens. *AIMS Microbiol*. 3:529-563. doi:10.3934/microbiol.2017.3.529.

Blattner, R. F., G. Plunkett, C. A. Bloch, N. T. Perna, V. Burland, M. Riley, J. Collado-Vides, J. D. Glasner, C. K. Rode, G. F. Mayhew, J. Gregor, N. W. Davis, H. A. Kirkpatrick, M. A. Goeden, D. J. Rose, B. Mau, and Y. Shao. 1997. The complete genome sequence of *Escherichia coli* K-12. *Science*. 277:1453-1462. doi:10.1126/science.277.5331.1453.

Boerlin, P., S. A. McEwen, F. Boerlin-Petzold, J. B. Wilson, R. P. Johnson, and C. L. Gyles. 1999. Associations between virulence factors of shiga toxin-producing *Escherichia coli* and disease in humans. *J. Clin. Microbiol*. 37:497-503.

Bolger, A. M.., M. Lohse, and B. Usadel. 2014. Trimmomatic: a flexible trimmer for illumina sequence data. *Bioinformatics*. 30:2114-2120.

Bost, F., M. Aouadi, L. Caron, and B. Binetruy. 2005. The role of MAPKs in adipocyte differentiation and obesity. *Biochimie*. 87:51-56. doi:10.1016/j.biochi.2004.10.018

Bourgon, R., R. Gentleman, and W. Huber. Independent filtering increases detection power for high-throughput experiments. *Proc. Natl. Acad. Sci. U.S.A.* 107:9546-9551.

Bouton, P. E., F. D. Carroll, P. V. Harris, and W. R. Shorthouse. 1973. Influence of pH and fiber contraction state upon factors affecting the tenderness of bovine muscle. *J. Food. Sci*. 38:404-407. doi:10.1111/j.1365-2621.1973.tb01440.x

Boykin C. A., L. C. Eastwood, M. K. Harris, D. S. Hale, C. R. Kerth, D. B. Griffin, A. N. Arnold, J. D. Hasty, K. E. Belk, D. R. Woerner, R. J. Delmore, J. N. Martin, D. L. VanOverbeke, G. G. Mafi, M. M. Pfeiffer, T. E. Lawrence, T. J. McEvers, T. B. Schmidt, R. J. Maddock, D. D. Johnson, C. C. Carr, J. M. Scheffler, T. D. Pringle, A. M. Stelzleni, J. Gottlieb, and J. W. Savell. 2017. National Beef Quality Audit - 2016: In-plant survey of carcass characteristics related to quality, quantity, and value of fed steers and heifers. *J Anim Sci*. 95:3003-3011. doi:10.2527/jas.2017.1544

Boža V., B. Brejová, and T. Vinař. 2017. Deepnano: deep recurrent neural networks for base calling in MinION nanopore reads. *PLos One*. 12:1-12.

Bracken, C. P., H. S. Scott, and G. J. Goodall. 2016. A network-biology perspective of microRNA function and dysfunction in cancer. *Nature Rev*. 17:719-732.

Braun, J. E., V. Truffault, A. Boland, E. Huntzinger, C. T. Chang, G. Haas, O. Weichenrieder, M. Coles, and E. Izaurralde. 2012. A direct interaction between DCP1 and XRN1 couples mRNA decapping to 5' exonucleolytic degradation. *Nat Struct Mol Biol*. 19:1324-31. doi:10.1038/nsmb.2413.

Braun, J. E., Huntzinger, E., Fauser, M. & Izaurralde, E. 2011. GW182 proteins directly recruit cytoplasmic deadenylase complexes to miRNA targets. *Mol. Cell* 44:120-133.

Bullard, H. J., A. E. Purdom, D. K. Hansen, S. Durinck, and S. Duboit. 2010. Evaluation of statistical methods for normalization and differential expression in mRNA-Seq experiments. *BMC Bioinformatics*. 11:94

Bushel, R. P., S. S. Ferguson, S. C. Ramaiahgari, R. S. Paules, and S. S. Auerbach. 2020. Comparison of normalization methods for analysis of tempo-seq targeted RNA sequencing data. *Front. Genet*. 11:594.

Busta, F. F., T. V. Suslow, M. E. Parish, L. R. Beuchat, J. N. Farber, E. H. Garrett, and L. J. Harris. 2006. The use of indicators and surrogate microorganisms for the evaluation of pathogens in fresh and fresh-cut produce. *Compr. Rev. Food. Sci. Food Saf.* 2:179-185.

Cabrera-Diaz, E., T. M. Moseley, L. M. Lucia, J. S. Dickson, A. Castillo, and G. R. Acuff. 2009. Fluorescent protein-marked *Escherichia coli* biotype I strains as surrogates for enteric pathogens in validation of beef carcass interventions. *J. Food Prot.* 2:295-303.

Cai, X., C. H. Hagedorn, and B. R. Cullen. 2004. Human microRNAs are processed from capped, polyadenylated transcripts that can also function as mRNAs. *RNA*. 10:1957-1966. doi:10.1261/rna.7135204.

Calkins, C. R. and J. M. Hodgen. 2007. A fresh look at meat flavor. *Meat Sci*. 77:63-80.

Caprioli, A., V. Falbo, M. Ruggeri, L. Baldassarri, R. Bisicchia, G. Ippolito, E. Romoli, and G. Donelli. 1987. Cytotoxic necrotizing factor production by hemolytic strains of *Escherichia coli* causing extraintestinal infections. *J. Clin. Microbiol*. 25:146-149.

Carver, T., S. R. Harris, M. Berriman, J. Parkhill, and J. A. McQuillan. 2012. Artemis: an integrated platform for visualization and analysis of high-throughput sequence-based experimental data. *Bioinformatics*. 28:464-469.

Castellani, A. and A. J. Chalmers. 1919. Manual of tropical medicine. Williams, Wood and Co., New York.

Ceelen, L. M., A. Decostere, R. Ductatelle, and F. Haesebrouck. 2006. Cytolethal distending toxin generates cell death by inducing a bottleneck in the cell cycle. *Microbiol. Res.* 161:109-120.

Centers for Disease Control and Prevention. 1993. Update: multistate outbreak of *Escherichia coli* O157:H7 infections from hamburgers--western United States, 1992-1993. *MMWR Morb. Mortal Wkly. Rep.* 42:258-263.

Centers for Disease Control and Prevention. 2014. *E. coli* (*Escherichia coli*): Questions & Answers. https://www.cdc.gov/ecoli/general/index.html (Accessed 15 May 2021.)

Centers for Disease Control and Prevention. 2015. Guide to confirming an etiology in foodborne disease outbreak. https://www.cdc.gov/foodsafety/outbreaks/investigating-outbreaks/confirming_diagnosis.html (Accessed 4 April 2018.)

Centers for Disease Control and Prevention. 2018a. Burden of foodborne illnesses in the United States. http://www.cdc.gov/foodborneburden/burden/index.html (Accessed 4 April 2018.)

Centers for Disease Control and Prevention. 2018b. Surveillance for foodborne disease outbreaks. https://www.cdc.gov/fdoss/pdf/2016_FoodBorneOutbreaks_508.pdf. Accessed 3 November 2018 (Accessed 4 April 2018.)

Chalfie, M., H. R. Horvitz, and J. E. Sulston. 1981. Mutations that lead to reiterations in the cell lineages of *C. elegans. Cell*. 24:59-69.

Chang, C., E. J. W. Kuek, C. Su, and P. Gean. 2020. MicroRNA-206 regulates stress-provoked aggressive behaviors in post-weaning social isolation mice. *Mol. Ther. Nucleic Acids*. 20:812-822.

Chekulaeva, M., H. Mathys, J. T. Zipprich, J. Attig, M. Colic, and R. Parker, W. Filipowicz. 2011. miRNA repression involves GW182-mediated recruitment of CCR4-NOT through conserved W-containing motifs. *Nat Struct Mol Biol*. 18:1218-26. doi:10.1038/nsmb.2166.

Chen, J. F., E. M. Mandel, J. M. Thomson, Q. Wu, T. E. Callis, S. M. Hammond, F. L. Conlon, and D. Z. Wang. 2006. The role of microRNA-1 and microRNA-133 in skeletal muscle proliferation and differentiation. *Nat. Genet*. 38:228-233.

Chen, L. H., J. Yang, J. Yu, Z. Yao, L. Sun, Y. Shen, and Q. Jin. 2005. VFDB: a reference database for bacterial virulence factors. *Nucleic Acids Res*. 33:D325-D328. doi:10.1093/nar/gki008.

Chen, L. H., Z. H. Xiong, L. L. Sun, J. Yang, and Q. Jin. 2012. VFDB 2012 update: toward the genetic diversity and molecular evolution of bacterial virulence factors. *Nucleic Acids Res*. 40: D641-D645. doi:10.1093/nar/gkr989.

Chen, L. H., D. D. Zeng, B. Lui, J. Yang, and Q. Jin. 2016. VFDB 2016: hierarchical and refined dataset for big data analysis-10 years on. *Nucleic Acids Res*. 44: D694-D697. doi:10.1093/nar/gkv1239.

Chen, S., L. Wang, B. Yao, Q. Liu, and C. Guo. 2019. miR-1307-3p promotes tumor growth and metastasis of hepatocellular carcinoma by repressing DAB2 interacting protein. *Biomed. Pharmacother*. 117:109055

Chen, Z., Y. Du, L. Wang, X. Liu, J. Guo, and X. Weng. 2018. MiR-543 promotes cell proliferation and metastasis of renal cell carcinoma by targeting dickkopf 1 through the Wnt/β-catenin signaling pathway. *J. Cancer*. 9:3660-3668.

Cheung, T. H., Quach, N. L., G. W. Charville, L. Lui, L. Park, A. Edalati, B. Yoo, P. Hoang, and T. A. Rando. 2012. Maintenance of muscle stem-cell quiescence by microRNA-489. *Nature*. 482:524-528.

Chomczynski, P. and K. Mackey. 1995. Substitution of chloroform by bromochloropropane in the single-step method of RNA isolation. *Anal. Biochem*. 1:163-164. doi:10.1006/abio.1996.1126.

Christie, M., A. Boland, E. Huntzinger, O. Weichenrieder, and E. Izaurralde. 2013. Structure of the PAN3 pseudokinase reveals the basis for interactions with the PAN2 deadenylase and the GW182 proteins. *Mol Cell*. 51:360-373. doi:10.1016/j.molcel.2013.07.011.

Chuang, T. Y., H. L. Wu, C. C. Chen, G. M. Gamboa, L. C. Layman, M. P. Diamond, R. Azziz, and Y. H. Chen. 2015. MicroRNA-223 expression is upregulated in insulin resistant human adipose tissue. *J. Diabet. Res*. 2015:943659.

Clevers, H. 2006. Wnt/beta-catenin signaling in development and disease. *Cell*. 127:469-480.

Cloonan, N., S. Wani, Q. Xu, J. Gu, K. Lea, S. Heater, C. Barbacioru, A. L. Steptoe, H. C. Martin, E. Nourbakhsh, K. Krishnan, B. Gardiner, X. Wang, K. Nones, J. A. Steen, N. A. Matigian, D. L. Wood, K. S. Kassahn, N. Waddell, J. Shepherd, C. Lee, J. Ichikawa, K. McKernan, K. Bramlett, S. Kuersten, and S. M. Grimmond. 2011. MicroRNAs and their isomirs function cooperatively to target common biological pathways. *Genome Biol*. 12:R126.

Code of Federal Regulations. 1996. Title 9 – Chapter III- Subchapter E- Part 417 – Hazard analysis and critical control point (HACCP) systems. https://ecfr.federalregister.gov/current/title-9/chapter-III/subchapter-E/part-417 (Accessed 9 May 2021.)

Conesa, A., P. Madrigal, S. Tarazona, D. Gomez-Cabrero, A. Cervera, A. McPherson, M. W. Szczesniak, D. J. Gaffney, L. L. Elo, X. Zhang, and A. Mortazavi. 2016. A survey of best practices for RNA-seq data analysis. *Genome Biol*. 17:13. doi:10.1186/s13059-016-0881-8

Cooper, G. M. 2000. Chapter 1: Cells as Experimental Models – *E. coli*. In: The Cell: A Molecular Approach, 2nd Edition, Sinauer Associates, Sunderland, MA.

Cornforth, D. P. and W. Egbert. 1985. Effect of rotenone and pH on the color of pre-rigor muscle. *J. Food Sci*. 50:34-35.

Cornforth, D., C. R. Calkins, and C. Faustman. 1991.Methods for identification and prevention of pink color in cooked meat. *Reciprocal Meat Conf. Proc*. 44:53-58

Cross, H. R., S. O. Sorinmade, and K. Ono. 1983. Effect of electrical stimulation on carcass from stressed and unstressed steers. *J. Food Quality*. 6:73-79.

Croxen, M. A., R. J Law, R. Scholz, K. M. Keeney, M. Wlodarska, and B. B. Finlay. 2013. Recent advances in understanding enteric pathogenic *Escherichia coli. Clin. Micrbiol. Rev*. 26:822-880.

D'Souza, R. F., J. F. Markworth, K. M. M. Aasen, N. Zeng, D. Cameron-Smith, C. J. Mitchell. 2017. Acute resistance exercise modulates microRNA expression profiles: combined tissue and circulatory targeted analyses. *PLoS One*. 12:e0181594.

Das, K., O. Garnica, and S. Dhandayuthapani. 2016. Modulation of host miRNAs by intracellular bacterial pathogens. *Fron. Cell Infect. Microbiol*. 6:79. doi:10.3389/fcimb.2016.00079

Davidsen, P. K., I. J. Gallagher, J. W. Hartman, M. A. Tarnopolsky, F. Delta, J. W. Helge, J. A. Timmons, and S. M. Phillips. 2011. High responders to resistance exercise training demonstrate differential regulation of skeletal muscle microRNA expression. *J. Appl. Physiol. (1985)*. 110:309-311. doi:10.1152/japplphysiol.00901.2010.

Davis-Dusenbery, B. N. and A. Hata. 2010. Mechanisms of control of microRNA biogenesis. J. Biochem. 148:381-392.

Dawes, M., K. J. Kochan, P. K. Riggs, and T. Lightfoot. 2015. Differential miRNA expression in inherently high- and low-active inbred mice. *Physiol. Reports*. 3:1-13.

Delacre, M., D. Lakens, and C. Leys. 2017.Why psychologists should by default use welch's t-test instead of student's t-test. *Int. Rev. Social Psych*. 30:92-101.

Deng, X., H. C. Bakker, and R. S. Hendriksen. 2016. Genomic epidemiology: whole-genome sequencing powered surveillance and outbreak investigation of foodborne bacterial pathogens. *Annu. Rev. Food Sci. Technol*. 7:353-374. doi:10.1146/annurev-food-041715-033259.

Dice, L. R. 1945. Measures of the amount of ecologic association between species. *Ecology*. 26: 297-302. doi: 10.2307/1932409.

Dickson, J. S. (Iowa State Universiy, Ames, Iowa, United States). Personal Communication, 2017

Dikeman, M. E. 2007. Effects of metabolic modifiers on carcass traits and meat quality. *Meat Sci*. 77:121-135.

Dillies, M., A. Rau, J. Aubert, C. Hennequet-Antier, M. Jeanmougin, N. Servant, C. Keime, G. Marot, D. Castel, J. Estelle, G. Guernec, B. Jagla, L. Jouneau, D. Laloë, C. Gall, B. Schaëffer, S. Crom, M. Guedj, and F. Jaffrézic. 2013. A comprehensive evaluation of normalization methods for illumina high-throughput RNA sequencing data analysis. *Brief. Bioinformatics*. 14:671-83.

Do, D. N., P. Dudemaine, B. E. Fomenky, and E. M. Ibeagha-Awemu. 2019. Integration of miRNA weighted gene co-expression network and miRNA-mRNA co-expression analyses reveals potential regulatory functions of miRNAs in calf rumen development. *Genomics*. 111:849-859.

Doyle, M. P., M. C. Erickson, W. Alali, J. Cannon, X. Deng, Y. Ortega, M. A. Smith, and T. Zhao. 2015. The food industry's current and future role in preventing microbial foodborne illness within the United States. *Clin. Inf. Disease*. 61:252-259. doi:10.1093/cid/civ253

Doyle, M., B. Phipson, J. Maksimovic, A. Trigos, M. Ritchie, H. Dashnow, S. Su, and C. Law. 2021. 2: RNA-seq counts to genes. Available at: https://training.galaxyproject.org/archive/2021-07-01/topics/transcriptomics/tutorials/rna-seq-counts-to-genes/tutorial.html#citing-this-tutorial (Accessed 7 March 2022.)

Dransfield, E. 1981. Eating quality of beef. In: D. Hood and P. Tarrant, editors. The problem of dark-cutting in beef. Leiden, Boston: Martinus Nijhoff Publisher. p. 334-358.

Dubrez, L., S. Causse, N. B. Bonan, B. Dumetier, and C. Garrido. 2020. Heat-shock proteins: chaperoning DNA repair. *Oncogene*. 39:515-529. doi:10.1038/s41388-019-1016-y

Eichhorn, S. W., H. Guo, S. E. McGeary, R. A. Rodriguez-Mias, C. Shin, D. Baek, S. H. Hsu, K. Ghoshal, J. Villén, and D. P. Bartel. 2014. mRNA destabilization is the dominant effect of mammalian microRNAs by the time substantial repression ensues. *Mol Cell*. 56:104-115. doi:10.1016/j.molcel.2014.08.028

Elwell, C., K. Chao, K. Patel, and L. Dreyfus. 2001. *Escherichia coli* cdtb mediates cytolethal distending toxin cell cycle arrest. *Infect. Immun*. 69:3418-3422. doi:10.1128/IAI.69.5.3418-3422.2001

English, A. R., K. M. Willis, B. N. Harsh, G. G. Mafi, D. L. VanOverbeke, and R. Ramanathan. 2016. Effects of aging on the fundamental color chemistry of dark-cutting beef. *J. Anim. Sci*. 94:4040-4048. doi:10.2527/jas2016-0561

Escherich, T. 1885. Die darmbakterien des neugeborenen und säuglings. *Fortschr. Med*. 3:515-522.

Evans, C., J. Hardin, and D. M. Stoebel. 2018. Selecting between-sample RNA-seq normalization methods from the perspective of their assumptions. *Brief. Bioinformatics*. 19:776-792.

Evert, O. B., R. Nalavade, J. Jungverdorben, F. Matthes, S. Weber, A. Rajput, S. Bonn, O. Brustle, M. Peitz, and S. Kraus. 2018. Upregulation of miR-370 and miR-543 is associated with reduced expression of heat shock protein 40 in spinocerebellar ataxia type 3. *PLoS ONE*. 13:e0201794.

Fabbri, A., M. Gauthier, and P. Boquet. 1999. The 5’ region of cnf1 harbours a translational regulatory mechanism for cnf1 synthesis and encodes the cell-binding domain of the toxin. *Mol. Microbiol*. 33:108-118.

Fabbri, A., S. Travaglione, and C. Fiorentini. 2010. *Escherichia coli* cytotoxic necrotizing factor 1 (cnf1): toxin biology, in vivo applications and therapeutic potential. *Toxins*. 2:283-296. doi:10.3390/toxins2020282

Fagerland, W. M. 2012. t-tests, non-parametric tests, and large studies – a paradox of statistical practice? *BMC Med. Res. Methol*. 12:78.

Falbo, V., T. Pace, L. Picci, E. Pizzi, and A. Caprioli. 1993. Isolation and nucleotide sequence of the gene encoding cytotoxic necrotizing factor 1 of *Escherichia coli*. *Infect. Immun*. 61:4909-4914.

Fang, Z., J. Martin, and Z. Wang. 2012. Statistical methods for identifying differentially expressed genes in RNA-Seq experiments. *Cell Biosci*. 2:26.

Fard, E. M., S. Moradi, N. N. Salekdeh, B. Bakhshi, M. R. Ghaffari, M. Zeinalabedini, and G. H. Salekdeh. 2020. Plant isomirs: origins, biogenesis, and biological functions. *Genomics*. 112:3382-3395.

Fatima, A. and D. G. Morris. 2013. MicroRNAs in domestic livestock. *Physiol. Genomics*. 45:685-696.

Ferguson, D. M., H. L. Bruce, J. M. Thompson, A. F. Egan, D. Perry, and W. R. Shorthose. 2001. Factors affecting beef palatability-farm gate to chilled carcass. *Aust. J. Exp. Agric.* 41:879-891.

Frenzel, M. A., J. W. Savell, K. B. Gehring, T. M. Taylor, and G. C. Smith. 2017. Evaluation of antimicrobial interventions applied during further processing of raw beef products to reduce pathogen contamination. PhD Diss. Texas A&M Univ., College Station. https://oaktrust.library.tamu.edu/bitstream/handle/1969.1/166061/FRENZEL-DISSERTATION-2017.pdf?sequence=1&isAllowed=y. (Accessed 12 November 2018.)

Friedlander, M. R., Mackowiak, S. D., Li, N., Chen, W., Rajewsky, N. 2012. miRDeep2 accurately identifies known and hundreds of novel microRNA genes in seven animal clades. *Nucleic Acids Res*. 20:37-52.

Friedlander, M. R., E. Lizano, A. J. Houden, D. Bezdan, M. Banez-Coronel, G. Kudla, E. Muteu-Huertas, B. Kagerbauer, J. Gonzalez, K. C. Chen, E. M. LeProust, E. Marti, and X. Estivill. 2014. Evidence for the biogenesis of more than 1,000 novel human microRNAs. *Gen. Biol.* 15:R57.

Friedman, R. C., K. K. -H. Farh, C. B. Burge, and D. P. Bartel. 2009. Most mammalian mRNAs are conserved targets of microRNAs. *Genome. Res*. 19:92-105.

Friedrich, A. W., S. Lu, M. Bielaszewska, R. Prager, P. Bruns, J. Xu, H. Tschäpe, and H. Karch. 2006. Cytolethal distending toxin in *Escherichia coli* O157:H7: spectrum of conservation, structure, and endothelial toxicity. *J. Clin. Microbiol*. 44:1844-1846. doi:10.1128/JCM.44.5.1844.-1846.2006

Frömmel, U., A. Böhm, J. Nitschke, J. Weinreich, J. Grob, S. Rödiger, T. Wex, H. Ansorge, O. Zinke, C. Schröder, D. Roggenbuck, and P. Schierack. 2013. Adhesion patterns of commensal and pathogenic *Escherichia coli* from humans and wild animals on human and porcine epithelial cell lines. *Gut Pathog*. 5:1-8. doi:10.1186/1757-4749-5-31

Fu. S., X. Bai, R. Fan, H. Sun, Y. Xu, and Y. Xiong. 2018. Genetic diversity of the enterohaemolysin gene (*ehxA*) in non-O157 Shiga toxin-producing *Escherichia coli* strains in China. *Sci. Rep*. 8:1-8.

Fulton, R. W., B. J. Cook, D. L. Step, A. W. Confer, J. T. Saliki, M. E. Payton, L. J. Burge, R. D. Welsch, and K. S. Blook. 2002. Evaluation of health status of calves and the impact on feedlot performance: assessment of a retained ownership program for postweaning calves. *Can. J. Vet. Res*. 66:173-180.

Galkin, V. E., S. Kolappan, D. Ng, Z. Zong, J. Li, X. Yu, E. H. Egelman, and L. Craig. 2013. The structure of the cs1 pilus of enterotoxigenic *Escherichia coli* reveals structural polymorphisms. *J. Bacteriol*. 195:1360-1370.

Garcia, A., J. G. Fox, and T. E. Besser. 2010. Zoonotic enterhemorrhagic *Escherichia coli*: a one health perspective. *ILAR*. J. 51:221-232.

Gardner, B. A., H. G. Dolezal, L. K. Bryant, F. N. Owens, and R. A. Smith. 1999. Health of finishing steers: effects on performance, carcass traits, and meat tenderness. *J. Anim. Sci.* 77:3168-3175. doi:10.2527/1999.77123168x

Garmire, X. L. and S. Subramaniam. 2012. Evaluation of normalization methods in mammalian microRNA-Seq data. *RNA*. 18:1279-1288. doi:10.1261/rna.030916.111

Gerbert, L. F. R. and I. J. MacRae. 2019. Regulation of microRNA function in animals. *Nature Rev*. 20:21-37.

Giani, A. M., G. R. Gallo, L. Gianfranceschi, and G. Formenti. 2020. Long walk to genomics: history and current approaches to genome sequencing and assembly. *Comp. and Struc. Biotech. Journal*. 18:9-19.

Gill, C. O. and K. G. Newton. 1977. The development of aerobic spoilage flora on meat stored at chill temperatures. *J. Appl. Bacteriol*. 43:189-195.

Gill, C. O. and K. G. Newton. 1979. Spoilage of vacuum-packaged dark, firm, dry meat at chill temperatures. *Appl. Environ. Microbiol*. 37:362-364.

Gill, C. O. and K. G. Newton. 1981. Microbiology of DFD beef. In: D. Hood and P. Tarrant, editors, The problem of dark-cutting in beef. Martinus Nijhoff Publisher, Leiden, Boston. p. 305-322.

Gill, C. O. and K. G. Newton. 1982. Effect of lactic acid concentration on growth on meat of gram-negative psychrotrophs from a meatworks. *Appl. Environ. Microbiol*. 43:284-288.

Giordano, F., L. Aigrain, M. A. Quail, P. Coupland, J. K. Bonfield, R. M. Davies, G. Tischler, D. K. Jackson, T. M. Keane, J. Yue, G. Liti, R. Durbin, and Z. Ning. 2017. De novo yeast genome assemblies from MinION, pacbio, and miseq platforms. *Sci. Rep*. 7:3935

Goetz, G. S., A. Mahmood, S. J. Hultgren, M. J. Engle, K. Dodson, and D. H. Alpers. 1999. Binding of pili from uropathogenic *Escherichia coli* to membranes secreted by human colonocytes and enterocytes. *Infect. Immun*. 67:6161-6163.

Goldstein, P. B. 2014. Resistance to rifampicin: a review. *J. Antibiotics.* 67:625-630.

Gómez-Duarte, O. G. and J. B. Kaper. 1995. A plasmid-encoded regulatory region activates chromosomal *eaeA* expression in enteropathogenic *Escherichia coli*. *Infect. Immun*. 63:1767-1776.

Goodwin, S., J. Gurtowski, S. Ethe-Sayers, P. Deshpande, M. C. Schatz, and W. R. McCombie. 2015. Oxford nanopore sequencing, hybrid error correction, and de novo assembly of a eukaryotic genome. *Gen Research*. 25:1750-1756. doi:10.1101/gr.191395.115

Goodwin, S., J. D. McPherson, and W. R. McCombie. 2016. Coming of age: ten years of next-generation sequencing technologies. *Nat. Rev. Genet*. 17:333-351. doi:10.1038/nrg.2016.49

Gordon, D. M. 2013. Chapter 1 – The ecology of *Escherichia coli*. In: M. S. Donnenberg, editor, *Escherichia coli*: Pathotypes and Principles of Pathogenesis, 2nd ed. p.3-20.

Grandin T. 1992. Problems with bruises and dark cutters in harvest steers/heifers. In: Improving the Consistency and Competitiveness of Beef – A Blueprint for Total Quality Management in the Fed-Beef Industry – The Final Report of the National Beef Quality Audit – 1991. Colorado State University, Fort Collins; Texas A&M University, College Station.

Grandin, T. 2020. Livestock handling at the abattoir: effects on welfare and meat quality. *Meat and Muscle Biol*. 4:1-11. doi:10.22175/mmb.9457.

Grayson, A. L., S. D. Shackelford, R. O. McKeith, D. A. King, R. K. Miller, and T. L. Wheeler. 2016. Effect of degree of dark cutting on tenderness and flavor attributes of beef. *J. Anim. Sci*. 94:2583-2591.

Grozdanov, L., C. Raasch, J. Schulze, U. Sonnenborn, G. Gottschalk, J. Hacker, and U. Dobrindt. 2004. Analysis of the genome structure of the nonpathogenic probiotic Escherichia coli strain Nissle 1917. *J. Bacteriol*. 186:5432-5441. doi:10.1128/JB.186.16.5432-5441.2004

Guerra, L., X. Cortes-Bratti, R. Guidi, and T. Frisan. 2011. The biology of the cytolethal distending toxins. *Toxins.* 3:172-190. doi:10.3390/toxins3030172

Gulyaeva, L. F. and N. E. Kushlinskiy. 2016. Regulatory mechanisms of microRNA expression. *J. Transl. Med*. 14:143. doi:10.1186/s12967-016-0893-x

Guo, J., W. Zhao, S. Zhan, L. Li, T. Zhong, L. Wang, Y. Dong, and H. Zhang. 2016. Identification and expression profiling of miRNAome in goat *longissimus dorsi* muscle from prenatal stages to a neonatal stage. *PLoS ONE.* 11:e0165764.

Guo, J., J. Yuan, H. R. Lui, S. Lian, H. Ji, L. Zhen, X. Zhang, S. Li, and H. Yang. 2020. Identification of transport stress miRNAs in beef cattle by high-throughput

sequencing and bioinformatics functional analysis. *Int. J. Agri. Biol*. 23:589-596. doi:10.17957/IJAB/15.1328

Guo, Y., X. Zhang, W. Huang, and X. Miao. 2017. Identification and characterization of differentially expressed miRNAs in subcutaneous adipose between wagyu and holstein cattle. *Nature: Sci. Reports*. 7:44026

Ha, M. and V. N. Kim. 2014. Regulation of microRNA biogenesis. *Nature Rev*. 15:509-524.

Hale, D. S., H. R. Cross, J. W. Savell, and G. C. Smith. 1988. USDA beef carcass grades: purpose and application. Texas Agricultural Extension Service. Available at: https://oaktrust.library.tamu.edu/handle/1969.1/174957 (Accessed 15 June 2021.)

Hale, D. S., K. Goodson, and J. W. Savell. 2013. USDA Beef Quality and Yield Grades. Available at: https://meat.tamu.edu/beefgrading/ (Accessed 15 June 2021.)

Hammond, S. 2015. An overview of microRNAs. *Adv. Drug Deliv. Rev*. 87:3-14. doi:10.1016/j.addr.2015.05.001

Han, J., Y. Lee, K. Yeom, J. Nam., I. Heo, J. Rhee, S. Y. Sohn, Y. Cho, B. Zhang, and V. N. Kim. 2006. Molecular basis for the recognition of primary microRNAs by the drosha-DGCR8 complex. *Cell*. 125:887-901.

Hanif, Q., M. Farooq, I. Amin, S. Mansoor, Y. Zhang, and Q. M. Khan. 2018. *In silico* identification of conserved miRNAs and their selective target gene prediction in indicine (*Bos indicus*) cattle. *PLoS One*. 12:e0206154.

Hardy Diagnostics. 2016. Instruction for Use: *Escherichia*. https://catalog.hardydiagnostics.com/cp_prod/Content/hugo/Escherichia.htm (Accessed 15 May 2021.)

Harfe, B. D., M. T. McManus, J. H. Mansfield, E. Hornstein, and C. J. Tabin. 2005. The rnaseIII enzyme dicer is required for morphogenesis but not patterning of the vertebrate limb. *Proc. Natl. Acad. Sci. USA.* 102:10898-10903. doi:10.1073/pnas.0504834102

Harris, J. J., H. R., Cross, J. W. Savell. 1996. History of Meat Grading in the United States. Available at: https://meat.tamu.edu/meat-grading-history/ (Accessed 10 June 2021.)

Harris, K. S., Z. Zhang, M. T. McManus, B. D. Harfe, and X. Sun. 2006. Dicer function is essential for lung epithelium morphogenesis. *Proc. Natl. Acad. Sci. USA.* 103:2208-2213. doi:10.1073/pnas.0510839103

Heather, J. M. and B. Chain. 2016. The sequence of sequencers: the history of sequencing DNA. *Genomics*. 107:1-8

Hedrick, H. B., J. B. Boillot, D. E. Brady, and H. D. Naumann. 1959. Etiology of dark-cutting beef. Research Bulletin 717. University MO, Agri. Exp. Stn., Columbia.

Hemsworth, P. H., M. Rice, M. G. Karlen, L. Calleja, J. L. Barnett, J. Nash, and G. J. Coleman. 2011. Human–animal interactions at abattoirs: relationships between handling and animal stress in sheep and cattle. *Appl. Anim. Behav. Sci*. 135:24-33.

Herbison, P. 2011. Analysing count data. Available at: https://www.ics.org/Abstracts/Publish/44/000161.pdf (Accessed 8 March 2022.)

Hoffman, S., B. B. Michael, and J. G. Morris. 2012. Annual cost of illness and quality-adjusted life year losses in the United States due to 14 foodborne pathogens. *J. Food. Saf.* 75:1292-1302. doi:10.4315/0362-028X.JFP-11-417

Hogue, A. T., P. L. White, and J. A. Heminover. 1998. Pathogen reduction and hazard analysis and critical control point (HACCP) systems for meat and poultry. *Micro. Foodborne Patho*. 14:151-164.

Hollins, S. L. and M. J. Cairns. 2016. MicroRNAs: small RNA mediators of the brain's genomic response to environmental stress. *Prog. Neurobiol*. 143:61-81.

Hood, L. and D. Galas. 2003. The digital code of DNA. *Nature*. 421:444-448.

Horak, M., J. Novak, and J. Bienertova-Vasku. 2016. Muscle-specific microRNAs in skeletal muscle development. *Dev. Biol*. 410:1-13.

Horvitz, H. R. and J. E. Sulston. 1980. Isolation and genetic characterization of cell-lineage mutants of the nematode *Caenorhabditis elegans*. *Genetics*. 96:435-454.

Howard, A. and R. A. Lawrie. 1956. Part II: Physiological and Biochemical Effects of Various Preslaughter Treatments. In: Studies on Beef Quality. H. M. Stationary Office, Melbourne, Australia. p. 1-79.

Hu, M. and B. J. Gurtler. 2017. Selection of surrogate bacteria for use in food safety challenge studies: a review. *J. Food Proc.* 80:1506-1536. doi:10.4315/0362-028XJFP-16-536

Huang, Y., X. J. Shen, Q. Zou, S. P. Wang, S. M. Tang, and G. Z. Zhang. 2011. Biological functions of microRNAs: a review. *J. Physiol. Biochem*. 67:129-139. doi:10.1007/s12105-010-0050-6

Humphreys, D. T., B. J. Westman, D. I. Martin, and T. Preiss. 2005. MicroRNAs control translation initiation by inhibiting eukaryotic initiation factor 4E/cap and poly(A) tail function. *Proc. Natl. Acad. Sci*. 102:16961-6.

Hutt, B. P. and B. P. Hutt II. 1984. A history of government regulation of adulteration and misbranding of food. *Food Drug Cosm Law J*. 39: 2-73.

Illumina. 2010. Illumina Sequencing Technology. https://www.illumina.com/documents/products/techspotlights/techspotlight_sequencing.pdf (Accessed 20 May 2021.)

Illumina. 2017. An Introduction to Next-Generation Sequencing Technology. https://www.illumina.com/content/dam/illumina-marketing/documents/products/illumina_sequencing_introduction.pdf. (Accessed 20 May 2021.)

Illumina. 2021. Explore Illumina sequencing technology. https://www.illumina.com/science/technology/next-generation-sequencing/sequencing-technology.html (Accessed 20 May 2021.)

Immonen, K., M. Ruusunen, K. Hissa, and E. Puolanne. 2000. Bovine muscle glycogen concentration in relation to finishing diet, slaughter and ultimate pH. *Meat Sci*. 55:25-31. doi:10.1016/s0309-1740(99)00121-7

Ingham, S. C., R. J. Algino, B. H. Ingham, and R. F. Schell. 2010. Identification of *Escherichia coli* O157:H7 surrogate organisms to evaluate beef carcass intervention treatment efficacy. *J. Food. Prot.* 73:1864-1874.

Inui, M., G. Martello, and S. Piccolo. 2010. MicroRNA control of signal transduction. *Nature*. 11:252-263.

Iqbal, A., J. Ping, S. Ali, G. Zhen, L. Juan, J. Z. Kang, P. Ziyi, L. Huixian, and Z. Zhihui. 2020. Role of microRNAs in myogenesis and their effects on meat quality in pig – a review. *AJAS*. 33:1873-1884.

Izumiya, M., N. Tsuchiya, K. Okamoto, and H. Nakagama. 2011. Systematic exploration of cancer-associated microRNA through functional screening assays. *Cancer Sci*. 102:1615-1621.

Jackson B. R., C. Tarr, E. Strain, K. A. Jackson, A. Conrad, H. Carleton, L. S. Katz, S. Stroika, L. H. Gould, R. K. Mody, B. J. Silk, J. Beal, Y. Chen, R. Timme, M. Doyle, A. Fields, M. Wise, G. Tillman, S. Defibaugh-Chavez, Z. Kucerova, A. Sabol, K. Roache, E. Trees, M. Simmons, J. Wasilenk, K. Kubota, H. Pouseele, W. Klimke, J. Besser, E. Brown, M. Allard, and P. Gerner-Smidt. 2016. Implementation of nationwide real-time whole-genome sequencing to enhance listeriosis outbreak detection and investigation. *Clin. Infect. Dis*. 63:380-386. doi:10.1093/cid/ciw242

Jacob, R. 2020. Implications of the variation in bloom properties of red meat: a review. *Meat Sci*. 162:108040.

Jagadeesan, B., P. Gerner-Smidt, M. W. Allard, S. Leuillet, A. Winkler, Y. Xiao, S. Chaffron, J. V. D. Vossen, S. Tang, M. Katase, P. McClure, B. Kimura, L. C. Chai, J. Chapman, and K. Grant. 2019. The use of next generation sequencing for improving food safety: translation into practice. *Food Microbiol.* 79:96-115.

Jain, M., S. Koren, K. H. Miga, J. Quick, A. C. Rand, T. A. Sasani, J. R. Tyson, A. D. Beggs, A. T. Dilthey, I. T. Fiddes, S. Malla, H. Marriott, T. Nieto, J. O'Grady, H. E. Olsen, B. S. Pederson, A. Rhie, H. Richardson, A. R. Quinlan, T. P. Snutch, L. Tee, B. Paten, A. M. Phillippy, J. T. Simpson, N. J. Loman, and M. Loose. 2018. Nanopore sequencing and assembly of a human genome with ultra-long reads. *Nat. Biotechnol*. 36:338-345.

Janka, A., M. Bielaszewska, U. Dobrindt, L. Greune, M. A. Schmidt, and H. Karch. 2003. Cytolethal distending toxin gene cluster in enterohemorrhagic *Escherichia coli* O157:H7: characterization and evolutionary considerations. *Infect. Immun*. 71:3634-3638. doi:10.1128/IAI.71.6.3634-3638.2003

Jeffries, C. D., H. M. Fried, and D. O. Perkins. 2009. Additional layers of gene regulatory complexity from recently discovered microRNA mechanism. *Intern. J. Biochem. Cell Biol.* 42:1236-1242.

Jego, G., A. Hazoumé, R. Seigneuric, and C. Garrido. 2013. Targeting heat shock proteins in cancer. *Cancer Lett*. 332:275-285

Jin, J. D. and C. A. Gross. 1988. Mapping and sequencing of mutations in the *Escherichia coli rpoB* gene that lead to rifampicin resistance. *J. Mol. Biol*. 202:45-58.

Jing, L., Y. Hou, H. Wu, Y. Miao, X. Li, J. Cao, J. M. Brameld, T. Parr, and S. Zhao. 2015. Transcriptome analysis of mRNA and miRNA in skeletal muscle indicates an important network for differential residual feed intake in pigs. *Nature: Sci. Reports*. 5:11953. doi:10.1038/srep11953

Joensen, K. G., A. M. Tezchner, A. Iguchi, F. M. Aarestrup, and F. Scheutz. 2015. Rapid and easy in silico serotyping of *Escherichia coli* using whole genome sequencing (WGS) data. *J Clin. Microbiol*. 53:2410-2426. doi:JCM.00008-15

Jonas, S., and E. Izaurralde. 2015. Towards a molecular understanding of microRNA-mediated gene silencing. *Nat. Rev. Genet*. 16:421-433.

Jovanovic, M. and M. O. Hengartner. 2006. miRNAs and apoptosis: RNAs to die for. *Oncogene*. 25:6176-6187.

Kalla, R., N. T. Ventham, N. A. Kennedy, J. F. Quintana, E. R. Nimmo, A. H. Buck, and J. Satsangi. 2015. MicroRNAs: new players in IBD. *Gut*. 64:504-517.

Kapps, M. and W. R. Lamberson. 2017. biostatistics for animal science. 3rd ed. CPI Group (UK) Ltd, Croydon, CR0.

Karlinski, J. 1889. Zur kenntnis des Bacillus enteritidis Gaertner. *Zentralbl. Bakteriol. Parasitenkd*. 6:289-292.

Kaspar, C. W., and M. L. Tamplin. 1993. Effects of temperature and salinity on the survival of *Vibrio vulnificus* in seawater and shellfish. *Appl. Environ. Microbiol*. 59:2425-2429.

Kauffmann, F. 1947. Review: the serology of the coli group. *J. Immun*. 57:71.100.

Kaur, M., A. Kumar, N. K. Siddaraju, M. N. Fairoze, P. Chhabra, S. Ahlawat, R. K. Vijh, A. Yadav, and R. Arora. 2020. Differential expression of miRNAs in skeletal muscles of Indian sheep with diverse carcass and muscle traits. *Nature: Sci. Reports*. 10:16332.

Kawamata, T and Y. Tomari. 2010. Making RISC. *Trends Biochem. Sci*. 35:368-376.

Kchouk, M., J. Gibrat, and M. Elloumi. 2017. Generations of sequencing technologies: from first to next generation. *Bio. Med*. 9:1-8. doi:10.4172/0974-8369.10000395

Keeling, C., S. E. Niebuhr, G. R. Acuff, and J. S. Dickson. 2009. Evaluation of *Escherichia coli* O157:H7 for cooking, fermentation, freezing, and refrigerated storage in meat processes. *J. Food Prot.* 72:728-732.

Kenny, F. J. and P. V. Tarrant. 1987. The behaviour of young Friesian bulls during social re-grouping at an abattoir. Influence of an overhead electrified wire grid. *App. Anim. Behav. Sci*. 18:233-246.

Ketting, R. F., S. E. J. Fischer, E. Bernstein, T. Sijen, G. J. Hannon, and R. H. A. Plasterk. 2001. Dicer functions in RNA interference and in synthesis of small RNA involved in developmental timing in C-elegans. *Genes Dev*. 15:2654-2659. doi:10.1101/gad.927801

Khan, N. A., Y. Wang, K. J. Kim, J. W. Chung, C. A. Wass, and K. S. Kim. 2002. Cytotoxic necrotizing factor-1 contributes to *Escherichia coli* K1 invasion of the central nervous system. *J. Biol. Chem.* 277:15607-15612.

Khvorova, A., A. Reynolds, and S. D. Jayasena. 2003. Functional siRNAs and miRNAs exhibit strand bias. *Cell*. 115:209-216.

Kiess, O. H. and B. A. Green. 2010. Statistical concepts for the behavioral sciences. 4th ed. Pearson Education, Boston, MA.

Kim, H. K., Y. S. Lee, U. Sivaprasad, A. Malhotra, and A. Dutta. 2006. Muscle-specific microRNA miR-206 promotes muscle differentiation. *J. Cell. Biol*. 174:677-687.

Kim, J., S. Park, and H. Lee. 2020. Diagnostic value of miR-1260b in cervical cancer: a pilot study. *Biomed. Sci. Letters*. 26:8-13.

Kim, V. N., J. Han, and M. C. Siomi.2009. Biogenesis of small RNAs in animals. *Nature Rev. Mol. Cell Biol*. 10:126-139.

Kirby, T. J. and J. J. McCarthy. 2013. MicroRNAs in skeletal muscle biology and exercise adaptation. *Free Radical Biol*. Med. 64:95-105.

Kloosterman, W. P. and R. H. Plasterk. 2006. The diverse function of micro-RNAs in animal development and disease. *Dev. Cell*. 11:441-450.

Knust, Z., B. Blumenthal, K. Aktories, and G. Schimdt. 2009. Cleavage of *Escherichia coli* cytotoxic necrotizing factor 1 is required for full biological activity. *Inf. Imm*. 77:1835-1841. doi:10.1128/IAI.01145-08

Kochan, K. J., S. E. Forman, A. E. Hillhouse, H. R. Cross, and P. K. Riggs. 2017. Methodology for quantification of circulating cell-free microRNA from bovine plasma for analysis of meat quality traits. *Proc. Assoc. Advmt. Anim. Breed Genet*. 22:469-472.

Kong, Z., C. Zhou, B. Li., J. Jiao, A. Ren, H. Jie, and Z. Tan. 2019. Integrative plasma proteomic and microRNA analysis of Jersey cattle in response to high-altitude hypoxia. *J. Dairy Sci*. 102:4606-4618.

Koren. S., B. P. Walenz, K. Berlin, J. R. Miller, N. H. Bergman, and A. M. Phillippy. 2017. Canu: scalable and accurate long-read assembly via adaptive k-mer weighting and repeat separation. *Genome Research*. 27:722-736.

Kozomara, A., M. Birgaoanu, and S. Griffiths-Jones. 2019. miRBase: from microRNA sequences to function. *Nucl. Acids Res*. 47:D155-D162.

Kramer, A., J. Green, J. Pollard, and S. Tugendreich. 2014. Causal analysis approaches in ingenuity pathway analysis. *Bioinformatics*. 30:523-30

Krol, J., I. Loedige, and W. Filipowicz. 2010. The widespread regulation of microRNA biogenesis, function and decay. *Nature Rev. Genet*. 11:597-610.

Kuehn, M. J., J. Hueser, S. Normark, and S. J. Hultgren. 1992. P pili in uropathogenic *E. coli* are composite fibres with distinct fibrillary adhesive tips. *Nature*. 356:252-255.

Lagos-Quintana, M., R. Rauhut, A. Yalcin, J. Meyer, W. Lendeckel, and T. Tuschl. 2002. Identification of tissue-specific microRNAs from mouse. *Curr. Biol*. 12:735-739. doi:10.1016/S0960-9822(02)00809-6

Lakicevic, B., I. Nastasijevic, and M. Dimitrijevic. 2017. Whole genome sequencing: an efficient approach to ensuring food safety. *IOP Conf. Ser.: Earth and Environ. Sci*. 85:012052. doi:10.1088/1755-1315/85/1/012052

Landgraf, P. M. Rusu, R. Sheridan, A. Sewer, N. Iovino, A. Aravin, S. Pfetter, A. Rice, A. O. Kamphorst, M. Landthaler, C. Lin, N. D. Socci, L. Herminda, V. Fulci, S. Chiaretti, R. Foa, J. Schliwka, U. Fuchs, A. Novosel, R. Muller, B. Schermer, U. Bissels, J. Inman, Q. Phan, M. Chien, D. B. Weir, R. Choksi, G. D. Vita, D. Frezzetti, H. Trompeter, V. Hornung, G. Teng, G. Hartmann, M. Palkovits, R. D. Lauro, P. Wernet, G. Macino, C. E. Rogler, J. W. Nagle, J. Ju, F. N. Papavasiliou, T. Benzing, P. Lichter, W. Tam, M. J. Brownstein, A. Bosio, A. Borkhardt, J. J. Russo, C. Sander, M. Zavolan, and T. Tuschl. 2007. A mammalian microRNA expression atlas based on small RNA library sequencing. *Cell*. 129:1401-1414. doi:10.1016/j.cell.2007.04.040

Lane, M. C., and H. L. T. Mobley. 2007. Role of p-fimbrial-mediated adherence in pyelonephritis and persistence of uropathogenic *Escherichia coli* (UPEC) in the mammalian kidney. *Kid. Int.* 72:19-25.

Lannoy, C., D. Riddler, and J. Risse. 2019. The long reads ahead: de novo genome assembly using the MinION [version 2; peer review: 2 approved]. *F1000 Research*. 6:1-26. doi:10.12688/f1000research.12012.2

Larsen, M. V., S, Cosentino, S. Rasmussen, C. Friis, H. Hasman, R. L. Marvig, L. Jelsback, T. Sicheritz-Pontén, D. W. Ussery, F. M. Aarestrup, and O. Lund. 2012. Multilocus sequence typing of total genome sequenced bacteria. *J. Clin. Microbiol*. 50:1355-1361. doi:10.12.0/JCM.06094-11

Lau, N. C., L. P. Lim, E. G. Weinstein, and D. P. Bartel. 2001. An abundant class of tiny RNAs with probable regulatory roles in *Caenorhabditis elegans*. *Science*. 294:858-862.

Law, C. W., M. Alhamdoosh, S. Su, X. Dong, L. Tian, G. K. Smyth, and M. E. Ritchie. 2018. RNA-seq analysis is easy as 1-2-3 with limma, glimma and edgeR. *F1000 Research*. 5:1408.

Law, D. 2000. A review: virulence factors of *Escherichia coli* O157 and other shiga toxin-producing *E. coli. J. App. Microbio*. 88:729-745.

Lawless, N., P. Vegh, C. O'Farrelly, and D. J. Lynn. 2014. The role of microRNAs in bovine infection and immunity. *Front. Immunol*. 5:611.

Lawrie, R. A. 1958. Physiological stress in relation to dark-cutting beef. *J. Sci. Food Agric*. 9:721-727.

Lean, I. J., J. M. Thompson, and F. R. Dunshea. 2014. A meta-analysis of zilpaterol and ractopamine effects on feedlot performance, carcass traits and shear strength of meat in cattle. *PloS One*. 9:e115904.

Ledward, D. A. 1985. Post-slaughter influences on the formation of metmyoglobin in beef muscles. *Meat Sci*. 15:149-171.

Lee, H., J. Gurtowski, S. Yoo, M. Nattestad, S. Marcus, S. Goodwin, W. R. McCombie, and M. C. Schatz. 2016. Third-generation sequencing and the future of genomics. *bioRxiv*. doi:10.1101/048603

Lee, R. C. and V. Ambros. 2001. An extensive class of small RNAs in *Caenorhabditis elegans*. *Science*. 294:862-864. doi:10.1126/science.1065329

Lee, R. C., R. L. Feinbaum, and V. Ambros. 1993. The *C. elegans* heterochronic gene *lin-4* encodes small RNAs with antisense complementarity to *lin-14*. *Cell*. 75:843-854. doi:10.1016/0092-8674(93)90529-Y

Lee, Y., K. Jeon, J. T. Lee, S. Kim, and V. N. Kim. 2002. MicroRNA maturation: stepwise processing and subcellular localization. *EMBO J*. 21:4463-4670.

Lee, Y., M. Kim, J. Han, K. Yeom, S. Lee, S. H. Baek, and V. N. Kim. 2004. MicroRNA genes are transcribed by RNA polymerase II. *EMBO J*. 23:4051-4060.

Lemichez, E., G. Flatau, M. Bruzzone, P. Boquet, and M. Gauthier. 1997. Molecular localization of the *Escherichia coli* cytotoxic necrotizing factor cnf1 cell-binding and catalytic domains. *Mol. Microbiol.* 24:1061-1070.

Leung, A. K. L., and P. A. Sharp. 2010. MicroRNA functions in stress responses. *Mol. Cell*. 40:205-215. doi:10.1016/j.molcel.2010.09.027

Leung, A. K. L. 2015. The whereabouts of miRNA actions: cytoplasm and beyond. *Trends Cell Biol.* 25:601-610. doi:10.1016/j.tcb.2015.07.005

Li, J., X. Qian, and B. Sha. 2009. Heat shock protein 40: structural studies and their functional implications. *Protein Pept. Lett.* 16:606-612.

Li, K., C. Wong, C. Cheng, S. Cheng, M. Li, S. Mansveld, A. Bergsma, T. Huang, M. J. T. Eijk, H. Lam. 2021. GmDNJ1, a type-I heat shock protein 40 (HSP40), is responsible for both growth and heat tolerance in soybean. *Plant Direct*. 5:e00298.

Li, Q., C. Yang, J. Du, B. Zhang, Y. He, Q. Hu, Q. Hu, M. Li, Y. Zhang, C. Wang, and J. Zhong. 2018. Characterization of miRNA profiles in the mammary tissue of dairy cattle in response to heat stress. *BMC Genomics*. 19:975.

Li, S. C., W. C. Chan, L. Y. Hu, C. H. Lai, C. N. Hsu, and W. C. Lin. 2010. Identification of homologous microRNAs in 56 animal genomes. *Genomics* 96:1-9. doi:10.1016/j.ygeno.2010.03.009

Li, X., N. G. F. Cooper, T. E. O'Toole, and E. C. Rouchka. 2020. Choice of library size normalization and statistical methods for differential gene expression analysis in balanced two-group comparisons for RNA-seq studies. *BMC Genomics*. 21:75.

Liao, R., Y. Lv, L. Zhu, and Y. Lin. 2019. Altered expression of miRNAs and mRNAs reveals the potential regulatory role of miRNAs in the developmental process of early weaned goats. *PLoS One*. 14:e0220907.

Liao, Y., G. K. Smyth, and W. Shi. 2014. featureCounts: an efficient general purpose program for assigning sequence reads to genomic features. *Bioinformatics*. 7:923-930.

Lillington, J., S. Geibel, and G. Waksman. 2014. Biogenesis and adhesion of type 1 and p pili. *Biochimica et Biophysica Acta.* 1840:2783-2793.

Lim, L. P., N. C. Lau, E. G. Weinstein, A. Abdelhakim, S. Yekta, M. W. Rhoades, C. B. Burge, and D. P. Bartel. 2003. The microRNAs of *Caenorhabditis elegans*. *Genes & Dev*. 17:991-1008. doi:10.1101/gad.1074403

Lim, Y. J., J. W. Yoon, and C. J. Hovde. 2010. A brief overview of *Escerichia coli* O157:H7 and its plasmid O157. *J. Microbiol. Biotechnol*. 20:5-14.

Lin, S., and R. I. Gregory. 2015. MicroRNA biogenesis pathways in cancer. *Nat Rev Cancer*. 15:321-33.

Liu, D., Q. Guan, M. Gao, L. Jiang, and H. Kang. 2016. miR-1260b is a potential prognostic biomarker in colorectal cancer. *Med. Sci. Monit*. 22:2417-2423. doi:10.12659/msm.898733

Liu, N., A. H. Williams, J. M. Maxeiner, S. Bezprozvannaya, J. M. Shelton, J. A. Richardson, R. Bassel-Duby, and E. N. Olson. 2012. microRNA-206 promotes skeletal muscle regeneration and delays progression of duchenne muscular dystrophy in mice. *J. Clin. Investig*. 122:2054-2065.

Logan, C. Y. and R. Nusse. 2004. The Wnt signaling pathway in development and disease. *Annu. Rev. Cell. Dev. Biol*. 20:781-810.

Loman, N. J. and M. J. Pallen. 2015. Twenty years of bacterial genome sequencing. *Nat. Rev. Microbiol*. 13:787-794. doi:10.1038/nrmicro3565

Loredo-Osti, J., E. Sánchez-López, A. Barreras-Serrano, F. Figueroa-Saaverdra, C. Pérez-Linares, M. Ruiz-Albarrán, and M. Á. Domínguez-Muñoz. 2019. An evaluation of environmental, intrinsic and pre- and post-slaughter risk factors associated to dark-cutting beef in federal inspected type slaughter plant. *Meat Sci.* 150:85-92.

Love, M. I., W. Huber, and S. Anders. 2014. Moderated estimation of fold change and dispersion for RNA-seq data with DESeq2. *Genome Biol*. 15:550. doi:10.1186/s13059-014-0550-8

Love, M. I., S. Anders, and W. Huber. 2021. Analyzing RNA-seq data with DESeq2. Available at: http://bioconductor.org/packages/devel/bioc/vignettes/DESeq2/inst/doc/DESeq2.html#the-deseq2-model (Accessed 1 December 2021.)

Lu. H., R. J. Buchan, and S. A. Cook. 2010. MicroRNA-233 regulates glut4 expression and cardiomyocyte glucose metabolism. *Cardiovasc. Res*. 86:410-420.

Lui, J., M. A. Valencia-Sanchez, G. J. Hannon, and R. Parker. 2005. MicroRNA-dependent localization of targeted mRNAs to mammalian p-bodies. *Nat. Cell Biol*. 7:719-723. doi:10.1038/ncb1274

Lund, E., S. Guttinger, A. Calado, J. E. Dahlberg, and U. Kutay. 2004. Nuclear export of microRNA precursors. *Science*. 303:95-98.

Luo, W., Q. Nei, and X. Zhang. 2013. MicroRNAs involved in skeletal muscle differentiation. *J. Genet. Genomics*. 40:107-116.

Lüth, S., S. Kleta, and S. A. Dahouk. 2018. Whole genome sequencing as a typing tool for foodborne pathogens like *Listeria monocytogenes* – The way towards global harmonization and data exchange. *Trends in Food Sci. & Tech*. 73:67-75.

Lysty, B., L. Engstrand, Å, Gustafsson, and R. Kaden. 2017. Time to review the gold standard for genotyping vancomycin-resistant enterococci in epidemiology: comparing whole-genome sequencing with pfge and mlst in three suspected outbreaks in Sweden during 2013-2015. *Inf. Gen. and Evo*. 54:74-80.

Ma, G., Y. Wang, Y. Li, L. Cui, Y. Zhao, and K. Li. 2015. MiR-206, a key modulator of skeletal muscle development and disease. *Int. J. Biol. Sci*. 11:345-352.

Ma, X., D. Wei, G. Cheng, S. Li, L. Wang, Y. Wang. X. Wang, S. Zhang, H. Wang, and L. Zan. 2018. Bta-miR-130a/b regulates preadipocyte differentiation by targeting *PPARG* and *CYP2U1* in beef cattle. *Mol. Cell. Probes*. 42:10-17.

MacDougall, D. B., B. G. Shaw, G. R. Nute, and D. N. Rhodes. 1979. Effect of pre-slaughter handling on the quality and microbiology of venison from farmed young red deer. *J. Sci. Food Agr.* 30:1160-1167.

MacRae, I. J., K. Zhou, and J. A. Doudna. 2007. Structal determinants of RNA recognition and cleavage by dicer. *Nat. Struct. Mol. Biol*. 14:934-940. doi:10.1038/nsmb1293

Mahjoub N, S. Dhorne-Pollet, W. Fuchs, M. E. Ahanda, E. Lange, B. Klupp, A. Arya, J. E. Loveland, F. Lefevre, T. C. Mettenleiter, and E. Giuffra. 2015. A 2.5-kilobase deletion containing a cluster of nine microRNAs in the latency-associated-transcript locus of the pseudorabies virus affects the host response of porcine trigeminal ganglia during established latency. *J. Virol*. 89:428-442. doi:10.1128/JVI.02181-14

Mahmood, S., B. C. Roy, I. L. Larsen, J. L. Aalhus, W. T. Dixon, and H. L. Bruce. 2017. Understanding the quality of typical and atypical dark cutting beef from heifers and steers. *Meat Sci*. 133:75-85. doi:10.1016/j.meatsci.2017.06.010

Maio, N. D., L. P. Shaw, A. Hubbard, S. George, N. Sanderson, J. Swann, R. Wick, M. AbuOun, E. Stubberfield, S. J. Hoosdally, D. W. Crook, T. E. A. Peto, A. E. Sheppard, M. J. Bailey, D. S. Read, M. F. Anjum, A. S. Walker, and N. Stoesser. 2019. Comparison of long-read sequencing technologies in the hybrid assembly of complex bacterial genomes. *bioRxiv*. doi:10.1101/530824

Marioni, C. J., E. C. Mason, M. S. Mane, M. Stephens, and Y. Gilad. 2008. RNA-seq: an assessment of technical reproducibility and comparison with gene expression arrays. *Genome Res*. 18:1509-1517.

Marshall, K. M., S. E. Niebuhur, G. R. Acuff, L. M. Lucia, and J. S. Dickson. 2005. Identification of *Escherichia coli* O157:H7 meat processing indicators for fresh meat through comparison of the effects of selected antimicrobial interventions. *J. Food. Prot.* 68:2580-2586.

Massey, J. F. 1951. The Kolmogorov-smirnov test for goodness of fit. *J. American Stat. Ass*. 46:68-78.

Mathys, H. J. Basquin, S. Ozgur, M. Czarnocki-Cieciura, F. Bonneau, A. Aartse, A. Dziembowski, M. Nowotny, E. Conti, and W. Filipowicz. 2014. Structural and biochemical insights to the role of the CCR4-NOT complex and DDX6 ATPase in microRNA repression. *Mol Cell*. 54:751-65. doi:10.1016/j.molcel.2014.03.036

McCarthy. 2008. MicroRNA-206: the skeletal muscle-specific myomiR. *Biochim. Biophys. Acta.* 1779:682-601

McGilchrist, P., C. L. Alston, G. E. Gardner, K. L. Thomson, D. W. Pethick. 2012. Beef carcass with larger eye muscle areas, lower ossification scores and improved nutrition have a lower incidence of dark cutting. *Meat Sci.* 92:474-480. doi:10.1016/j.meatsci.2012.014

McGregor, R. A. and M. S. Choi. 2011. microRNAs in the regulation of adipogenesis and obesity. *Curr. Mol. Med*. 11:304-316.

McKeith, R. O., D. A. King, A. L. Grayson, S. D. Shackelford, K. B. Gehring, J. W. Savell, and T. L. Wheeler. 2016. Mitochondrial abundance and efficiency contribute to lean color of dark cutting beef. *Meat Sci*. 116:165-173. doi: 10.1016/j.meatsci.2016.01.016

McNeill, J. W. 1999. ASWeb-026. Available at: http://animalscience.tamu.edu/wp-content/uploads/sites/14/2012/04/beef-r2r-4yrsummary.pdf (Accessed 12 January 2022.)

Mellies, J. L., S. J. Elliot, V. Sperandio, M.S. Donnenberg, and J. B. Kaper. 1999. The Per regulon of enteropathogenic *Escherichia coli*: identification of a regulatory cascade and a novel transcriptional activator, the locus of enterocyte effacement (LEE)-encoded regulator (Ler). *Mol. Microbiol.* 33:296-306.

Melton-Celsa, A. R., S. C. Darnell, and A. D. O'Brien. 1996. Activation of shiga-like toxins by mouse and human intestinal mucus correlates with virulence of enterohemorrhagic *Escherichia coli* O91:H21 isolates in orally infected, streptomycin-treated mice. *Infect. Immun*. 64:1569-1576.

Mendell, T. J. and E. N. Olson. 2012. MicroRNAs in stress signaling and human disease. *Cell*. 148:1172-1187.

Mendenhall, V.T. 1989. Effect of pH and total pigment concentration on the internal color of cooked ground beef patties. *J. Food Sci*. 54: 1-2

Michino, H., K. Araki, S. Minami, S. Takaya, N. Sakai, M. Miyazaki, A. Ono, and H. Yanagawa. 1998. Massive outbreak of *Escherichai coli* O157:H7 infection in schoolchildren in Sakai City, Japan, associated with consumption of white radish sprouts. *Am. J. Epidemiol*. 8:787-796. doi:10.1093/oxfordjournals.aje.a010082

Miller, D. J. and P. E. Fort. 2018. Heat shock proteins regulatory role in neurodevelopment. *Front. Neurosci*. 12:821. doi:10.3389/fnins.2018.00821

Miller, M. 2007. Dark, firm, and dry beef. BEEF FACTS Product Enhancement. Available at: https://fyi.extension.wisc.edu/wbic/files/2011/04/Dark-Firm-and-Dry-Beef.pdf (Accessed 26 August 2021.)

Miretti, S., C. Lecchi, F. Ceciliani, and M. Baratta. 2020. MicroRNAs as biomarkers for animal health and welfare in livestock. *Front. Vet. Sci*. 7:578193.

Moiseev, I. V. and D. P. Cornforth. 1999. Treatments for prevention of persistent pinking in dark-cutting beef patties. *J. Food Sci*. 64:738-743.

Moore M. C., G. D. Gray, D. S. Hale, C. R. Kerth, D. B. Griffin, J. W. Savell, C. R. Raines, K. E. Belk, D. R. Woerner, J. D. Tatum, J. L. Igo, D. L. VanOverbeke, G. G. Mafi, T. E. Lawrence, R. J. Delmore Jr., L. M. Christensen, S. D. Shackelford, D. A. King, T. L. Wheeler, L. R. Meadows, and M. E. O'Connor. 2012. National Beef Quality Audit–2011: In-plant survey of targeted carcass characteristics related to quality, quantity, value, and marketing of fed steers and heifers. *J. Anim. Sci*. 90:5143–5151. doi:10.2527/jas.2012-5550

Morenikeji, O. B., M. E. Hawkes, A. O. Hudson, and B. N. Thomas. 2019. Computational network analysis identifies evolutionarily conserved miRNA gene interactions potentially regulating immune response in bovine typanosomosis. *Front. Microbiol*. 10:1-14.

Mortezaei, N., C. R. Epler, P. P. Shao, M. Shirdel, B. Singh, A. McVeigh, B. E. Uhlin, S. J. Savarino, M. Andersson, and E. Bullitt. 2015. Structure and function of enterotoxigenic *Escherichia coli* fimbriae from differing assembly pathways. *Mol. Microbiol.* 95:116-126. doi:10.1111/mmi.12847

Mounier, L. H. Dubroeucq, S. Andanson, and I. Veissier. 2006. Variations in meat pH of beef bulls in relation to conditions of transfer to slaughter and previous history of the animals. *J. Anim. Sci*. 84:1567-1576.

Murano, A. E., H. R. Cross, and P. K. Riggs. 2018. The outbreak that changed meat and poultry inspection system worldwide. *Animal Frontiers*. 8:4-8. doi:10.1093/af/vfy017

Nada, R. A., H. I. Shaheen, S. B. Khalil, A. Mansour, N. El-Sayed, I. Touni, M. Weiner, A. W. Armstrong, and J. D. Klena. 2011. Discovery and phylogenetic analysis of novel members of class b enterotoxigenic *Escherichia coli* adhesive fimbriae. *J. Clin. Microbiol*. 49:1403-1410. doi:10.1128/JCM.02006-10

Nakasa, T., M. Ishikawa, M. Shi, H. Shibuya, N. Adachi, and M. Ochi. 2010. Acceleration of muscle regeneration by local injection of muscle-specific microRNAs in rat skeletal muscle injury model. *J. Cell. Mol. Med*. 14: 495-2505.

Naseer, U., I. Lobersli, M. Hindrum, T. Bruvik, and L. T. Brandal. 2017. Virulence factors of shiga toxin-producing *Escherichia coli* and the risk of developing haemolytic uraemic syndrome in Norway, 1992-2013. *Eur. J. Clin. Microbiol. Infect. Dis*. 36:1613-1620. doi:10.1007/s10096-017-2974-z

Nataro, J. P. and J. B. Kaper. 1998. Diarrheagenic *Escherichia coli. Clin. Microbiol. Rev*. 11:142-201.

National Advisory Committee on Microbiological Criteria for Foods. 1992. National Advisory Committee on Microbiological Criteria for Foods, Hazard Analysis and Critical Control Point System. *Int. J. Food. Microbio*. 16:1-23

National Center for Biotechnology Information. 2017. Genome. Available at: https://www.ncbi.nlm.nih.gov/genome (Accessed 1 December 2021.)

Nesic D., Y. Hsu, and C. E. Stebbins. 2004. Assembly and function of a bacterial genotoxin. *Nature.* 429:429-433.

Nicholson, A. W. 2014. Ribonuclease III mechanisms of double-stranded RNA cleavage. *WIREs RNA*. 5:31-48.

Niebuhr, S. E., A. Laury, G. R. Acuff, and J. S. Dickson. 2008. Evaluation of nonpathogenic surrogate bacteria as process validation indicators for *Salmonella entericia* for selected antimicrobial treatments, cold storage, and fermentation in meat. *J. Food. Prot.* 71:714-718.

Nottrott, S., M. J. Simard, and J. D. Richter. 2006. Human let-7a miRNA blocks protein production on actively translating polyribosomes. *Nature Struct. Mol. Biol*. 13:1108-1114.

O'Brien, J., H. Hayder, Y. Zayed, and C. Peng. 2018. Overview of microRNA biogenesis, mechanisms of action, and circulation. *Front. Endocrin*. 9:1-12. doi:10.3389/frendo.2018.00402

O'Rourke, J. R., S. A. Georges, H. R. Seay, S. J. Tapscott, M. T. McManus, D. J. Goldhamer, M. S. Swanson, and B. D. Harfe. 2007. Essential role for dicer during skeletal muscle development. *Dev. Biol*. 311:359-368.

Okada, C., E. Yamashita, S. J. Lee, S. Shibata, J. Katahira, A. Nakagawa, Y. Yoneda, and T. Tsukihara. 2009. A high-resolution structure of the pre-microRNA nuclear export machinery. *Science*. 326:1275-1279.

Olejniczak, M., A. Kotowska-Zimmer, and W. Kryzyzosiak. 2018. Stress-induced changes in miRNA biogenesis and functioning. *Cell. Mol. Life Sci*. 75:177-191.

Oliveira, P. S. N., L. L Coutinho, A. S. M. Cesar, W. J. S. Diniz, M. M. Souza, B. G. Andrade, J. E. Koltes, G. B. Mourao, A. Zerlotini, J. M. Reecy, and L. C. A. Regitano. 2019. Co-expression networks reveal potential regulatory roles of miRNAs in fatty acid composition of nelore cattle. *Front. Genet*. 10:651. doi:10.3389/fgene.2019.00651

Ostroff, S. M., P. I. Tarr, M. A. Neill, J. H. Lewis, N. Hargrett-Bean, and J. M. Kobayashi. 1989. Toxin genotypes and plasmid profiles as determinants of systemic sequelae in *Escherichia coli* O157:H7 infections. *J. Infect. Dis.* 160:994-998.

Ott, L. R. and M. Longnecker. 2016. An introduction to statistical methods & data analysis. 7th ed. Cengage Learning, Boston, MA.

Oxford Nanopore Technologies. 2016. Sequencing library preparation for MinION and PromethION. https://nanoporetech.com/sites/default/files/s3/2016-07/libprepv1.pdf (Accessed 15 May 2021.)

Oxford Nanopore Technologies. 2018. Rapid Barcoding Sequencing (SQK-RBK004). https://community.nanoporetech.com/protocols/rapid-barcoding-kit-96-sqk-rbk110-96/checklist_example.pdf (Accessed 15 May 2021.)

Oxford Nanopore Technologies. 2020. Rapid Barcoding Kit 96. https://store.nanoporetech.com/us/catalog/product/view/id/508/s/rapid-barcoding-kit-96/category/28/ (Accessed 15 May 2021.)

Page, J. K., D. M. Wulf, and T. R. Schwotzer. 2001. A survey of beef muscle color and pH. *J. Anim. Sci*. 79:598-604.

Park, J. I. Heo, Y. Tian, D. K. Simanshu, H. Chang, D. Jee, D. J. Patel, and V. N. Kim. 2011. Dicer recognizes the 5' end of the RNA for efficient and accurate processing. *Nature*. 475:201-205.

Park, Y. C., Y. S. Choi, and M. T. McManus. 2010. Analysis of microRNA knockouts in mice. *Hum. Mol. Genet*. 19:R169-R175.

Parker, R. and U. P. Sheth. 2007. P bodies and the control of mRNA translation and degradation. *Mol. Cell*. 25:635-646. doi:10.1016/j.molcel.2007.02.011

Pasquinelli, A. E., B. J. Reinhart, F. Slack, M. Q. Martindale, M. I. Kuroda, B. Maller, D. C. Hayward, E. E. Ball, B. Degnan, P. Muller, J. Spring, A. Srinivasan, M. Fishman, J. Finnerty, J. Corbo, M. Levine, P. Leahy, E. Davidson, and G. Ruvkun. 2000. Conservation of the sequence and temporal expression of *let-7* heterochronic regulatory RNA. *Nature*. 408:86-89. doi:10.1038/35040556

Pasquinelli, A. E. 2012. MicroRNAs and their targets: recognition, regulation and an emerging reciprocal relationship. *Nat. Rev. Genet*. 13:271-282.

Paton, A. W. and J. C. Paton. 1999. Direct detection of shiga toxigenic *Escherichia coli* strains belonging to serogroups O111, O157, and O113 by multiplex pcr. *J. Clin. Microbiol*. 37:3362-3365.

Paul, P., A. Chakraborty, D. Sarkar, M. Langthasa, M. Rahman, M. Bari, R. K. S. Singha, A. K. Malakar, and S. Chakraborty. 2017. Interplay between miRNAs and human disease. J. Cell. Phys. 233:2007-2018. doi:10.1002/jcp.25854

Payne, A., N. Holmes, V. Rakyan, and M. Loose. 2019. BulkVis: a graphical viewer for oxford nanopore bulk FAST5 files. *Bioinformatics*. 35:349-353.

Peltier, H. J. and G. J. Latham. 2008. Normalization of microRNA expression levels in quantitative RT-PCR assays: Identification of suitable reference RNA targets in normal and cancerous human solid tissues. *RNA*. 14:844-852.

Percival, S. L. and D. W. Williams. 2014. Chapter six – Escherichia coli. In: S. L. Percival, M. V. Yates, D. W. Williams, R. M. Chalmers, and N. F. Gray, editors, Microbiology of Waterborne Diseases, 2nd edition. Academic Press, San Diego, CA. p. 89-117.

Pickett, C. L., and C. A. Whitehouse. 1999. The cytolethal distending toxin family. *Nat. Rev*. 7:292-297.

Pillai, R. S., S. N.Bhattacharyya, C. G. Artus, T. Zoller, N. Cougot, E. Basyuk, E. Bertrand, and W. Filipowicz. 2005. Inhibition of translational initiation by *let-7* MicroRNA in human cells. *Science*. 309:1573-1576. doi:10.1126/science.1115079

Place, R. F., L. Li, D. Pookot, E. J. Noonan, and R. Dahiya. 2008. MicroRNA-373 induces expression of genes with complementary promoter sequences. *PNAS*. 105:1608-1613.

Pollard, M. O., D. Gurdasani, A. J. Mentzer, T. Porter, and M. S. Sandhu. 2018. Long reads: their purpose and place. *Hum. Mol. Gen*. 27:R234-R241. doi:10.1093/hmg/ddy177

Ponnampalam, E. N., D. L. Hopkins, H. Bruce, D. Li, G. Baldi, and A. E. Bekhit. 2017. Causes and contributing factors to “dark cutting” meat: current trends and future directions: a review. *Comp. Rev. in Food Sci. and Food Saf.* 16:400-430. doi:10.1111/1541-4337.12258

Portmann, A., C. Fournier, J. Gimonet, C. Ngom-Bru, C. Barretto, and L. Baert. 2018. A validation approach of an end-to-end whole genome sequencing workflow for source tracking of *Listeria monocytogenes* and *Salmonella enterica*. *Front. Microbiol*. 9:1-13. doi:10.3389/fmicb.2018.00446

Qi, L., K. Wang, H. Chen, X. Lui, J. Lv, S. Hou, Y. Zhang, and Y. Sun. 2019. Host microRNA miR-1307 suppresses foot-and-mouth disease virus replication by promoting VP3 degradation and enhancing innate immune response. *Virology*. 535:162-70. doi:10.1016/j.virol.2019.07.009

Qi, R., H. Liu, Q. Wang, J. Wang, F. Yang, D. Long, and J. Huang. 2018. Expressions and regulatory effects of P38/ERK/JNK mapks in the adipogenic trans-differentiation of C2C12 myoblasts. *Cell. Phys. Biochem*. 44:2467-2475.

Quinn, P. T., T. M. Crowley, and M. F. Richardson. 2018. Benchmarking differential expression analysis tools for RNA-Seq: normalization-based vs. log-ratio transformation-based methods. *BMC Bioinformatics*. 19:274.

Quinlan, R. A. and I. M. Hall. 2010. Bedtools: a flexible suite of utilities for comparing genomic features. *Bioinformatics*. 26:841-842.

Rajesh, T. and M. Jaya. 2017. Chapter 7 – Next-Generation Sequencing Methods. In: P. Gunasekaran, S. Noronha, and A. Pandey, editors, Current Developments in Biotechnology and Bioengineering: Functional Genomics and Metabolic Engineering, 1st ed. Elsevier, San Diego, CA. p. 143-158.

Rantsiou, K., S. Kathariou, A. Winkler, P. Skandamis, M. J. Saint-Cyr, K. Rouzeau-Szynalski, and A. Amézquita. 2018. Next generation microbial risk assessment: opportunities of whole genome sequencing (WGS) for foodborne pathogen surveillance, source tracking and risk assessment. *Int. J. Food Microbiol*. 287:3-9. doi:10.1016/j.ijfoodmicro.2017.11.007

Rao, M., Z. Zeng, L. Tang, G. Cheng, W. Xia, and C> Zhu. 2017. Next-generation sequencing-based microRNA profiling of mice testis subjected to transient heat stress. *Oncotarget*. 8:111672-111682.

Raza, S. H. A., N. Kaster, R. Khan, S. A. Abdelnour, M. E. A. El-Hack, A. F. Khafaga, A. Taha, H. Ohran, A. A. Swelum, N. M. Schreurs, and L. Zan. 2020. The role of microRNAs in muscle tissue development in beef cattle. *Genes*. 11:295.

Reinhart, B. J., F. J. Slack, M. Basson, A. E. Pasquinelli, J. C. Bettinger, A. E. Rougvie, H. R. Horvitz, and G. Ruvkun. 2000. The 21-nucleotide *let-7* RNA regulates developmental timing in *Caenorhabditis elegans*. *Nature*. 403:901-906.

Ren, J., D. Wang, H. Huang, X. Li, X. Zhuang, and J. Li. 2020. miR-1260b activates wnt signaling by targeting secreted frizzled-related Protein 1 to regulate taxane resistance in lung adenocarcinoma. *Front. Oncol*. 10:557327.

Rendón, A. M., Z. Saldaña, A. L. Erdem, V. Monteiro-Neto, A. Vázquez, J. B. Kaper, J. L. Puente, and J. A. Girón. 2007. Commensal and pathogenic *Escherichia coli* use a common pilus adherence factor for epithelial cell colonization. *Proc. Natl. Acad. Sci. USA*. 104:10637-10642. doi:10.1073/pnas.0704104104

Riggs, P. K. 2019. Expansion of knowledge and advances in genetics for quantitative analyses. In: J. T. Lightfoot, M. J. Hubal, and S. M. Roth, editors, Routledge handbook of sport and exercise systems genetics. Routledge, New York, NY. p. 16-27.

Riley, D. G., R. K. Miller, K. L. Nicholson, C. A. Gill, A. D. Herring, P. K. Riggs, J. E. Sawyer, J. W. Savell, and J. O. Sanders. 2019. Genome association of carcass and palatability traits from *Bos indicus-Bos taurus* crossbred steers within electrical stimulation status and correspondence with steer temperament 1. carcass. Livestock Science. 229:150-158.

Riley, L. W., R. S. Remis, S. D. Helgerson, H. B. McGee, J. G. Wells, B. R. Davis, R. J. Hebert, E. S. Olcott, L. M. Johnson, and N. T. Hargett. 1983. Hemorrhagic colitis associated with a rare *Escherichia coli* serotype. *New Eng. J. Med*. 308:681-685.

Risso, D., K. Schwartz, G. Sherlock, and S. Dudoit. 2011. GC-content normalization for RNA-Seq data. *BMC Bioinform*. 12:480.

Robbertse, L., S. A. Richards, and C. Maritz-Oliver. 2017. Bovine immune factors underlying tick resistance: integration and future directions. *Front. Cell. Infect. Microbiol*. 7:522. doi:10.3389/fcimb.2017.00522

Robinson, D. M. and G. K. Smyth. 2007. Moderated statistical tests for assessing differences in tag abundance. *Bioinformatics*. 23:2881-2887.

Robinson, D. M. and A. Oshlack. 2010. A scaling normalization method for differential expression analysis of RNA-seq data. *Genome Biol*. 11:R25.

Robles, J. A., S. E. Qureshi, S. J. Stephen, S. R. Wilson, C. J. Burden, and J. M. Taylor. 2012. Efficient experimental design and analysis strategies for the detection of differential expression using RNA-sequencing. *BMC Genomics*. 13:484.

Rocke, M. D., L. Ruan, J. J. Gossett, B. Durbin-Johnson, and S. Aviran. 2015. Controlling false positive rates in methods for differential gene expression analysis using RNA-seq data. *bioRxiv*. 018739.

Rodriguez, A., S. Griffiths-Jones, J. L. Ashurst, and A. Bradley. 2004. Identification of mammalian microRNA host genes and transcription units. *Genome Res*. 14:1902-1910.

Ronholm, J., N. Nasheri, N. Petronella, and F. Pagotto. 2016. Navigating microbiological food safety in the era of whole-genome sequencing. *Clin. Micro. Rev.* 29:837-856.

Roush, S. and F. J. Slack. 2008. The *let-7* family of microRNAs. *Cell Biol*. 18:505-516. doi:10.1016/j.tcb.2008.07.007

Rudel, S., Y. Wang, R. Lenobel, R. Korner, H. Hsiao, H. Urlaub, D. Patel, and G. Meister. 2011. Phosphorylation of human argonaute proteins affects small RNA binding. *Nucleic Acids Res*. 39:2330-2343. doi:10.1093/nar/gkq1032

Rupaimoole, R., G. A. Calin, G. Lopez-Berestein, and A. K. Sood. 2016. miRNA deregulation in cancer cells and the tumor microenvironment. *Cancer Discov.* 6:235-246.

Saliminejad, K., H. R. K. Khorshid, S. S. Fard, and S. H. Ghaffari. 2018. An overview of microRNAs: biology, functions, therapeutics, and analysis methods. *J. Cell Physiol*. 234:5451-5465.

Sanger, F., S. Nicklen, and A. R. Coulson. 1977. DNA sequencing with chain-terminating inhibitors. *Proc. Nat. Acad. Sci*. 74:5463-5467. doi:10.1073/pnas.74.12.5463

Sathipati, S. Y. and S. Ho. 2018. Identifying a miRNA signature for predicting the stage of breast cancer. *Sci. Rep*. 8:16138.

Savell, J. W. and G. C. Smith. 2009. Meat Science Laboratory Manual. 8th ed. American Press, Boston.

Savell, J. W. 2012. Beef Carcass Chilling: Current Understanding, Future Challenges. Available at: http://agrilifecdn.tamu.edu/animalscience/files/2012/04/BeefCarcassChilling_White_Paper_final.pdf (Accessed 1 December 2021.)

Savell, J. 2013. Meat Science: Dark-cutting beef. Available at: https://meat.tamu.edu/2013/01/22/dark-cutting-beef/ (Accessed 30 August 2021.)

Savell, J. and K. Gehring. 2018. Investigating dark cutters. Available at: https://www.meatpoultry.com/articles/20129-investigating-dark-cutters (Accessed 26 August 2021.)

Sawyer, J. T., J. K. Apple, Z. B. Johnson, R. T. Baublits, and J. W. S. Yancey. 2009. Fresh and cooked color of dark-cutting beef can be altered by post-rigor enhancement with lactic acid. *Meat Sci*. 83:263-270. doi:10.1016/j.meatsci.2009.05.008

Scanga, A. J., K. E. Belk, J. D. Tatum, T. Grandin, and G. C. Smith. 1998. Factors contributing to the incidence of dark cutting beef. *J. Anim. Sci*. 76:2040-1171.

Scannell, A. G. M. 2012. Overview of foodborne pathogens. *Handbook of Food Safety Engineering*. 18-56. doi:10.1002/9781444355321.ch2

Schwartz, D. S., G. Hutvagner, T. Du, Z. Xu, N. Aronin, and P. D. Zamore. 2003. Asymmetry in the assembly of the RNAi enzyme complex. *Cell*. 115:199-208.

Seideman, S. C., H. R. Cross, G. C. Smith, and P. R. Durland. 1984. Factors associated with fresh meat color: a review. *J. Food Quality*. 6:211-237.

Sekse, C., A. Holst-Jensen, U. Dobrindt, G. S. Johannessen, W. Li, B. Spilsberg, and J. Shi. 2017. High throughput sequencing for detection of foodborne pathogens. *Frontiers in Micro*. 8:1-26. doi:10.3389/fmicb.2017.02029

Selbach, M., B. Schwanhausser, N. Thierfelder, Z. Fang, R. Khanin, and N. Rajewsky. 2008. Widespread changes in protein synthesis induced by microRNAs. *Nature*. 244:58-63.

Seong, M. and H. Kang. 2020. Hypoxia-induced miR-1260b regulates vascular smooth muscle cell proliferation by targeting GDF11. *BMB Rep*. 4:206-211.

Seppey, M., M. Manni, and E. M. Zdobnov. 2019. BUSCO: assessing genome assembly and annotation completeness. In: M. Kollmar, editor, Gene Prediction. Methods in Molecular Biology, vol 1962. Humana, New York, NY.

Sha, Y., J. H. Phan, and M. D. Wang. 2015. Effect of low-expression gene filtering on detection of differentially expressed genes in RNA-seq data. *Conf. Proc. IEEE Eng. Med. Biol. Soc*. 2015:6461-6464.

Shackelford, S. D., M. Koohmaraie, T. L. Wheeler, L. V. Cundiff, and M. E. Dikeman. 1994. Effects of biological type of cattle on the incidence of the dark, firm, and dry condition in the longissimus muscle. *J. Anim. Sci*. 72:337-343.

Shapiro, S. S. and M. B. Wilk. 2965. An analysis of variance test for normality (complete samples). *Biometrika*. 52:591-611.

Sharma, M., Y. Luo, and R. Buchanan. 2011. Chapter 8 – Microbial safety of tropical and subtropical fruits. In: E. M. Yahia, editor, Postharvest Biology and Technology of Tropical and Subtropical Fruits. Woodhead Publishing. p. 288-314.

Shi, M., X. Yan, P. Han, Y. Tang, and H. Li. 2020. Microarray and bioinformatics analysis of differentially-expressed microRNAs in wnt/b-catenin signaling-activated Bovine skeletal muscle satellite cells. *Pakistan J. Zool*. 52:2071-2080.

Shin, S., M. Castanie-Cornet, J. W. Foster, J. A. Crawford, C. Brinkley, and J. B. Kaper. 2001. An activator of glutamate decarboxylase genes regulates the expression of enteropathogenic *Escherichia coli* virulence genes through control of the plasmid-encoded regulator, per. *Mol. Microbiol.* 41:1133-1150.

Sinclair, G. R., J. B. Rose, S. A. Hashsham, C. P. Gerba, and C. N. Haas. 2012. Criteria for selection of surrogates used to study the fate and control of pathogens in the environment. *J. Appl. Environ. Microbiol*. 78:1969-1977.

Singh, J., J. K. Dhanoa, R. K. Choudhary, A. Singh, R. S. Sethi, S. Kaur, and C. S. Mukhopadhyay. 2020. MicroRNA expression profiling in PBMCs of Indian water Buffalo (*Bubalus bubalis*) infected with Brucella and Johne's disease. *ExRNA*. 2:8.

Sjögren, R. J. O., M. H. L. Lindgren Niss, and A. Krook. 2018. Skeletal muscle microRNAs: roles in differentiation, disease and exercise. In: B. Spiegelman, editor. Hormones, Metabolism and the Benefits of Exercise. Springer, Cham, CH. p. 67-81.

Smith, G. C., J. D. Tatum, and J. B. Morgan. 1993. Dark cutting beef: physiology, biochemistry and occurrence. Colorado State University, Fort Collins.

Smith, L. M., J. Z. Sanders, R. J. Kaiser, P. Hughes, C. Dodd, C. R. Connell, C. Heinder, S. B. H. Kent, and L. E. Hood. 1986. Fluorescence detection in automated DNA sequence analysis. *Nature*. 321:674-679.

Smith, S., C. Gill, D. Lunt, and M. Brooks. 2009. Regulation of fat and fatty acid composition in beef cattle. *J. Anim. Sci*. 22:1225-1233. doi:10.5713/ajas.2009.r.10

Sørensen, T. 1948. A method of establishing groups of equal amplitude in plant sociology based on similarity of species and its application to analyses of the vegetation on Danish commons. *Kongelige Danske Videnskabernes Selskab*. 5: 1-34.

Soneson, C. and M. Delorenzi. 2013. A comparison of methods for differential expression analysis of RNA-seq data. *BMC Bioinformatics*. 14:91.

Staal, F. J. T., T. C. Luis, and M. M. Tiemessen. 2008. WNT signalling in the immune system: WNT is spreading its wings. *Nature. Rev. Immun*. 8:581-593.

Sun, J., T. S. Sonstegard, C. Li, Y. Huang, Z. Li, X. Lan, C. Zhang, C. Lei, X. Zhao, and H. Chen. 2015. Altered microRNA expression in bovine skeletal muscle with age. *Anim. Genet*. 46:227-238. doi:10.1111/age.12272

Sun, J. L., L. L. Zhao, K. He, Q. Liu, J. Luo, D. M. Zhang, J. Liang, L. Liao, and S. Yang. 2020. MiRNA-mRNA integration analysis reveals the regulatory roles of miRNAs in the metabolism of largemouth bass (*Micropterus salmoides*) livers during acute hypoxic stress. *Fish Physiol. Biochem*. 46:2227-2242.

Taboada, E. N., M. R. Graham, J. A. Carrico, and G. V. Domselaar. 2017. Food safety in the age of next generation sequencing, bioinformatics, and open data access. *Front. Micro*. 8:1-10. doi:10.3389/fmicb.2017.00909

Takekawa, M., F. Posas, and H. Saito. 1997. A human homolog of the yeast ssk2/ssk22 map kinase kinase kinases, MTK1, mediates stress-induced activation of the p38 and JNK pathways. *EMBO J*. 16:4973-4982.

Tam, S., M. Tsao, and J. D. McPherson. 2015. Optimization of miRNA-seq data preprocessing. *Brief. Bioinformatics*. 16:950-963.

Tang, W., Z. Liao, and Q. Zou. 2016. Which statistical significance test best detects oncomiRNAs in cancer tissues? an exploratory analysis. *Oncotarget*. 7:85613-86623.

Tarrant, P. V. 1989. Animal behavior and environment in the dark-cutting condition in beef – a review. *Irish. J. Food. Sci. and Tech*. 13:1-21.

Tatum, D. 2007. Beef Grading. Available at: https://fyi.extension.wisc.edu/wbic/files/2011/04/Beef-Grading.pdf (Accessed 1 December 2021.)

Tatum, D. 2020. Fact Sheet: Beef Grading. Available at: https://www.beefresearch.org/resources/product-quality/fact-sheets/beef-grading (Accessed 1 December 2021.)

Tatusova, T., M. DiCuccio, A. Badretdin, V. Chetvernin, E. P. Nawrocki, L. Zaslavsky, A. Lomsadze, K. D. Pruitt, M. Borodovsky, and J. Ostell. 2016. NCBI prokaryotic genome annotation pipeline. *Nucleic Acids Res*. 44:6614-6624. doi:10.1093/nar/gkw569

Tauxe, R. V., and A. T. Pavia. 1998. Salmonellosis: nontyphoidal. In: A. S. Evans and P. S. Brachman, editors, Bacterial infection of humans: epidemiology and control, 2nd ed. Plenum Publishing Corporation, New York, NY, p. 613-630.

Tejero, M. L., and J. E. Galán. 2001. Cdta, cdtb, and cdtc form a tripartite complex that is required for cytolethal distending toxin activity. *Inf. Imm.* 69:4358-4365. doi:10.1128/IAI.69.7.4358-4365.2001

Tennent, J. M., F. Lindberg, and S. Normark. 1990. Integrity of *Escherichia coli* P pili during biogenesis: properties and role of PapJ. *Mol. Microbiol*. 4:747-758.

The Center for Food Security & Public Health. 2016. Enterohemorrhagic *Escherichia coli* and Other *E. coli* Causing Hemolytic Uremic Syndrome. https://www.cfsph.iastate.edu/Factsheets/pdfs/e_coli.pdf (Accessed 15 May 2021.)

The National Human Research Institute. 2019. https://www.genome.gov/about-genomics/fact-sheets/DNA-Sequencing-Costs-Data (Accessed 14 August 2019.)

Therrien, D. A., K. Konganti, J. J. Gill, B. W. Davis, A. E. Hillhouse, J. Michalik, H. R. Cross, G. C. Smith, T. M. Taylor, and P. K. Riggs. 2021. Complete whole genome sequences of *Escherichia coli* surrogate strains and comparison of sequence methods with application to the food industry. *Microorganisms*. 9:608.

Tobe, T., G. K. Schoolnik, I. Sohel, V. H. Bustamante, and J. L. Puente. 1996. Cloning and characterization of *bfpTVW*, genes required for the transcriptional activation of *bfpA* in enteropathogenic *Escherichia coli*. *Mol. Microbio*. 21:963-975.

Tobe, T., T. Hayashi, C. Han, G. K. Schoolnik, E. Ohtsubo, and C. Sasakwaw. 1999. Complete DNA sequence and structural analysis of the enteropathogenic *Escherichia coli* adherence factor plasmid. *Infect. Immun*. 67:5455-5462.

Tomasello, L., R. Distefano, G. Nigita, and C. M. Croce. 2021. The microRNA family gets wider: the isomirs classification and role. *Front. Cell Dev. Biol*. 9:1-15. doi:10.3389/fcell.2021.668648

Trout, G.R. 1989. Variation in myoglobin denaturation and color of cooked beef, pork and turkey meat as influenced by pH, sodium chloride, sodium tripolyphosphate and cooking temperature. *J. Food Sci*. 54: 536

Tsutsumi, A., T. Kawamata, N. Izumi, H. Seitz, and Y. Tomari. 2011. Recognition of the pre-miRNA structure by *drodophila* dicer-1. *Nature*. 18:1153-1158.

Tyler, D. A., L. Mataseje, C. J. Urfano, L. Schmidt, K. S. Antonation, M. R. Mulvey, and C. R. Corbett. 2018. Evaluation of oxford nanopore's MinION sequencing device for microbial whole genome sequencing applications. *Nature: Sci. Reports*. 8:1-12.

Ud-Din, A. and S. Wahid. 2014. Relationship among shigella spp. and enteroinvasive *Escherichia coli* (EIEC) and their differentiation. *Braz. J. Microbiol*. 45:1131-1138. doi:10.1590/s1517-83822014000400002

Ueno, K., H. Hirata, S. Majid, S. Yamamura, V. Shahryari, Z. L. Tabatabai, Y. Hinoda, and R. Dahiya. 2012. Tumor suppressor microRNA-493 decreases cell motility and migration ability in human bladder cancer cells by downregulating RhoC and FZD4. *Mol. Cancer Ther*. 11:244-253.

Uhlmann, S., H. Mannsperger, J. D. Zhang, E. Horvat, C. Schmidt, M. Kublbeck, F. Henjes, A. Ward, U. Tschulena, K. Zweif, U. Korf, S. Wiemann, and O. Sahin. 2012. Global microRNA level regulation of EGFR-driven cell-cycle protein network in breast cancer. *Mol. Syst. Biol*. 8:570. doi:10.1038/msb.2011.100

United States Department of Agriculture. 1993. Immediate actions: cattle clean meat program. FSIS correlation packet, interim guidelines for inspectors. U.S. Department of Agriculture, Food Safety and Inspection Service. Washington, D.C.

United States Department of Agriculture. 1999. Beef products contaminated with *Escherichia coli* O157:H7. *Federal Register*. 64:2803-2805.

United States Department of Agriculture. 2012. USDA Targeting Six Additional Strains of *E. coli* in Raw Beef Trim Starting Monday. Available at: https://www.usda.gov/media/press-releases/2012/05/31/usda-targeting-six-additional-strains-ecoli-raw-beef-trim-starting. (Accessed 10 May 2021.)

United States Department of Agriculture. 2015a. FSIS Compliance Guideline: HACCP Systems Validation. Available at: https://www.fsis.usda.gov/guidelines/2015-0011 (Accessed 10 May 2021.)

United States Department of Agriculture. 2015b. Use of non-pathogenic *Escherichia coli* (*E. coli*) cultures as surrogate indicator organisms in validation studies. https://askfsis.custhelp.com/app/answers/detail/a_id/1392/~/use-of-non-pathogenic-escherichia-coli-%28e.-coli%29-cultures-as-surrogate (Accessed 10 November 2018.)

United States Department of Agriculture. 2020. Microbiology. Available at: https://www.fsis.usda.gov/science-data/data-sets-visualizations/microbiology (Accessed 10 May 2021.)

United States Department of Agriculture. 2021. Livestock Slaughter 2020 Summary. Available at:

https://usda.library.cornell.edu/concern/publications/r207tp32d?locale=en#release-items (Accessed 31 August 2021.)

United States Department of Agriculture: Agricultural Marketing Service. 2017a. United States Standards for Grades of Carcass Beef. Available at: https://www.ams.usda.gov/sites/default/files/media/CarcassBeefStandard.pdf (Accessed 9 June 2021.)

United States Department of Agriculture: Agricultural Marketing Service. 2017b. United States Standards for Grades of Carcass Beef. Federal Register. 82:27782-27786.

United States Department of Agriculture: Agricultural Marketing Service. 2021. Beef Grading Shields. Available at: https://www.ams.usda.gov/grades-standards/beef/shields-and-marbling-pictures (Accessed 15 June 2021.)

United States Department of Agriculture: Economic Research Service. 2013. Cost of foodborne illness estimate for *Escherichia coli* O157. Available at: https://www.ers.usda.gov/data-products/cost-estimates-of-foodborne-illnesses/ (Accessed 1 November 2018.)

United States Department of Agriculture: Food Safety and Inspection Service. 1996. Pathogen reduction: hazard analysis and critical control point (HACCP) systems; final rule. Federal Register. 61:38806-38989. (Accessed 15 May 2021.)

United States Food & Drug Administration. 2017. Sharing Whole Genome Sequencing with the World. Available at: https://www.fda.gov/food/conversations-experts-food-topics/sharing-whole-genome-sequencing-world (Accessed 12 May 2021.)

United States Food & Drug Administration. 2018a. Hazard Analysis Critical Control Point (HACCP). Available at: https://www.fda.gov/food/guidance-regulation-food-and-dietary-supplements/hazard-analysis-critical-control-point-haccp (Accessed 15 May 2021.)

United States Food & Drug Administration. 2018b. Whole Genome Sequencing (WGS) Program. Available at: https://www.fda.gov/food/science-research-food/whole-genome-sequencing-wgs-program (Accessed 15 May 2021.)

United States Food & Drug Administration. 2021a. GenomeTrakr Fast Facts. Available at: https://www.fda.gov/food/whole-genome-sequencing-wgs-program/genometrakr-fast-facts (Accessed 10 May 2021.)

United States Food & Drug Administration. 2021b. GenomeTrakr Network. Available at: https://www.fda.gov/food/whole-genome-sequencing-wgs-program/genometrakr-network (Accessed 10 May 2021.)

United States National Institute of Health. 2021a. GenBank and WGS Statistics. Available at: https://www.ncbi.nlm.nih.gov/genbank/statistics/ (Accessed 23 May 2021.)

United States National Institute of Health. 2021b. Human Genome Project Timeline of Events. Available at: https://www.genome.gov/human-genome-project/Timeline-of-Events (Accessed 19 May 2021.)

Valvatne, H., H. Steinsland, H. M. S. Grewal, K. Mølbak, J. Vuust, and H. Sommerfelt. 2004. Identification and molecular characterization of the gene encoding coli surface antigen 20 of enterotoxigenic *Escherichia coli. FEMS Microbio. Letters*. 239:131-138.

Vanderzant, C., L. K. Chesser, J. W. Savell, F. A. Gardner, and G. C. Smith. 1983. Effect of addition of glucose, citrate and citric-lactic acid on microbiological and sensory characteristics of steaks from normal and dark, firm and dry beef carcasses displayed in polyvinyl chloride film and in vacuum packages. *J. Food Prot*. 9:775-780.

Vasudevan, S., Y. Tong, and J. A. Steitz. 2007a. Switching from repression to activation: microRNAs can up-regulate translation. *Science*. 318:1931-1934.

Vasudevan, S. and J. A. Steitz. 2007b. AU-rich-element-mediated upregulation of translation by FXR1 and argonaute 2. *Cell*. 128:1105-1118. doi:10.1016/j.cell.2007.01.038

Voisinet, B. D., T. Grandin, S. F. O'Connor, J. D. Tatum, and M. J. Deesing. 1997a. *Bos indicus*-cross feedlot cattle with excitable temperaments have tougher meat and a higher incidence of borderline dark cutters. Meat Sci. 46:367-377.

Voisinet, B. D., T. Grandin, J. D. Tatum, S. F. O'Connor, and J. J. Struthers. 1997b. Feedlot cattle with calm temperaments have higher average daily gains than cattle with excitable temperaments. *J. Anim. Sci*. 75:892-896.

Waksman, G. and S. J. Hultgren. 2009. Structural biology of the chaperone- usher pathway of pilus biogenesis. *Nat. Rev. Microbiol.* 7:765-774. doi:10.1038.nrmicro2220

Walker, J. A. 2021. Applied statistics for experimental biology. Available at: https://www.middleprofessor.com/files/applied-biostatistics_bookdown/_book/index.html (Accessed 8 March 2022.)

Walker, J. B., T. Abeel, T. Shea, M. Priest, A. Abouelliel, S. Sakthikumar, C. A. Cuomo, Q. Zeng, J. Worman, S. K. Young, and A. M. Earl. 2014. Pilon: an intergrated tool

for comprehensive microbial variant detection and genome assembly improvement. *PLoS One*. 9:1-14. doi:10.1371/journal.pone.0112963

Wang, H., R. Peng, J. Wang, Z. Quin, and L. Xue. 2018. Circulating microRNAs as potential cancer biomarkers: the advantage and disadvantage. *Clin. Epigene*. 10:1-10.

Wang, H., Y. Zheng, G. Wang, and H. Li. 2013. Identification of microRNA and bioinformatics target gene analysis in beef cattle intramuscular fat and subcutaneous fat. *Mol. BioSystems*. 9:2154-2162. doi:10.1039/c3mb70084d

Wang, S., W. Daniel, J. Falardeau, L. K. Strawn, F. O. Mardones, A. D. Adell, and A. I. M. Switt. 2016. Food safety trends: from globalization of whole genome sequencing to application of new tools to prevent foodborne disease. *Trends Food Sci. & Tech*. 57:188-198. doi:10.1016/j.tifs.2016.09.016

Wang, Y., R. Medvid, C. Melton, R. Jaenisch, and R. Blelloch. 2007. DGCR8 is essential for microRNA biogenesis and silencing of embryonic stem cell self-renewal. *Nat. Genet.* 39:380-385.

Wang, Y. and T. Taniguchi. 2013. MicroRNAs and DNA damage response. *Cell Cycle*. 12:32-42. doi: 10.4161/cc.23051

Wang, Y., B. Wang., X. Shao, M. Liu, K. Jiang, M. Wang, and L. Wang. 2020. Identification and profiling of microRNAs during embryogenesis in the red claw Crayfish *Cherax quadricarinatus*. *Front. Physiol.* 11:878. doi:10.3389/fphys.2020.00878

Wang, Z., M. Gerstein, and M. Snyder. 2009. RNA-Seq: a revolutionary tool for transcriptomics. *Nat. Rev. Genet*. 10:57-63. doi:10.1038/nrg2484

Warren, L. A., I. B. Mandell, and K. G. Bateman. 2010. Road transport conditions of slaughter cattle: effects on the prevalence of dark, firm and dry beef. *Canadian J. Anim. Sci.* 90:471-482.

Warriss, P. D., S. C. Kestin, S. N. Brown, and L. J. Wilkins. 1984. The time required for recovery from mixing stress in young bulls and the prevention of dark cutting beef. *Meat Sci*. 10:53-68.

Weidemann, A. and R. S. Johnson. 2008. Biology of HIF-α. *Cell Death Diff*. 15:621-627.

Welch, B. L. 1947. The generalization of 'student's' problem when several different population variances are involved. *Biometrika*. 34:28-35.

Whitaker, L. 1914. On the poisson law of small numbers. *Biometrika*. 10:36-71.

Wick, R. R., L. M. Judd, C. L. Gorrie, and K. E. Holt. 2017a. Unicycler: resolving bacterial genome assemblies from short and long read sequencing reads. *PLoS Comp. Biology*. 13:1-22. doi:10.1371/journal.pcbi.1005595

Wick, R. R., L. M. Judd, C. L. Gorrie, and K. E. Holt. 2017b. Completing bacterial genome assemblies with multiplex MinION sequencing. *Micro. Gen*. 3:1-7.

Wienholds, E., M. J. Koudijs, F. J. M. Eeden, E. Cuppen, and R. H. A. Plasterk. 2003. The microRNA-producing enzyme dicer1 is essential for zebrafish development. *Nat Genet.* 35:217-218.

Wightman, B., I. Ha, and G. Ruvkun. 1993. Posttranscriptional regulation of the heterochronic gene *lin-14* by *lin-4* mediates temporal pattern formation in *C. elegans*. *Cell*. 75:855-862. doi:10.1016/0092-8674(93)90530-4

Wiley, J. M., L. M. Sherwood, and C. J. Woolverton. 2010. Prescott's Microbiology, 8th ed. McGraw-Hill Higher Education, New York, NY.

Wills, M. K., R. M. Mitacek, G. G. Mafi, D. L. VanOverbeke, D. Jaroni, R. Jadeja, and R. Ramanathan. 2017. Improving the lean muscle color of dark-cutting beef by aging, antioxidant-enhancement, and modified atmospheric packaging. *J. Anim. Sci*. 95:5378-5387. doi:10.2527/jas2017.1967

World Health Organization. 2018. *E. coli*. Available at: https://www.who.int/news-room/fact-sheets/detail/e-coli (Accessed 17 May 2021)

World Health Organization. 2019. Food Safety. Available at: https://www.who.int/en/news-room/fact-sheets/detail/food-safety (Accessed 1 November 2018.)

Wu, L., Fan, J. and J. G. Belasco. 2006. MicroRNAs direct rapid deadenylation of mRNA. *Proc. Natl. Acad. Sci*. 103:4034-4039.

Wulf, D. M., R. S. Emnett, J. M. Leheska, and S. J. Moeller. 2002. Relationships among glycolytic potential, dark cutting (dark, firm, and dry) beef, and cooked beef palatability. *J. Animal Sci*. 80:1895-1903.

Wult. B., G. Bergsten, M. Samuelsson, and C. Svanborg. 2002. The role of p fimbriae for *Escherichia coli* establishment and mucosal inflammation in the human urinary tract. *Int. J. Antimicro. Agents.* 19:522-538.

Xia, Y., K. Wei, F. Yang, L. Hu, C. Pan, X. Pan, W. Wu, J. Wang, W. Wen, Z. He. J. Xu, X. Xu, Q. Zhu, and L. Chen. 2019. miR-1260b, mediated by YY1, activates KIT signaling by targeting SOCS6 to regulate cell proliferation and apoptosis in NSCLC. *Cell Death & Disease*. 10:112.

Yadav, P., B. Yadav, D. K. Swain, M. Anand, S. Yadav, and A. K. Madan. 2021. Differential expression of miRNAs and related mRNAs during heat stress in buffalo heifers. *J. Thermal Biol*. 97:102904.

Yan, M., X. Li, D. Tong, C. Han, R. Zhao, Y. He, and X. Jin. 2016. miR-136 suppresses tumor invasion and metastasis by targeting RASAL2 in triple-negative breast cancer. *Oncol. Rep*. 36:65-71. doi:10.3892/or.2016.4767

Yancey, E., M. Dikeman, K. Hachmeister, E. Chambers, and G. Milliken. 2005. Flavor characterization of top-blade, top-sirloin, and tenderloin steaks as affected by pH, maturity, and marbling. *J. Anim. Sci*. 83:2618-2623.

Yang, J., L. H. Chen, L. L. Sun, J. Yu, and Q. Jin. 2008. VFDB 2008 release: an enhanced web-based resource for comparative pathogenomics. *Nucleic Acids Res.* 36:D539-D542. doi:10.1093/nar/gkm951

Yang, R., Z. Dai, S. Chen, and L. Chen. 2011. MicroRNA-mediated gene regulation plays a minor role in the transcriptomic plasticity of cold-acclimated zebrafish brain tissue. *BMC Genomics*. 12:1-17.

Yang, W., K. Tang, Y. Wang, and L. Zan. 2018. MiR-27a-5p increases steer fat deposition partly by targeting calcium-sensing receptor (CASR). *Nature: Sci. Reports*. 8:3012. doi:10.1038/s41598-018-20168-9

Yao, C. Jiang, F. Wang, H. Yan, D. Long, J. Zhao, J. Wang, C. Zhang, Y. Li, X. Tian, Q. K. Wang, G. Wu, and Z. Zhang. 2019. Integrative analysis of miRNA and mRNA expression profiles associated with human atrial aging. *Front. Physiol*. 10:1226. doi:10.3389/fphys.2019.01226

Zeng, Y., R. Yi, and B. R. Cullen. 2005. Recognition and cleavage of primary microRNA precursors by the nuclear processing enzyme drosha. *EMBO. J*. 24:138-148. doi:10.1038/sj.emboj.7600491

Zeng, Y. 2006. Principles of micro-RNA production and maturation. *Oncogene*. 25:6156-6162.

Zhang, H., F. A. Kolb, L. Jaskiewicz, E. Westhof, and W. Filipowicz. 2004. Single processing center models for human dicer and bacterial RNase III. *Cell*. 118:57-68.

Zhang, H., X. Guo, X. Feng, T. Wang, Z. Hu, X. Que, Q. Tian, T. Zhu, G. Guo, Q. Huang, and X. Li. 2017. MiRNA-543 promotes osteosarcoma cell proliferation and glycolysis by partially suppressing PRMT9 and stabilizing HIF-1α protein. *Oncotarget*. 8:2342-2355.

Zhang, J., Z. Cao, G. Yang, L. You, T. Zhang, and Y. Zhao. 2019. MicroRNA-27a (miR-27a) in solid tumors: a review based on mechanisms and clinical observations. *Front. Oncol*. 9:893. doi:10.3389/fonc.2019.00893

Zhang, Z., D. J. Jhaveri, V. M. Marshall, D. C. Bauer, J. Edson, R. K. Narayanan, G. J. Robinson, A. E. Lundberg, P. F. Barlett, N. R. Wray, and Q. Zhao. 2014. A comparative study of techniques for differential expression analysis on RNA-seq data. *PLoS ONE*. 9:e103207. doi:10.1371/journal.pone.0103207

Zhao, C., F. Tian, Y. Yu, G. Liu, L. Zan, M. S. Updike, and J. Song. 2012. miRNA-dysregulation associated with tenderness variation induced by acute stress in angus cattle. *J. Anim. Sci. Biotechn*. 3:12.

Zhao, L., H. Lui, S. Luo, K. M. Walsh, W. Li, and Q. Wei. 2020. Associations of novel variants in *PIK3C3, INSR* and *MAP3K4* of the ATM pathway genes with pancreatic cancer risk. *Am. J. Cancer Res*. 10:2128-2144.

Zhao, Q., Y. Kang, H. Wang, W. Guan, X. Li, L. Jiang, X. He, Y. Pu, J. Han, Y. Ma, and Q. Zhao. 2016. Expression profiling and functional characterization of miR-192 throughout sheep skeletal muscle development. *Nature: Sci. Reports*. 6:30281. doi:10.1038/srep30281

Zheng, Y., K. Chen, X. Zheng, H. Li, and G. Wang. 2014. Identification and bioinformatics analysis of microRNAs associated with stress and immune response in serum of heat-stressed and normal holstein cows. *Cell Stress Chaperones*. 19:973-981. doi:10.1007/s12192-014-0521-8

Zheng, Y., Y. Zheng, W. Lei, L. Xiang, and M. Chen. 2019. miR-1307-3p overexpression inhibits cell proliferation and promotes cell apoptosis by targeting ISM1 in colon cancer. *Mol. Cell. Probes*. 48:101445.

Zhou, R., S. P. O'Hara, and X. Chen. 2011. MicroRNA regulation of innate immune responses in epithelial cells. *Cell. Mol. Immunol*. 8:371-379.

Zhou, X., H. Lindsay, and M. D. Robinson. 2014. Robustly detecting differential expression in RNA sequencing data using observation weights. *Nucleic Acids Res*. 42:e91. doi:10.1093/nar/gku310

Zhou, Y., K. Xia, and F. A. Wright. 2011. A powerful and flexible approach to the analysis of RNA sequence count data. *Bioinformatics*. 27:2672-2678. doi:10.1093/bioinformatics/btr449

Zhu, Y., S. Shao, H. Pan, Z. Cheng, and X. Rui. 2018. MicroRNA-136 inhibits prostate cancer cell proliferation and invasion by directly targeting mitogen-activated protein kinase kinase 4. *Mol. Med. Rep*. 17:4803-4810.

Zimmerman, D. W. 1996. Some properties of preliminary tests of equality of variances in the two-sample location problem. *J. Gen. Psych*. 123:217-231.

APPENDIX A:

FOOD SAFETY

Figure 1.1 MinION assemblies: Distribution of contig lengths.

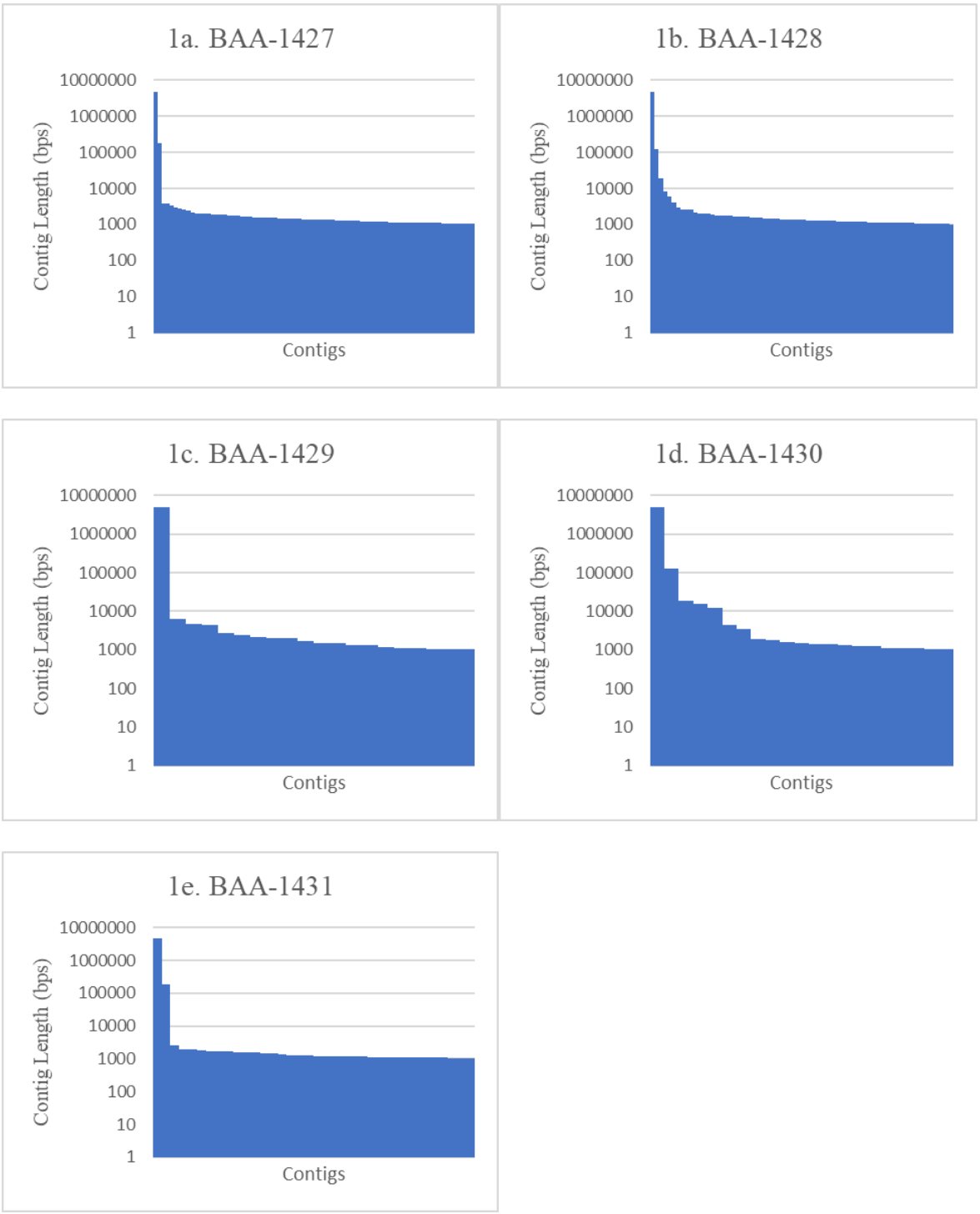

Figure 1.2 Miseq assemblies: Distribution of contig lengths.

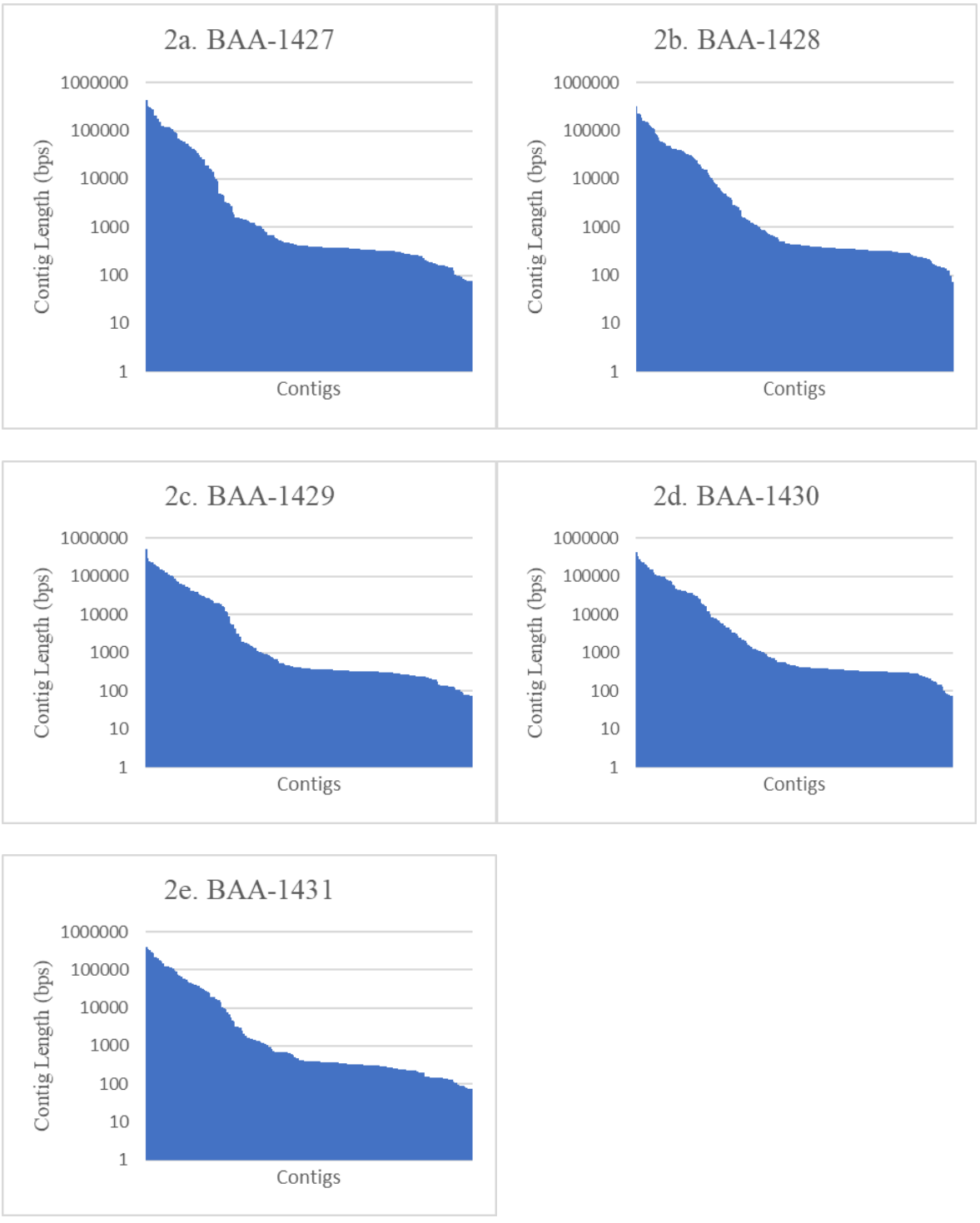

Table 1.1 Surrogate *E. coli* strains with ATCC accession numbers and designated strain identification. (Marshall et al., 2005, ATCC, 2012a).

ATCC accession number	Strain designation[1]
BAA-1427	P1
BAA-1428	P3
BAA-1429	P8
BAA-1430	P14
BAA-1431	P68

[1] The associated strain ID as listed on the ATCC website from where the strains were purchased.

Table 1.2 Summary of virulence testing performed by the *E. coli* Reference Center of Pennsylvania State University (provided by the depositor). (ATCC, 2012b)

ATCC No.	Strain	O Type	H Type	STa	SLT1	SLT2	CNF1	CNF2	EAE	K99	CS31A	F1845	O157	H7	BFP
BAA-1427	P1	-	4	-	-	-	-	-	-	-	-	-	-	-	-
BAA-1428	P3	154	-	-	-	-	-	-	-	-	-	-	-	-	-
BAA-1429	P8	-	34	-	-	-	-	-	-	-	-	-	-	-	-
BAA-1430	P14	85	34	-	-	-	+	-	-	-	-	-	-	-	-
BAA-1431	P68	106	12	-	-	-	-	+	-	-	-	-	-	-	-

Table 1.3 List of virulence attributes examined as seen on VFDB with NCBI accession numbers.

Virulence Factor[1]	Related Gene	Pathogroup[2]	Function	NCBI Accession Number[3]
Afa/Dr family	afaE-I, afaE-III, daaE, draE, draE2	DAEC	Adherence	CAW30801, CAA54121, AAA23661, AAK16480, AAB65153
AAF's	aafA, aafB, aafC, aafD, agg3A, agg3B, agg3C, agg3D, aggA, aggB, aggC, aggD, aggR	EAEC	Adherence	AAB82330, AAD27809, AAD27810, AAD26595, AAM88298, AAM88297, AAM88296, AAM88295, AAA57454, AAA57453, AAA57452, AAA57451, CAA83535
Dispersin	aap/aspU, aatA, aatB, aatC, aatD, aatP	EAEC	Adherence	YP_006099176, YP_006099144, YP_006099145, YP_006099146, YP_006099147, YP_006099143
EAST-1	astA	EAEC	Toxin	BAA94855
Pet	pet	EAEC	Toxin	YP_006099165
Pic	pic	EAEC		YP_006098864
ShET1	set1A, set1B	EAEC	Toxin	YP_006098866, YP_006098865
ECP	yagV/ecpE, yagW/ecpD, yagX/ecpC, yagY/ecpB, yagZ/ecpA, ykgK/ecpR	EHEC	Adherence	NP_286006, NP_286007, NP_286008, NP_286009, NP_286010, NP_286011
Efa-1/LifA	efa1	EHEC	Adherence	AAD49229
Intimin	eae	EHEC	Adherence	NP_290259
Paa	paa	EHEC	Adherence	NP_287515
ToxB	toxB	EHEC	Adherence	YP_325655
Afa/Dr family	afaE-I, afaE-III, daaE, draE, draE2	DAEC	Adherence	CAW30801, CAA54121, AAA23661, AAK16480, AAB65153

Table 1.3 Continued.

AAF's	aafA, aafB, aafC, aafD, agg3A, agg3B, agg3C, agg3D, aggA, aggB, aggC, aggD, aggR	EAEC	Adherence	AAB82330, AAD27809, AAD27810, AAD26595, AAM88298, AAM88297, AAM88296, AAM88295, AAA57454, AAA57453, AAA57452, AAA57451, CAA83535
Dispersin	aap/aspU, aatA, aatB, aatC, aatD, aatP	EAEC	Adherence	YP_006099176, YP_006099144, YP_006099145, YP_006099146, YP_006099147, YP_006099143
EAST-1	astA	EAEC	Toxin	BAA94855
Pet	pet	EAEC	Toxin	YP_006099165
Pic	pic	EAEC		YP_006098864
ShET1	set1A, set1B	EAEC	Toxin	YP_006098866, YP_006098865
ECP	yagV/ecpE, yagW/ecpD, yagX/ecpC, yagY/ecpB, yagZ/ecpA, ykgK/ecpR	EHEC	Adherence	NP_286006, NP_286007, NP_286008, NP_286009, NP_286010, NP_286011
Efa-1/LifA	efa1	EHEC	Adherence	AAD49229
Intimin	eae	EHEC	Adherence	NP_290259
Paa	paa	EHEC	Adherence	NP_287515
ToxB	toxB	EHEC	Adherence	YP_325655
Afa/Dr family	afaE-I, afaE-III, daaE, draE, draE2	DAEC	Adherence	CAW30801, CAA54121, AAA23661, AAK16480, AAB65153
AAF's	aafA, aafB, aafC, aafD, agg3A, agg3B, agg3C, agg3D, aggA, aggB, aggC, aggD, aggR	EAEC	Adherence	AAB82330, AAD27809, AAD27810, AAD26595, AAM88298, AAM88297, AAM88296, AAM88295, AAA57454, AAA57453, AAA57452, AAA57451, CAA83535
Dispersin	aap/aspU, aatA, aatB, aatC, aatD, aatP	EAEC	Adherence	YP_006099176, YP_006099144, YP_006099145, YP_006099146, YP_006099147, YP_006099143

Table 1.3 Continued.

EAST-1	astA	EAEC	Toxin	BAA94855
Pet	pet	EAEC	Toxin	YP_006099165
SigA	sigA	EIEC	Protease	NP_708742
T2SS (S. dysenteriae)	gspC, gspD, gspE, gspF, gspG, gspH, gspI, gspJ, gspK, gspL, gspM	EIEC	Secretion System	YP_404599, YP_404600, YP_404601, YP_404602, YP_404603, YP_404604, YP_404605, YP_404606, YP_404607, YP_404608, YP_404609
shET1, shET2	set1A, set1B, senB	EIEC	Toxin	YP_177614, YP_177613, YP_406304
Stx (S. dysenteriae (serotype 1))	stxA, stxB	EIEC	Toxin	YP_403025, YP_403026
BFP	bfpA, bfpB, bfpC, bfpD, bfpE, bfpF, bfpG, bfpH, bfpI, bfpJ, bfpK, bfpL, bfpP, bfpU	EPEC	Adherence	BAA84838, YP_002332159, YP_002332160, BAA84843, YP_002332163, BAA84845, YP_002332158, BAA84847, BAA84848, YP_002332168, BAA84850, YP_002332170, YP_002332165, BAA84842
Intimin	eae	EPEC	Adherence	AAC38392
Lymphostatin/ LifA	lifA/efa1	EPEC	Adherence	YP_002330705
Paa	paa	EPEC	Adherence	YP_006158657
EspC	espC	EPEC	Protease	AAG37043
Ler	ler	EPEC	Regulation	AAC38364
Per	perA/bfpT, perB/bfpV, perC/bfpW	EPEC	Regulation	BAA84859, BAA84860, BAA84861
CDT	cdtA, cdtB, cdtC	EPEC	Toxin	CAD48849, CAD48850, CAD48851
EAST1	east1	EPEC	Toxin	AHY03744
Cif	cif	EPEC	Type III translocate protein	PRJEA32571

Table 1.3 Continued.

EspA, EspB, EspD, EspF, EspG, EspH	espA, espB, espD, espF, espG, espH	EPEC	Type III translocate protein	AAC38394, AAC38396, AAC38395, AAC38400, AAC38363, AAC38387
Map	orf19	EPEC	Type III translocate protein	AAC38389
NleA/EspI, NleC, NleD	nleA, nleC, nleD	EPEC	Type III translocate protein	EIQ72111, YP_003498583, YP_003498587
Tir	tir	EPEC	Type III translocate protein	AAC38390
Adhesive fimbriae	cfaB, cofA, cooA, cs3, csbA, cseA, csfA, csnA, cssA, csvA, cswA	ETEC	Adherence	AAC41415, BAB62897, AAT07441, AAA23614, AAS89777, AAD30557, CAA11820, AAL31637, AAC45093, AAK09045, AAK09047
EtpA	etpA, etpB	ETEC	Adherence	YP_006203830, CBJ04459
Heat-labile toxin (LT)	eltA, eltB	ETEC	Toxin	AAA24685, AAA98064
Heat-stable toxin (ST)	estIa	ETEC	Toxin	YP_003294006
FdeC	fdeC	NMEC	Adherence	YP_002390132
S fimbriae	sfaA, sfaB, sfaC, sfaD, sfaE, sfaF, sfaG, sfaH, sfaS	NMEC	Adherence	YP_006100306, YP_006100305, YP_006100304, YP_006100307, YP_006100308, YP_006100309, YP_006100310, YP_006100312, YP_006100311
AslA	aslA	NMEC	Invasion	AAG10151
Ibes	ibeA, ibeB, ibeC	NMEC	Invasion	AAF98391, AAD30205, AAD28716
K1 capsule	kpsD, kpsM, kpsT	NMEC	Invasion	AAA21682, AAA24046, AAA24047
OmpA	ompA	NMEC	Invasion	AAF37887

Table 1.3 Continued.

TraJ	traJ	NMEC	Invasion	AAA92657
CNF-1	cnf1	NMEC	Toxin	CAA50007
Dr adhesins	draA, drab, draC, draD, draE, draP	UPEC	Adherence	AAK16475, AAK16476, AAK16477, AAK16478, AAK16480, AAK16479
F1C fimbriae	focA, focC, focD, focF, focG, focH focI	UPEC	Adherence	NP_753153, NP_753155, NP_753156, NP_753157, NP_753158, NP_753159, NP_753154
P fimbriae	papA, papA, papB, papB, papC, papC, papD, papD, papE, papE, papF, papF, papG, papG, papH, papH, papI, papI, papJ, papJ, papK, papK	UPEC	Adherence	NP_755467, NP_757036, -, -, NP_755465, NP_757034, NP_755464, NP_757033, NP_755460, NP_757029, NP_755459, NP_757028, NP_755458, NP_757027, NP_755466, NP_757035, NP_755468, NP_757037, NP_755463, NP_757032, NP_755461, NP_757030
S fimbriae	sfaA, sfaB, sfaC, sfaD, sfaE, sfaF, sfaG, sfaH, sfaS, sfaX, sfaY	UPEC	Adherence	YP_540124, YP_540123, YP_540122, YP_540125, YP_540126, YP_540127, YP_540128, YP_540130, YP_540129, YP_540132, YP_540131
Type 1 fimbriae	fimA, fimB, fimC, fimD, fimE, fimF, fimG, fimH, fimI	UPEC	Adherence	NP_757241, NP_757239, NP_757243, NP_757244, NP_757240, NP_757245, NP_757247, NP_757248, NP_757242
TcpC	tcpC	UPEC	Immune Evasion	NP_754290
Aerobactin	iucA, iucB, iucC, iucD, iutA	UPEC	Iron Uptake	NP_755502, NP_755501, NP_755500, NP_755499, NP_755498
Chu	chuA, chuS, chuT, chuU, chuV, chuW, chuX, chuY	UPEC		NP_756170, NP_756169, NP_756175, NP_756179, NP_756180, NP_756176, NP_756177, NP_756178

Table 1.3 Continued.

Enterobactin	entA, entB, entC, entD, entE, entF, fepA, fepB, fepC, fepD, fepE, fepG	UPEC	Iron Uptake	NP_752614, NP_752613, NP_752611, NP_752599, NP_752612, NP_752604, NP_752600, NP_752610, NP_752606, NP_752608, NP_752605, NP_752607
IroN	iroN	UPEC	Iron Uptake	NP_753164
Pic	pic	UPEC	Protease	NP_752289
Sat	sat	UPEC	Protease	NP_755494
Tsh	vat	UPEC	Protease	NP_752330
CNF-1	cnf1	UPEC	Toxin	YP_543855
Hemolysin	hlyA, hlyB, hlyC hlyD	UPEC	Toxin	NP_755445, NP_755448, NP_755444, NP_755449

[1] Table was constructed from pre-existing *E. coli* data located on the VFDB (Chen et al., 2005; Chen et al., 2012; Chen et al., 2016; Yang et al., 2008).
[2] Diffusely adherent *E. coli* (DAEC), Enteroaggregative *E. coli* (EAEC), Enterohemorrhagic *E. coli* (EHEC), Enteroinvasive *E. coli* (EIEC), Enteropathogenic *E. coli* (EPEC), Enterotoxigenic *E. coli* (ETEC), Neonatal meningitis-associate *E. coli* (NMEC), Uropathogenic *E. coli* (UPEC).
[3] NCBI accession numbers are listed in the same order as the related gene they are associated with (Chen et al., 2005; Chen et al., 2012; Chen et al., 2016; Yang et al., 2008).

Table 1.4 Long-read Oxford Nanopore MinION assembly sequence statistics.

Bacterial Strains	O Type	H Type	MLST[1]	Contigs	Assembled Length (bps)	Largest Contig (bps)	Average Coverage
BAA-1427	-	4	n/a	74	5,034,864	4,743,343	323.673x
BAA-1428	154	16	n/a	67	5,050,340	4,806,641	311.819x
BAA-1429	166	12	n/a	20	4,856,504	4,816,131	362.642x
BAA-1430	28ac/42	21	n/a	19	5,217,837	5,022,067	310.567x
BAA-1431	-	4	n/a	34	4,982,422	4,753,397	306.167x

[1] MLST types could not be determined due to imperfect matches.

Table 1.5 Short-reads Illumina Miseq assembly sequence statistics.

Bacterial Strains	O Type	H Type	MLST	Contigs	Assembled Length (bps)	Largest Contig (bps)	Average Coverage
BAA-1427	-	4	10	91	4,825,300	434,834	51.211x
BAA-1428	154	16	165	127	4,758,825	319,570	57.141x
BAA-1429	166	12	10	87	4,739,915	523,910	60.601x
BAA-1430	28ac/42	21	278	103	5,009,161	421,121	49.422x
BAA-1431	-	4	10	91	4,829,685	404,666	47.608x

Table 1.6 Hybrid assembly sequence statistics.

Bacterial Strains	O Type	H Type	MLST	Pilon[1]	BUSCO[2]	Contigs	Assembled Length (bps)	Largest Contig (bps)	Average Coverage	GenBank Accession No.
BAA-1427	-	4	10	6	99.9%	1	4,886,306	4,886,306	152x	CP063979
BAA-1428	154	16	165	5	99.8%	2	4,876,786	4,870,024	151x	CP063956-CP063967
BAA-1429	166	12	10	4	99.9%	1	4,812,017	4,812,017	186x	CP063969
BAA-1430	28ac/42	21	278	8	99.9%	5	5,106,612	4,988,672	138x	CP063970-CP063974
BAA-1431	-	4	10	6	99.9%	1	4,889,455	4,889,455	135x	CP063958

[1] Indicates the number of rounds of error correction each assembly underwent during Pilon processing.
[2] Indicates the predicted completeness of each assembly generated by BUSCO after comparison to the lineage enterobacteriales.

Table 1.7 Virulence attributes observed in bacterial surrogates. Genes that encode subunits of virulence factors that were detected in each strain are indicated. An e-value limit of <0.00001 was adopted as a cut-off for protein identity. (The GenBank accession numbers for the virulence factors and their corresponding subunits within this table are provided in Table 1.3).

Virulence Factors	BAA-1427	BAA-1428	BAA-1429	BAA-1430	BAA-1431
BFP	bfpB$^{*(-)}$, bfpE$^{*(-)}$, bfp$^{HI(-)}$	-	-	bfpB$^{IH(-)}$, bfpE$^{IH(-)}$, bfpH$^{IH(-)}$	bfpB$^{*(-)}$, bfpE$^{*(-)}$, bfpH$^{I(-)}$
Per	-	-	perC/bfpW$^{*(-)}$	perC/bfpW$^{*(-)}$	-
CDT	cdtA$^{*(56.03\%)}$, cdtB$^{*(68.87\%)}$, cdtC$^{*(40.56\%)}$	-	-	-	cdtA$^{*(56.03\%)}$, cdtB$^{*(68.87\%)}$, cdtC$^{*(40.56\%)}$
Adhesive fimbriae	csnA$^{IH(-)}$, cswA$^{I(-)}$	csnA$^{I(-)}$, cswA$^{IH(-)}$	csn$^{I(-)}$, cswA$^{IH(-)}$	cfaB$^{*(-)}$, cooA$^{*(-)}$, csbA$^{IH(-)}$, csnA$^{*(-)}$, cswA$^{IH(-)}$	csnA$^{IH(-)}$, cswA$^{I(-)}$
CNF1	cnf1$^{*(53.48\%)}$	-	-	-	cnf1$^{*(53.48\%)}$
P fimbriae	-	-	papE$^{*(-)}$, papG$^{*(-)}$, papJ$^{*(-)}$	-	-

$^{(\#)}$ Indicates the %ID that the identified protein shares with its virulent counterpart.
$^{(-)}$ indicates that a %ID was not calculated due to no toxin being present or due to the overall structure being non-functional due to other required subunits not being present.
^{I} Gene was detected in the assembly from Illumina Miseq.
^{H} Gene was detected in the hybrid assembly.
* Gene was detected in every dataset.

Table 1.8 Comprehensive list of alterations within the *rpoB* genes of each sample and assembly type.

Assembly	Sample	Codon [1]	Mutation	Alteration	Amino Acid Shift
MiSEQ	1427	206*	Transition	GCG → GCA	A to A
	1428	486*	Transition	ACC → ACT	T to T
	1430	489*	Transversion	CCA → CCT	P to P
	1430	623*	Transition	TTG → CTG	L to L
	1430	846*	Transversion	GGT → GGG	G to G
MINION	1427	9	Deletion	AAA → AA-	-
	1427	115	Deletion	AAA → AA-	-
	1427	206*	Transition	GCG → GCA	A to A
	1427	265	Deletion	AAA → AA-	-
	1427	319	Deletion	CTG → C-G	-
	1427	431	Deletion	AAG → A-G	-
	1427	468	Transition	CTG → CCG	L to P
	1427	618	Deletion	CAG → C-G	-
	1427	643	Deletion	CTG → C-G	-
	1427	671	Transition	CTG → CCG	L to P
	1427	941	Deletion	AAA → AA-	-
	1427	1117	Deletion	CCT → C--	-
	1427	1238	Deletion	CTG → --G	-
	1428	8	Deletion	AAA → AA-	-
	1428	83	Deletion	CAG → C-G	-
	1428	114	Deletion	GTA → GT-	-
	1428	226	Deletion	GAA → G-A	-
	1428	264	Deletion	GAA → G-A	-
	1428	278	Deletion	GAA → G-A	-
	1428	319	Deletion	CTG → C-G	-
	1428	372	Deletion	CCT → CC-	-
	1428	468	Deletion	CTG → C-G	-
	1428	486*	Transition	ACC → ACT	A to A

Table 1.8 Continued

1428	563	Deletion	ACC → A-C	-
1428	618	Transition	CAG → CGG	Q to R
1428	643	Deletion	CTG → C-G	-
1428	649	Transition	CAG → CGG	Q to R
1428	671	Deletion	CTG → C-G	-
1428	940	Deletion	GAA → G-A	-
1428	987	Deletion	GAG → GA-	-
1428	1038	Transition	CAG → CGG	Q to R
1428	1062	Transition	CCT → CCC	R to P
1428	1117	Deletion	CTG → C-G	-
1428	1238	Deletion	CTG → --G	-
1430	4	Transition	TCC → CTC	S to L
1430	8	Deletion	AAA → -AA	-
1430	83	Deletion	CAG → C--	-
1430	112	Transition	GGC → AGC	G to S
1430	113	Deletion	AAC → AA-	-
1430	114	Deletion	GGT → --T	-
1430	115	Deletion	ACC → -CC	-
1430	183	Transition	TGG → CGG	W to R
1430	227	Deletion	AAA → AA-	-
1430	265	Deletion	AAA → AA-	-
1430	319	Deletion	CTG → C-G	-
1430	372	Deletion	CCT → C-G	-
1430	431	Deletion	AAG → A-G	-
1430	468	Transition	CTG → CCG	L to P
1430	489*	Transversion	CCA → CCT	P to P
1430	535	Deletion	CCA → CC-	-
1430	618	Transition	CAG → CGG	Q to R
1430	623*	Transition	TTG → CCG	L to P

Table 1.8 Continued

	1430	633	Deletion	CTG → C-G	-
	1430	846*	Transversion	GGT → GGG	G to G
	1430	1038	Deletion	CAG → C-G	-
	1430	1062	Transition	CCT → CCC	P to P
	1430	1117	Deletion	CTG → C--	-
	1430	1238	Deletion	CTG → C-G	-
	1430	1253	Transition	CTG → CCG	L to P
Hybrid	1427	206*	Transition	GCG → GCA	A to A
	1428	486*	Transition	ACC → ACT	T to T
	1430	489*	Transversion	CCA → CCT	P to P
	1430	623*	Transition	TTG → CTG	L to L
	1430	846*	Transversion	GGT → GGG	G to G
Rif-Mutant	1427	206*	Transition	GCG → GCA	A to A
	1427	533R	Transition	CTC → CCC	L to P
	1428	486*	Transition	ACC → ACT	T to T
	1428	512R	Transition	TCT → CCT	S to P
	1430	489*	Transversion	CCA → CCT	P to P
	1430	526R	Transition	CAC → TAC	H to Y
	1430	623*	Transition	TTG → CTG	L to L
	1430	846*	Transversion	GGT → GGG	G to G

[1] Codon number within the *rpoB* gene of the *E. coli* str. K-12 substr. MG1655 (NC_000913.3) reference strain.
[*] Indicates that this mutation was found within all four assemblies.
[R] Documented to confer rif-resistance.

APPENDIX B:

MEAT QUALITY

Figure 2.1 Dark cutter incidence across sires in 2010 contemporary group.

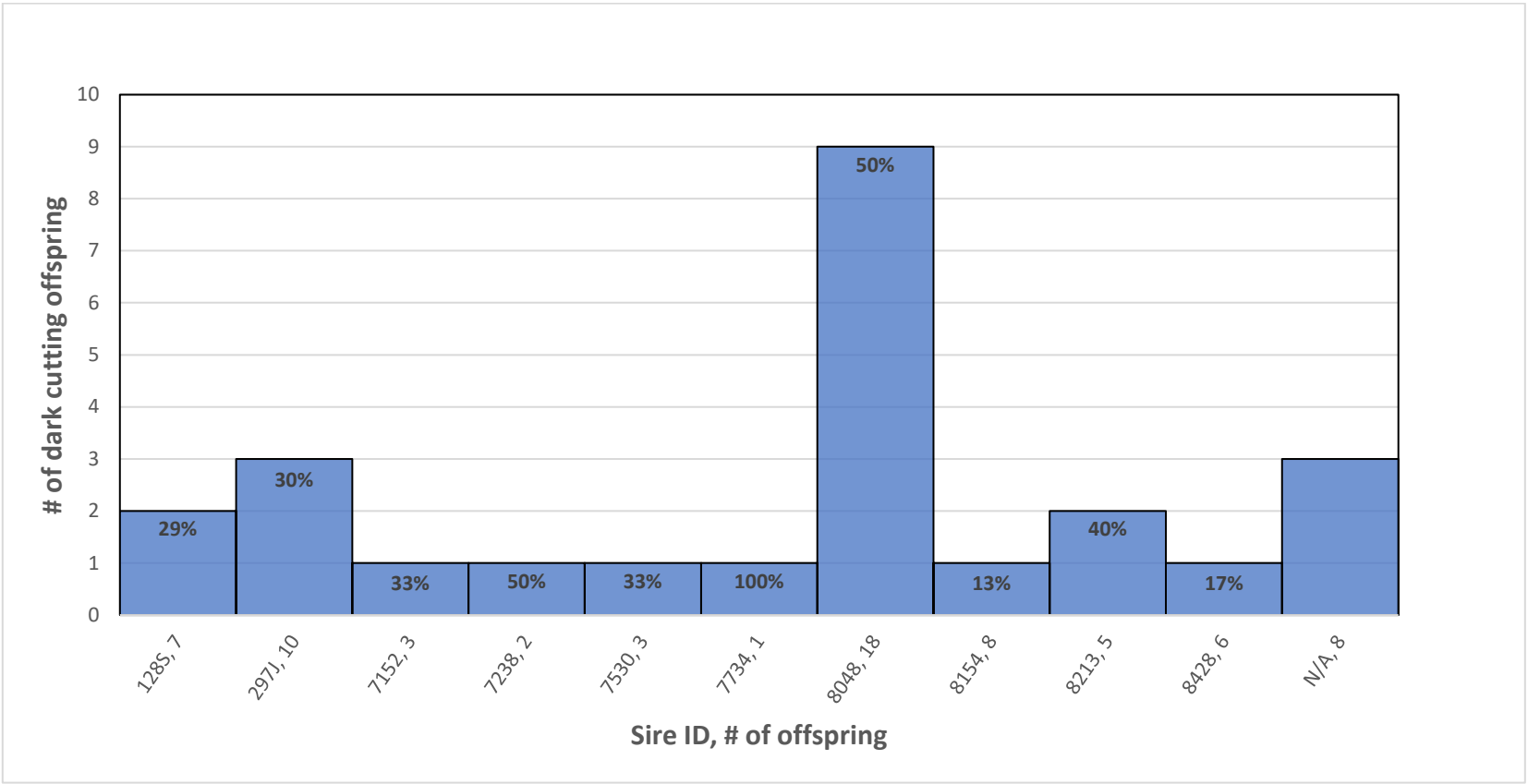

Figure 2.2 miRNA counts per million.

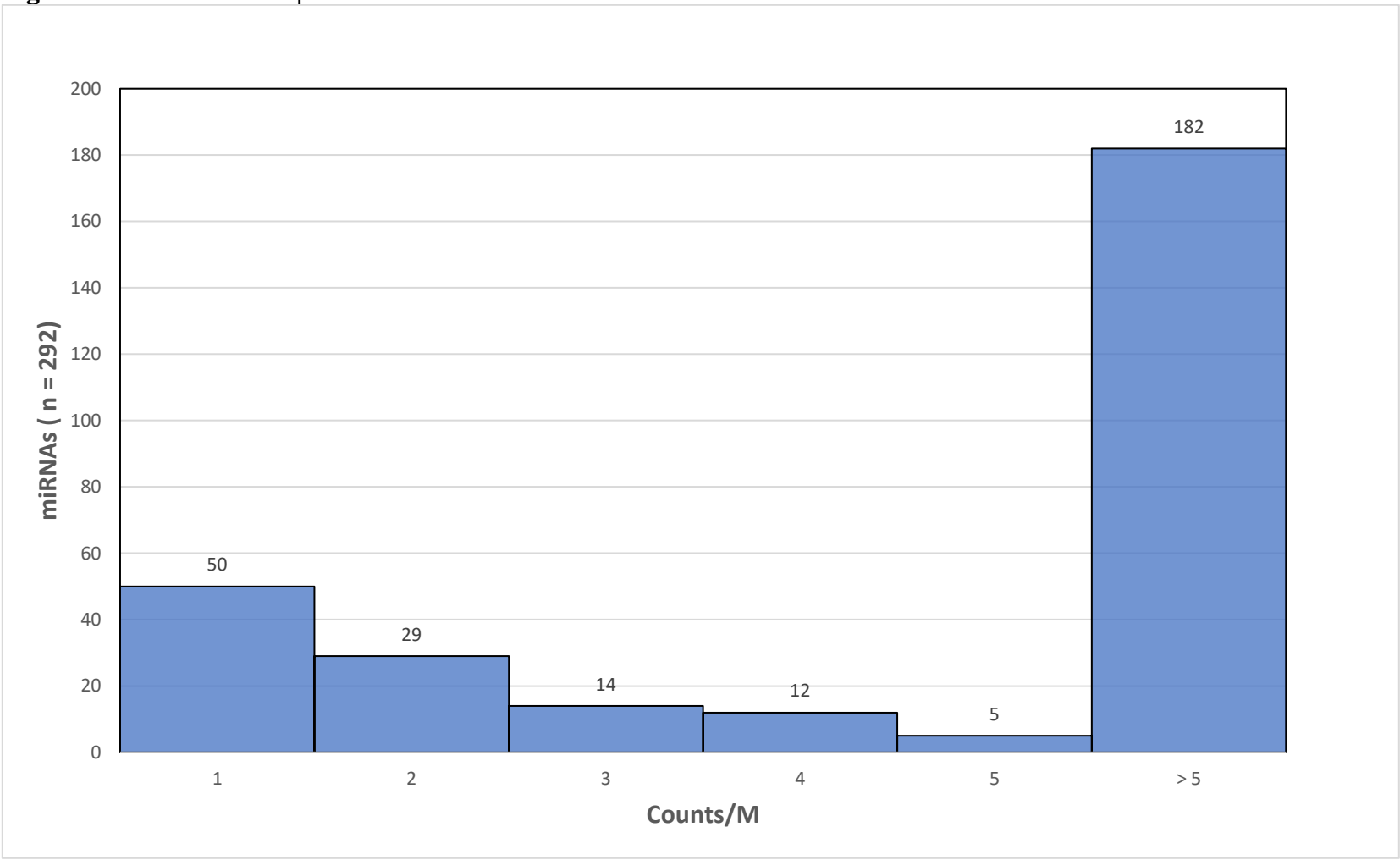

Figure 2.3 Distribution of miRNA fold difference expression ratios (DFD/NON) that were calculated prior to the Welch *t*-test.

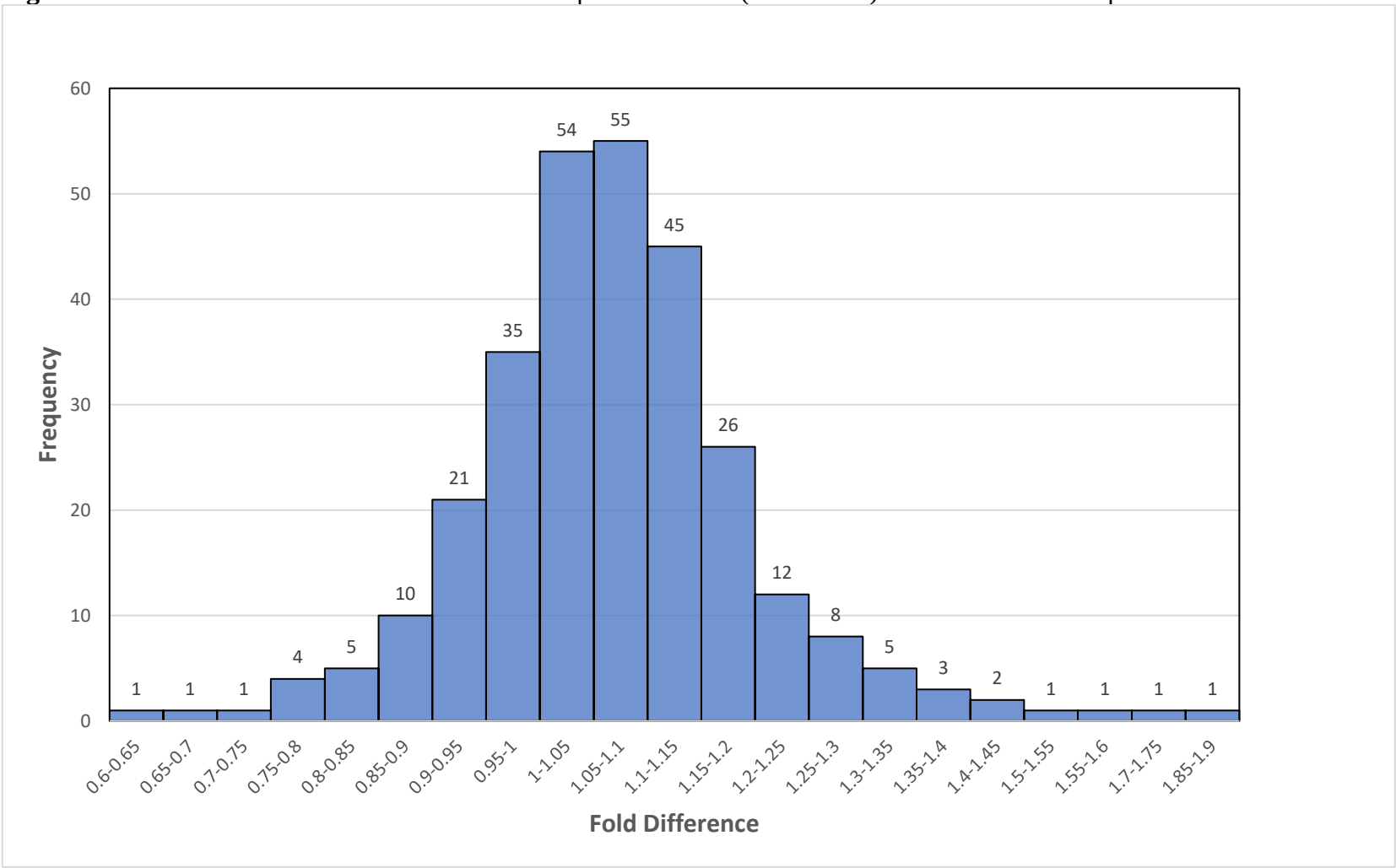

Figure 2.4 Distribution of miRNA fold difference (log_{10}) expression ratios (DFD/NON) that were estimated via the DESeq2 software package.

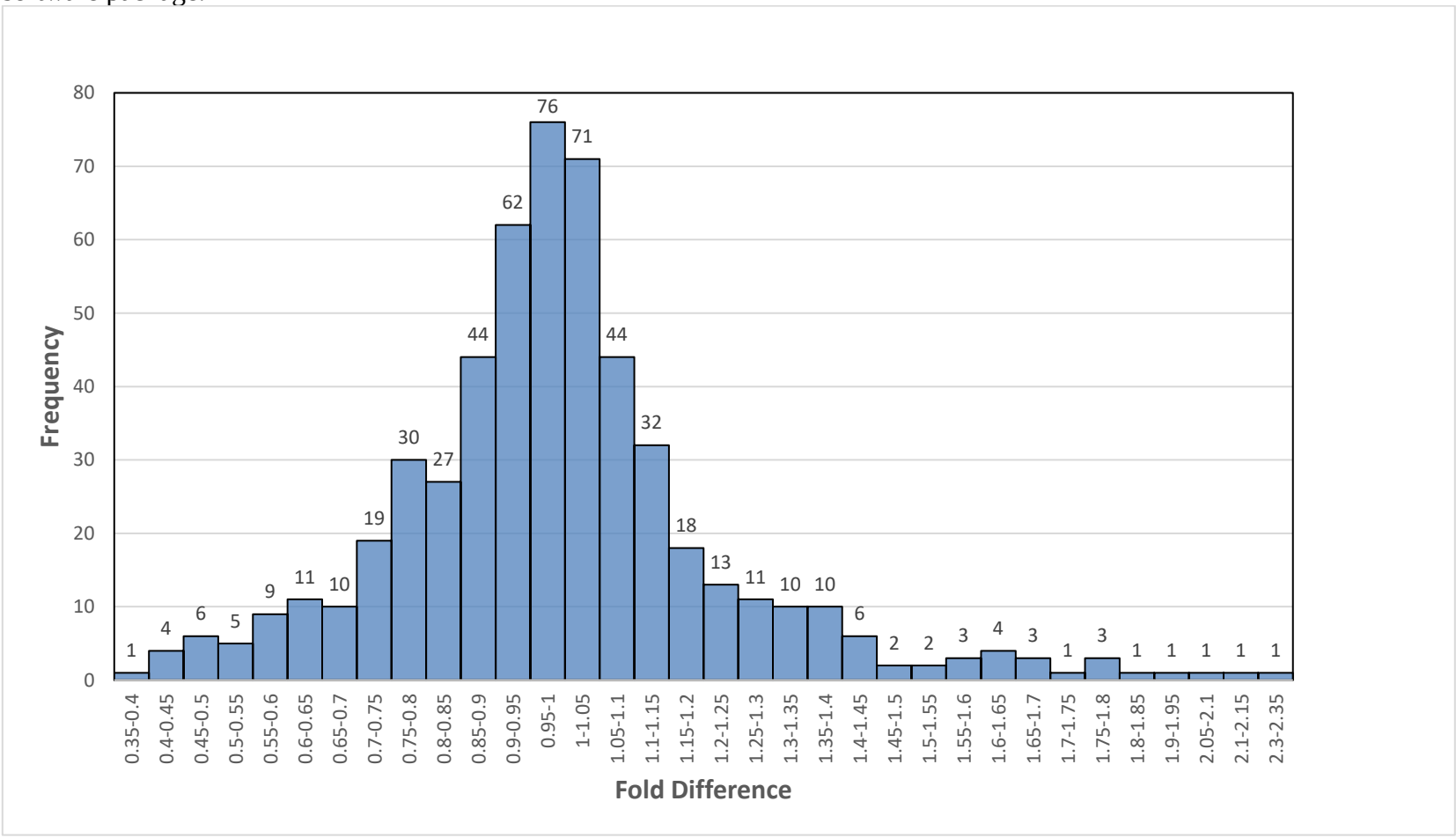

Table 2.1 Descriptions of project steer groups.

Cycle 1	Cycle 2	Cycle 3
NA x NA	4 crosses of NA and AN F_1 parents	Cycle 1 parents
Born 2003-2007	Born 2009-2013	Born 2009-2013

All animals are 50% Nellore (N, *Bos indicus*) and 50% Angus (A, *Bos taurus*). A pair of letters indicate the breeds of sire and dam in the cross, respectively.

Table 2.2 Summary of each animal's background and the characteristics of their corresponding carcasses. Contains related identification numbers, lineage, treatments, and the previously generated quality assessment values of each animal's carcass.

			Parents											
Calf ID	Ranch Tag	Family ID	SIRE	DAM	HCW[1]	Act. PYG[2]	Adj. PYG[3]	REA[4]	%KPH[5]	MARB[6]	QG[7]	Avg. SF[8]	DC[9]	BVD Trt[10]
32	520084	210203	297J	753G	900.5	3.5	3.5	12.2	2.0	470	CH-	2.132	no	MLV
66	520077	223001	414S	559J	777.5	2.7	2.9	14.0	1.5	320	SE	2.101	no	MLV
93	520211	222703	128S	281G	723.5	2.7	2.9	12.1	1.5	420	CH-	2.87	no	NON
136	520231	210209	297J	954H	711.5	3.1	3.3	11.7	2.0	320	SE	2.391	no	MLV
138	520220	210210	297J	323P	806.0	4.1	4.3	12.1	2.0	460	CH-	2.055	no	NON
139	520-	210211	297J	640H	833.0	3.0	3.2	14.8	2.0	310	SE	2.372	no	MLV
176	520239	223003	414S	117J	802.5	3.2	3.6	12.1	2.0	530	Cho	2.662	no	MLV
249	520089	210214	297J	725J	904.5	3.8	3.8	12.6	1.5	410	CH-	2.345	no	MLV
327	520093	222709	128S	389J	726.0	3.1	3.4	12.1	2.0	320	SE	1.767	no	MLV
328	520242	210218	297J	417H	841.0	3.2	3.3	14.4	2.0	470	CH-	2.029	no	MLV
345	520217	222710	128S	477J	792.5	3.0	3.3	12.8	2.0	420	CH-	2.010	no	MLV
346	520226	N/A	N/A	N/A	838.0	3.1	3.3	14.1	2.0	330	SE	2.872	no	NON
378	520170	222711	128S	572H	834.5	3.5	3.6	13.4	1.5	380	SE	2.272	no	MLV
379	520240	222903	262S	422H	923.0	3.6	3.8	14.1	1.5	650	CH+	1.681	no	MLV
382	520205	222712	128S	849H	849.5	3.3	3.7	12.6	1.0	620	CH+	2.523	no	MLV
446	520210	N/A	N/A	N/A	832.0	3.0	3.2	13.3	1.5	420	CH-	2.141	no	NON
458	520235	210221	297J	633H	820.5	3.7	4.0	13.0	2.0	340	SE	3.658	no	MLV
507	520083	N/A	N/A	N/A	746.0	3.5	3.7	10.5	2.0	320	SE	2.070	no	Killed
602	520219	315601	8154	8401	822.0	3.1	3.3	13.1	1.5	400	CH-	2.496	no	MLV
604	520206	315301	7530	7119	733.5	3.3	3.5	13.4	2.0	380	SE	2.207	no	MLV
606	520207	315901	8428	8119	763.5	2.5	2.7	14.3	1.5	350	SE	3.534	no	MLV
621	520203	315503	8048	8310	743.5	3.2	3.4	12.7	2.0	450	CH-	3.289	no	NON
622	520086	315001	7146	8320	744.5	2.7	2.8	14.0	2.5	430	CH-	1.895	no	Killed
623	520099	315203	7238	8417	781.0	3.0	3.4	14.8	1.5	520	Cho	3.411	no	MLV
624	520229	315504	8048	8322	832.0	2.7	2.8	15.6	2.0	320	SE	3.358	no	MLV
626	520096	315002	7146	7201	868.0	3.6	3.9	11.2	2.0	380	SE	4.037	no	NON
630	520222	315608	8154	8405	718.5	3.4	3.8	13.2	2.5	340	SE	2.106	no	MLV

Table 2.1 Continued

633	520216	315507	8048	7515	809.5	3.0	3.4	14.6	2.0	410	CH-	2.590	no	NON
634	520209	315703	8213	7124	995.5	3.9	4.2	15.2	2.0	380	SE	2.152	no	MLV
636	520224	315609	8154	7103	770.5	3.9	4.0	12.2	2.0	380	SE	2.181	no	MLV
641	520247	315611	8154	7137	790.5	4.0	4.2	12.6	2.0	370	SE	2.597	no	NON
642	520244	315005	8048	7520	682.5	3.2	3.4	11.4	2.0	320	SE	N/A	no	MLV
646	520249	315511	7146	7516	746.0	3.2	3.5	11.6	2.5	420	CH-	2.387	no	MLV
652	520166	315006	8048	7403	857.5	3.0	3.3	14.4	1.5	370	SE	2.527	no	NON
653	520228	315903	7146	8329	824.0	3.5	3.9	12.4	2.0	430	CH-	3.031	no	Killed
654	N/A	315514	8428	7522	645.0	3.0	3.3	11.1	2.0	320	SE	2.115	no	MLV
656	520201	315516	8048	8202	608.0	3.0	3.0	11.5	2.0	380	SE	2.194	no	MLV
659	520088	315904	8048	7304	824.5	2.6	2.7	16.4	2.0	310	SE	1.594	no	MLV
664	520094	315616	8048	8103	869.5	3.9	4.0	14.1	2.0	350	SE	2.878	no	MLV
666	520248	315102	8154	7725	811.0	2.7	2.9	13.2	1.5	300	SE	2.149	no	MLV
667	520085	315520	7152	8201	685.0	2.7	2.9	12.8	2.5	340	SE	2.444	no	Killed
675	520095	315521	8428	8321	786.5	3.5	3.8	12.8	2.5	420	CH-	2.317	no	MLV
680	520223	315522	8048	7224	807.5	2.7	2.9	13.3	1.5	400	CH-	2.028	no	NON
687	520171	N/A	8154	7133	777.5	4.0	4.3	13.7	2.5	420	CH-	2.853	no	NON
688	520087	N/A	N/A	N/A	733.5	3.0	3.2	13.4	2.5	320	SE	2.265	no	NON
689	520081	315523	N/A	N/A	673.0	3.1	3.5	12.1	2.0	420	CH-	3.8076	no	NON
693	520202	315622	8428	8302	786.5	3.0	3.4	13.9	2.5	300	SE	4.319	no	NON
694	520250	315908	8154	7148	765.5	3.5	4.2	11.9	2.5	430	CH-	2.620	no	MLV
695	520098	315707	8428	8210	826.0	3.3	3.4	14.8	2.0	450	CH-	2.990	no	MLV
701	520100	315526	8213	8034	800.5	3.5	4.0	12.5	2.0	410	CH-	3.671	no	MLV
704	520241	315708	7152	7237	810.0	3.0	3.5	15.4	2.5	450	CH-	3.085	no	MLV
713	520225	315306	8213	7140	751.0	3.3	3.5	13.0	2.0	500	Cho	2.375	no	NON
716	520090	315307	7530	8423	628.5	2.8	3.0	11.3	2.5	320	SE	2.297	no	MLV
57	520208	210204	297J	635H	849.0	2.7	2.9	16.0	2.5	380	SE	2.988	1/4	NON
130	520236	210208	297J	365J	741.0	2.6	2.8	12.5	2.0	310	SE	3.326	1/4	Killed
263	520204	N/A	N/A	N/A	768.0	2.9	3.0	12.8	2.0	370	SE	2.350	1/4	MLV
635	520221	315508	8048	7502	783.5	2.6	2.8	13.3	1.5	430	CH-	2.280	1/4	Killed
648	520092	315512	8048	8325	762.5	3.2	3.3	15.1	2.0	520	Cho	2.597	1/4	NON

Table 2.1 Continued

650	520237	315614	8048	7212	864.5	3.4	3.6	13.5	2.0	420	CH-	2.344	1/4	Killed
669	520227	315206	8048	7235	702.5	2.7	2.9	13.5	2.0	630	CH+	2.590	1/4	Killed
684	520215	315621	8213	7713	692.5	3.4	3.6	13.0	2.0	380	SE	3.631	1/4	Killed
140	520168	210212	297J	852H	761.0	2.8	3.2	12.3	1.5	420	CH-	3.047	1/3	NON
177	520243	N/A	N/A	N/A	851.5	4.2	4.5	12.6	1.5	550	Cho	3.149	1/3	MLV
209	520213	N/A	N/A	N/A	797.0	4.2	4.2	13.5	2.0	660	CH+	4.567	1/3	Killed
631	520082	315505	8048	8107	829.5	3.7	3.9	14.1	1.5	600	CH+	3.296	1/3	Killed
651	520091	315513	8154	8022	804.5	3.1	3.4	15.3	3.0	460	CH-	4.133	1/3	MLV
671	520214	315103	7238	7113	847.0	3.0	3.1	16.6	2.0	500	Cho	3.512	1/3	Killed
674	520232	315905	7152	8203	708.0	3.3	3.5	14.5	2.5	400	CH-	2.729	1/3	NON
682	520167	315705	8048	7517	775.0	2.8	2.9	14.0	2.0	440	CH-	3.379	1/3	MLV
692	520218	315907	8213	7704	799.5	4.0	4.5	12.6	2.0	540	Cho	2.663	1/3	NON
427	520233	222714	128S	715J	811.0	2.4	2.7	13.5	2.0	380	SE	2.913	1/2	NON
703	520246	315105	8048	8205	726.0	2.7	2.9	15.7	1.5	380	SE	3.793	1/2	Killed
771	520076	N/A	7530	8023	619.5	2.7	2.7	11.9	2.0	350	SE	2.863	1/2	NON
289	520238	222707	128S	684G	708.5	2.5	2.8	11.4	2.5	310	SE	2.269	2/3	Killed
601	520230	N/A	7734	N/A	832.0	3.5	3.8	14.3	2.0	460	CH-	2.690	2/3	MLV
662	520234	315518	8428	7406	803.5	2.5	2.6	15.8	2.0	340	SE	3.157	2/3	NON
691	N/A	315706	8048	8118	738.5	3.0	3.2	14.0	1.5	330	SE	2.836	2/3	MLV
608	520097	315502	8048	8311	712.0	3.0	3.0	12.6	2.0	350	SE	2.291	3/4	Killed

[1] Hot carcass weight
[2] Actual preliminary yield grade
[3] Adjusted preliminary yield grade
[4] Ribeye Area
[5] Percentage of kidney, pelvic, and heart fat
[6] Marbling
[7] Quality grade
[8] Average shear force value
[9] Degree of dark cutting
[10] Bovine Viral Diarrhea vaccination: Killed (killed vaccine), NON (control), and MLV (modified live vaccine)

Table 2.3 Differentially expressed miRNAs between normal beef carcasses and those exhibiting the DFD phenotype according to analysis via Welch's *t* test. The threshold for statistical significance for differential expression was set as p_{adj} (≤ 0.05). Bold text indicates significance.

miRNA[1]	All samples Geometric $\bar{x}$	NON Geometric $\bar{x}$	DFD Geometric $\bar{x}$	Fold difference[2] (DFD/NON)	*p*-value	p_{adj}[3]
bta-miR-206	2773.709	2612.441	3149.281	**1.205**	**0.00073**	0.216
bta-miR-2422	1.330	1.108	1.902	**1.716**	**0.00081**	0.119
bta-miR-2285q	0.946	1.111	0.691	**0.622**	**0.00260**	0.255
bta-miR-1260b	2.783	2.294	4.262	**1.858**	**0.00302**	0.222
bta-let-7f	6610.166	6415.680	7042.197	1.098	**0.00589**	0.347
bta-miR-493	5.357	4.885	6.514	**1.333**	**0.00696**	0.341
bta-miR-27a-5p	2.500	2.175	3.357	**1.544**	**0.00819**	0.344
bta-miR-380-3p	13.286	12.376	15.441	**1.248**	**0.01067**	0.392
bta-miR-3613a	96.984	102.997	85.373	0.829	**0.01578**	0.515
bta-miR-146a	60.269	64.413	52.345	0.813	**0.01748**	0.514
bta-miR-28	107.069	102.929	116.406	1.131	**0.01803**	0.482
bta-miR-17-5p	16.474	15.473	18.813	**1.216**	**0.01938**	0.475
bta-miR-543	3.197	2.916	3.870	**1.327**	**0.02284**	0.516
bta-miR-6522	0.954	0.863	1.215	**1.407**	**0.02499**	0.525
bta-miR-24	14.249	13.545	15.865	1.171	**0.02523**	0.494
bta-miR-378c	189.076	179.833	210.273	1.169	**0.02614**	0.480
bta-miR-1307	3.089	2.797	3.813	**1.363**	**0.02703**	0.467
bta-miR-142-5p	36.986	39.001	33.051	0.847	**0.02928**	0.478
bta-miR-11994	1.734	1.596	2.054	**1.287**	**0.03069**	0.475
bta-miR-378b	12.994	12.060	15.222	**1.262**	**0.03444**	0.506
bta-miR-378d	28.707	27.347	31.818	1.163	**0.03465**	0.485
bta-miR-181d	2.519	2.271	3.124	1.376	**0.03553**	0.475
bta-miR-148a	374.651	385.479	352.691	0.915	**0.03708**	0.474
bta-miR-487b	26.537	24.915	30.333	**1.217**	**0.03773**	0.462
bta-miR-136	2.010	2.261	1.550	**0.686**	**0.03880**	0.456
bta-let-7a-5p	3604.010	3468.475	3909.114	1.127	**0.04268**	0.483
bta-miR-196a	128.449	123.898	138.658	1.119	**0.04522**	0.492

Table 2.2 Continued

bta-miR-103	203.663	194.164	225.368	1.161	**0.04532**	0.476
bta-miR-10174-3p	967.189	922.089	1070.231	1.161	**0.04611**	0.467
bta-miR-23b-3p	962.762	918.085	1064.798	1.160	**0.04724**	0.463
bta-miR-361	61.545	58.945	67.443	1.144	**0.05074**	0.481
bta-miR-486	470.111	450.176	515.342	1.145	0.05138	0.472
bta-miR-423-5p	79.654	75.619	88.936	1.176	0.05250	0.468
bta-miR-378	2943.043	2821.481	3218.353	1.141	0.05268	0.455
bta-miR-432	2.052	1.859	2.529	**1.360**	0.05719	0.480
bta-miR-484	18.722	17.866	20.676	1.157	0.05764	0.471
bta-miR-299	1.499	1.310	2.043	**1.559**	0.05847	0.465
bta-miR-2478	8.113	7.456	9.705	**1.302**	0.05924	0.458
bta-miR-411c-5p	6.669	6.135	7.961	**1.298**	0.06009	0.453
bta-miR-29d-5p	6.853	6.491	7.687	1.184	0.06127	0.450
bta-miR-32	226.952	236.703	207.588	0.877	0.06193	0.444
bta-miR-6123	1.313	1.432	1.090	**0.761**	0.06196	0.434
bta-miR-144	5.033	5.594	4.024	**0.719**	0.06326	0.433
bta-miR-376c	2.209	2.049	2.584	**1.261**	0.06439	0.430
bta-miR-423-3p	389.085	372.211	427.431	1.148	0.06513	0.426
bta-miR-532	56.979	55.058	61.276	1.113	0.06648	0.425
bta-miR-2887	4.798	4.388	5.798	**1.321**	0.07184	0.449
bta-miR-98	457.133	446.380	480.795	1.077	0.07245	0.444
bta-miR-151-5p	642.937	619.365	695.921	1.124	0.07729	0.464
bta-miR-495	11.078	10.469	12.488	1.193	0.08349	0.491
bta-miR-362-5p	73.064	70.573	78.639	1.114	0.08467	0.488
bta-miR-1343-3p	5.735	5.430	6.440	1.186	0.08468	0.479
bta-miR-503-5p	3.654	3.391	4.282	**1.263**	0.09066	0.503
bta-miR-23a	912.155	866.248	1017.684	1.175	0.09099	0.495
bta-miR-2284x	90.708	88.123	96.442	1.094	0.09380	0.501
bta-let-7g	3420.305	3355.754	3561.288	1.061	0.09423	0.495
bta-miR-424-3p	4.371	4.052	5.133	**1.267**	0.09712	0.501
bta-miR-1248	12.929	13.488	11.818	0.876	0.10665	0.541

Table 2.2 Continued

bta-miR-409a	4.223	3.969	4.814	**1.213**	0.10789	0.538
bta-miR-192	36.819	35.563	39.630	1.114	0.11172	0.547
bta-miR-320a	96.488	92.791	104.819	1.130	0.11193	0.539
bta-miR-382	6.696	6.261	7.719	**1.233**	0.11276	0.535
bta-miR-193a-5p	40.781	38.953	44.947	1.154	0.11442	0.534
bta-miR-365-3p	177.290	171.022	191.350	1.119	0.11531	0.530
bta-miR-191	250.248	242.430	267.665	1.104	0.11610	0.525
bta-miR-655	10.255	9.613	11.762	**1.224**	0.11859	0.528
bta-miR-2285o	5.925	6.109	5.551	0.909	0.11910	0.523
bta-miR-410	4.577	4.269	5.306	**1.243**	0.12007	0.519
bta-miR-151-3p	116.414	113.382	123.113	1.086	0.12063	0.514
bta-miR-22-5p	301.935	293.437	320.774	1.093	0.12557	0.527
bta-miR-2904	46.092	43.273	52.690	**1.218**	0.12743	0.528
bta-miR-133b	225.109	217.546	242.024	1.113	0.12798	0.523
bta-miR-208b	57.244	60.216	51.421	0.854	0.12823	0.516
bta-miR-1434-5p	9.316	9.699	8.553	0.882	0.12883	0.512
bta-let-7e	104.650	100.874	113.131	1.122	0.12958	0.508
bta-miR-30e-5p	6878.272	6996.432	6634.332	0.948	0.13145	0.509
bta-miR-664b	11.946	11.584	12.750	1.101	0.13397	0.512
bta-miR-1388-3p	3.256	3.361	3.044	0.906	0.13785	0.520
bta-miR-2336	1.913	1.992	1.756	0.881	0.13877	0.516
bta-miR-106b	76.657	74.423	81.617	1.097	0.14110	0.519
bta-miR-30d	2236.142	2177.603	2365.500	1.086	0.14255	0.517
bta-let-7d	191.426	185.980	203.505	1.094	0.14491	0.520
bta-miR-154c	10.120	9.585	11.356	1.185	0.14882	0.527
bta-miR-31	1.010	1.095	0.831	**0.759**	0.14894	0.521
bta-miR-27b	2878.943	2796.286	3062.346	1.095	0.15214	0.526
bta-miR-1247-5p	1.224	1.086	1.573	**1.448**	0.15316	0.524
bta-miR-143	20578.245	21154.560	19407.853	0.917	0.16131	0.545
bta-miR-2285ba	2.121	2.236	1.897	0.849	0.16277	0.544
bta-miR-331-5p	12.279	11.894	13.136	1.104	0.16594	0.548

Table 2.2 Continued

bta-miR-145	190.158	181.773	209.237	1.151	0.16801	0.549
bta-miR-125b	1016.020	987.476	1079.294	1.093	0.16923	0.547
bta-let-7c	411.321	399.462	437.640	1.096	0.17057	0.545
bta-miR-107	27.883	26.715	30.530	1.143	0.17226	0.545
bta-miR-2285cf	1.357	1.298	1.490	1.148	0.17383	0.544
bta-miR-653	2.392	2.512	2.157	0.858	0.18671	0.578
bta-miR-494	17.403	16.768	18.829	1.123	0.18724	0.573
bta-miR-197	5.910	5.636	6.536	1.160	0.18987	0.575
bta-miR-331-3p	37.235	36.025	39.936	1.109	0.19251	0.578
bta-miR-1306	0.999	0.918	1.194	**1.301**	0.19278	0.572
bta-miR-326	1.190	1.135	1.297	1.142	0.20022	0.589
bta-miR-193b	51.088	49.340	55.002	1.115	0.20478	0.596
bta-miR-222	9.292	8.895	10.193	1.146	0.20592	0.594
bta-miR-127	27.814	26.897	29.864	1.110	0.21184	0.605
bta-miR-15a	110.277	106.451	118.848	1.116	0.21422	0.606
bta-miR-140	110.676	107.755	117.133	1.087	0.21759	0.609
bta-miR-1249	1.449	1.369	1.644	**1.201**	0.21841	0.606
bta-miR-7859	10.650	10.268	11.506	1.120	0.22000	0.604
bta-miR-2285bf	38.644	39.836	36.233	0.910	0.22069	0.601
bta-let-7b	383.972	373.403	407.379	1.091	0.22217	0.599
bta-miR-1468	82.256	80.231	86.719	1.081	0.22581	0.604
bta-miR-1	732578.607	736155.512	725052.942	0.985	0.24092	0.638
bta-miR-9-5p	5.021	4.856	5.391	1.110	0.24114	0.633
bta-miR-2285f	9.922	10.303	9.161	0.889	0.24324	0.633
bta-miR-30b-5p	258.687	253.577	269.862	1.064	0.24539	0.633
bta-miR-502b	2.828	2.616	3.338	**1.276**	0.25049	0.640
bta-miR-93	105.688	102.975	111.677	1.085	0.25129	0.637
bta-miR-134	0.972	0.911	1.105	**1.212**	0.25286	0.635
bta-miR-411b	2.104	1.993	2.361	1.185	0.25343	0.631
bta-miR-301a	2.004	1.897	2.260	1.191	0.25401	0.628
bta-miR-194	84.677	82.624	89.200	1.080	0.25749	0.631

Table 2.2 Continued

bta-miR-381	67.903	65.348	73.656	1.127	0.25793	0.627
bta-miR-660	171.623	167.038	181.763	1.088	0.25799	0.622
bta-miR-16a	540.640	549.344	522.639	0.951	0.26182	0.626
bta-miR-497	32.563	31.229	35.581	1.139	0.26358	0.625
bta-miR-92a	250.424	244.925	262.493	1.072	0.26373	0.620
bta-miR-885	20.586	21.249	19.248	0.906	0.26902	0.628
bta-miR-10a	93.049	91.070	97.387	1.069	0.27514	0.637
bta-miR-130a	8.257	8.484	7.796	0.919	0.27532	0.632
bta-miR-10b	2159.979	2120.440	2246.256	1.059	0.27926	0.636
bta-miR-154b	1.262	1.232	1.322	1.073	0.29262	0.662
bta-miR-100	141.886	138.767	148.730	1.072	0.29372	0.659
bta-miR-369-3p	51.944	50.580	54.959	1.087	0.29441	0.656
bta-miR-20a	17.805	17.361	18.783	1.082	0.30007	0.663
bta-miR-15b	30.512	29.763	32.164	1.081	0.30032	0.659
bta-miR-6120-3p	2.186	2.075	2.441	1.177	0.30085	0.655
bta-miR-30f	47.578	46.574	49.778	1.069	0.30092	0.651
bta-miR-374a	116.374	118.212	112.570	0.952	0.30757	0.660
bta-miR-365-5p	1.286	1.241	1.400	1.128	0.30859	0.657
bta-miR-132	1.824	1.715	2.074	**1.209**	0.31030	0.656
bta-miR-125a	332.564	326.455	345.894	1.060	0.31213	0.655
bta-miR-2284ab	4.460	4.302	4.808	1.118	0.31246	0.652
bta-miR-29b	31.915	32.420	30.869	0.952	0.31304	0.648
bta-miR-105a	2.094	1.993	2.325	1.166	0.31519	0.648
bta-miR-10020	1.636	1.514	1.926	**1.272**	0.31832	0.650
bta-miR-210	1.308	1.274	1.378	1.081	0.32659	0.662
bta-miR-149-5p	6.343	6.089	6.920	1.137	0.32663	0.658
bta-miR-2284z	4.743	4.555	5.169	1.135	0.33048	0.661
bta-miR-505	5.331	5.146	5.745	1.116	0.33498	0.665
bta-miR-204	5.163	5.560	4.412	**0.794**	0.33690	0.665
bta-miR-2285x	1.745	1.682	1.885	1.120	0.34210	0.671
bta-miR-1296	0.998	0.946	1.126	1.190	0.34958	0.681

Table 2.2 Continued

bta-miR-451	111.173	110.746	112.082	1.012	0.35126	0.679
bta-miR-34a	7.933	7.527	8.870	1.179	0.35736	0.687
bta-miR-99b	56.461	55.241	59.137	1.071	0.36028	0.688
bta-miR-2285bg	1.201	1.226	1.151	0.939	0.36385	0.690
bta-miR-33a	1.463	1.481	1.428	0.965	0.36733	0.692
bta-miR-26b	1620.186	1586.504	1693.976	1.068	0.36836	0.690
bta-miR-345-3p	4.050	4.197	3.755	0.895	0.37392	0.696
bta-miR-450a	68.154	66.729	71.278	1.068	0.38511	0.712
bta-miR-30a-5p	3989.850	3939.001	4099.831	1.041	0.39336	0.723
bta-miR-3432a	19.091	18.654	20.050	1.075	0.39385	0.719
bta-miR-148b	80.397	80.966	79.204	0.978	0.39452	0.716
bta-miR-139	46.772	45.832	48.829	1.065	0.39566	0.714
bta-miR-6529a	2.836	2.725	3.089	1.134	0.39664	0.711
bta-miR-199c	30.447	31.015	29.276	0.944	0.39680	0.707
bta-miR-339a	87.993	86.975	90.189	1.037	0.39896	0.707
bta-miR-99a-5p	1265.341	1243.479	1312.969	1.056	0.39957	0.703
bta-miR-26a	8743.192	8594.159	9067.746	1.055	0.40738	0.713
bta-miR-22-3p	8915.550	9020.773	8696.518	0.964	0.41360	0.720
bta-miR-652	102.116	100.353	105.956	1.056	0.41492	0.718
bta-miR-106a	1.599	1.553	1.701	1.096	0.41937	0.721
bta-miR-7	77.106	77.855	75.542	0.970	0.41957	0.717
bta-miR-3431	8.185	7.965	8.670	1.089	0.43221	0.735
bta-miR-223	5.615	5.646	5.551	0.983	0.43451	0.734
bta-miR-30b-3p	3.038	2.979	3.166	1.063	0.43578	0.732
bta-miR-95	99.228	97.675	102.604	1.050	0.43932	0.734
bta-miR-760-3p	0.988	0.947	1.073	1.133	0.44290	0.736
bta-miR-199a-5p	153.312	153.826	152.228	0.990	0.44474	0.735
bta-miR-504	11.798	11.718	11.970	1.022	0.45474	0.747
bta-miR-196b	82.234	81.197	84.477	1.040	0.45695	0.746
bta-miR-185	20.910	20.469	21.877	1.069	0.45798	0.744
bta-miR-133a	15858.437	15569.912	16487.915	1.059	0.46140	0.745

Table 2.2 Continued

bta-miR-215	4.901	4.639	5.506	1.187	0.46346	0.745
bta-miR-6119-5p	107.442	108.385	105.470	0.973	0.46689	0.746
bta-miR-25	114.967	113.302	118.578	1.047	0.46780	0.743
bta-miR-338	6.793	7.186	6.029	0.839	0.47288	0.747
bta-miR-302b	1.351	1.411	1.228	0.870	0.48164	0.757
bta-miR-362-3p	21.982	22.205	21.519	0.969	0.48557	0.759
bta-miR-433	1.017	0.968	1.120	1.158	0.49590	0.771
bta-miR-455-3p	12.180	11.702	13.258	1.133	0.49611	0.768
bta-miR-181c	10.108	10.210	9.895	0.969	0.50795	0.782
bta-miR-199a-3p	432.177	435.118	426.008	0.979	0.51085	0.782
bta-let-7i	1444.203	1451.113	1429.660	0.985	0.51408	0.783
bta-miR-7862	1.046	1.080	0.981	0.908	0.51998	0.788
bta-miR-1388-5p	2.992	3.055	2.861	0.936	0.52174	0.787
bta-miR-2484	52.982	54.017	50.852	0.941	0.52371	0.786
bta-miR-221	11.903	11.504	12.796	1.112	0.52866	0.789
bta-miR-152	82.770	83.161	81.946	0.985	0.53740	0.798
bta-miR-224	6.612	6.749	6.331	0.938	0.53907	0.796
bta-miR-2284y	8.283	8.160	8.552	1.048	0.54010	0.794
bta-miR-767	3.963	3.880	4.147	1.069	0.55636	0.814
bta-miR-425-3p	2.189	2.142	2.290	1.069	0.55701	0.811
bta-miR-302d	1.653	1.586	1.798	1.134	0.56144	0.813
bta-miR-7180	4.034	3.988	4.131	1.036	0.56869	0.820
bta-miR-29d-3p	9.996	9.800	10.425	1.064	0.57310	0.822
bta-miR-128	281.309	279.039	286.184	1.026	0.58671	0.837
bta-miR-11986b	2.215	2.423	1.832	**0.756**	0.58716	0.834
bta-miR-181b	27.769	27.394	28.579	1.043	0.58830	0.832
bta-miR-421	2.805	2.680	3.088	1.152	0.58854	0.828
bta-miR-2285av	3.275	3.253	3.322	1.021	0.59273	0.830
bta-miR-30c	729.003	723.983	739.762	1.022	0.60360	0.841
bta-miR-328	3.372	3.543	3.038	0.858	0.60408	0.838
bta-miR-218	9.291	9.286	9.301	1.002	0.60418	0.834

Table 2.2 Continued

bta-miR-500	20.655	20.308	21.409	1.054	0.61108	0.840
bta-miR-2284aa	1.164	1.196	1.099	0.920	0.61773	0.845
bta-miR-19b	19.207	19.122	19.390	1.014	0.61981	0.844
bta-miR-339b	11.171	11.104	11.316	1.019	0.62147	0.842
bta-miR-11977	2.070	2.021	2.175	1.076	0.62289	0.840
bta-miR-2419-5p	3.338	3.264	3.500	1.072	0.62446	0.838
bta-miR-188	2.212	2.125	2.403	1.131	0.63358	0.847
bta-miR-101	1487.268	1480.894	1500.871	1.013	0.63490	0.845
bta-miR-376d	2.388	2.340	2.493	1.065	0.63591	0.842
bta-miR-126-5p	467.650	463.082	477.485	1.031	0.63923	0.843
bta-let-7a-3p	54.936	54.677	55.489	1.015	0.64383	0.845
bta-miR-2285ce	1.823	1.810	1.854	1.025	0.64642	0.845
bta-miR-502a	4.597	4.458	4.907	1.101	0.64914	0.844
bta-miR-99a-3p	2.721	2.721	2.720	0.999	0.65049	0.842
bta-miR-142-3p	4.645	4.647	4.640	0.998	0.65334	0.842
bta-miR-574	2.933	2.969	2.859	0.963	0.65504	0.841
bta-miR-374b	41.860	41.174	43.353	1.053	0.66651	0.852
bta-miR-450b	78.887	78.256	80.243	1.025	0.67464	0.859
bta-miR-29c	218.606	215.356	225.661	1.048	0.67678	0.858
bta-miR-324	1.088	1.030	1.220	1.184	0.67888	0.857
bta-miR-335	54.585	55.082	53.546	0.972	0.69705	0.876
bta-miR-452	3.663	3.687	3.611	0.979	0.69779	0.873
bta-miR-411a	223.164	223.897	221.616	0.990	0.71078	0.885
bta-miR-376e	21.870	21.541	22.584	1.048	0.72732	0.902
bta-miR-2285u	1.681	1.677	1.689	1.007	0.73030	0.902
bta-miR-21-5p	2725.559	2702.198	2775.754	1.027	0.73125	0.900
bta-miR-150	13.562	13.860	12.952	0.935	0.73151	0.896
bta-miR-1839	24.432	24.233	24.860	1.026	0.73427	0.896
bta-miR-2285cm	1.314	1.312	1.318	1.005	0.73483	0.893
bta-miR-6119-3p	7.329	7.323	7.343	1.003	0.74249	0.898
bta-miR-2404	1.039	1.022	1.079	1.056	0.74389	0.896

Table 2.2 Continued

bta-miR-369-5p	6.630	6.619	6.654	1.005	0.74438	0.893
bta-miR-181a	492.236	486.177	505.333	1.039	0.74536	0.891
bta-miR-130b	1.007	1.015	0.993	0.978	0.75980	0.904
bta-miR-4286	1.238	1.200	1.325	1.104	0.76077	0.902
bta-miR-2285k	1.233	1.226	1.249	1.019	0.77110	0.910
bta-miR-27a-3p	722.408	706.962	756.279	1.070	0.77866	0.916
bta-miR-874	1.343	1.380	1.267	0.919	0.78001	0.914
bta-miR-499	4515.287	4538.226	4467.038	0.984	0.78173	0.912
bta-miR-379	113.073	113.253	112.693	0.995	0.78525	0.913
bta-miR-16b	244.391	244.833	243.456	0.994	0.78687	0.911
bta-miR-18a	4.615	4.714	4.414	0.936	0.78738	0.908
bta-miR-376b	1.060	1.079	1.019	0.944	0.79623	0.914
bta-miR-146b	9.909	9.866	10.001	1.014	0.79707	0.912
bta-miR-425-5p	37.940	37.699	38.457	1.020	0.80003	0.912
bta-miR-1271	5.692	5.611	5.867	1.046	0.80253	0.911
bta-miR-342	32.411	32.667	31.874	0.976	0.80274	0.908
bta-miR-454	1.134	1.124	1.153	1.025	0.81396	0.917
bta-miR-302a	1.751	1.729	1.794	1.038	0.83496	0.937
bta-miR-126-3p	4056.995	4057.827	4055.233	0.999	0.83838	0.937
bta-miR-19a	3.997	3.989	4.013	1.006	0.84971	0.946
bta-miR-195	207.952	207.582	208.740	1.006	0.85256	0.946
bta-miR-193a-3p	1.719	1.678	1.810	1.079	0.85259	0.942
bta-miR-340	7.732	7.671	7.864	1.025	0.85895	0.946
bta-miR-2285b	2.963	2.988	2.911	0.974	0.86518	0.949
bta-miR-370	2.046	2.015	2.111	1.048	0.86662	0.947
bta-miR-424-5p	42.832	42.395	43.773	1.033	0.87948	0.958
bta-miR-24-3p	2950.605	2918.819	3019.140	1.034	0.88680	0.962
bta-miR-199b	79.371	79.000	80.162	1.015	0.88735	0.959
bta-miR-2332	1.986	1.996	1.964	0.984	0.90195	0.971
bta-miR-2285t	3.470	3.418	3.583	1.048	0.90392	0.970
bta-miR-2285bn	1.923	1.975	1.818	0.921	0.90399	0.966

Table 2.2 Continued

bta-miR-2285ad	1.320	1.323	1.315	0.994	0.90404	0.963
bta-miR-214	14.176	14.120	14.295	1.012	0.91224	0.968
bta-miR-2387	1.008	0.995	1.037	1.043	0.92144	0.974
bta-miR-190b	2.265	2.250	2.298	1.021	0.92441	0.974
bta-miR-769	1.728	1.728	1.727	1.000	0.92782	0.974
bta-miR-3432b	2.104	2.089	2.136	1.022	0.93330	0.976
bta-miR-186	698.625	696.569	703.003	1.009	0.93534	0.975
bta-miR-155	8.882	8.783	9.095	1.036	0.94359	0.980
bta-miR-2284a	1.567	1.576	1.549	0.983	0.94373	0.977
bta-miR-708	3.745	3.721	3.797	1.021	0.95213	0.982
bta-miR-190a	6.700	6.744	6.607	0.980	0.95668	0.983
bta-miR-628	7.857	7.822	7.932	1.014	0.95862	0.982
bta-miR-363	3.292	3.362	3.150	0.937	0.96355	0.984
bta-miR-491	2.276	2.257	2.316	1.026	0.97119	0.988
bta-miR-1246	1.292	1.288	1.300	1.009	0.98901	1.003
bta-miR-29a	926.627	924.503	931.147	1.007	0.98991	1.000
bta-miR-296-3p	2.071	2.095	2.021	0.965	0.999211385	1.006

[1] Of 292 miRNAs expressed at a minimum threshold of at least 1 CPM, 31 miRNAs exhibited differential expression with $p \leq 0.05$.

[2] Fold difference was calculated as (DFD/NON).

[3] Adjusted Welch's *t*-test *p*-values to control for multiple testing at FDR of 5% via the Benjamini-Hochberg method. (*p*-value*292/rank)

Table 2.4 Differentially expressed miRNAs between normal beef carcasses and those exhibiting the DFD phenotype according to DESeq2 analysis. Expression ratios shown as DFD/NON. The threshold for statistical significance for differential expression was set as p_{adj} (≤ 0.05).

miRNA[1]	baseMean[2]	Fold Difference[3] (log_2)	Fold difference[4] (log_{10})	lfcSE[5]	Stat[6]	*p*-value	p_{adj}[7]
bta-miR-2422*	**5.537225**	**0.782301**	**1.72**	**0.201046**	**3.891158**	**0.000099800**	**0.0541**
bta-miR-1260b*	12.130828	0.657147	**1.58**	0.199356	3.296344	**0.000979521**	0.2534
bta-miR-144	25.261124	-0.842237	**0.56**	0.266125	-3.164821	**0.001551782**	0.2534
bta-miR-10174-5p	2.684507	0.948680	**1.93**	0.305026	3.110164	**0.001869836**	0.2534
bta-miR-148a	1389.298815	-0.223801	0.86	0.073570	-3.041997	**0.002350141**	0.2548
bta-miR-2285e	3.140881	0.683174	**1.61**	0.234911	2.908225	**0.003634862**	0.2861
bta-miR-2285at	2.179531	0.819967	**1.77**	0.287829	2.848799	**0.004388459**	0.2861
bta-miR-142-5p	145.191977	-0.372611	**0.77**	0.131392	-2.835881	**0.004569941**	0.2861
bta-miR-206	10196.55151	0.168747	1.12	0.059765	2.823511	**0.004750072**	0.2861
bta-miR-3613a	375.894830	-0.336897	**0.79**	0.120946	-2.785511	**0.005344335**	0.2897
bta-miR-493*	20.736229	0.334943	**1.26**	0.123069	2.721581	**0.006497047**	0.3201
bta-miR-27a-5p*	10.569774	0.467175	**1.38**	0.174474	2.677614	**0.007414854**	0.3349
bta-miR-136*	8.859364	-0.549883	**0.68**	0.213603	-2.574327	**0.010043536**	0.4001
bta-miR-146a	246.050892	-0.417407	**0.75**	0.164238	-2.541480	**0.01103843**	0.4001
bta-miR-23b-5p	1.555601	1.087160	**2.12**	0.427946	2.540417	**0.011072048**	0.4001
bta-miR-32	876.046909	-0.279171	0.82	0.118582	-2.354242	**0.018560538**	0.5545
bta-miR-2285r	1.562110	-1.003818	**0.50**	0.427714	-2.346936	**0.018928517**	0.5545
bta-miR-1307*	12.526238	0.369588	**1.29**	0.157492	2.346706	**0.018940201**	0.5545
bta-miR-2285aa	1.324645	-1.151635	**0.45**	0.494519	-2.328798	**0.019869749**	0.5545
bta-miR-2285o	22.986542	-0.286760	0.82	0.125228	-2.289910	**0.022026506**	0.5545
bta-miR-31	4.477936	-0.674125	**0.63**	0.294719	-2.287348	**0.022175541**	0.5545
bta-miR-10162-5p	1.316099	0.881745	**1.84**	0.388739	2.268220	**0.023315787**	0.5545
bta-miR-30e-5p	25467.20372	-0.164962	0.89	0.072841	-2.264689	**0.023531784**	0.5545
bta-miR-2299-5p	1.894945	-0.835436	**0.56**	0.376643	-2.218109	**0.026547434**	0.5803
bta-miR-2284k	1.444190	-0.899801	**0.54**	0.406246	-2.214915	**0.026765926**	0.5803
bta-miR-2285q*	3.657111	-0.599624	**0.66**	0.277126	-2.163723	**0.030485626**	0.6045
bta-miR-2478	32.272897	0.311441	**1.24**	0.144154	2.160473	**0.030736063**	0.6045

Table 2.3 Continued

bta-miR-431	1.261808	1.057601	**2.08**	0.494122	2.140362	**0.032325514**	0.6045
bta-miR-543*	12.774199	0.351976	**1.28**	0.164918	2.134247	**0.032822528**	0.6045
bta-miR-671	2.165656	-0.735509	**0.60**	0.348527	-2.110332	**0.034829787**	0.6045
bta-miR-380-3p	50.307019	0.209695	1.16	0.100985	2.076501	**0.037847602**	0.6045
bta-miR-16a	2008.088667	-0.161258	0.89	0.077870	-2.070877	**0.038370338**	0.6045
bta-miR-361	225.670813	0.115881	1.08	0.057232	2.024755	**0.042892528**	0.6045
bta-miR-1434-5p	37.678583	-0.315719	**0.80**	0.156242	-2.020710	**0.043309787**	0.6045
bta-miR-130a	31.408686	-0.217856	0.86	0.108816	-2.002062	**0.045278078**	0.6045
bta-miR-18b	0.473127	-1.425416	**0.37**	0.715235	-1.992934	**0.046268641**	0.6045
bta-miR-11994*	6.873714	0.352410	**1.28**	0.177269	1.987994	**0.046812349**	0.6045
bta-miR-186	2545.507985	-0.080731	0.95	0.040761	-1.980565	**0.04764009**	0.6045
bta-miR-10174-3p	3554.332911	0.120053	1.09	0.060657	1.979223	**0.047790905**	0.6045
bta-miR-6123	5.081524	-0.453418	**0.73**	0.229257	-1.977767	**0.047954982**	0.6045
bta-miR-1388-3p	13.014946	-0.296196	0.81	0.150404	-1.969332	**0.048914969**	0.6045
bta-miR-23b-3p	3538.095095	0.118983	1.09	0.060702	1.960114	**0.049982437**	0.6045
bta-miR-487b	99.567564	0.179214	1.13	0.091780	1.952649	0.050861191	0.6045
bta-miR-103	749.187220	0.121546	1.09	0.062533	1.943725	0.051928602	0.6045
bta-miR-17-5p	61.363272	0.157361	1.12	0.080960	1.943684	0.051933564	0.6045
bta-miR-143	79197.29846	-0.225916	0.86	0.117024	-1.930505	0.053544238	0.6045
bta-miR-2336	7.863337	-0.333769	**0.79**	0.174410	-1.913701	0.055658372	0.6045
bta-miR-378c	698.608000	0.132992	1.10	0.070365	1.890034	0.05875341	0.6045
bta-miR-2285co	0.516628	-1.258545	**0.42**	0.670300	-1.877586	0.060437812	0.6045
bta-miR-2285bf	148.635782	-0.219350	0.86	0.117125	-1.872779	0.061098879	0.6045
bta-miR-29b	121.042753	-0.194785	0.87	0.104626	-1.861721	0.062642468	0.6045
bta-miR-208b	236.095631	-0.322285	**0.80**	0.173505	-1.857495	0.063240802	0.6045
bta-miR-2285f	39.005543	-0.248802	0.84	0.135148	-1.840963	0.06562705	0.6045
bta-miR-199c	116.764442	-0.213315	0.86	0.115882	-1.840800	0.065650818	0.6045
bta-miR-342	119.332468	-0.119748	0.92	0.065315	-1.833389	0.066744803	0.6045
bta-miR-148b	296.908636	-0.127920	0.92	0.069845	-1.831495	0.067026671	0.6045
bta-miR-9851	0.625384	-1.226108	**0.43**	0.670390	-1.828946	0.067407663	0.6045
bta-miR-22-3p	33266.05868	-0.154357	0.90	0.084467	-1.827412	0.06763788	0.6045

Table 2.3 Continued

bta-miR-152	306.177384	-0.133030	0.91	0.072938	-1.823886	0.068169257	0.6045
bta-miR-432	8.486918	0.303306	**1.23**	0.167268	1.813288	0.069787409	0.6045
bta-miR-665	3.363249	0.480928	**1.40**	0.266243	1.806347	0.070864192	0.6045
bta-miR-16b	897.290510	-0.106676	0.93	0.059095	-1.805149	0.071051347	0.6045
bta-miR-376c	8.794361	0.288536	**1.22**	0.159968	1.803712	0.071276491	0.6045
bta-miR-411c-5p	25.994368	0.229931	1.17	0.127523	1.803046	0.071381019	0.6045
bta-miR-1248	56.495181	-0.361698	**0.78**	0.204206	-1.771239	0.076520976	0.6312
bta-miR-23a	3383.538828	0.135248	1.10	0.076446	1.769200	0.076860527	0.6312
bta-let-7i	5330.247959	-0.120825	0.92	0.068645	-1.760157	0.078381258	0.6341
bta-miR-378b	50.531875	0.219045	1.16	0.126139	1.736540	0.082468326	0.6573
bta-miR-2285bu	0.702651	-1.006294	**0.50**	0.593083	-1.696715	0.089750581	0.6806
bta-miR-1	2711501.555	-0.123981	0.92	0.073267	-1.692181	0.090611395	0.6806
bta-miR-2285ba	9.997531	-0.403472	**0.76**	0.238465	-1.691954	0.090654709	0.6806
bta-miR-383	2.354576	0.519694	**1.43**	0.308120	1.686662	0.091668291	0.6806
bta-miR-362-3p	82.769434	-0.164507	0.89	0.097536	-1.686640	0.091672654	0.6806
bta-miR-135b	2.208272	0.752006	**1.68**	0.451710	1.664798	0.09595305	0.6890
bta-miR-29a	3397.268768	-0.093603	0.94	0.056426	-1.658874	0.097141094	0.6890
bta-miR-653	9.958054	-0.350388	**0.78**	0.211362	-1.657764	0.097365016	0.6890
bta-miR-885	83.904730	-0.265861	0.83	0.160621	-1.655212	0.097881599	0.6890
bta-miR-7	286.937844	-0.130791	0.91	0.081867	-1.597599	0.110132321	0.7653
bta-miR-345-5p	2.698728	-0.450174	**0.73**	0.284484	-1.582423	0.11355302	0.7791
bta-miR-199a-3p	1645.355806	-0.169708	0.89	0.107780	-1.574582	0.115352914	0.7815
bta-miR-410	18.308140	0.228836	1.17	0.146933	1.557419	0.119371068	0.7871
bta-miR-378	10828.00925	0.098669	1.07	0.063362	1.557244	0.119412489	0.7871
bta-miR-2285bt	0.493781	-1.123207	**0.46**	0.723896	-1.551614	0.120754556	0.7871
bta-miR-382	25.958405	0.199065	1.15	0.128719	1.546517	0.121979689	0.7871
bta-miR-326	4.634574	0.352643	**1.28**	0.229826	1.534393	0.124933094	0.7966
bta-miR-345-3p	16.415557	-0.237489	0.85	0.156714	-1.515425	0.12966471	0.8013
bta-miR-423-3p	1432.351275	0.097705	1.07	0.064595	1.512589	0.130384163	0.8013
bta-miR-105b	0.645057	0.838915	**1.79**	0.558995	1.500758	0.133418188	0.8013
bta-miR-24	53.207732	0.130087	1.09	0.086781	1.499030	0.13386573	0.8013

Table 2.3 Continued

bta-miR-224	25.645335	-0.192814	0.87	0.128910	-1.495729	0.134724272	0.8013
bta-miR-2285bc	1.886244	-0.626023	**0.65**	0.419384	-1.492720	0.135510578	0.8013
bta-miR-328	13.516421	-0.228137	0.85	0.153561	-1.485647	0.137372554	0.8013
bta-miR-2431-3p	0.863246	0.749575	**1.68**	0.504689	1.485223	0.137484769	0.8013
bta-miR-374a	458.251217	-0.202106	0.87	0.136708	-1.478373	0.139307972	0.8032
bta-miR-375	0.514126	-0.970412	**0.51**	0.671222	-1.445739	0.14825039	0.8218
bta-miR-6536	0.404843	-0.995304	**0.50**	0.692505	-1.437252	0.150646327	0.8218
bta-miR-11990	0.443264	-1.142514	**0.45**	0.795566	-1.436101	0.150973683	0.8218
bta-miR-2484	210.706411	-0.206621	0.87	0.144618	-1.428735	0.153080439	0.8218
bta-miR-2285n	3.455000	-0.368796	**0.77**	0.258377	-1.427357	0.153477054	0.8218
bta-miR-199a-5p	603.126182	-0.193264	0.87	0.136368	-1.417230	0.156415566	0.8218
bta-miR-551b	0.398500	-1.213975	**0.43**	0.856738	-1.416973	0.156490774	0.8218
bta-miR-423-5p	297.541866	0.122065	1.09	0.086720	1.407571	0.159258262	0.8218
bta-miR-495	42.312871	0.158296	1.12	0.112553	1.406412	0.159601956	0.8218
bta-miR-223	23.142448	-0.236958	0.85	0.168897	-1.402971	0.160625356	0.8218
bta-miR-153	2.772881	0.599468	**1.52**	0.428730	1.398241	0.162040586	0.8218
bta-miR-302b	5.892360	-0.327401	0.80	0.236222	-1.385987	0.165750854	0.8218
bta-miR-2285dd	2.107016	-0.448539	**0.73**	0.327538	-1.369427	0.170865887	0.8218
bta-miR-2285j	3.111133	-0.416243	**0.75**	0.305284	-1.363461	0.172737275	0.8218
bta-miR-1277	1.773030	-0.500609	**0.71**	0.367263	-1.363081	0.172857028	0.8218
bta-miR-29d-5p	26.096595	0.153493	1.11	0.112713	1.361802	0.17326033	0.8218
bta-miR-378d	106.957619	0.114979	1.08	0.084543	1.360009	0.173827025	0.8218
bta-miR-409a	16.511953	0.180943	1.13	0.133204	1.358396	0.174338017	0.8218
bta-miR-154b	5.409412	0.306130	**1.24**	0.225558	1.357212	0.174713812	0.8218
bta-miR-126-3p	14992.99965	-0.096702	0.94	0.071266	-1.356929	0.174803619	0.8218
bta-miR-150	51.514142	-0.144178	0.90	0.106263	-1.356798	0.174845259	0.8218
bta-miR-2285da	2.404445	-0.399828	**0.76**	0.295962	-1.350944	0.17671335	0.8218
bta-miR-181c	39.314570	-0.165598	0.89	0.122771	-1.348838	0.177388965	0.8218
bta-miR-6119-5p	411.118692	-0.151152	0.90	0.112994	-1.337708	0.180991744	0.8269
bta-miR-200c	0.710835	0.735526	**1.67**	0.551283	1.334208	0.182135716	0.8269
bta-miR-424-3p	17.381185	0.186840	1.14	0.140338	1.331363	0.18306963	0.8269

Table 2.3 Continued

bta-miR-181d	10.003412	0.197520	1.15	0.149293	1.323035	0.185823748	0.8324
bta-miR-654	1.192537	0.562778	**1.48**	0.427967	1.315005	0.188508113	0.8362
bta-miR-92b	1.841029	-0.476541	**0.72**	0.363416	-1.311283	0.189762009	0.8362
bta-miR-1185	1.497167	0.475986	**1.39**	0.367121	1.296538	0.194790068	0.8514
bta-miR-193a-5p	151.673650	0.105237	1.08	0.081902	1.284902	0.19882655	0.8556
bta-miR-2285cz	0.252163	1.226963	**2.34**	0.958401	1.280218	0.200468441	0.8556
bta-miR-503-5p	14.785375	0.204023	1.15	0.159713	1.277436	0.201448424	0.8556
bta-miR-11986b	9.379115	-0.232075	0.85	0.181917	-1.275718	0.202055242	0.8556
bta-miR-484	70.043492	0.111471	1.08	0.089793	1.241422	0.214450051	0.8756
bta-miR-2285bb	2.329083	-0.471394	**0.72**	0.380239	-1.239731	0.215074882	0.8756
bta-miR-877	0.804576	0.688219	**1.61**	0.559516	1.230026	0.218687376	0.8756
bta-miR-1388-5p	11.970133	-0.186320	0.88	0.151799	-1.227410	0.219668404	0.8756
bta-miR-2411-5p	2.482697	-0.344585	**0.79**	0.281223	-1.225311	0.220458228	0.8756
bta-miR-2468	1.581010	-0.544118	**0.69**	0.444097	-1.225223	0.220491328	0.8756
bta-miR-2285bl	0.602364	-0.698799	**0.62**	0.570524	-1.224837	0.220636668	0.8756
bta-miR-2320-3p	0.926677	-0.668781	**0.63**	0.546140	-1.224558	0.220741866	0.8756
bta-miR-11995	2.213751	0.402408	**1.32**	0.329031	1.223009	0.221326417	0.8756
bta-miR-151-5p	2360.830520	0.072856	1.05	0.060045	1.213360	0.22499239	0.8831
bta-miR-1343-3p	21.985193	0.144060	1.11	0.119154	1.209017	0.226656308	0.8831
bta-let-7a-5p	13269.81013	0.078463	1.06	0.065101	1.205247	0.228108023	0.8831
bta-miR-11987	2.702641	-0.634640	**0.64**	0.534020	-1.188420	0.234667871	0.8958
bta-miR-28	393.906166	0.076225	1.05	0.064204	1.187224	0.235139226	0.8958
bta-miR-204	20.960468	-0.213630	0.86	0.181139	-1.179368	0.238251614	0.8958
bta-miR-411a	834.081374	-0.103279	0.93	0.087690	-1.177778	0.238884948	0.8958
bta-let-7e	387.667781	0.088907	1.06	0.075682	1.174740	0.240098701	0.8958
bta-miR-2285br	0.549934	-0.752962	**0.59**	0.642598	-1.171745	0.241299281	0.8958
bta-miR-2354	0.321247	-0.997379	**0.50**	0.855685	-1.165591	0.243779926	0.8988
bta-miR-11991	3.303437	-0.323141	**0.80**	0.279174	-1.157490	0.247072163	0.9047
bta-miR-154c	39.117969	0.142076	1.10	0.123248	1.152761	0.249008672	0.9047
bta-miR-320a	359.771998	0.096990	1.07	0.084753	1.144381	0.2524657	0.9047
bta-miR-2285by	1.929721	-0.393064	**0.76**	0.344219	-1.141899	0.253495811	0.9047

Table 2.3 Continued

bta-miR-338	29.139630	-0.213770	0.86	0.188710	-1.132797	0.257299694	0.9047
bta-miR-301b	0.251069	-1.020329	**0.49**	0.901334	-1.132021	0.257625446	0.9047
bta-miR-499	16961.84389	-0.106155	0.93	0.093888	-1.130656	0.258200039	0.9047
bta-miR-3956	1.718955	0.394081	**1.31**	0.350610	1.123988	0.26101827	0.9047
bta-miR-6522	3.842564	0.265391	**1.20**	0.236312	1.123057	0.261413258	0.9047
bta-miR-2887	19.196556	0.168105	1.12	0.150104	1.119925	0.262745631	0.9047
bta-miR-299	6.755569	0.259573	**1.20**	0.232256	1.117616	0.26373105	0.9047
bta-miR-655	41.238377	0.169774	1.12	0.152979	1.109786	0.267091216	0.9093
bta-miR-1842	1.314967	0.452056	**1.37**	0.409401	1.104188	0.269511684	0.9093
bta-miR-2285ad	5.372519	-0.244801	0.84	0.222354	-1.100950	0.270918277	0.9093
bta-miR-21-5p	9979.089096	-0.059102	0.96	0.053933	-1.095842	0.273148043	0.9093
bta-miR-11993	2.807307	0.274087	**1.21**	0.251060	1.091719	0.274956541	0.9093
bta-miR-195	773.564535	-0.088959	0.94	0.081514	-1.091338	0.275124043	0.9093
bta-miR-574	11.878680	-0.166777	0.89	0.157030	-1.062072	0.288203071	0.9463
bta-miR-6524	3.636119	-0.266678	0.83	0.252664	-1.055464	0.291213027	0.9463
bta-miR-18a	17.839315	-0.123481	0.92	0.117660	-1.049468	0.293962594	0.9463
bta-miR-425-5p	139.260685	-0.063859	0.96	0.061061	-1.045814	0.29564679	0.9463
bta-miR-196a	474.034431	0.072533	1.05	0.069427	1.044743	0.296141995	0.9463
bta-miR-369-5p	25.739660	-0.133215	0.91	0.127748	-1.042797	0.29704216	0.9463
bta-miR-2320-5p	0.377974	-0.711234	**0.61**	0.685388	-1.037710	0.299405235	0.9463
bta-miR-335	211.698578	-0.130538	0.91	0.126029	-1.035773	0.300308108	0.9463
bta-miR-2443	0.729681	0.531492	**1.45**	0.516583	1.028862	0.303544417	0.9496
bta-miR-362-5p	269.640382	0.070897	1.05	0.069095	1.026083	0.304852634	0.9496
bta-miR-141	1.013909	0.493266	**1.41**	0.483033	1.021186	0.307166434	0.9513
bta-miR-11986c	0.442435	-0.754583	**0.59**	0.742543	-1.016214	0.309527712	0.9516
bta-miR-99a-3p	10.980521	-0.157097	0.90	0.154983	-1.013641	0.310754108	0.9516
bta-miR-2284f	0.216005	-1.163279	**0.45**	1.162094	-1.001020	0.316817205	0.9567
bta-miR-2285bo	0.772962	-0.551947	**0.68**	0.552354	-0.999264	0.317666655	0.9567
bta-miR-455-5p	3.157259	-0.251334	0.84	0.251543	-0.999172	0.317711375	0.9567
bta-miR-107	104.315348	0.087838	1.06	0.089061	0.986267	0.324001872	0.9678
bta-miR-1247-5p	5.067449	0.229148	1.17	0.232986	0.983526	0.325348753	0.9678

Table 2.3 Continued

bta-miR-191	913.984981	0.047244	1.03	0.048177	0.980635	0.326773007	0.9678
bta-miR-218	36.654491	-0.137563	0.91	0.141415	-0.972759	0.330672913	0.9737
bta-miR-486	1758.974709	0.086250	1.06	0.089255	0.966337	0.333875388	0.9737
bta-miR-33a	6.077309	-0.199919	0.87	0.206996	-0.965815	0.334136908	0.9737
bta-miR-2431-5p	1.362674	0.388333	**1.31**	0.407574	0.952791	0.340696012	0.9772
bta-miR-2285i	0.418597	0.713781	**1.64**	0.749359	0.952522	0.340832469	0.9772
bta-miR-19b	70.758941	-0.066584	0.95	0.069977	-0.951517	0.341341888	0.9772
bta-miR-210	5.021054	0.209178	1.16	0.220395	0.949107	0.342565992	0.9772
bta-miR-2285cs	0.594381	0.643034	**1.56**	0.685221	0.938434	0.348021616	0.9796
bta-miR-134	3.821725	0.210336	1.16	0.224502	0.936897	0.348811336	0.9796
bta-miR-101	5504.446518	-0.069263	0.95	0.074036	-0.935530	0.34951528	0.9796
bta-miR-2904	179.336798	0.120071	1.09	0.128641	0.933386	0.350620866	0.9796
bta-miR-379	429.338910	-0.097423	0.93	0.106146	-0.917823	0.358711538	0.9922
bta-miR-677	1.589466	-0.398916	**0.76**	0.436731	-0.913414	0.361024594	0.9922
bta-miR-744	0.648763	-0.540411	**0.69**	0.592454	-0.912158	0.361685763	0.9922
bta-miR-1306	4.423368	0.194015	1.14	0.215009	0.902357	0.366867045	0.9922
bta-miR-2285cf	5.337997	0.177523	1.13	0.202081	0.878474	0.379686754	0.9922
bta-miR-138	0.222335	-0.860848	**0.55**	0.982772	-0.875939	0.381063409	0.9922
bta-miR-532	210.509555	0.062506	1.04	0.071966	0.868554	0.385091257	0.9922
bta-miR-199b	298.970818	-0.084814	0.94	0.097733	-0.867809	0.3854989	0.9922
bta-miR-1839	90.364861	-0.064225	0.96	0.074028	-0.867583	0.385622493	0.9922
bta-miR-30c	2688.628475	-0.059234	0.96	0.068390	-0.866124	0.386422349	0.9922
bta-miR-135a	1.764273	0.348743	**1.27**	0.404265	0.862659	0.388324814	0.9922
bta-miR-2285as	0.633987	-0.502732	**0.71**	0.583392	-0.861740	0.388830859	0.9922
bta-miR-106b	279.938767	0.041730	1.03	0.048590	0.858815	0.390442701	0.9922
bta-miR-491	8.975289	-0.139489	0.91	0.162478	-0.858514	0.390608622	0.9922
bta-miR-452	14.463493	-0.127863	0.92	0.148975	-0.858284	0.390735899	0.9922
bta-miR-376a	2.015638	-0.273889	0.83	0.319228	-0.857974	0.390906852	0.9922
bta-miR-11992	0.892877	0.500792	**1.41**	0.584349	0.857007	0.391440941	0.9922
bta-miR-760-3p	3.837806	0.204239	1.15	0.238843	0.855120	0.392484608	0.9922
bta-miR-2415-3p	0.185312	-0.934939	**0.52**	1.094143	-0.854494	0.392831344	0.9922

Table 2.3 Continued

bta-miR-2284aa	4.962748	-0.180733	0.88	0.213679	-0.845815	0.397655859	0.9922
bta-miR-377	0.548308	0.500471	**1.41**	0.597478	0.837639	0.40223355	0.9922
bta-miR-6523a	1.986607	-0.312078	0.81	0.374900	-0.832430	0.405166302	0.9922
bta-let-7a-3p	205.680747	-0.074434	0.95	0.090826	-0.819514	0.412493303	0.9922
bta-miR-365-3p	656.423538	0.060925	1.04	0.074946	0.812913	0.416267687	0.9922
bta-miR-2285bg	5.646569	-0.227897	0.85	0.280557	-0.812304	0.416617137	0.9922
bta-miR-2285dl-3p	1.403683	-0.332886	**0.79**	0.410827	-0.810282	0.41777818	0.9922
bta-miR-15a	410.151572	0.065936	1.05	0.081836	0.805709	0.420410793	0.9922
bta-miR-542-5p	2.778166	-0.221654	0.86	0.275757	-0.803801	0.421511771	0.9922
bta-miR-127	103.886793	0.070454	1.05	0.088057	0.800095	0.423655619	0.9922
bta-miR-146b	38.583400	-0.105429	0.93	0.132382	-0.796403	0.425797787	0.9922
bta-miR-497	123.075035	0.080251	1.06	0.100906	0.795303	0.426437361	0.9922
bta-miR-2284c	0.284542	-0.694259	**0.62**	0.873192	-0.795082	0.426565767	0.9922
bta-miR-27b	10508.40025	0.036780	1.03	0.046575	0.789685	0.42971168	0.9922
bta-miR-145	716.250573	0.076588	1.05	0.097524	0.785331	0.432259656	0.9922
bta-miR-132	7.527233	0.146547	1.11	0.186915	0.784029	0.433023299	0.9922
bta-miR-331-3p	139.312466	0.070125	1.05	0.090148	0.777878	0.436640962	0.9922
bta-miR-11984	1.199468	-0.392196	**0.76**	0.506303	-0.774628	0.438559404	0.9922
bta-miR-133b	833.478060	0.057842	1.04	0.074938	0.771870	0.440191294	0.9922
bta-miR-582	0.513995	0.471203	**1.39**	0.611374	0.770727	0.440868514	0.9922
bta-miR-2285aw	2.065789	-0.277935	0.82	0.360913	-0.770089	0.441246999	0.9922
bta-miR-128	1046.213488	-0.062401	0.96	0.081427	-0.766348	0.443469051	0.9922
bta-miR-2285bs	0.210431	0.831092	**1.78**	1.085171	0.765862	0.44375816	0.9922
bta-miR-6520	1.486840	0.285342	**1.22**	0.374335	0.762266	0.445901514	0.9922
bta-miR-2285u	7.105578	-0.141429	0.91	0.185814	-0.761134	0.446576951	0.9922
bta-miR-340	29.020602	-0.074454	0.95	0.098575	-0.755304	0.450066874	0.9922
bta-miR-2311	0.386824	-0.572898	**0.67**	0.764572	-0.749306	0.453672829	0.9922
bta-miR-2285x	7.842257	0.155579	1.11	0.209003	0.744387	0.456642241	0.9922
bta-miR-449a	0.240220	0.699378	**1.62**	0.947055	0.738477	0.460224854	0.9922
bta-miR-628	29.610962	-0.074597	0.95	0.101053	-0.738205	0.460390163	0.9922
bta-miR-411b	8.486104	0.118462	1.09	0.160521	0.737985	0.460523609	0.9922

Table 2.3 Continued

bta-miR-346	0.789994	0.419847	**1.34**	0.570706	0.735662	0.461936601	0.9922
bta-miR-483	0.976055	-0.378042	**0.77**	0.518333	-0.729343	0.465792119	0.9922
bta-miR-19a	16.089875	-0.110479	0.93	0.151875	-0.727435	0.466959455	0.9922
bta-miR-222	36.074524	0.092531	1.07	0.127422	0.726179	0.467729322	0.9922
bta-miR-376b	4.105146	-0.204219	0.87	0.284733	-0.717228	0.473233209	0.9922
bta-miR-155	34.020427	-0.084075	0.94	0.117298	-0.716762	0.473521036	0.9922
bta-miR-2334	0.611317	0.428566	**1.35**	0.598561	0.715994	0.473994869	0.9922
bta-miR-2285g	2.457431	0.270521	**1.21**	0.378245	0.715201	0.474484916	0.9922
bta-miR-2440	2.717350	-0.326366	**0.80**	0.456576	-0.714812	0.47472537	0.9922
bta-let-7f	24221.82248	0.039837	1.03	0.055985	0.711567	0.476732988	0.9922
bta-miR-125b	3717.743482	0.037458	1.03	0.052839	0.708910	0.478380379	0.9922
bta-miR-193b	191.708150	0.065383	1.05	0.093511	0.699199	0.484427402	0.9922
bta-miR-2285h	0.386984	-0.588043	**0.67**	0.843643	-0.697028	0.485785102	0.9922
bta-miR-367	0.289243	-0.598610	**0.66**	0.860636	-0.695544	0.486714605	0.9922
bta-miR-190a	25.907191	-0.087395	0.94	0.125892	-0.694205	0.487553694	0.9922
bta-miR-2285cp	0.195536	-0.812037	**0.57**	1.174710	-0.691266	0.489398467	0.9922
bta-miR-9-5p	19.791013	0.095686	1.07	0.138690	0.689924	0.490241897	0.9922
bta-miR-25	422.708389	-0.043808	0.97	0.063538	-0.689472	0.490526111	0.9922
bta-miR-6119-3p	27.889959	-0.073541	0.95	0.107419	-0.684616	0.493586201	0.9922
bta-miR-10172-3p	1.579993	0.250803	1.19	0.367966	0.681592	0.495497098	0.9922
bta-miR-2284m	0.735354	-0.373811	**0.77**	0.555331	-0.673131	0.500863702	0.9922
bta-miR-7857-5p	0.511560	0.409283	**1.33**	0.608412	0.672707	0.501133865	0.9922
bta-miR-2284x	330.726191	0.028705	1.02	0.043168	0.664953	0.506080723	0.9922
bta-miR-2285az	0.540594	0.432492	**1.35**	0.652807	0.662511	0.507643579	0.9922
bta-miR-24-3p	11009.18943	-0.056237	0.96	0.085874	-0.654877	0.512547198	0.9922
bta-miR-339b	41.653764	-0.057562	0.96	0.087916	-0.654741	0.512634233	0.9922
bta-miR-874	5.410180	-0.132966	0.91	0.203093	-0.654707	0.512656556	0.9922
bta-miR-126-5p	1727.254403	-0.046398	0.97	0.071031	-0.653204	0.513624893	0.9922
bta-miR-197	22.743396	0.075410	1.05	0.116522	0.647179	0.517516381	0.9922
bta-miR-2285ao	0.254748	-0.628990	**0.65**	0.977220	-0.643652	0.519800904	0.9922
bta-miR-2284b	0.366002	0.443249	**1.36**	0.689160	0.643173	0.520111895	0.9922

Table 2.3 Continued

bta-miR-494	65.521111	0.062598	1.04	0.098178	0.637594	0.52373815	0.9922
bta-miR-142-3p	20.760095	-0.132336	0.91	0.207824	-0.636772	0.52427344	0.9922
bta-miR-3432b	8.421300	-0.099148	0.93	0.156063	-0.635309	0.525226978	0.9922
bta-miR-202	2.331771	0.394052	**1.31**	0.620998	0.634545	0.525724908	0.9922
bta-miR-214	56.890001	-0.097312	0.93	0.153479	-0.634043	0.526053032	0.9922
bta-miR-433	3.991900	0.157480	1.12	0.248813	0.632924	0.526783467	0.9922
bta-miR-2396	0.563717	0.404480	**1.32**	0.641220	0.630798	0.52817275	0.9922
bta-miR-2447	0.288619	0.608130	**1.52**	0.968050	0.628201	0.529872445	0.9922
bta-miR-2284h-5p	0.547564	-0.408983	**0.75**	0.659616	-0.620032	0.535236922	0.9922
bta-miR-2397-5p	0.250197	0.667719	**1.59**	1.078328	0.619217	0.535773508	0.9922
bta-miR-2285l	2.789117	-0.167780	0.89	0.271759	-0.617386	0.53698032	0.9922
bta-miR-184	0.423117	0.457285	**1.37**	0.743997	0.614633	0.538797051	0.9922
bta-let-7c	1516.304286	0.041573	1.03	0.067808	0.613100	0.53981008	0.9922
bta-miR-191b	0.151309	-0.826914	**0.56**	1.355540	-0.610025	0.541845072	0.9922
bta-miR-2285ax	1.095948	-0.267867	0.83	0.442213	-0.605741	0.544686549	0.9922
bta-miR-181a	1816.744674	-0.042198	0.97	0.069747	-0.605012	0.545171213	0.9922
bta-miR-2483-3p	0.432842	-0.396326	**0.76**	0.664355	-0.596557	0.550803054	0.9922
bta-miR-2427	1.199144	0.254813	1.19	0.427511	0.596039	0.551149034	0.9922
bta-miR-194b-3p	1.170656	-0.291011	0.82	0.489750	-0.594204	0.552375734	0.9922
bta-miR-194b	1.170656	-0.291011	0.82	0.489750	-0.594204	0.552375734	0.9922
bta-miR-10020	6.748249	0.274998	**1.21**	0.466272	0.589780	0.555338431	0.9922
bta-miR-1249	5.780181	0.125855	1.09	0.213564	0.589305	0.555656771	0.9922
bta-let-7b	1410.332374	0.035800	1.03	0.061118	0.585758	0.558038061	0.9922
bta-miR-708	14.887943	-0.087328	0.94	0.149213	-0.585259	0.558373583	0.9922
bta-miR-2457	0.796285	-0.305813	0.81	0.524134	-0.583462	0.559582022	0.9922
bta-miR-339a	322.797181	-0.034349	0.98	0.058955	-0.582637	0.560137491	0.9922
bta-miR-7862	4.165871	-0.121237	0.92	0.209773	-0.577945	0.563300958	0.9922
bta-miR-34a	32.857985	0.097987	1.07	0.170296	0.575393	0.565025555	0.9922
bta-miR-1197	0.316979	-0.463740	**0.73**	0.807999	-0.573936	0.566011356	0.9922
bta-miR-12003	0.399141	-0.534442	**0.69**	0.953842	-0.560304	0.575271816	0.9922
bta-miR-2285ab	0.511614	-0.381434	**0.77**	0.681552	-0.559655	0.575714466	0.9922

Table 2.3 Continued

bta-miR-485	1.432017	0.217197	1.16	0.393692	0.551692	0.581159701	0.9922
bta-miR-330	0.354124	0.476000	**1.39**	0.867451	0.548734	0.583187736	0.9922
bta-miR-2285ac	0.590304	0.317897	**1.25**	0.582915	0.545357	0.585507805	0.9922
bta-let-7d	701.745048	0.030815	1.02	0.056731	0.543177	0.587007841	0.9922
bta-miR-424-5p	161.665878	-0.054115	0.96	0.099806	-0.542207	0.587675877	0.9922
bta-miR-7859	39.933445	0.052021	1.04	0.096332	0.540019	0.589184069	0.9922
bta-miR-30a-5p	14758.00792	-0.039250	0.97	0.073376	-0.534919	0.592705564	0.9922
bta-miR-381	262.724289	0.066475	1.05	0.124305	0.534778	0.592803615	0.9922
bta-miR-2285c	1.399519	0.218588	1.16	0.410044	0.533083	0.593976069	0.9922
bta-miR-2355-3p	1.978777	-0.216000	0.86	0.407940	-0.529490	0.596465337	0.9922
bta-miR-1271	21.714341	-0.059552	0.96	0.113246	-0.525865	0.598982038	0.9922
bta-miR-2285ay	0.855136	-0.263299	0.83	0.503250	-0.523197	0.600837362	0.9922
bta-miR-1301	0.312742	0.472133	**1.39**	0.903450	0.522589	0.601260183	0.9922
bta-miR-147	0.600785	-0.343957	**0.79**	0.668172	-0.514774	0.606711081	0.9922
bta-miR-33b	2.038173	-0.170651	0.89	0.334908	-0.509544	0.610370754	0.9922
bta-miR-2285t	14.432719	-0.089180	0.94	0.176500	-0.505269	0.613369751	0.9922
bta-miR-12020	0.179701	-0.657057	**0.63**	1.303120	-0.504219	0.614107785	0.9922
bta-miR-451	420.085124	-0.068707	0.95	0.137057	-0.501302	0.616158379	0.9922
bta-miR-105a	8.487427	0.082300	1.06	0.164895	0.499104	0.617706128	0.9922
bta-miR-7860	0.219406	-0.535186	**0.69**	1.074014	-0.498305	0.618269304	0.9922
bta-miR-6516	1.968418	0.182172	1.13	0.367355	0.495903	0.619963143	0.9922
bta-miR-2436-3p	0.294541	-0.471014	**0.72**	0.955245	-0.493081	0.62195521	0.9922
bta-miR-2285ci	0.333737	-0.382135	**0.77**	0.775467	-0.492780	0.622167732	0.9922
bta-miR-2284v	0.683303	0.268488	**1.20**	0.548136	0.489820	0.624261389	0.9922
bta-miR-192	137.706027	0.043612	1.03	0.089245	0.488675	0.625071866	0.9922
bta-miR-331-5p	45.949250	0.044841	1.03	0.091868	0.488105	0.625475277	0.9922
bta-miR-95	365.377970	-0.032035	0.98	0.066096	-0.484665	0.627914168	0.9922
bta-miR-2285cj	2.198910	0.149717	1.11	0.308935	0.484622	0.627944587	0.9922
bta-miR-450b	296.559415	-0.045925	0.97	0.095497	-0.480906	0.630583403	0.9922
bta-miR-21-3p	0.756938	-0.248427	0.84	0.517835	-0.479742	0.631410992	0.9922
bta-miR-2299-3p	2.140754	-0.154212	0.90	0.321896	-0.479073	0.631886367	0.9922

Table 2.3 Continued

bta-miR-545-5p	0.537721	0.292769	**1.22**	0.626834	0.467059	0.64045775	0.9922
bta-miR-22-5p	1109.575496	0.028782	1.02	0.062122	0.463316	0.643137532	0.9922
bta-miR-4286	5.189836	-0.095153	0.94	0.207038	-0.459590	0.64581063	0.9922
bta-miR-329a	1.808898	0.178708	1.13	0.389120	0.459263	0.646045271	0.9922
bta-miR-11997	0.135846	-0.718031	**0.61**	1.564247	-0.459027	0.646214866	0.9922
bta-miR-502b	11.852985	0.077786	1.06	0.171242	0.454246	0.649651705	0.9922
bta-miR-2285bn	7.839144	-0.077880	0.95	0.172275	-0.452067	0.651220428	0.9922
bta-miR-374b	158.934907	-0.048237	0.97	0.107116	-0.450328	0.652474137	0.9922
bta-miR-2339	0.209587	-0.419764	**0.75**	0.932807	-0.450001	0.65270977	0.9922
bta-miR-2285ap	2.058782	-0.146249	0.90	0.328064	-0.445794	0.655745791	0.9922
bta-miR-212	0.383216	0.330249	**1.26**	0.742345	0.444873	0.65641132	0.9922
bta-miR-2285dh	0.239030	-0.413915	**0.75**	0.935584	-0.442414	0.658190002	0.9922
bta-miR-98	1679.788368	0.027185	1.02	0.061942	0.438881	0.660747914	0.9922
bta-miR-182	0.659161	-0.271736	0.83	0.628098	-0.432633	0.665281512	0.9922
bta-miR-425-3p	8.597577	0.070554	1.05	0.163274	0.432116	0.665656959	0.9922
bta-miR-122	0.211546	-0.473274	**0.72**	1.101664	-0.429599	0.667487045	0.9922
bta-miR-2285am-5p	0.398157	-0.331211	**0.79**	0.774588	-0.427596	0.668944958	0.9922
bta-miR-411c-3p	1.147714	0.179570	1.13	0.420270	0.427273	0.669180248	0.9922
bta-miR-1949	0.833383	0.207257	1.15	0.490872	0.422223	0.672862373	0.9922
bta-miR-6775	0.480615	-0.302047	0.81	0.718237	-0.420539	0.674091536	0.9922
bta-miR-2466-3p	0.185771	0.461203	**1.38**	1.105320	0.417258	0.676490008	0.9922
bta-miR-2285cw	0.198285	-0.480667	**0.72**	1.154004	-0.416521	0.677028571	0.9922
bta-miR-2285be	0.299914	-0.343307	**0.79**	0.826662	-0.415293	0.677927689	0.9922
bta-miR-3065	0.182480	0.489218	**1.40**	1.181112	0.414201	0.678726635	0.9922
bta-miR-374c	1.280394	-0.183406	0.88	0.443582	-0.413465	0.679266181	0.9922
bta-miR-96	0.187073	-0.480667	**0.72**	1.166328	-0.412120	0.68025114	0.9922
bta-miR-190b	9.263329	-0.066962	0.95	0.163180	-0.410360	0.68154195	0.9922
bta-miR-2346	0.174356	0.538944	**1.45**	1.335443	0.403570	0.68652919	0.9922
bta-miR-2284z	18.563903	0.054756	1.04	0.137084	0.399430	0.689576448	0.9922
bta-miR-10164-3p	0.159078	-0.826913	**0.56**	2.072034	-0.399083	0.689832271	0.9922
bta-miR-301a	7.981873	0.068421	1.05	0.171777	0.398311	0.690400886	0.9922

Table 2.3 Continued

bta-miR-6120-3p	8.812281	0.065572	1.05	0.164871	0.397719	0.690837052	0.9922
bta-miR-20b	1.726740	-0.151859	0.90	0.382151	-0.397379	0.691088232	0.9922
bta-miR-664b	44.199744	0.031466	1.02	0.080216	0.392259	0.694866539	0.9922
bta-miR-11985	0.269936	0.392497	**1.31**	1.005966	0.390170	0.696411083	0.9922
bta-miR-2285k	4.950132	-0.085843	0.94	0.222360	-0.386052	0.699457932	0.9922
bta-miR-29c	824.915820	-0.038258	0.97	0.099821	-0.383264	0.701524171	0.9922
bta-miR-2285ce	7.266113	-0.064589	0.96	0.168884	-0.382447	0.702129593	0.9922
bta-miR-29e	0.226361	-0.365252	**0.78**	0.961242	-0.379979	0.703960942	0.9922
bta-miR-369-3p	196.509242	0.039129	1.03	0.103062	0.379667	0.704192312	0.9922
bta-miR-2387	4.290339	-0.085286	0.94	0.232118	-0.367424	0.71330248	0.9922
bta-miR-106a	6.750927	0.068394	1.05	0.186503	0.366720	0.713827972	0.9922
bta-miR-10b	7924.452581	-0.021501	0.99	0.058698	-0.366299	0.714141923	0.9922
bta-miR-539	1.231665	-0.164964	0.89	0.455422	-0.362222	0.717186179	0.9922
bta-miR-2285dk	0.152848	-0.487201	**0.71**	1.345256	-0.362162	0.7172311	0.9922
bta-miR-500	76.763307	-0.029011	0.98	0.080136	-0.362021	0.717336452	0.9922
bta-miR-26a	31965.95583	-0.018308	0.99	0.050932	-0.359466	0.719246857	0.9922
bta-miR-652	375.418571	-0.022619	0.98	0.063228	-0.357740	0.720537586	0.9922
bta-miR-2408	0.238278	0.331151	**1.26**	0.925675	0.357740	0.720538015	0.9922
bta-miR-2284ab	16.706263	0.041388	1.03	0.116284	0.355921	0.721899419	0.9922
bta-miR-6529a	11.315226	0.055532	1.04	0.156592	0.354629	0.72286724	0.9922
bta-miR-181b	102.958144	-0.027004	0.98	0.076626	-0.352420	0.724523414	0.9922
bta-miR-2285ar	0.172628	-0.419775	**0.75**	1.195224	-0.351210	0.725430494	0.9922
bta-miR-2285dc	0.306955	-0.297523	0.81	0.848020	-0.350845	0.725704993	0.9922
bta-miR-193a-3p	6.658669	-0.065979	0.96	0.188849	-0.349374	0.726808719	0.9922
bta-miR-11973	0.192960	-0.426226	**0.74**	1.223507	-0.348364	0.727566539	0.9922
bta-miR-10167-3p	0.377641	0.251586	1.19	0.731105	0.344118	0.730757335	0.9922
bta-miR-323b-3p	0.285359	-0.338923	**0.79**	0.995163	-0.340570	0.733426949	0.9922
bta-miR-1343-5p	0.333574	-0.301501	0.81	0.886410	-0.340137	0.733753136	0.9922
bta-miR-302d	7.033617	0.072921	1.05	0.214971	0.339215	0.734447959	0.9922
bta-miR-11975	0.163203	-0.426226	**0.74**	1.259219	-0.338485	0.734997951	0.9922
bta-miR-656	0.876221	-0.171023	0.89	0.508238	-0.336501	0.736493056	0.9922

Table 2.3 Continued

bta-miR-2285bq	2.223049	-0.106789	0.93	0.318824	-0.334948	0.737664488	0.9922
bta-miR-2285bj	0.608131	-0.214216	0.86	0.645458	-0.331883	0.739977937	0.9922
bta-miR-935	0.752533	-0.181114	0.88	0.556090	-0.325692	0.744657469	0.9922
bta-miR-8549	0.826442	0.158775	1.12	0.489301	0.324493	0.745564988	0.9922
bta-miR-151-3p	429.626835	0.022373	1.02	0.069207	0.323280	0.746483475	0.9922
bta-miR-2285b	12.493765	-0.059865	0.96	0.186052	-0.321763	0.747632496	0.9922
bta-miR-2285m	0.177809	0.371687	**1.29**	1.173316	0.316783	0.751407976	0.9922
bta-miR-11998	2.569181	-0.109373	0.93	0.356441	-0.306848	0.758958868	0.9922
bta-miR-505	20.572308	0.035512	1.02	0.115840	0.306563	0.759175827	0.9922
bta-miR-2302	0.117941	-0.772472	**0.59**	2.527801	-0.305590	0.759916573	0.9922
bta-miR-99a-5p	4646.720376	-0.018348	0.99	0.060673	-0.302410	0.762339528	0.9922
bta-miR-2463	0.470591	0.191163	1.14	0.642095	0.297717	0.765919244	0.9922
bta-miR-2483-5p	1.051718	-0.146640	0.90	0.497372	-0.294830	0.768124052	0.9922
bta-miR-6517	1.940389	0.097437	1.07	0.330999	0.294373	0.768473245	0.9922
bta-miR-2285bp	0.276116	-0.241733	0.85	0.821292	-0.294333	0.768503746	0.9922
bta-miR-363	13.288365	-0.050063	0.97	0.170271	-0.294019	0.768743526	0.9922
bta-miR-208a	2.245573	-0.095189	0.94	0.324263	-0.293555	0.769097948	0.9922
bta-miR-29d-3p	37.703296	-0.029509	0.98	0.101339	-0.291188	0.770907224	0.9922
bta-miR-2285cm	5.691419	-0.070157	0.95	0.241956	-0.289959	0.77184744	0.9922
bta-miR-660	637.888887	0.023304	1.02	0.080694	0.288791	0.772741501	0.9922
bta-miR-2284d	0.140956	-0.371785	0.77	1.288730	-0.288489	0.77297214	0.9922
bta-miR-17-3p	3.073899	0.073301	1.05	0.256894	0.285336	0.775386747	0.9922
bta-miR-412	0.189255	0.374115	1.30	1.315512	0.284388	0.776113311	0.9922
bta-miR-370	8.592721	-0.051300	0.97	0.180952	-0.283502	0.776791815	0.9922
bta-miR-130b	4.159717	-0.064870	0.96	0.229757	-0.282340	0.777682629	0.9922
bta-miR-149-5p	24.333666	0.033109	1.02	0.117462	0.281874	0.778039837	0.9922
bta-miR-2397-3p	0.434889	-0.231071	0.85	0.827402	-0.279273	0.780035573	0.9924
bta-miR-296-3p	8.463941	-0.048242	0.97	0.179369	-0.268956	0.787963743	0.9928
bta-miR-6525	0.202593	-0.249836	0.84	0.938024	-0.266343	0.789974699	0.9928
bta-miR-7857-3p	0.140866	0.362819	**1.29**	1.367028	0.265407	0.790695865	0.9928
bta-miR-93	390.895297	0.019389	1.01	0.073218	0.264814	0.79115246	0.9928

Table 2.3 Continued

bta-miR-11977	8.859774	0.053253	1.04	0.209989	0.253601	0.799803663	0.9928
bta-miR-2285y	1.440972	-0.097089	0.93	0.384335	-0.252616	0.800565247	0.9928
bta-miR-302a	7.152005	0.056802	1.04	0.225839	0.251514	0.801417049	0.9928
bta-miR-2284y	31.614225	-0.027289	0.98	0.110643	-0.246641	0.805185841	0.9928
bta-miR-2285cn	0.275855	-0.239371	0.85	1.007381	-0.237617	0.812178324	0.9928
bta-miR-2285av	12.787976	-0.031249	0.98	0.135538	-0.230555	0.817660245	0.9928
bta-miR-487a	1.675509	-0.082524	0.94	0.358663	-0.230089	0.818022824	0.9928
bta-miR-27a-3p	2724.551883	-0.022810	0.98	0.099136	-0.230084	0.818026597	0.9928
bta-miR-2284n	0.172926	0.288786	**1.22**	1.264827	0.228320	0.819397162	0.9928
bta-miR-20a	66.519284	0.020143	1.01	0.089288	0.225598	0.82151421	0.9928
bta-miR-2332	10.286969	-0.073064	0.95	0.328759	-0.222243	0.82412489	0.9928
bta-miR-1468	304.726200	0.016683	1.01	0.076020	0.219462	0.826290083	0.9928
bta-miR-133a	59175.47412	-0.018594	0.99	0.086179	-0.215761	0.829173935	0.9928
bta-miR-6535	0.154135	0.253903	1.19	1.198669	0.211820	0.832247075	0.9928
bta-miR-2465	0.347164	-0.174470	0.89	0.833670	-0.209279	0.834230108	0.9928
bta-miR-504	44.470776	-0.021163	0.99	0.101663	-0.208168	0.835097404	0.9928
bta-miR-455-3p	47.311603	0.026477	1.02	0.127311	0.207973	0.835250178	0.9928
bta-miR-2284a	9.221262	-0.085701	0.94	0.418493	-0.204785	0.837740418	0.9928
bta-miR-2284j	0.235728	-0.188794	0.88	0.927654	-0.203517	0.838730707	0.9928
bta-miR-376e	83.018913	-0.020979	0.99	0.106324	-0.197316	0.843579882	0.9928
bta-miR-1296	3.751748	0.052401	1.04	0.268017	0.195515	0.844989681	0.9928
bta-miR-2411-3p	1.282127	-0.089976	0.94	0.468938	-0.191871	0.847843259	0.9928
bta-miR-2285bm	0.290425	0.150908	1.11	0.790603	0.190877	0.848622303	0.9928
bta-miR-185	78.694796	0.018714	1.01	0.098163	0.190646	0.848802658	0.9928
bta-miR-376d	10.076343	0.033566	1.02	0.176098	0.190612	0.848829233	0.9928
bta-miR-30d	8237.794209	0.012473	1.01	0.066657	0.187125	0.851562327	0.9928
bta-miR-769	6.905377	-0.034917	0.98	0.186672	-0.187050	0.851621334	0.9928
bta-miR-3431	31.457865	0.022202	1.02	0.120229	0.184662	0.853494367	0.9928
bta-miR-496	0.479272	0.136822	1.10	0.742387	0.184300	0.853778032	0.9928
bta-miR-10172-5p	0.134862	0.246667	1.19	1.373146	0.179636	0.857438066	0.9928
bta-miR-1291	1.088113	-0.091530	0.94	0.524371	-0.174553	0.861431246	0.9928

Table 2.3 Continued

bta-miR-2285af	0.236204	0.187261	1.14	1.076006	0.174033	0.861839262	0.9928
bta-miR-2285aj-5p	2.047472	-0.056967	0.96	0.333791	-0.170668	0.86448487	0.9928
bta-miR-129	0.324462	-0.152783	0.90	0.921379	-0.165820	0.868298793	0.9928
bta-miR-129-5p	0.324462	-0.152783	0.90	0.921379	-0.165820	0.868298793	0.9928
bta-miR-502a	18.104509	-0.022534	0.98	0.137466	-0.163922	0.86979216	0.9928
bta-miR-380-5p	0.281697	0.155540	1.11	0.972096	0.160005	0.872877319	0.9928
bta-miR-11982	0.176749	0.199474	1.15	1.252978	0.159200	0.873511442	0.9928
bta-miR-2419-5p	14.379339	0.035777	1.03	0.234031	0.152874	0.878497495	0.9928
bta-miR-758	0.211378	-0.134421	0.91	0.894675	-0.150246	0.880570927	0.9928
bta-miR-215	22.082416	0.031519	1.02	0.213231	0.147814	0.882489234	0.9928
bta-miR-503-3p	0.200494	0.144949	1.11	0.985081	0.147144	0.883018002	0.9928
bta-miR-302c	0.361561	-0.105729	0.93	0.726469	-0.145538	0.884286186	0.9928
bta-miR-296-5p	3.072260	0.034129	1.02	0.239577	0.142454	0.886721183	0.9928
bta-miR-194	313.741492	0.010835	1.01	0.076447	0.141739	0.887286469	0.9928
bta-miR-200b	0.166230	-0.201929	0.87	1.424967	-0.141708	0.887311003	0.9928
bta-miR-2284o	0.151534	-0.201929	0.87	1.451367	-0.139130	0.889347443	0.9928
bta-miR-221	45.770822	0.016262	1.01	0.119476	0.136110	0.891734105	0.9928
bta-miR-2419-3p	0.688577	-0.093705	0.94	0.694790	-0.134869	0.892715745	0.9928
bta-let-7g	12513.48514	-0.007009	1.00	0.052609	-0.133228	0.894013292	0.9928
bta-miR-2285ai-5p	0.860369	-0.071329	0.95	0.540121	-0.132061	0.894936177	0.9928
bta-miR-2404	4.398902	-0.035430	0.98	0.269135	-0.131645	0.895264834	0.9928
bta-miR-3660	0.189703	0.144993	1.11	1.101989	0.131574	0.895321289	0.9928
bta-miR-30b-5p	948.768317	-0.007357	0.99	0.058220	-0.126369	0.899440061	0.9928
bta-miR-211	3.327422	-0.047744	0.97	0.377946	-0.126325	0.899474502	0.9928
bta-miR-99b	207.759254	0.008021	1.01	0.065331	0.122773	0.902286609	0.9928
bta-miR-2285bz	0.415033	0.104608	1.08	0.874593	0.119607	0.904794248	0.9928
bta-miR-1246	6.779791	-0.044582	0.97	0.373144	-0.119478	0.904897001	0.9928
bta-miR-2284ac	0.797568	0.066913	1.05	0.561715	0.119122	0.905178567	0.9928
bta-miR-216b	0.170769	0.137785	1.10	1.250368	0.110195	0.912254424	0.9928
bta-miR-26b	5926.236586	-0.005554	1.00	0.052031	-0.106740	0.914995505	0.9928
bta-miR-2285cy	1.330210	0.041413	1.03	0.402600	0.102865	0.918070178	0.9928

Table 2.3 Continued

bta-miR-2285p	2.557105	0.030614	1.02	0.300371	0.101922	0.918818733	0.9928
bta-miR-12030	0.151166	0.137785	1.10	1.361344	0.101212	0.919382044	0.9928
bta-miR-15b	112.543318	0.007101	1.00	0.070306	0.101000	0.919550294	0.9928
bta-miR-421	11.213634	-0.015154	0.99	0.151556	-0.099988	0.920353933	0.9928
bta-miR-7180	15.935931	-0.014134	0.99	0.142588	-0.099123	0.921040546	0.9928
bta-miR-2285au	2.940639	0.026104	1.02	0.265364	0.098369	0.921639118	0.9928
bta-miR-2285cc	1.071513	0.046773	1.03	0.479121	0.097623	0.922231333	0.9928
bta-miR-188	8.927327	0.016199	1.01	0.167751	0.096567	0.923070237	0.9928
bta-miR-2285ak-5p	0.123289	0.131252	1.10	1.392137	0.094281	0.924886237	0.9928
bta-miR-30b-3p	11.980698	-0.013483	0.99	0.143078	-0.094237	0.924920589	0.9928
bta-miR-125a	1216.593863	-0.004833	1.00	0.052377	-0.092281	0.926474724	0.9928
bta-miR-2415-5p	0.109903	0.131251	1.10	1.525060	0.086063	0.931416367	0.9928
bta-miR-9-3p	2.268764	-0.028380	0.98	0.336892	-0.084241	0.93286458	0.9928
bta-miR-2382-3p	0.185393	-0.079980	0.95	1.000590	-0.079933	0.936290872	0.9928
bta-miR-140	408.035874	0.005290	1.00	0.068526	0.077198	0.938466297	0.9928
bta-miR-323	2.822013	0.021574	1.02	0.284766	0.075759	0.939610452	0.9928
bta-miR-767	15.279437	-0.009251	0.99	0.125134	-0.073927	0.941068084	0.9928
bta-miR-12034	0.697123	-0.042414	0.97	0.602122	-0.070440	0.943843185	0.9928
bta-miR-196b	306.961263	-0.005966	1.00	0.086984	-0.068590	0.945316215	0.9928
bta-miR-11971	0.134059	-0.093046	0.94	1.374781	-0.067681	0.94603976	0.9928
bta-miR-2284r	0.130452	-0.093046	0.94	1.382275	-0.067314	0.946331876	0.9928
bta-miR-12049	0.221194	-0.079980	0.95	1.207462	-0.066238	0.947188303	0.9928
bta-miR-2285d	0.156494	-0.093046	0.94	1.423698	-0.065355	0.947891074	0.9928
bta-miR-2399-3p	0.148651	0.131250	1.10	2.048030	0.064086	0.948901891	0.9928
bta-miR-299-2	0.127688	-0.093046	0.94	1.484007	-0.062699	0.950005849	0.9928
bta-miR-10a	344.557402	0.004418	1.00	0.075350	0.058636	0.953241812	0.9928
bta-miR-545-3p	0.326384	-0.041674	0.97	0.760541	-0.054796	0.95630133	0.9928
bta-miR-2285cx	0.119535	0.076810	1.05	1.406641	0.054605	0.956452783	0.9928
bta-miR-324	4.253168	0.012799	1.01	0.238952	0.053564	0.957282905	0.9928
bta-miR-2285an	0.387780	-0.036689	0.97	0.758391	-0.048378	0.961415288	0.9928
bta-miR-139	174.595777	0.004140	1.00	0.087553	0.047291	0.962281091	0.9928

Table 2.3 Continued

bta-miR-7861	0.838028	-0.023509	0.98	0.537753	-0.043716	0.965130556	0.9928
bta-miR-11976	0.627359	0.022236	1.02	0.567418	0.039189	0.968739841	0.9928
bta-miR-2284w	3.145485	-0.009018	0.99	0.258134	-0.034937	0.972130376	0.9928
bta-miR-454	4.895207	0.007851	1.01	0.230934	0.033995	0.97288132	0.9928
bta-miR-450a	255.966846	0.002987	1.00	0.094701	0.031541	0.974837728	0.9928
bta-miR-2350	2.605869	-0.009364	0.99	0.300114	-0.031202	0.975108142	0.9928
bta-miR-12060	0.126143	-0.038605	0.97	1.589131	-0.024293	0.980618574	0.9928
bta-miR-365-5p	4.970535	-0.005733	1.00	0.243953	-0.023499	0.981252629	0.9928
bta-miR-592	3.605422	0.005926	1.00	0.257446	0.023017	0.981637096	0.9928
bta-miR-2399-5p	0.174277	-0.032072	0.98	1.411730	-0.022718	0.981874998	0.9928
bta-miR-34c	0.644248	-0.012069	0.99	0.564117	-0.021394	0.982930976	0.9928
bta-miR-100	524.150301	-0.001450	1.00	0.071516	-0.020278	0.98382163	0.9928
bta-miR-92a	917.666691	0.001042	1.00	0.056403	0.018473	0.985261494	0.9928
bta-miR-2448-3p	0.139959	0.022369	1.02	1.287893	0.017369	0.986142284	0.9928
bta-miR-30f	175.084405	-0.001085	1.00	0.065762	-0.016504	0.986832	0.9928
bta-miR-10182-5p	0.170463	0.022369	1.02	1.404910	0.015922	0.987296536	0.9928
bta-miR-3432a	70.750733	0.000349	1.00	0.077112	0.004525	0.996389979	0.9999
bta-miR-2308	0.315545	-0.000227	1.00	0.734880	-0.000309	0.999753343	0.9999
bta-miR-183	0.374006	-0.000067	1.00	0.861935	-0.000077	0.999938276	0.9999

[*] Selected for further investigation. Possessed expression fold difference ≤ 0.8 and ≥ 1.2 with *p*-value of ≤ 0.05, via both DESeq2 analysis and Welch's *t*-test method.

[1] Out of the initial 542 miRNAs that were tested, 42 miRNAs were different between groups with *p*-values ≤ 0.05.

[2] The average of the normalized count values taken over all samples.

[3] The differential miRNA expression ratio between normal and DFD groups (DFD/NON), reported in values transformed to logbase$_2$.

[4] Fold difference expression ratios expressed in conventional $\log_{10}$.

[5] The standard error estimate for the $\log_2$ fold difference estimate.

[6] Wald statistic. The value of the test statistic for the miRNA.

[7] Adjusted Wald test *p*-values to control for multiple testing at FDR of 5% via the Benjamini-Hochberg method. (*p*-value*542/rank)